NASA Contractor Report - 179544

Isolated Testing of Highly Maneuverable Inlet Concepts

W.P. Norby
B.A. Haeffele
McDonnell Aircraft Company
St. Louis, Missouri

R.R. Burley
NASA-Lewis Research Center
Cleveland, Ohio

IN-07
19372
167

December 1986

NASA

NASA Contractor Report - 179544

Isolated Testing of Highly Maneuverable Inlet Concepts

W.P. Norby
B.A. Haeffele
McDonnell Aircraft Company
St. Louis, Missouri

R.R. Burley
NASA-Lewis Research Center
Cleveland, Ohio

[redacted] until December 1988.

Prepared for
Lewis Research Center
December 1986

National Aeronautics and
Space Administration
Lewis Research Center
Cleveland, Ohio 44135

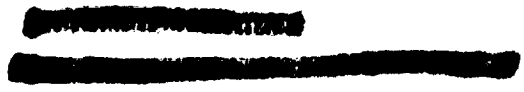

FOREWORD

This report was prepared by personnel in the inlet technology area of the Propulsion and Thermodynamics Department of the McDonnell Aircraft Company. It is the culmination of a cooperative wind tunnel testing effort between MCAIR and the NASA Lewis Research Center in Cleveland, Ohio.

The NASA research engineer was Mr. R. R. Burley, whom the MCAIR authors would like to commend for his outstanding work during the course of the program.

The authors wish to acknowledge the assistance of the following MCAIR personnel: P. V. Reagan, M. A. McGarry, and W. T. Torgerson. Also, the authors would also like to recognize M. S. Taich and J. L. Mark, who made valuable contributions during the test program and the preparation of this report.

Special acknowledgement is due to D. N. Bowditch who initiated the program within NASA.

TABLE OF CONTENTS

TABLE OF CONTENTS (Concluded)

LIST OF FIGURES

LIST OF FIGURES

LIST OF FIGURES (Continued)

LIST OF FIGURES (Continued)

LIST OF FIGURES (Continued)

LIST OF FIGURES (Concluded)

NOMENCLATURE

A	Area, $in.^2$
A_c	Inlet capture area at zero degrees angle of attack, $in.^2$
A_o	Area of the freestream streamtube captured by the inlet, $in.^2$
CR	Contraction ratio of auxiliary inlets, capture area divided by throat area
D	Engine face diameter, in.
L	Distance from inlet throat plane to engine face rake, in.
K_{a_2}	Pratt & Whitney F100 engine fan distortion descriptor
$(K_{a_2})_{\text{limit}}$	Distortion screening limit of engine fan distortion descriptor for the Pratt & Whitney F100
M	Mach number
M_o	Freestream Mach number
P_s	Static pressure, psi
P_T	Total pressure, psi
$P_{T_{RMS}}$	Root mean square value of the dynamic total pressure deviation from the steady state level, psi
P_{T_o}	Freestream total pressure, psi
P_{T_2}	Average total pressure at the engine face station, psi
RALPHA	Average angle of attack over a mass flow sweep, degrees
RBETA	Average angle of sideslip over a mass flow sweep, degrees
RMACH	Average freestream Mach number over mass flow sweep
SF	Scale factor. For both the axisymmetric and 2-D inlets, SF = 0.1
T	Temperature, °Rankine
T_{T_2}	Total Temperature at the engine face station, °Rankine
$\dot{W}$	Mass flow rate, lbm/sec
WAK2P	Full scale inlet corrected airflow evaluated at the engine face:

$$WAK2P = \frac{1}{SF^2} \quad \frac{\dot{W}\ \theta_{T_2}}{\delta_{T_2}} \frac{P_{\text{sea level}}}{T_{\text{sea level}}}, \text{ lbm/sec}$$

W_c	Model scale inlet corrected airflow
α	Angle of attack, measured from the inlet centerline to the freestream direction (positive is inlet up), degrees

β	Angle of sideslip (positive is inlet left), degrees
δ	Total pressure divided by sea level standard pressure
θ	Total temperature divided by sea level standard temperature

SUMMARY

Current supersonic fighter aircraft inlets generally require a compromise between a sharp cowl lip for low drag at supersonic velocities and a blunt cowl lip for good static and angle of attack performance at subsonic velocities. By incorporating flow improvement concepts, increased performance can be obtained over the entire Mach number/angle of attack regime of fighter inlets.

McDonnell Aircraft Company (MCAIR) conducted a wind tunnel test program on isolated inlets to evaluate the effectiveness of several flow improvement concepts on subsonic/transonic maneuvering performance. These concepts were incorporated in 10% scale models of 2-D and axisymmetric external compression inlets. The 2-D inlet was a Mach 2.2, two ramp, overhead compression inlet. The axisymmetric inlet was a Mach 2, single translating cone inlet.

The objective of the test program was to experimentally evaluate inlet concepts designed to delay the onset of internal flow separation at high angles of attack. Flow separation can be controlled or delayed by reducing the flow velocity near the leading edge of the cowl lip. Flow improvement designs included a rotating cowl lip, auxiliary inlets, and retractable centerbody (axisymmetric inlet only). The rotating cowl lip and retracting centerbody reduce the Mach number at the cowl lip by increasing the ratio of the area at the inlet entrance plane to the throat area. This is defined as the inlet contraction ratio. In addition, the rotating cowl lip provides a Mach number reduction at the cowl by more closely aligning the lip leading edge with the inlet approach flow field. Auxiliary inlets reduce the flow velocity by reducing the mass flow through the main inlet.

Testing was conducted from Mach 0.6 to 1.4 in the 8 x 6 foot wind tunnel at the NASA-Lewis Research Center. Inlet angle of attack was varied from 0° to +40° at Mach 0.6 and 0.9 and up to +25° at Mach 1.2 and 1.4. Sideslip angles were 0° to 10°. The freestream Reynolds number ranged from 3.5 to 4.5 million per foot.

Results showed the rotating cowl lip to be an effective concept for improving angle of attack performance for both 2-D and axisymmetric inlets in the Mach number range of 0.6 to 0.9. Cowl lip rotation angles of 20° and 40° were tested. The 20° lip rotation provided the largest performance improvement throughout the angle of attack range. At Mach 0.9 and 40° angle of attack, total pressure recovery was 20% higher than the baseline axisymmetric inlet and 7.5% higher than the baseline 2-D inlet. Average turbulence levels were reduced by a factor of 4.6 for the 2-D inlet and 2.2 for the axisymmetric inlet.

The rotating cowl lip concepts were ineffective on the 2-D and axisymmetric inlets above Mach 1.2 and 1.4 due to a bow shock generated by the rotated cowl lip. Recovery levels dropped from one to four percent relative to the baseline over the entire angle of attack range.

Auxiliary inlets provided only small improvements in inlet performance, and then only at angles of attack above 30°. Opening auxiliary inlets below 30° degraded inlet performance. Auxiliary inlet location and throat area were varied on the axisymmetric inlet, on which only flush auxiliary inlets were tested. Auxiliary inlets were effective only on the lower inlet surface. This was due to the ram effect of the flow at angle of attack.

On the 2-D inlet, tests included two flush inlets and one external scoop auxiliary inlet. Addition of an external door or scoop provided only a small performance improvement above the flush configurations. In general, inlet distortion increased when auxiliary inlets were opened.

Flush auxiliary inlet configurations were not tested above Mach 0.9 since they were ineffective at subsonic Mach numbers. However, the external scoop auxiliary inlet was tested on the 2-D inlet at Mach 1.2 , α = 20° and 25°. Inlet performance was reduced when this auxiliary inlet was opened.

The retracted centerbody configuration provided a small improvement in axisymmetric inlet performance at angles of attack above 20°, where flow separation begins to occur in the baseline inlet. However, above 20°, inlet distortion levels increased. Below 20°, performance was similar to the baseline inlet.

This report presents inlet performance in terms of total pressure recovery, average turbulence, and inlet distortion as a function of angle of attack. Engine face total pressure contour plot comparisons are shown to illustrate how cowl lip and auxiliary inlet devices effect the duct flow. A final comparison is made between the 2-D and axisymmetric inlet baselines and the 20° rotated lip configurations at all Mach numbers.

1. INTRODUCTION

Projected requirements for some advanced fighters include a sustained supersonic cruise capability, and subsonic maneuvering capabilities beyond that of current fighters. However, efficient supersonic performance and high maneuverability are conflicting inlet design requirements. Efficient supersonic performance requires an inlet which is properly matched to the engine airflow requirements and sharp leading edges to minimize lip drag at supersonic speeds. For effective maneuvering performance, including low distortion, a high contraction ratio is required along with blunt leading edges to prevent flow separation. In general, a compromise is made in the inlet design to provide acceptable subsonic and supersonic performance.

The major cause of reduced inlet performance at high angles of attack is flow separation on the lower cowl lip. The flow stagnation point moves below the lip highlight, forcing flow to accelerate around the leading edge. The sharper the cowl lip (for improved supersonic performance), the worse the separation problem becomes.

For 2-D inlets, flow separation results in increased distortion while inlet recovery is not as significantly affected. However, for an axisymmetric inlet, cowl lip separation is further complicated by flow separation on the leeward side of the inlet centerbody, resulting in low recovery and high distortion. Angle of attack performance of axisymmetric inlets has traditionally been poor.

Several concepts have been identified in this program for improving the subsonic high angle of attack performance of supersonic inlets. The flow improvement devices designed included a rotating cowl lip, auxiliary inlets, and a retracting centerbody on the axisymmetric inlet. Ideally, the inlet could be designed with a sharp cowl lip, to provide low supersonic drag, and incorporate variable geometry features to improve maneuvering performance. These concepts would be actuated as the aircraft angle of attack is increased.

Analytical codes have recently become available for predicting the performance of inlets at high angles of attack, but have not been sufficiently verified due to lack of experimental data. Therefore, wind tunnel testing was conducted to identify the performance increments, and increase the data base for verification of inlet performance prediction codes.

The 2-D inlet flowfield with the baseline and rotated cowl lip was analyzed using a recently developed 2-D Navier-Stokes code. Analytical results verified that eliminating the separated region at the cowl lip reduced the boundary layer thickness at the engine face and improved total pressure recovery.

This report presents a summary of the test results and analysis of the data. Inlet performance was measured in terms of engine face total pressure recovery, distortion, and average turbulence. The operating point at each Mach number was selected to be the corrected airflow corresponding to 95 percent of critical inlet mass flow for the baseline inlet at zero degrees angle of attack.

This test was performed with the support and under the auspices of the NASA-Lewis Research Center to investigate inlet technology for enhanced maneuverability. NASA Lewis provided the use of the 8 x 6 foot wind tunnel test facility from July through August 1982. NASA engineers developed the software for the data reduction, display, and plotting capabilities. A total of 4150 data points were recorded in 86 runs. The NASA research engineer was Mr. Richard R. Burley.

2. TEST FACILITY

2.1 8X6 FOOT TUNNEL - The NASA Lewis Research Center 8x6 foot Supersonic Wind Tunnel can attain test section Mach numbers ranging from 0.36 to 2.0. The tunnel, illustrated in Figure 2-1, may be operated in an open or closed loop mode, Reference 1. In the closed loop mode, air is recirculated through the test section, with dry air being added only as required to maintain the desired test conditions. In the open mode, outside air is drawn in through the air dryer and exhausted to the atmosphere. For this test, the tunnel was operated in the open mode. The four test section walls are perforated to reduce boundary layer thickness. The wall porosity was further adjusted to compensate for the flow blockage of the test model.

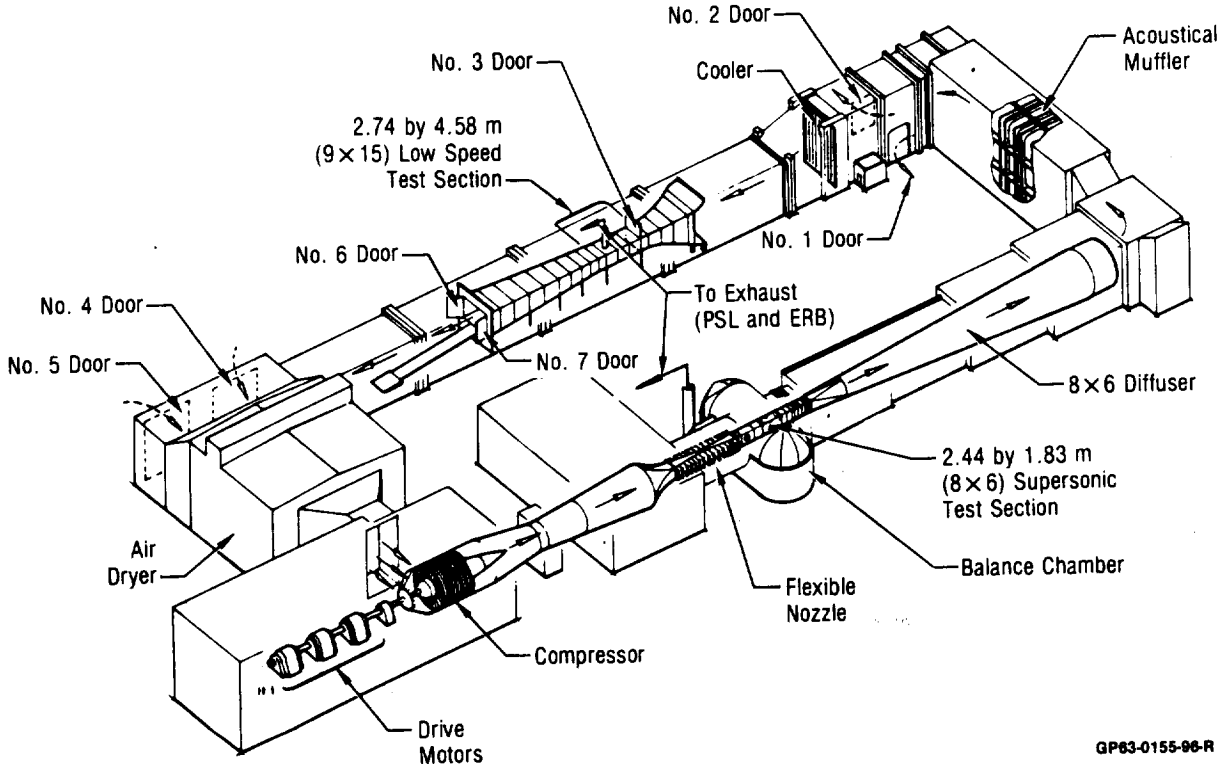

Figure 2-1. NASA-Lewis Research Center 8 x 6 Ft Wind Tunnel

2.2 MODEL SUPPORT SYSTEM - NASA-Lewis provided the support and interface hardware for installing the MCAIR inlet models in the tunnel. The major hardware elements were (1) the mass flow plug adapter, (2) the model mount strongback, and (3) the remote actuation pitch and yaw sting. These interface elements connected the models to the facility transonic strut, as shown in the installation drawing, Figure 2-2.

The MCAIR inlets were attached to the NASA mass flow plug adapter, establishing the interface between MCAIR and NASA hardware elements. The NASA Lewis mass flow plug was supported from the aft end of the adapter.

The adapter is supported from the model mount strongback, which provides the load path for model aerodynamic forces. Two additional support straps extend from the strongback to the mass flow plug, to improve model rigidity at angle of attack.

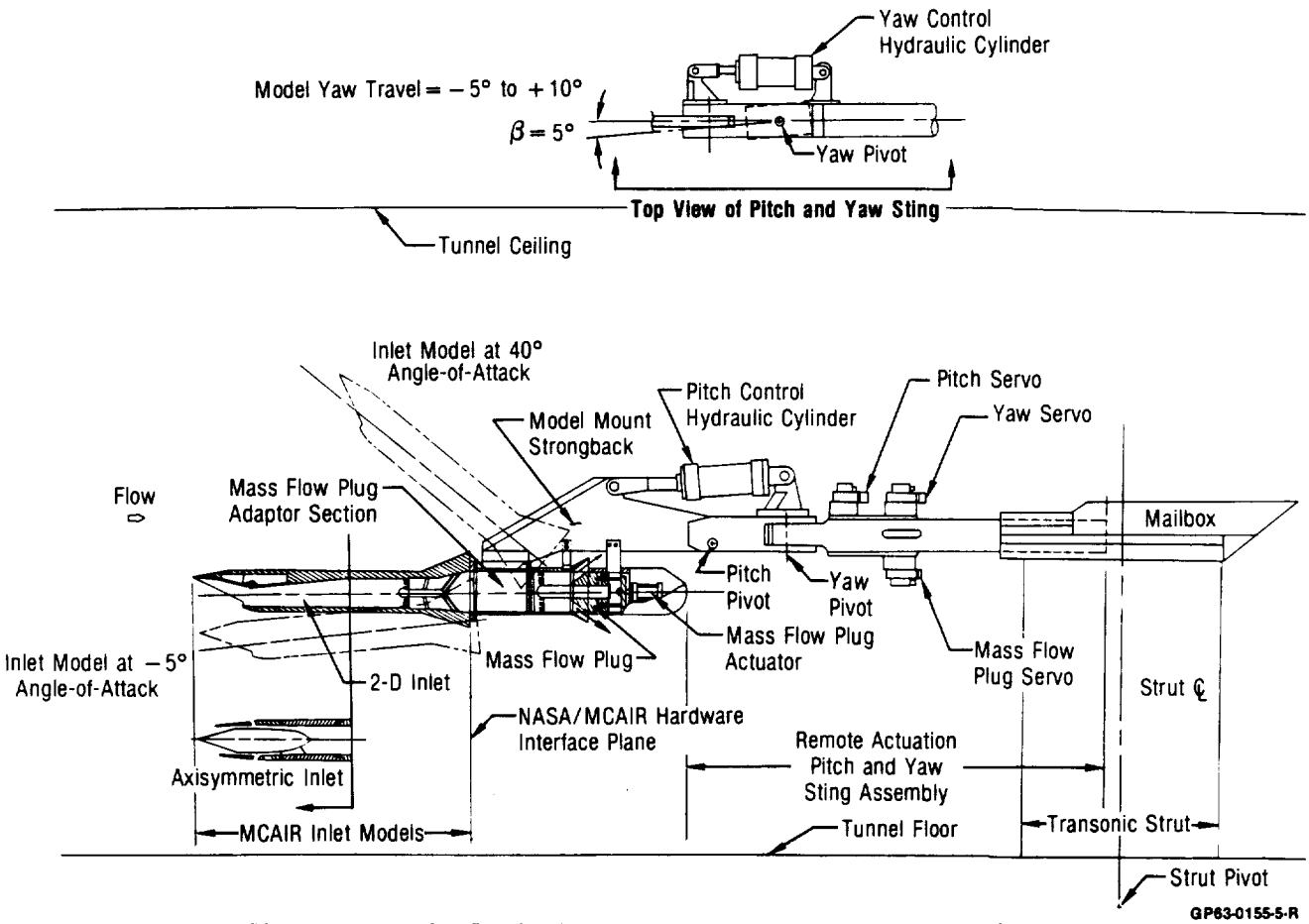

Figure 2-2. MCAIR Highly Maneuverable Inlet Model Installation
NASA-Lewis Research Center 8 x 6 Ft Wind Tunnel

The strongback is connected to a sting assembly via a pitch pivot connection. A pitch control actuator, attached to both the sting and strongback, provides remote pitch actuation for angle of attack testing.

The remote actuation pitch and yaw sting assembly connects the model strongback to the facility transonic strut. This sting provides the pivots for both pitch and yaw actuation. The pitch pivot is forward of the yaw pivot. The yaw control hydraulic cylinder is illustrated in a top view of Figure 2-2. Servo controls are mounted on the sting for hydraulic actuation of the pitch, yaw, and mass flow plug actuators.

The pitch range of the sting was from -5° to +25° and yaw capability was -5° to +10°. The facility transonic strut is floor mounted and capable of pitch over an angle of attack range from 0° to +15°. Therefore, combined sting and strut rotation provided a maximum model angle of attack range from -5° to +40°.

All electrical and pneumatic lines were routed in bundles along the model strongback and sting. These bundles were then enclosed in the top of the transonic strut, where connections were made to the facility control room instrumentation.

2.3 DATA ACQUISITION SYSTEM - The data acquisition system utilized ten pressure modules that could accommodate up to 32 pressure orifices each. Each orifice had its own transducer, and the outputs from the 32 transducers were scanned electronically. Each module also had two ports connected to reference pressures.

All transducers for the engine face and mass flow plug rakes were 50 psi transducers. Static pressures were measured on 15 psi transducers. Accuracy of the transducers was $\pm$.15% of full scale. The modules were automatically calibrated every 20 minutes for zero shifts and sensitivity changes by checking against the two reference pressures. New sensitivity factors were computed from these calibrations and the transducer sensitivity coefficients were updated. All pressure transducers were housed in a water cooled enclosure below the tunnel, to minimize temperature variations.

The NASA Lewis data acquisition system provided for recording test measurands and the effective real time computation of a large number of performance parameters. Data was obtained, performance parameters computed, and real time results were updated every five seconds on CRT monitors. As test variables were remotely altered, the monitors allowed test engineers to examine updated model pressure data as well as preselected performance parameters. Recorded data was also transmitted to a high speed digital computer, which provided complete hardcopy data reduction. The reduced data was also stored on disks, for post test data review and automated plotting.

NASA-Lewis engineers developed the software for calculating real time and post test inlet performance data.

3. MODEL DESCRIPTIONS

Maneuverability performance testing was conducted using ten percent scale MCAIR models of 2-D and axisymmetric supersonic inlets. Basic model features of both inlet types are described in Sections 3.1 and 3.2, together with instrumentation and flow improvement concepts. Descriptions of hardware common to both models, such as the engine face rake and mass flow plug, are contained in Section 3.3.

3.1 2-D INLET MODEL - The 2-D inlet model, Figure 3-1, was assembled from four model sections: (1) the main inlet, (2) the forward auxiliary inlet, (3) the diffuser, and (4) the aft auxiliary inlet. Immediately downstream of the aft auxiliary inlet section is the engine face rake, which is common for all inlet configurations.

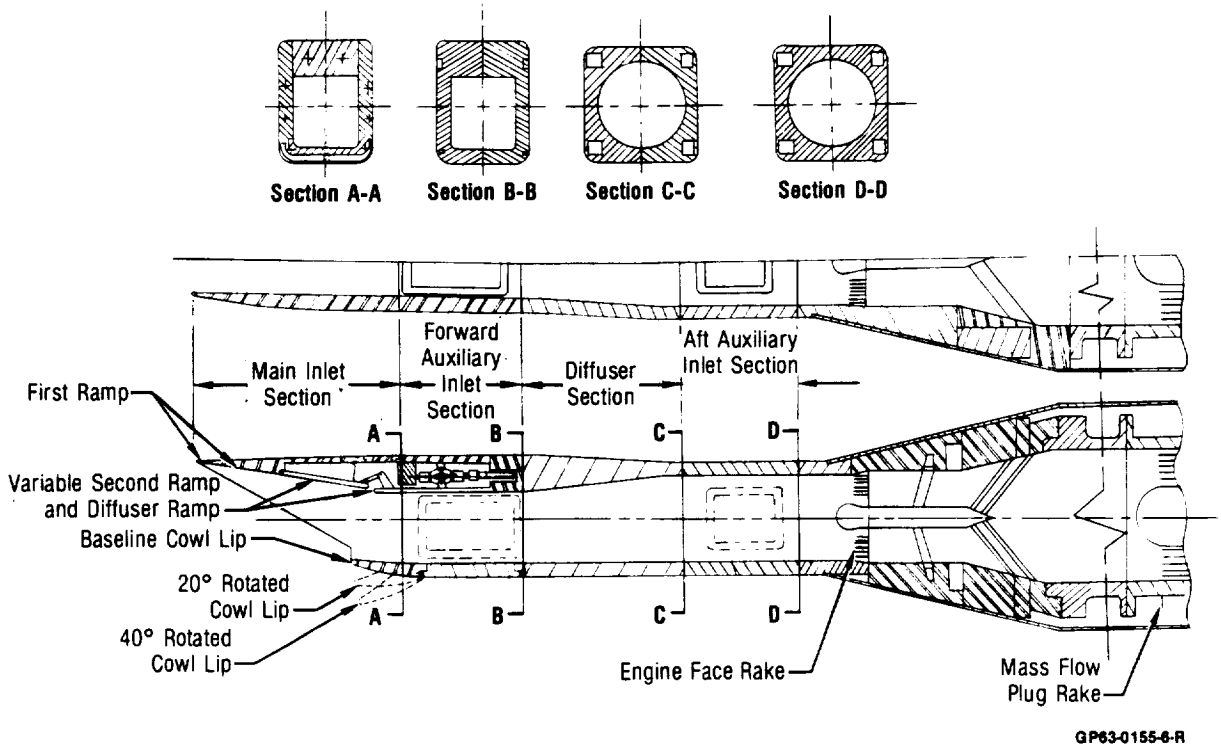

Figure 3-1. 2-D Inlet Model Design

The inlet configuration with all four component sections is referred to as the long diffuser configuration, Figure 3-2. In this configuration, the distance, L, from the inlet throat plane to the engine face rake is equal to 5.5 engine face diameters. The engine face diameter is 3.46 inches.

The 2-D inlet can also be tested with shorter ducts by removing one or both of the auxiliary inlet sections. The short diffuser configuration, Figure 3-3, is created by removing both auxiliary inlet sections from the long diffuser configuration, reducing the distance between the throat plane and engine face rake to 2.5 engine face diameters. A photograph of this configuration in the 8x6 foot wind tunnel, Figure 3-4, also shows the NASA support hardware downstream of the inlet model.

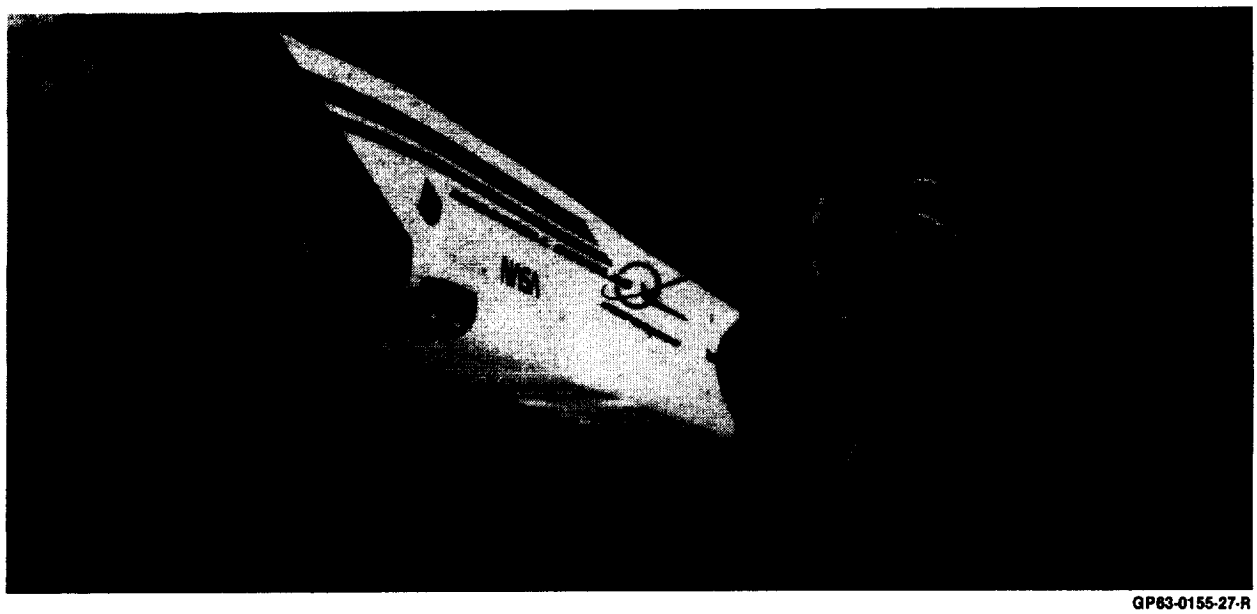

GP83-0155-27-R

Figure 3-2. 2-D Inlet Model Installation in the NASA-Lewis 8 x 6 Ft Wind Tunnel
Long Diffuser Configuration

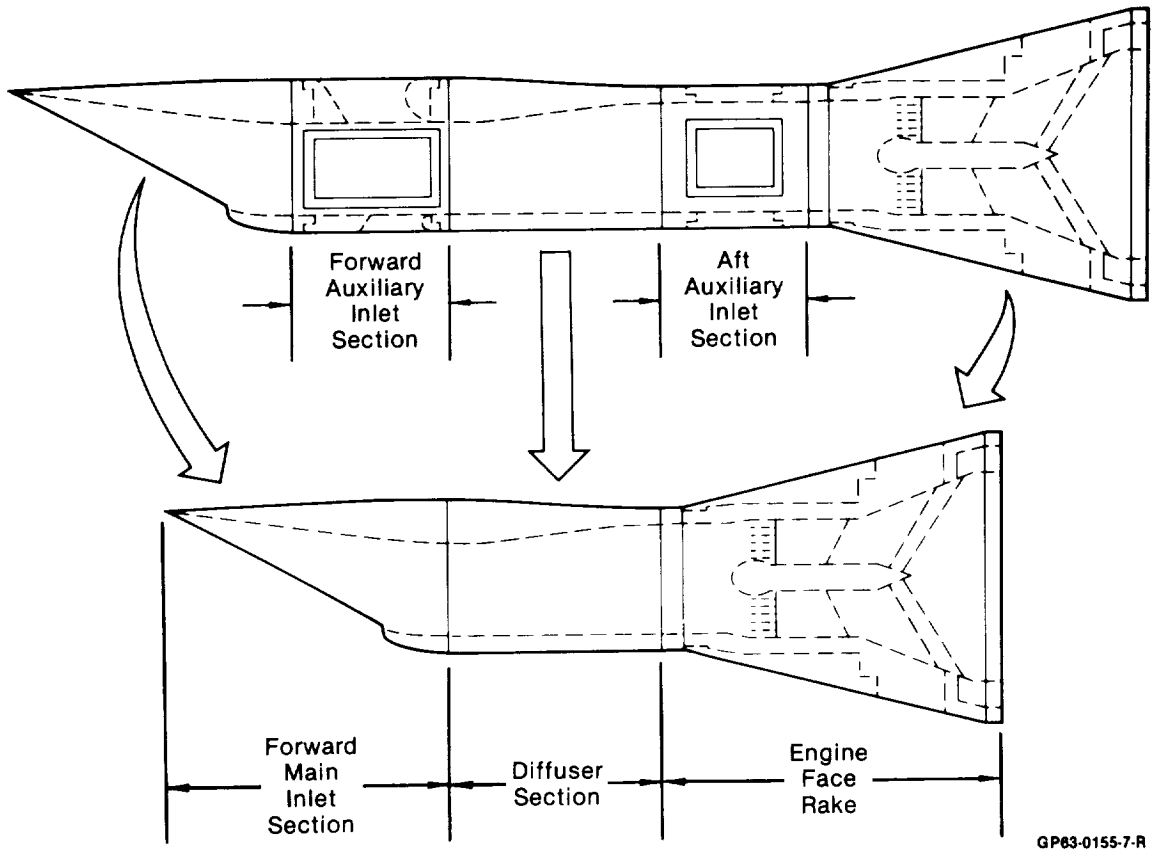

Figure 3-3. 2-D Inlet Model Long and Short Diffuser Configurations

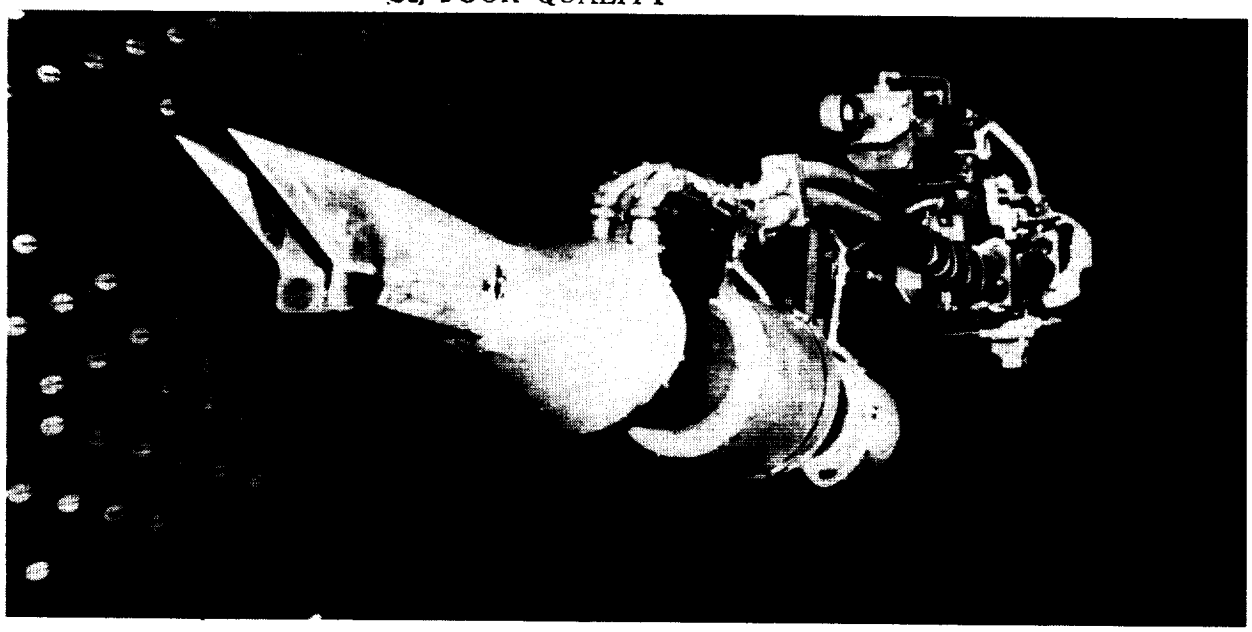

GP63-0155-22-R

Figure 3-4. 2-D Inlet Model Installation in the NASA-Lewis 8 x 6 Ft Wind Tunnel
Short Diffuser Configuration With 40° Rotated Lip

3.1.1 Main Inlet Section - The main inlet section of the 2-D inlet model contains the fixed first ramp, variable second ramp, cowl lip, and sideplates as shown in Figure 3-1. The first ramp provides 8° of compression. For testing with the short diffuser, the variable second ramp was replaced with a wedge block shown in the shaded area of Figure 3-5. This simulates a V/STOL inlet with no boundary layer bleed system in the throat slot or ramp. In this test, the variable second ramp in the long diffuser configuration was always tested in a colinear position with the first ramp, hence the overall compression angle was 8° for all 2-D inlet investigations.

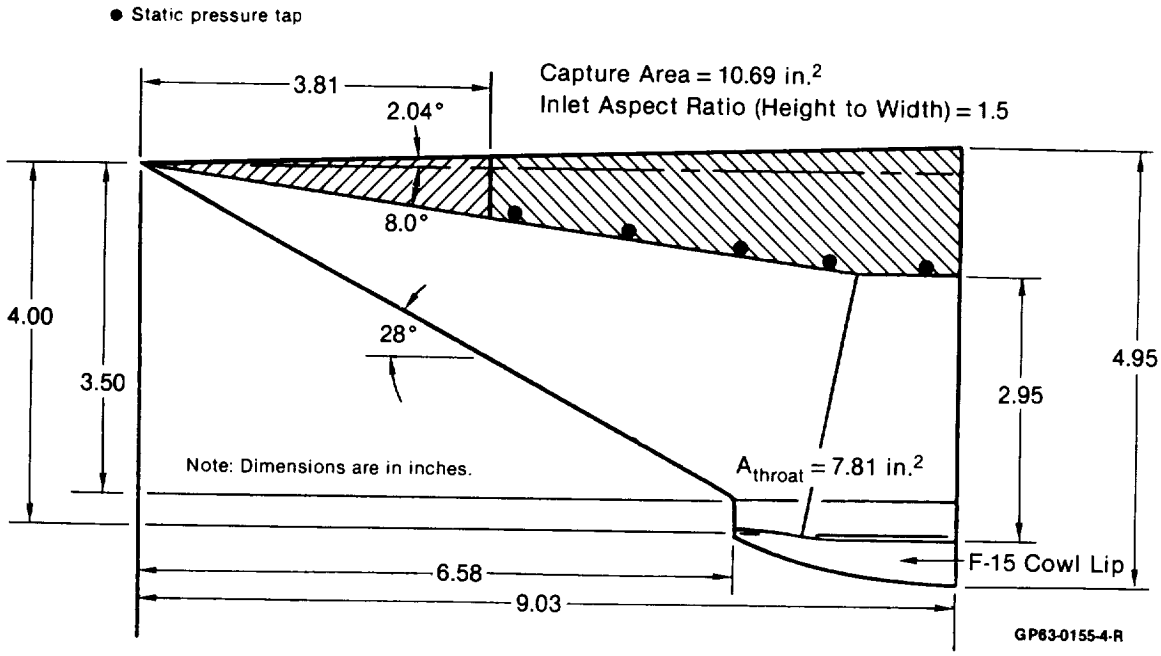

Figure 3-5. 2-D Main Inlet Section Design and Instrumentation
Short Diffuser Configuration

The short diffuser wedge block ramp has five static pressure orifices distributed along the centerline of the compression system, as shown in Figure 3-5. The variable ramp configuration has 10 static pressure orifices on the two compression and diffuser ramps, Figure 3-6. A three-probe total pressure rake is located at the end of the second ramp.

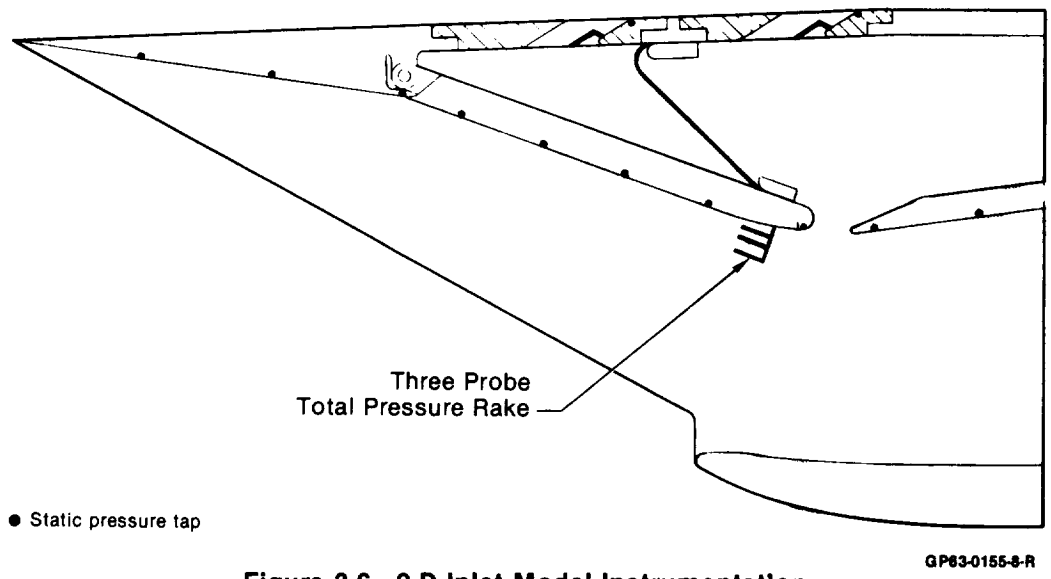

Figure 3-6. 2-D Inlet Model Instrumentation
Long Diffuser Configuration

The inlet sideplates have a 12.5% cutback, identical to that of the F-15 aircraft inlet. The cutback, defined as the ratio of the cutback height to the inlet height, Figure 3-5, is designed to improve supersonic stable range. The leading edges of the sideplates are swept 28°. The internal surfaces are planar, to avoid sidewall compression influences on the ramp flowfield.

Bleed systems were incorporated in the sideplates for boundary layer control in the regions where the second oblique and normal shocks occur during supersonic operation. Solid and porous plates were interchangeable. The unbled sideplates were tested on the short diffuser configuration and the long diffuser configuration was tested with sideplate bleed. The sideplates were not instrumented.

The baseline cowl lip contour was scaled from the F-15 aircraft inlet. This contour is a compromise between a sharp lip for low supersonic drag and a blunt cowl lip for good subsonic performance at angle of attack. The 2-D inlet was tested with the baseline cowl lip and with two rotated cowl lips, Figure 3-7. The rotated cowl lips utilized the same contour as the baseline, but were rotated 20° and 40° relative to a reference line from the baseline lip highlight through the theoretical hinge point. The three cowls are illustrated in Figure 3-8. The rotated cowl lip hardware contained a portion of the sideplate to simulate sideplates which rotated in concert with the cowl lip.

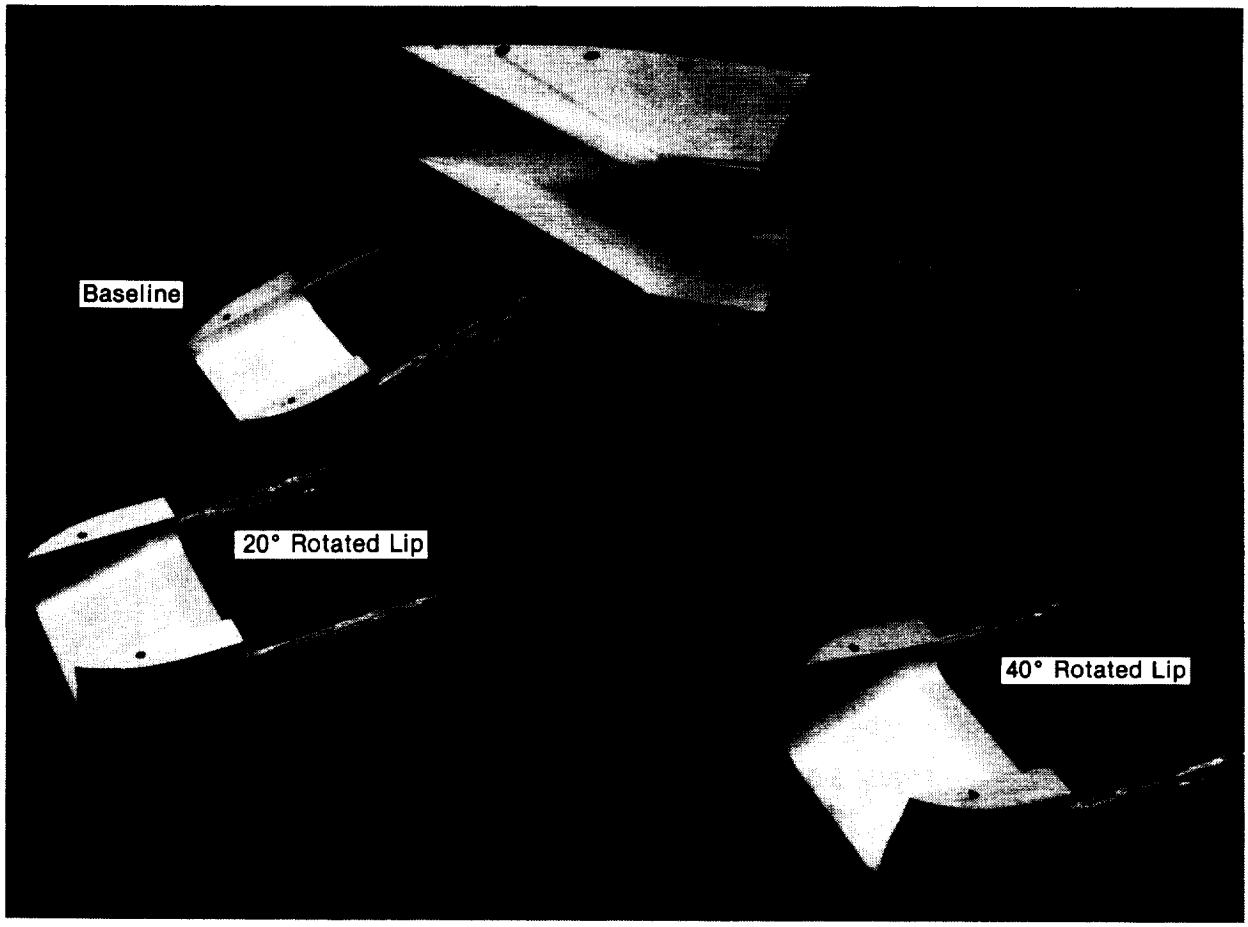

GP83-0155-21-R

Figure 3-7. 2-D Inlet Lower Cowl Lip Variations

Each cowl was instrumented with seventeen static pressure orifices, illustrated in Figure 3-8. This instrumentation was distributed along the centerline, both internally and externally.

3.1.2 Forward Auxiliary Inlet Section - The forward auxiliary inlet section of the model provides a constant area flow channel, spanning the length of the simulated diffusion ramp. The cross-sectional area is rectangular, with fillets in the lower corners, as shown in Sections AA and BB of Figure 3-1. The top, sides, and bottom were designed for incorporating the auxiliary inlets.

It was determined during the testing of the axisymmetric inlet, which was tested prior to the 2-D inlet, that upper auxiliary inlets were ineffective in the Mach range of this test program, and therefore only bottom mount auxiliary inlets were evaluated on the 2-D inlet in this program.

Three auxiliary inlet configurations were evaluated, two flush concepts and one external scoop concept, as illustrated in Figure 3-9. The throat centerlines of the auxiliary inlets are located 4.5 duct diameters forward of the engine face rake.

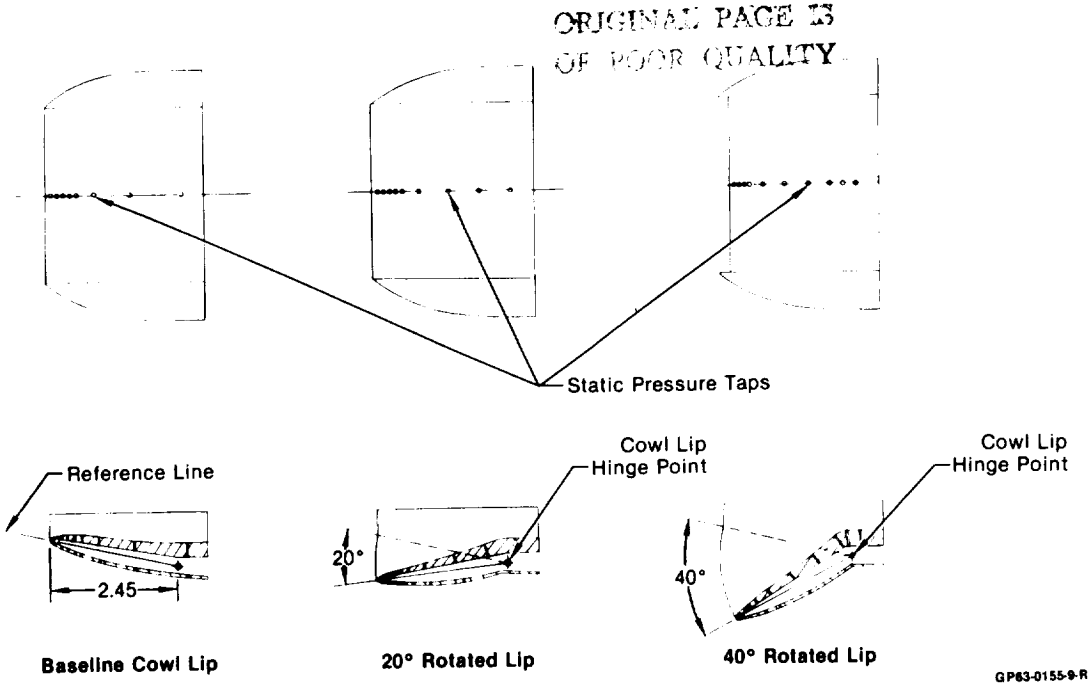

Figure 3-8. 2-D Inlet Rotated Cowl Lip Configurations

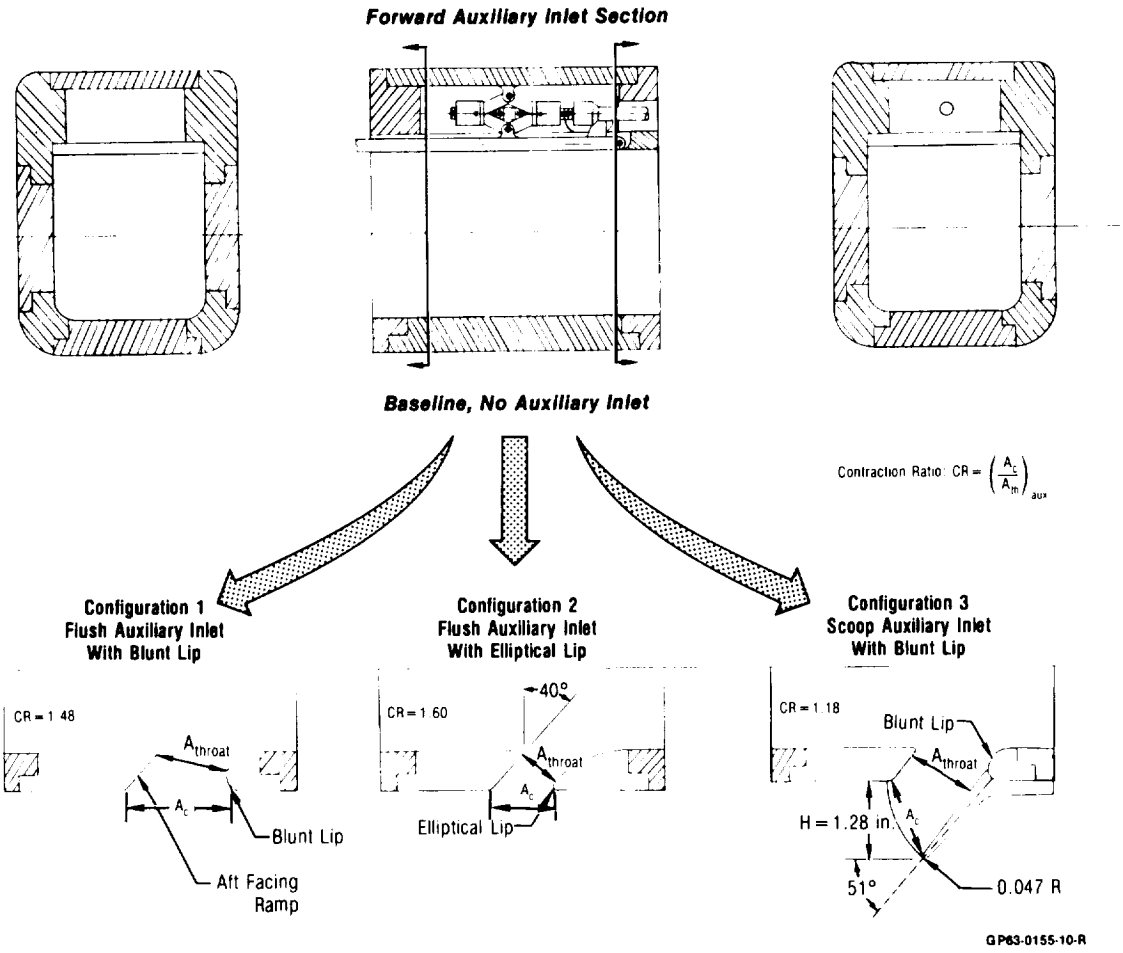

Figure 3-9. 2-D Inlet Model Auxiliary Inlet Configurations

All auxiliary inlets used the same forward lip contour, a simple aft facing ramp. This planar ramp was inclined 40° relative to the vertical.

The aft lip however, was different for each concept. A thick, circular, contoured section was used as the aft lip on auxiliary inlet configuration 1, Figure 3-9. The throat area was 35% of the main inlet throat area.

The second flush auxiliary inlet configuration incorporated a more elliptical shaped aft lip, to increase the distance utilized to turn the auxiliary flow parallel to the internal flow. This elliptical lip extended further forward than Configuration 1, reducing the auxiliary inlet throat area to 17.5% of the main inlet throat area.

The final auxiliary inlet concept added an external scoop, with sidewalls, to the circular aft lip on Configuration 1. The scoop angle was 51°, Figure 3-9. Hence, the throat area of Configuration 3 is equal to that of Configuration 1. A photograph of the 2-D inlet with the external scoop auxiliary inlet deployed is shown in Figure 3-10. The auxiliary inlets were not instrumented.

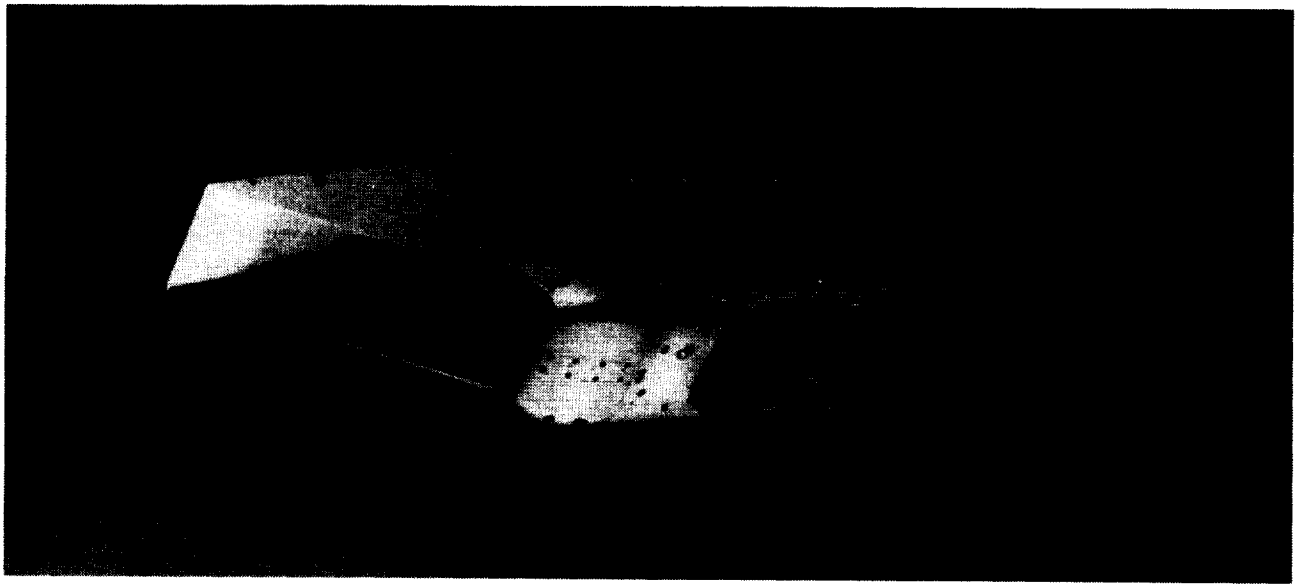

GP63-0155-23-R

Figure 3-10. 2-D Inlet With External Scoop Auxiliary Inlet

3.1.3 Diffuser Section - The duct transitions from a rectangular to a circular cross section in the diffuser section. This section also has a 20% increase in flow area and a slight vertical offset, as shown in Figure 3-11. The 20% increase provides the flow deceleration required between the throat and engine face rake. The diffuser offset is 0.07 engine face diameters in the vertical plane.

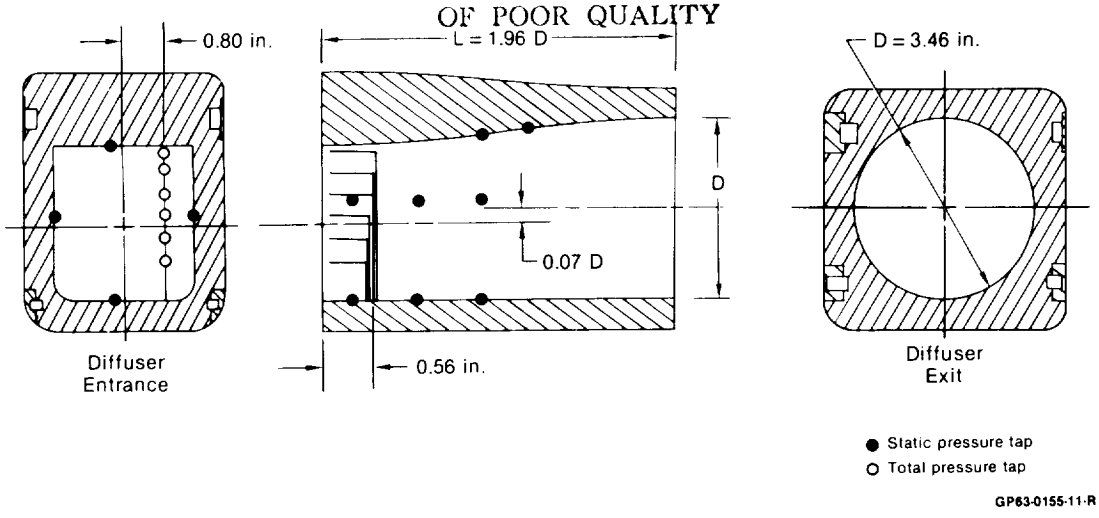

Figure 3-11. Diffuser Section Geometry and Instrumentation

Diffuser instrumentation consists of wall surface taps and a removable six probe total pressure rake. A total of 12 static pressure taps were located in three rows along the top, bottom, and side centerlines, as shown in Figure 3-11. The rake was located 0.56 inches aft of the diffuser entrance, offset 0.80 inches from the diffuser centerline, as pictured in Figure 3-11. The rake was installed only during tests with the long diffuser.

3.1.4 Aft Auxiliary Inlet Section - The aft auxiliary inlet section served as a constant area circular duct extension during the tests. Flush coverplates were used in the auxiliary inlet openings, similar to the baseline configuration of the forward auxiliary inlet. The length of this section is 1.4 engine face diameters. It contained no pressure instrumentation.

3.2 AXISYMMETRIC INLET MODEL - The axisymmetric inlet, Figure 3-12, is a 10% scale model of a Mach 2.0 single cone inlet. It has a capture area of 8.73 in^2 and a cone half angle of 25°. The design of the cowl lip contour was sharp for good supersonic performance. It had no boundary layer bleed systems for the subsonic/transonic testing in this program. The subsonic diffuser was not offset and the length from the inlet throat to the engine face rake is 5.4 engine face diameters.

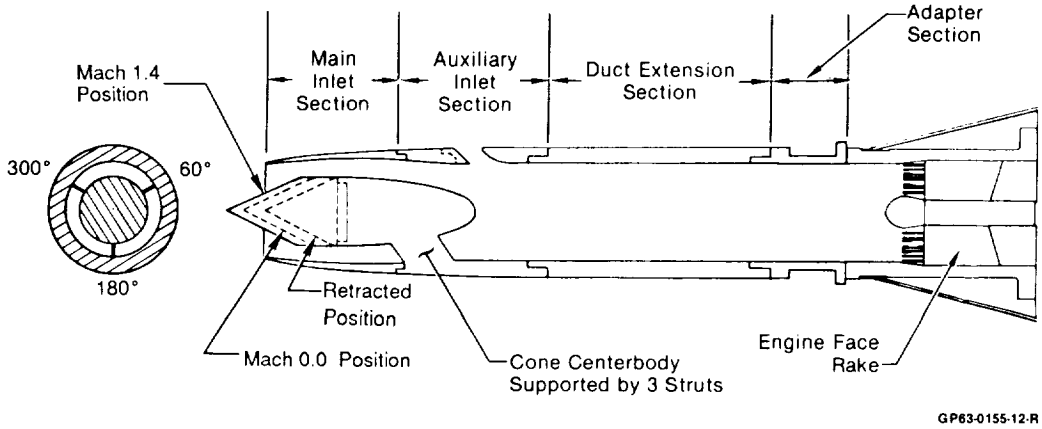

Figure 3-12. Axisymmetric Inlet Model Details

The axisymmetric inlet model is assembled from three sections: (1) the main inlet, (2) the auxiliary inlet, and (3) duct extension section. A short adapter section, L/D = 0.75, is used to connect the duct extension section and the engine face rake. Figure 3-13 shows the assembled model in the 8x6 foot wind tunnel.

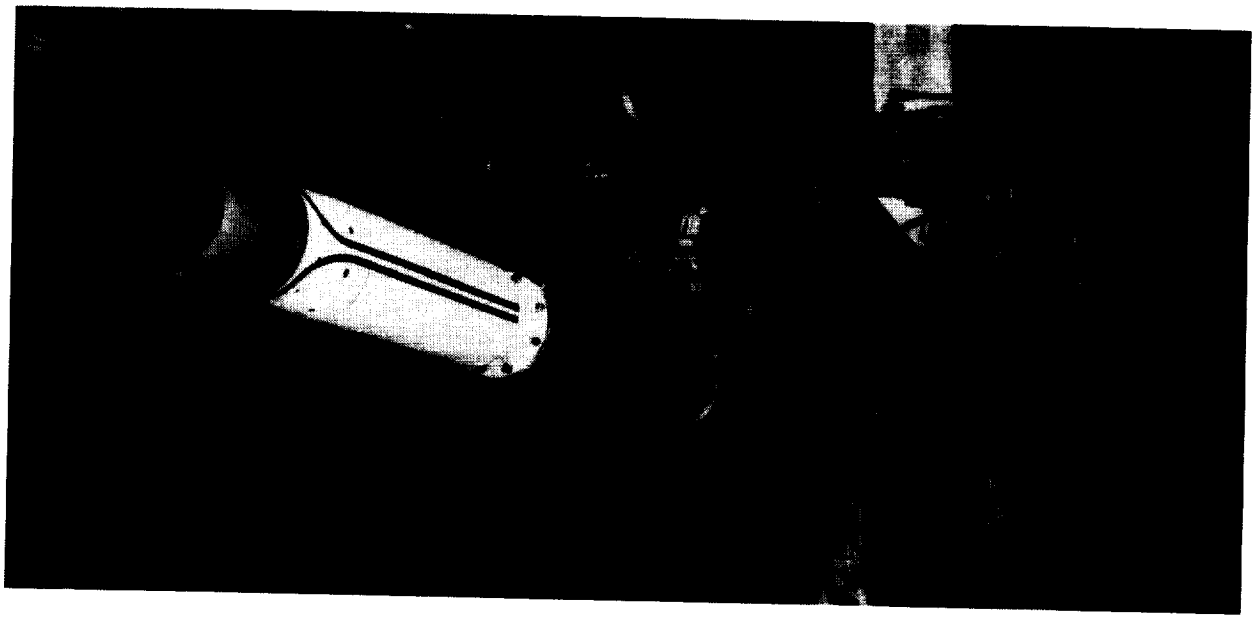

GP63-0155-25-R

Figure 3-13. Axisymmetric Inlet Model Installation in the NASA-Lewis 8 x 6 Ft Wind Tunnel

3.2.1 Main Inlet Section - The main inlet section of the axisymmetric inlet contains the forward portion of the cone centerbody assembly and the cowl lip portion of the inlet. The axial location of the cone is variable, to provide contraction ratio adjustments subsonically and to avoid oblique shock wave ingestion supersonically. The translating cone was simulated by adding or removing spacers to the centerbody.

The most forward cone position was tested at Mach 1.4, see Figure 3-12. This position was required in order to position the oblique shock ahead of the cowl lip. An intermediate cone location, aft of the Mach 1.4 position, provided increased flow contraction for inlet operation from static to low transonic speeds. The increased contraction reduces the Mach number in the vicinity of the cowl lip highlight.

The baseline cowl lip has a thin contour. Coordinates are given in Figure 3-14. The cowl contains nine static pressure orifices, six of which are internal. The centerbody has seven static pressure taps distributed along the conical compression surface and the afterbody. The instrumentation for the main inlet section is shown in Figure 3-14.

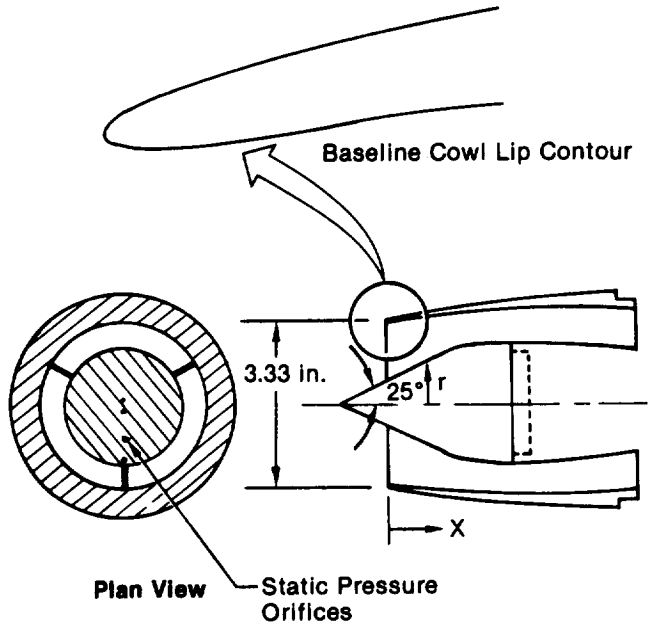

Baseline Cowl Lip Coordinates

X	External Cowl r	Internal Cowl r
0.006	1.667	1.667
0.01	1.677	1.664
0.014	1.682	1.661
0.018	1.686	1.659
0.024	1.690	1.657
0.032	1.693	1.655
0.04	1.697	1.655
0.05	1.702	1.654
0.07	1.710	1.655
0.08	1.714	1.656
0.10	1.721	1.657
0.14	1.733	1.661
0.18	1.745	1.667
0.22	1.756	1.673

GP63-0155-13-R

Figure 3-14. Main Inlet Section Design

Two maneuvering improvement concepts were incorporated into the main inlet section of the axisymmetric inlet. The first concept was a retracted centerbody, which increased the contraction ratio, or the ratio of the inlet highlight flow area to the throat area. By retracting the centerbody, the highlight area is increased while the throat area remains essentially unchanged.

A retracted cone, Figure 3-12, was fabricated to simulate a further aft translation of the centerbody. In the retracted position, the apex of the centerbody cone is in the cowl lip highlight plane. Theoretically, the increased flow area reduces the local Mach number at the lip, thereby reducing the potential for flow separation.

The second maneuvering improvement concept in the main inlet section is a rotating cowl lip. The axisymmetric inlet was tested with two lip rotation angles, 20° and 40°. These rotated cowl lips were simulated by rotating a 90° sector of the lower lip, Figure 3-15. Vertical sideplates were used to prevent spillage of the captured flow.

The 40° rotated lip was tested with two cowl lip contours: one that matched the contour of the baseline and one that was more blunt, to ensure attached flow near the lip highlight. The 20° rotated lip was tested with only the blunt lip contour. The lips were not instrumented.

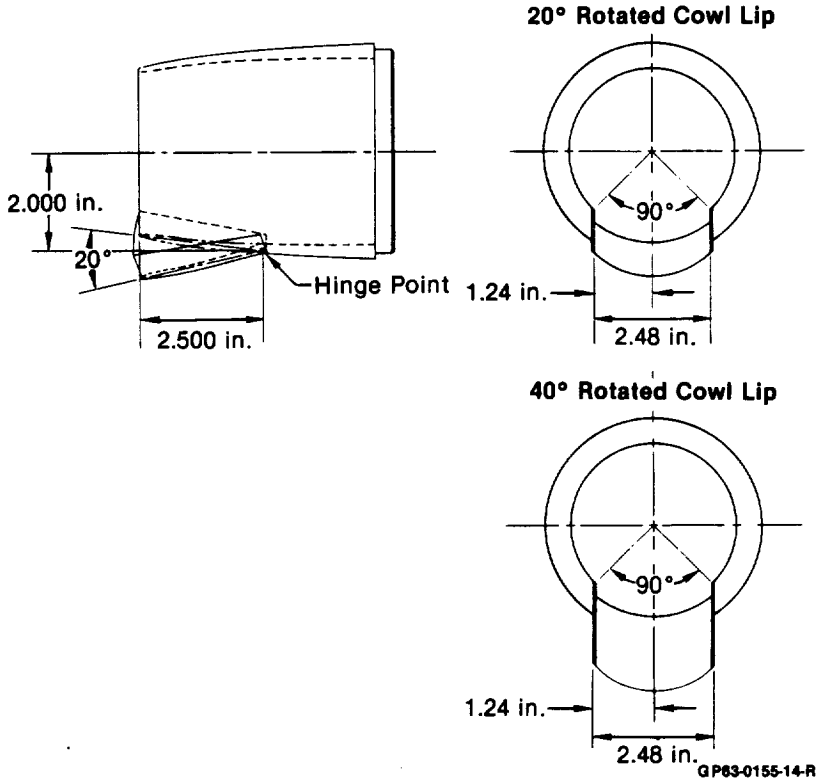

Figure 3-15. Axisymmetric Inlet Rotated Cowl Lip Geometry

The rotating cowl lip design on the axisymmetric inlet requires that the rotating lip sideplates retract into the inlet throat. A retracted sideplate configuration was tested to determine the effect of the sideplates on inlet performance. This configuration simulated the 40° rotated lip sideplates in their stowed position, Figure 3-16. The sideplate thickness was .063, with a leading edge radius equal to the plate thickness. The baseline cowl lip contour was utilized on this configuration.

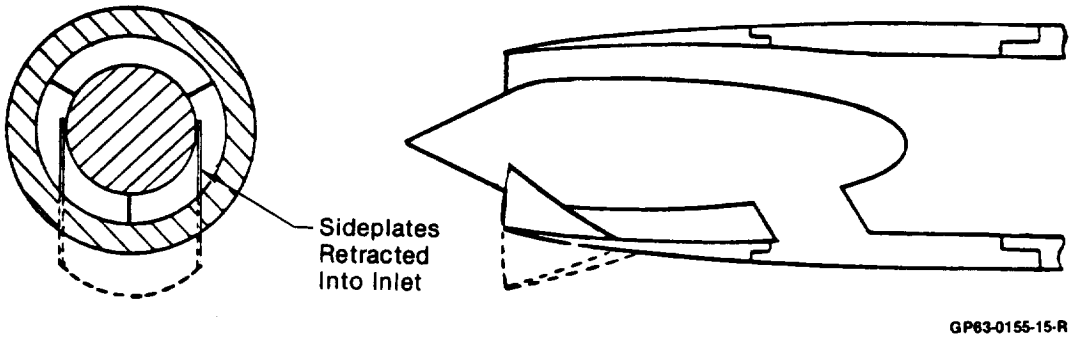

Figure 3-16. Axisymmetric Inlet With Retracted Sideplates

3.2.2 Auxiliary Inlet Section - This section of the axisymmetric inlet model accommodates hardware to simulate auxiliary inlets. It also contains the aft portion of the cone centerbody and support. The cone centerbody assembly is supported by three struts, at 60°, 180°, and 300° orientations, as shown in Figure 3-12. The internal walls are contoured to provide a slight contraction to compensate for the increased flow area which results from termination of the inlet centerbody.

Auxiliary inlets were tested at four circumferential locations just downstream of the centerbody termination. The model was oriented so that the auxiliary inlet centerlines were 45° from the duct vertical centerline, Figure 3-17. The auxiliary inlets were located 3.8 duct diameters ahead of the engine face rake. They were opened in pairs, either the two upper or two lower auxiliary inlets being opened simultaneously.

Each individual auxiliary inlet provided a maximum of 35% of the main inlet throat area when fully opened (with the centerbody in the M = 0.0 position). Hence, a pair of auxiliary inlets could provide up to a 70% increase in throat area. This area could be reduced by 50% with interchangeable forward ramp hardware. The contour of the forward ramp was linear with an approach angle of 45° relative to the inlet longitudinal axis.

Only one set of auxiliary inlet surfaces was instrumented. A total of eleven static pressure orifices were utilized to determine the pressure distribution along the entrance surfaces. Five orifices were located on the forward ramp and six on the aft surface. The instrumentation is shown in Figure 3-17.

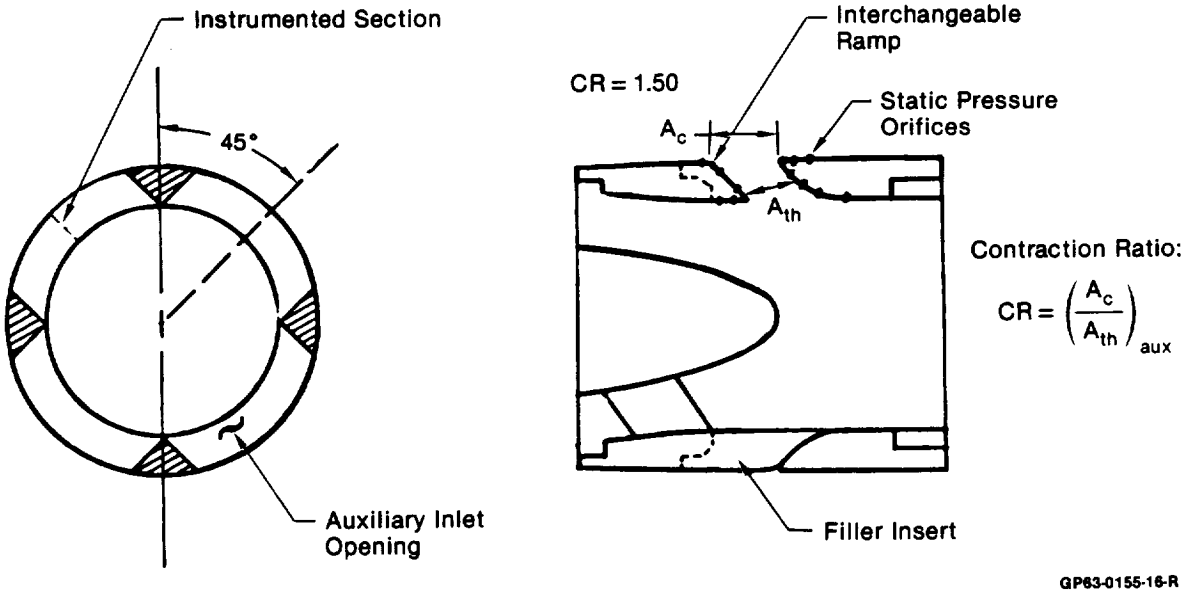

Figure 3-17. Auxiliary Inlet Section Instrumentation

3.2.3 Duct Extension Section - The duct extension section provides a constant flow area for 2.5 engine face diameters. The duct extension has a circular cross section, equal to the engine face diameter (3.46 inches). It connects to a short adapter section which allows the axisymmetric inlet to be tested with the same engine face rake as the 2-D inlet model. The duct extension, Figure 3-18, has four static pressure orifices each on its upper and lower surfaces.

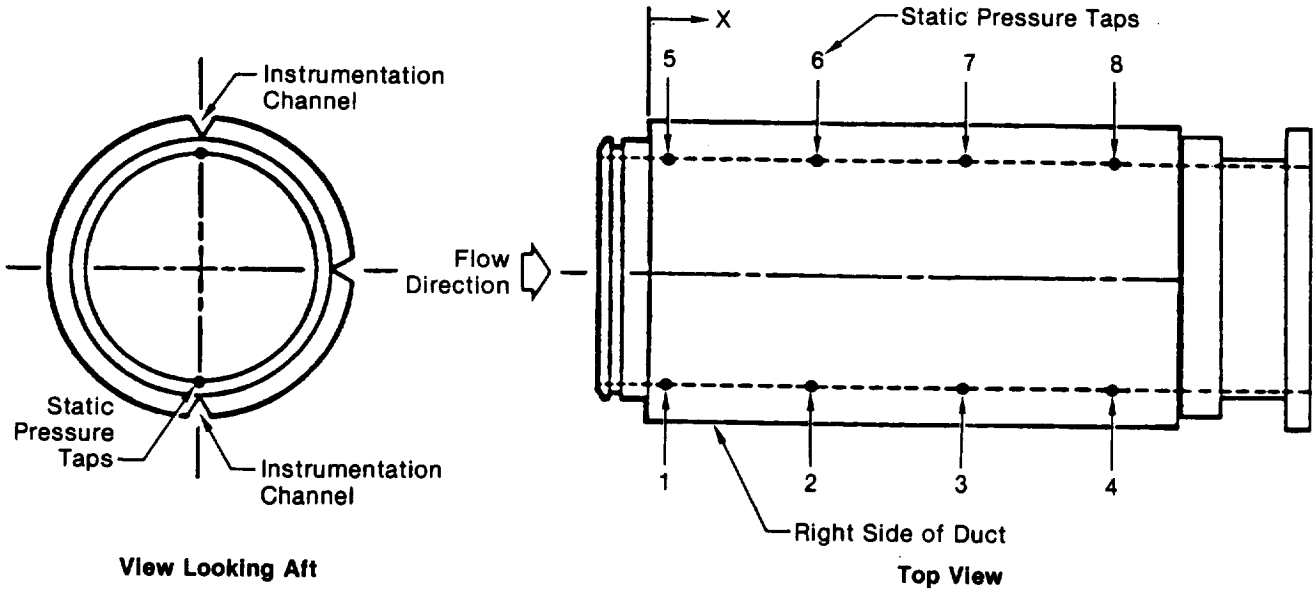

Pressure Locations

Duct Extension Tap Number	1	2	3	4	5	6	7	8	Duct Extension Length (in.)
Location, X (in.) Long Duct	0.25	2.50	4.75	7.00	0.25	2.50	4.75	7.00	8.00

GP83-0155-17-R

Figure 3-18. Duct Extension Details and Instrumentation

3.3 COMMON MODEL HARDWARE - The 2-D and axisymmetric inlet models utilized the same mass flow plug and engine face rake hardware for measuring inlet mass flow and the flow properties at the engine face.

The engine face rake used in this test consisted of 48 total pressure probes and 24 high response Kulite probes on eight radial legs about a center hub. The radial legs were spaced at 45° increments equally around the duct, as shown in Figure 3-19. Each leg had six steady state and three high response total pressure probes, as indicated in Figure 3-20. The pressure probes on each leg were located at the centroid of equal areas to allow direct averaging of the pressure data.

The center hub had eight static pressure orifices in line with each of the rake legs. The orifices were located at the same axial station as the total pressure probes on the engine face rake.

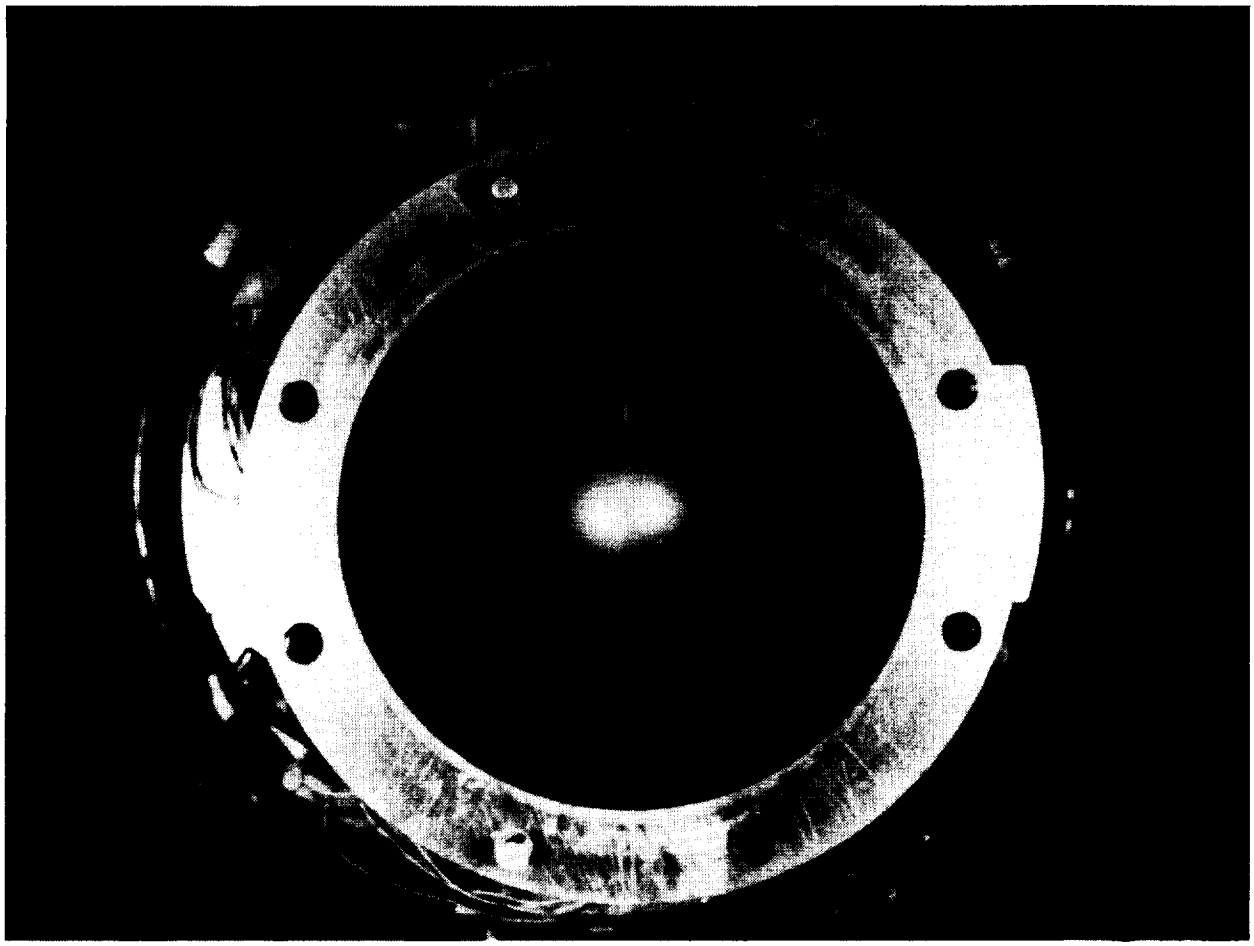

GP83-0155-24-R

Figure 3-19. Engine Face Rake Instrumentation Details

Dynamic pressure data was filtered through four pole bessel low pass filters with a cutoff frequency of 1700 hertz before being processed by RMS modules. This corresponds to a 170 hertz cutoff frequency for the full scale inlet.

The filtered analog signal from each of the high response probes was the input to the RMS modules. This data was used to compute the root mean square (RMS) fluctuation of the pressure data about the steady state pressure level. The RMS modules use a sliding window to continuously update the computed RMS level. A time constant of 0.5 seconds was specified to define the size of the window such that the output from the RMS modules varied much more slowly than the data acquisition rate.

The engine face rake housing and hub were relieved in the region of the rake legs to increase the flow area and thus compensate for the blockage associated with the legs, Figure 3-20. This increased flow area prevented the inlet mass flow from being limited due to the instrumentation hardware at the engine face for freestream Mach numbers above 0.6.

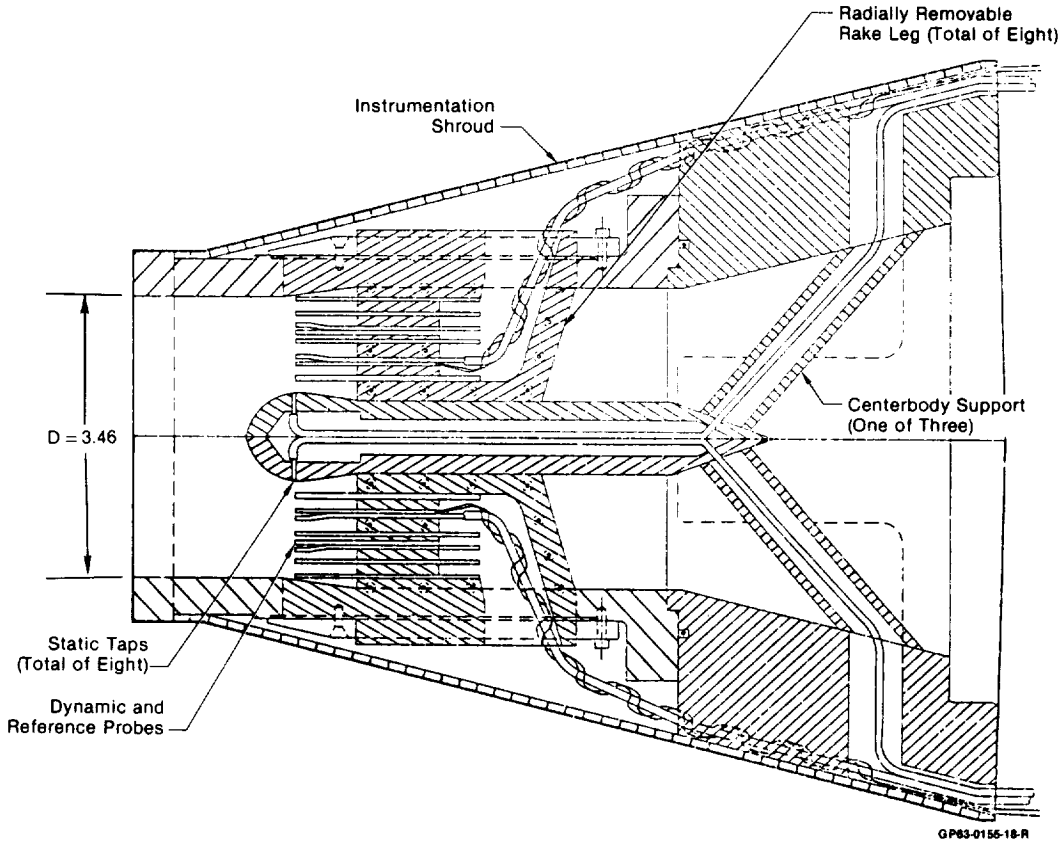

Figure 3-20. Sheer View of Engine Face Rake Showing Instrumentation Routing

An adapter section provided the transition from the rake hardware to the mass flow plug hardware and supported the model, as mentioned in Section 2.2. It had a constant circular cross section and a length of 3 duct diameters. The purpose of this section was to provide length behind the engine face rake so flow distortions could attenuate. The accuracy of the computed mass flow is improved by minimizing the flow distortion at the mass flow plug rake.

The inlet mass flow controller used in this test was the NASA Lewis HiMat mass flow plug. A sheer view of this hardware is shown in Figure 3-21. This plug utilized a 40 probe total pressure rake with center hub ahead of the flow measurement station. Inlet airflow was controlled by a translating conical plug, which was remotely driven by a hydraulic actuator. A calibrated linear potentiometer was used to determine plug position. The mass flow plug was calibrated in the 8x6 tunnel during April and May 1982.

Calibration curves for the mass flow plug are presented in Appendix A. Results of the plug calibration show the accuracy of the plug position to be $\pm$0.05 inches and the repeatability to be $\pm$0.005 inches. Accuracy of the computed corrected airflow is $\pm$0.1 lbm/sec.

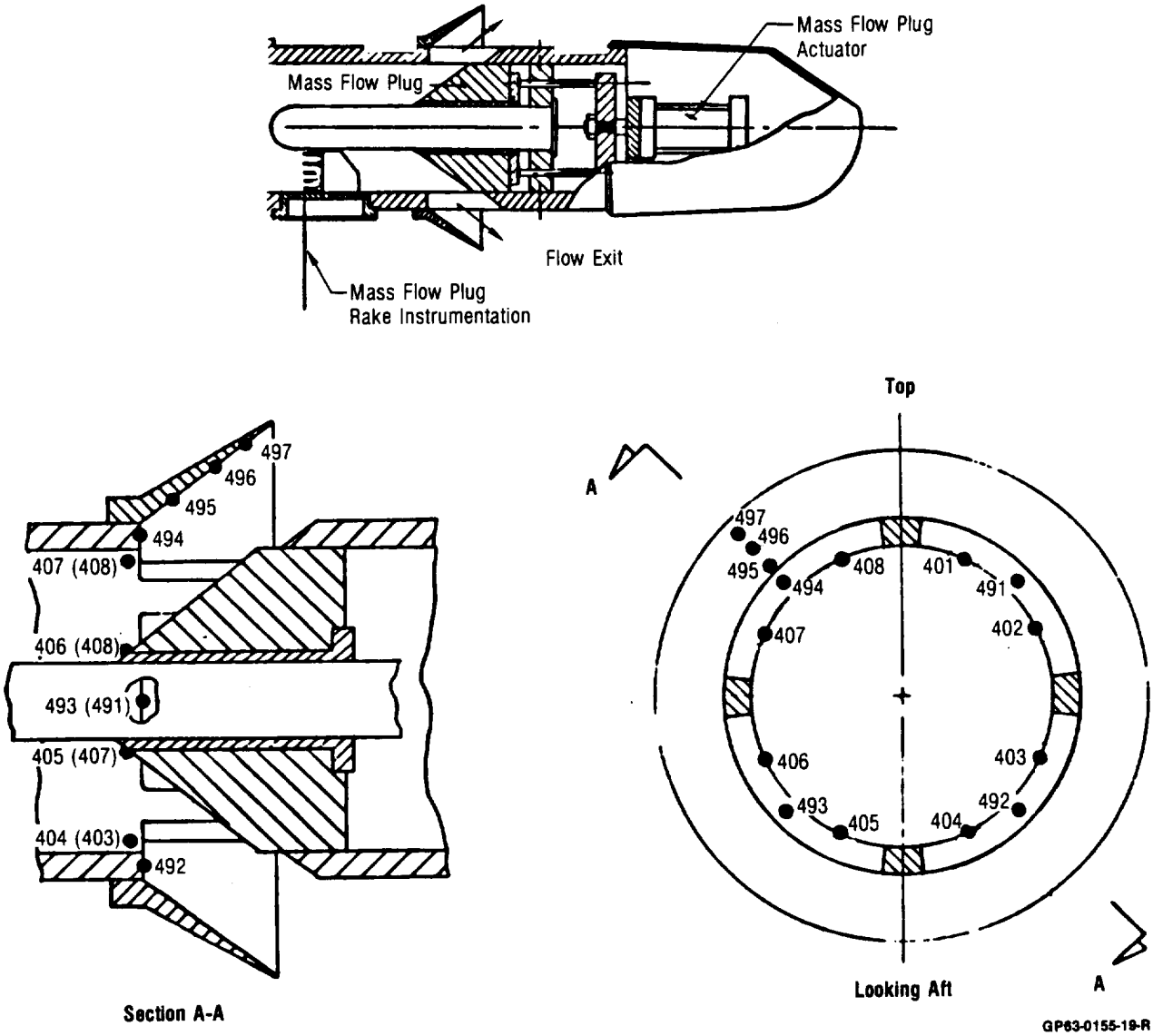

Figure 3-21. Mass Flow Plug Design and Instrumentation

The total pressure rake on the mass flow plug consisted of eight radial legs, spaced at equal angular positions. Each leg had five steady state total pressure probes spaced on equal area centers. Eight static pressure taps were located circumferentially around the rake housing at the measurement plane.

Six static pressure orifices, located near the exit were used to correlate the mass flow through the plug to the static-to-total-pressure ratio at the plug exit. A short external skirt was placed ahead of the flow exit, to reduce the base pressure in this region, Figure 3-21. The local reduction in exit pressure increased the mass flow range of the plug.

4. TEST PROCEDURE AND DATA REDUCTION

The baseline axisymmetric and 2-D inlets were tested initially to establish the reference performance level. The axisymmetric inlet was tested first.

The effects of the rotating cowl lip and auxiliary inlets on the axisymmetric inlet were tested from Mach 0.6 to 1.4. Data at Mach 1.4 was taken separately from the 0.6 to 1.2 data, because of the different centerbody position. Results showed the flow improvement concepts to be ineffective at Mach 1.2 and 1.4. Therefore, the subsequent 2-D inlet tests were concentrated in the Mach 0.6 to 0.9 speed regime, with only limited data taken at Mach 1.2.

4.1 OPERATIONAL SEQUENCE - During tunnel startup, the inlet was set to zero degrees pitch and yaw, to minimize starting loads on the model. The mass flow plug was set to a failsafe position which would definitely operate the inlet in the choked throat condition. Once the tunnel was brought up to the desired Mach number, the model was set to the desired test orientation. The mass flow plug was then moved from the failsafe position to the initial mass flow position, which provided the maximum inlet mass flow ratio.

Supercritical operation was achieved at all Mach numbers except 0.6. At Mach 0.6, freestream static pressure was high enough such that the 2-D inlet could not be run supercritically. Flow was allowed to stabilize for 10 to 15 seconds before data acquisition. The mass flow plug was then stepped into the next position, flow allowed to stabilize, and another data point taken. Five to seven mass flow points were recorded in order of decreasing mass flow. The lowest mass flow ratio was determined from typical engine flight idle airflow at subsonic conditions.

At supersonic Mach numbers, the output from three dynamic probes on the engine face rake was monitored to detect the onset of buzz. The lowest mass flow ratio was determined by engine idle airflow, unless buzz occurred beforehand. Upon completion of a mass flow sweep, the mass flow plug was returned to the failsafe position, the model orientation set to the next test condition, and the mass flow sweep repeated.

The mass flow plug schedule generally did not change with angle of attack at a fixed Mach number. The initial plug setting did vary with Mach number, however, to achieve supercritical inlet operation where possible.

4.2 RUN SCHEDULE - The 2-D and axisymmetric inlets were tested throughout a typical subsonic/transonic maneuvering envelope for advanced fighters. The angle of attack and sideslip angle ranges over which the model were tested are shown in Figure 4-1.

Figure 4-2 presents the run schedule for the axisymmetric inlet. The run schedule for the 2-D inlet is presented in Figure 4-3.

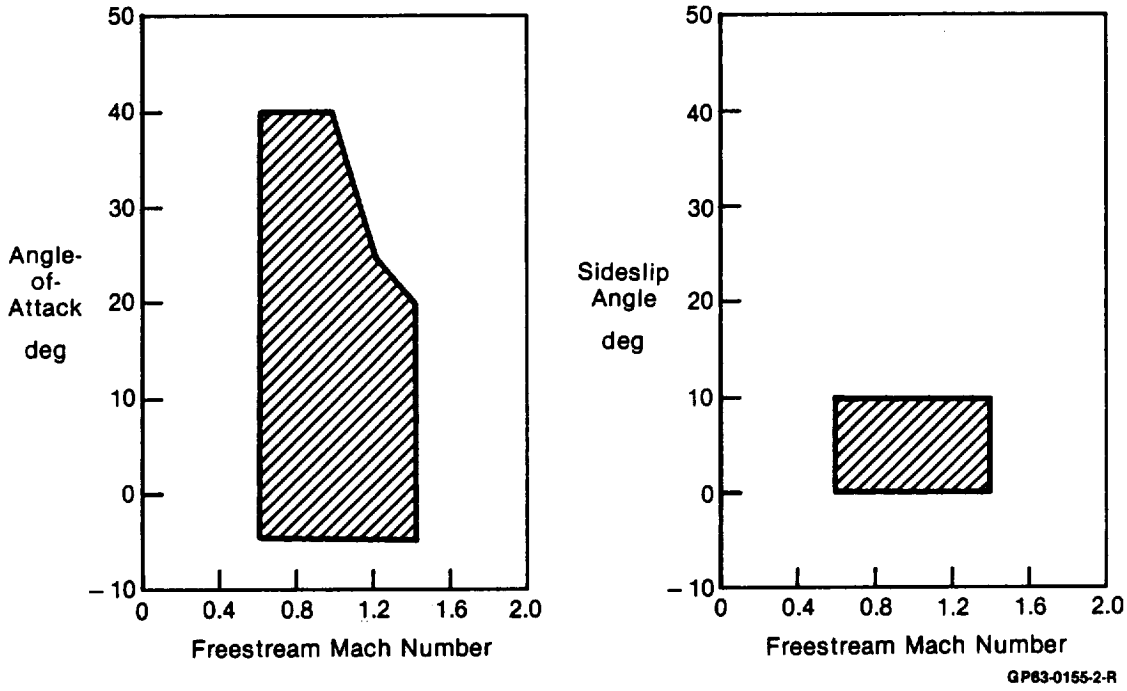

Figure 4-1. Angle-of-Attack and Sideslip Ranges for the 8 × 6 ft Wind Tunnel Test

Configuration Number	Description	Mach	Angle-of-Attack (deg)*	Cowl Lip	Centerbody (Mach)	Auxiliary Inlet
1.	0° Rotated Lip With Retracted Sideplates	1.4 0.9 0.6	0, 5, 10, 15, 20 0, 20, 40 0, 20, 40 (No Sideslip Data)	0° Rotated Lip With Retracted Sideplates	1.4 0	Closed
2.	Baseline Configuration	1.4 1.2 0.9 0.6	0, 5, 10, 15, 20 0, 10, 20, 25 0, 10, 20, 30, 40 0, 10, 20, 30, 40	Baseline (0° Rotated Lip)	1.4 0	Closed
3.	20° Rotated Lip	1.4 1.2 0.9 0.6	0, 5, 10, 15, 20 0, 10, 20, 25 −5, 0, 10, 20, 30, 40 0, 10, 20, 30, 40	20° Rotated Lip	1.4 0	Closed
4.	40° Rotated Lip (Blunt)	1.4 1.2 0.9 0.6	0, 5, 10, 15, 20 0, 10, 20, 25 −5, 0, 10, 20, 30, 40 0, 10, 20, 30, 40	40° Rotated Lip (Blunt)	1.4 0	Closed
5.	40° Rotated Lip (Sharp)	0.9 0.6	0, 20, 40 0, 20, 40 (No Sideslip Data)	40° Rotated Lip (Sharp)	1.4 0	Closed
6.	Lower Auxiliary Inlets Fully Open	1.4 1.2 0.9 0.6	0, 5, 10, 15, 20 0, 10, 20, 25 0, 10, 20, 30, 40 0, 10, 20, 30, 40	Baseline	1.4 0	Both Lower Auxiliary Inlets Fully Open (Flush)
7.	Lower Auxiliary Inlets Half Open	0.9 0.6	0, 20, 40 0, 20, 40	Baseline	1.4 0	Both Lower Auxiliary Inlets Half Open (Flush)
8.	Upper and Lower Auxiliary Inlets Half Open	0.9 0.6	0, 20, 40 0, 20, 40	Baseline	1.4 0	All 4 Auxiliary Inlets Half Open (Flush)
9.	Upper and Lower Auxiliary Inlets Fully Open	1.4 1.2 0.9 0.6	0, 5, 10, 15, 20 0, 10, 20 0, 10, 20, 30, 40 0, 10, 20, 30, 40	Baseline	1.4 0	All 4 Auxiliary Inlets Fully Open (Flush)
10.	Upper Auxiliary Inlets Fully Open	1.4 1.2 0.9 0.6	0, 5, 10, 15, 20 0, 10, 20, 25 0, 10, 20, 30, 40 0, 10, 20, 30, 40	Baseline	1.4 0	Both Upper Auxiliary Inlets Fully Open (Flush)
11.	Upper Auxiliary Inlets Half Open	0.9 0.6	0, 20, 40 0, 20, 40 (No Sideslip Data)	Baseline	1.4 0	Both Upper Auxiliary Inlets Half Open (Flush)
12.	Retracted Centerbody	0.9 0.6	0, 20, 30, 40 0, 20, 40	Baseline	Retracted Centerbody	Closed
13.	Best Rotated Lip and Auxiliary Inlet Configuration	1.2 0.9 0.6	0, 10, 20, 25 −5, 0, 10, 20, 30, 40 0, 10, 20, 30, 40	20° Rotated Lip	1.4 0	Both Lower Auxiliary Inlets Fully Open
14.	Best Rotated Lip and Auxiliary Inlet Configuration With Retracted Centerbody	0.9 0.6	−5, 0, 10, 20, 30, 40 0, 10, 20, 30, 40 (No Sideslip Data)	20° Rotated Lip	Retracted Centerbody	Both Lower Auxiliary Inlets Fully Open

*Sideslip angles of 5°, and 10° tested at $\alpha = 0°$ and 20° at Mach 0.9 unless noted.

GP63-0155-94-R

Figure 4-2. Axisymmetric Inlet Run Schedule

Configuration Number	Description	Mach	Angle-of-Attack (deg)*	Cowl Lip	Auxiliary Inlet
15.	Short Diffuser With 0° Rotated Lip	1.2 0.9 0.6	0, 10, 20, 25 −5, 0, 10, 20, 30, 40 0, 10, 20, 30, 40	Baseline (0° Rotated Lip) ↓	Closed
16.	Short Diffuser With 20° Rotated Lip	1.2 0.9 0.6	0, 10, 20, 25 −5, 0, 10, 20, 30, 40 0, 10, 20, 30, 40	20° Rotated Lip ↓	Closed
17.	Short Diffuser With 40° Rotated Lip	1.2 0.9 0.6	0, 10, 20, 25 −5, 0, 10, 20, 30, 40 0, 10, 20, 30, 40	40° Rotated Lip ↓	Closed
18.	Long Diffuser With 0° Rotated Lip (No Bleed)	1.4 1.2 0.9 0.6	−5, 0, 5, 10, 15, 20 0, 10, 20, 25 −5, 0, 10, 20, 30, 40 0, 10, 20, 30, 40 (No Sideslip Data)	Baseline (0° Rotated Lip) ↓	Closed
19.	Long Diffuser With 20° Rotated Lip*	1.2 0.9 0.6	20, 25 0, 10, 20, 30, 40 0, 10, 20, 30, 40	20° Rotated Lip ↓	Closed
20.	Long Diffuser With 40° Rotated Lip*	0.9 0.6	0, 20, 40 0, 20, 40	40° Rotated Lip ↓	Closed
21.	Long Diffuser With 0° Rotated Lip*	0.9	0, 10, 20, 30	Baseline (0° Rotated Lip)	Closed
22.	Lower Auxiliary Inlet With External Scoop*	1.2 0.9 0.6	20, 25 0, 10, 20, 30, 40 0, 10, 20, 30, 40	Baseline (0° Rotated Lip) ↓	Lower Auxiliary Inlet Fully Open With External Scoop
23.	Lower Auxiliary Inlet (Flush)*	0.9 0.6	0, 20, 40 0, 20, 40	Baseline ↓	Lower Auxiliary Inlet Fully Open. Circular Aft Ramp.
24.	Lower Auxiliary Inlet (Flush With Elliptical Aft Ramp)*	0.9 0.6	0, 20, 40 0, 20, 40	Baseline ↓	Lower Auxiliary Inlet Fully Open With Elliptical Aft Ramp

*Six probe total pressure rake installed in diffuser.

**Sideslip angles of 5° and 10° tested at $\alpha = 0°$ and 20° at Mach 0.9 unless noted.

Configurations 19 – 24 have second ramp, throat slot and sideplate bleed.

GP63-0155-95-R

Figure 4-3. 2-D Inlet Run Schedule

4.3 DATA REDUCTION - The major performance parameters computed were total pressure recovery, average turbulence, steady state distortion, inlet mass flow ratio, and inlet stable range. These parameters are defined below.

Inlet Total Pressure Recovery (P_{T_2}/P_{T_0}) - The ratio of the average of the 48 steady state total pressure values measured at the engine face rake, divided by the freestream total pressure:

$$P_{T_2}/P_{T_0} = \frac{1}{48} \sum_{i=1}^{48} (P_{T_2}/P_{T_0})_i$$

Average Engine Face Turbulence $\left(\frac{P_{T_{RMS}}}{P_{T_2}}\right)$ - The ratio of the average of the 24 dynamic pressure probes root mean square (RMS) pressure deviations from the steady state total pressure level, divided by the average engine face total pressure.

$$\frac{P_{T_{RMS}}}{P_{T_2}} = \frac{1}{24} \sum_{i=1}^{24} \left(\sqrt{(P_{T_{inst}} - P_{T_{2_{SS}}})^2}\right)_i / P_{T_2}$$

Steady State Distortion - The spatial variation in total pressure measured at the engine face. Distortion levels were computed using the Pratt & Whitney F100 engine fan descriptor, K_{a_2}. The technique used to compute K_{a_2} is presented in Figure 4-4.

A screening limit was defined by the engine manufacturer as a function of the engine corrected airflow. The screening limit curve used in this data analysis is shown in Figure 4-5 as a function of percent design fan airflow.

Distortion data results are presented in terms of the ratio of the steady state distortion level to the screening limit value. Ratios greater than 1.0 indicate distortion levels high enough to cause an engine surge or stall. Values between 0.9 and 1.0 are considered to be marginal situations and would require a stability audit using more rigorous methods involving time varient data.

Inlet Stable Range (Supersonic) - Inlet stable range is defined as the mass flow range between the critical (maximum) inlet mass flow ratio and the mass flow ratio at which flow becomes unstable (buzz onset), divided by the critical mass flow ratio.

Inlet Mass Flow Ratio - Inlet mass flow ratio is defined as the ratio of the mass flow entering the inlet duct at the cowl lip station to the mass flow in a freestream streamtube whose area equals the inlet capture area. The mass flow entering the inlet duct is equal to the sum of the measured mass flow at the mass flow plug plus the mass flow through any bleed system aft of the cowl highlight. Sideplate and ramp bleed flows on the 2-D inlet are removed ahead of the cowl lip, and therefore are not considered part of the inlet mass flow ratio. By relating the duct mass flows to streamtube areas in the freestream, the mass flow ratio can be defined in terms of area ratios.

Mass flow ratios used in this report are based upon the zero degree angle of attack inlet capture area. This simplifies the comparison between the baseline and rotated cowl lip configurations at angle of attack.

Fan Circumferential Distortion Descriptor

$$K_\Theta = \frac{\sum_{\text{Ring}=1}^{J}\left[\left(\frac{A_N}{N^2}\right)_{max}\right]_{ring} \times \frac{1}{D_{ring}}}{(q/P_{t_2})_{ref}\ \sum_{\text{Ring}=1}^{J}\frac{1}{D_{ring}}}$$

Where:

J = Number of Rings (Probes Per Leg)

D = Ring Diameter

$\left(\frac{q}{P_{t_2}}\right)_{ref}$ = Reference Value of Engine Face Dynamic Pressure Head, Function of Engine Face Mach Number.

$A_N = \sqrt{a_N^2 + b_N^2}$, N = 1, 2, 3, 4

Where:

$$a_N = \frac{\Delta\Theta}{180}\sum_{k=1}^{K}\frac{P_{t_2}/P_{t_0}\,(k\Delta\Theta)}{(P_{t_2}/P_{t_0})}\cos(Nk\,\Delta\Theta)$$

$$b_N = \frac{\Delta\Theta}{100}\sum_{k=1}^{K}\frac{P_{t_2}/P_{t_0}\,(k\Delta\Theta)}{(P_{t_2}/P_{t_0})}\sin(Nk\,\Delta\Theta)$$

and

$P_{t_2}/P_{t_0}\,(k\,\Delta\Theta)$ = Local Recovery at Angle, k $\Delta\Theta$

(P_{t_2}/P_{t_0}) = Face Average Recovery

K = Number of Rake Legs

$\Delta\Theta$ = Angular Distance Between Rake Legs (deg)

$\left(\frac{A_N}{N^2}\right)_{max}$ = Maximum Value for the Four Fourier Coefficients Calculated; Normally Turns Out to Be A_1.

Fan Radial Distortion Descriptor

$$K_{r_a} = \frac{\sum_{\text{Ring}=1}^{J}\left(\frac{\Delta P_{t_2}}{P_{t_2}}\right)_{ring}\frac{1}{D_{ring}}}{(q/P_{t_2})_{ref}\ \sum\frac{1}{D_{ring}}}$$

With:

$$\left(\frac{\Delta P_{t_2}}{P_{t_2}}\right)_{ring} = \frac{(P^*_{t_2}/P_{t_0})}{P_{t_2}/P_{t_0}} - \frac{P^*_{t_{2_{base}}}}{P_{t_2}}\quad\frac{P_{t_2}}{P^*_{t_{2_{base}}}}$$

Where:

$P^*_{t_2}/P_{t_0}$ = Ring Average Recovery

$\frac{P^*_{t_{2_{base}}}}{P_{t_2}}$ = Reference Radial Profile, Function of Engine Corrected Airflow.

b = Radial Distortion Weighting Factor, Function of Engine Corrected Airflow.

P_{t_0} = Freestream Total Pressure

For High Response Data Only

$$P_{t_{2j}}/P_{t_2} = \frac{1}{48}\sum_{j=1}^{48}[((P_{t_2})_j + (DP_{t_{2h}}))/P_{t_2}]$$

Where:

$(P_{t_2})_j$ = jth Value of the Low Response Engine Face Total Pressure (kPa)

$(DP_{t_{2h}})_j$ = jth Value of the Fluctuating Component of the High Response Engine Face Total Pressure (kPa)

$$K_{a_2} = K_\Theta + bK_{r_a}$$

GP83-0155-20-R

Figure 4-4. Summary of Distortion Descriptor Equations for the P&W F-100 Engine

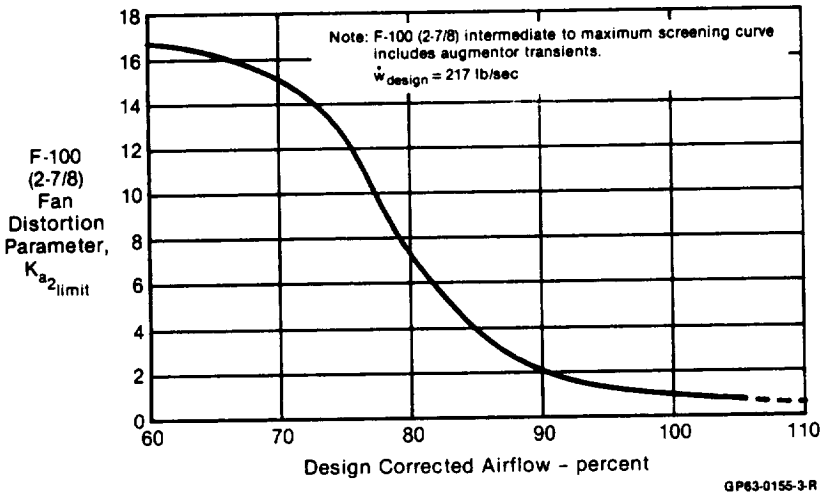

Figure 4-5. Distortion Screening Limit Curve

5. TEST RESULTS AND ANALYSIS

5.1 2-D INLET PERFORMANCE - The 2-D inlet was tested in a short and a long diffuser configuration. The rotating cowl lip was tested extensively with the short diffuser. A limited amount of testing was also conducted using the long diffuser, to verify results. Auxiliary inlets were tested with the long diffuser hardware only.

Each of these inlet designs was tested at Mach 0.6, 0.9, and 1.2. Because of the low Mach numbers, the second ramp angle was fixed at zero degrees relative to the first. This is equivalent to a single ramp configuration.

Test data for the baseline and the 20° and 40° rotating cowl lip configurations with the short diffuser were analyzed with a 2-D time-dependent Navier Stokes flow solver. This code uses a multiple zone approach to compute the flow field in two-dimensional inlets. The results are given in Section 5.1.2, to help explain flow phenomena observed in the tests.

Performance for the baseline configuration with the short diffuser is presented first to provide a comparative standard by which all others can be judged. The baseline with the long diffuser is then evaluated. Typical results for the rotated cowls and auxiliary inlets follow.

The operating point at which all inlet performance parameters are screened is defined to be the constant corrected airflow corresponding to 95% of the critical mass flow for the baseline configuration at zero degrees angle of attack, i.e., the corrected airflow remains constant along the inlet operating line and never changes with angle of attack. The critical mass flow of the inlet, however varies with Mach number, and hence the operating point becomes a function of Mach number.

5.1.1 Baseline 2-D Inlet - The baseline configuration for the rotating cowl lip concept is chosen to be the short diffuser configuration, since the rotating cowls were tested rigorously with the shorter duct. A discussion of its performance is given below. The auxiliary inlet configurations required the use of the auxiliary inlet section, and hence the long diffuser configuration is chosen to be the baseline for those investigations. Its performance is also discussed below.

Short Diffuser - The baseline with the short diffuser displayed good performance characteristics at low angles of attack. Engine face total pressure recovery was 98% at Mach 0.6 and $\alpha = 0.0°$, Figure 5-1. Turbulence was only 0.006 at this condition.

Inlet recovery decreased gradually with angle of attack to a level of 0.89 at $\alpha = 40°$. Similarly, turbulence showed a gradual increase as the inlet angle of attack increased. However, distortion, computed as the ratio of the P&W K_{a_2} factor divided by the limit K_{a_2} value, increased with angle of attack up to a maximum of 41% of the limit value at $\alpha = 20°$. Greater angles of attack result in decreased inlet distortion, Figure 5-2. The distortion screening assessment in Figure 5-2 indicates a large compatibility margin throughout the angle of attack maneuvering range.

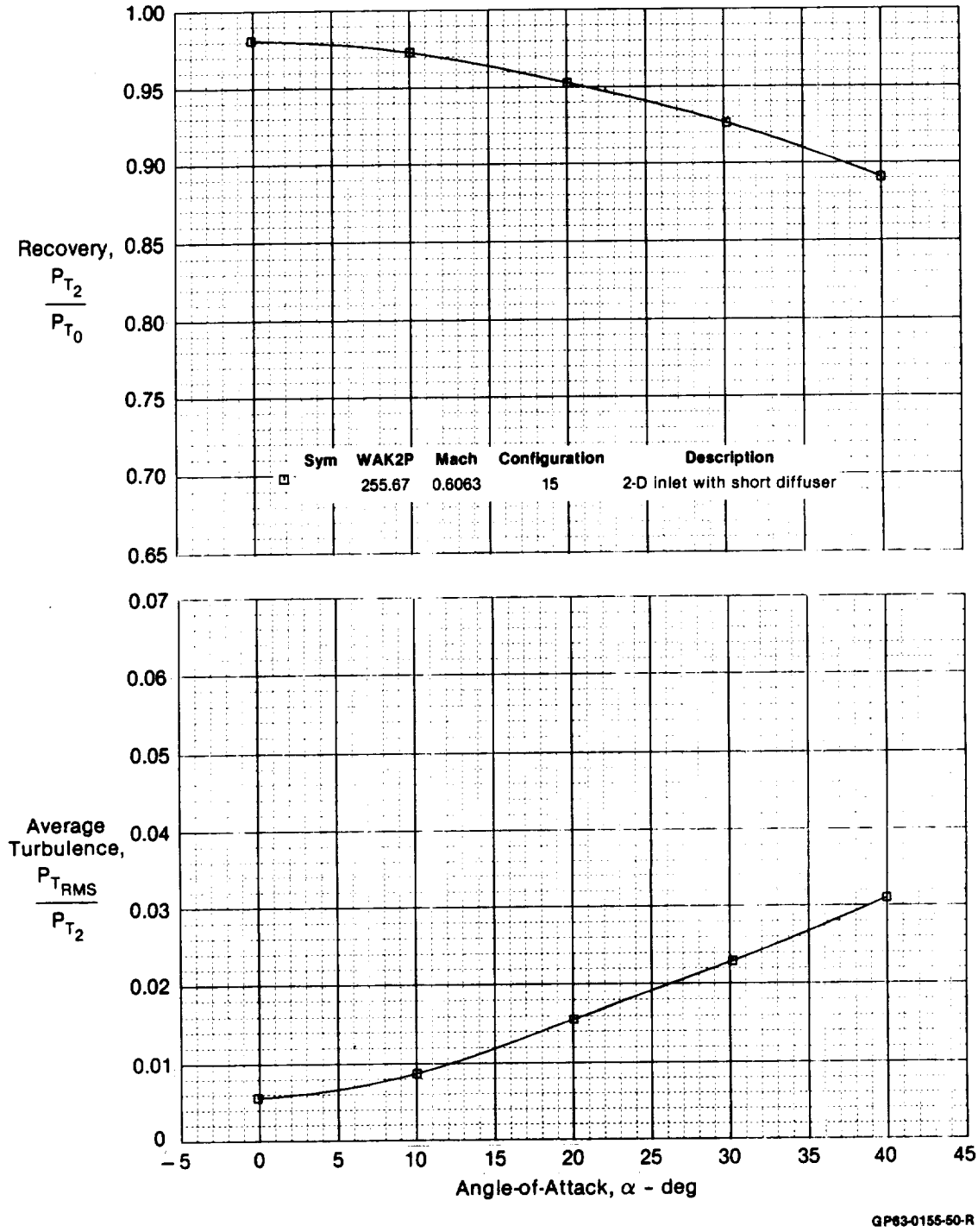

Figure 5-1. Baseline 2-D Inlet Recovery and Average Turbulence vs Angle-of-Attack $M_0 = 0.6$

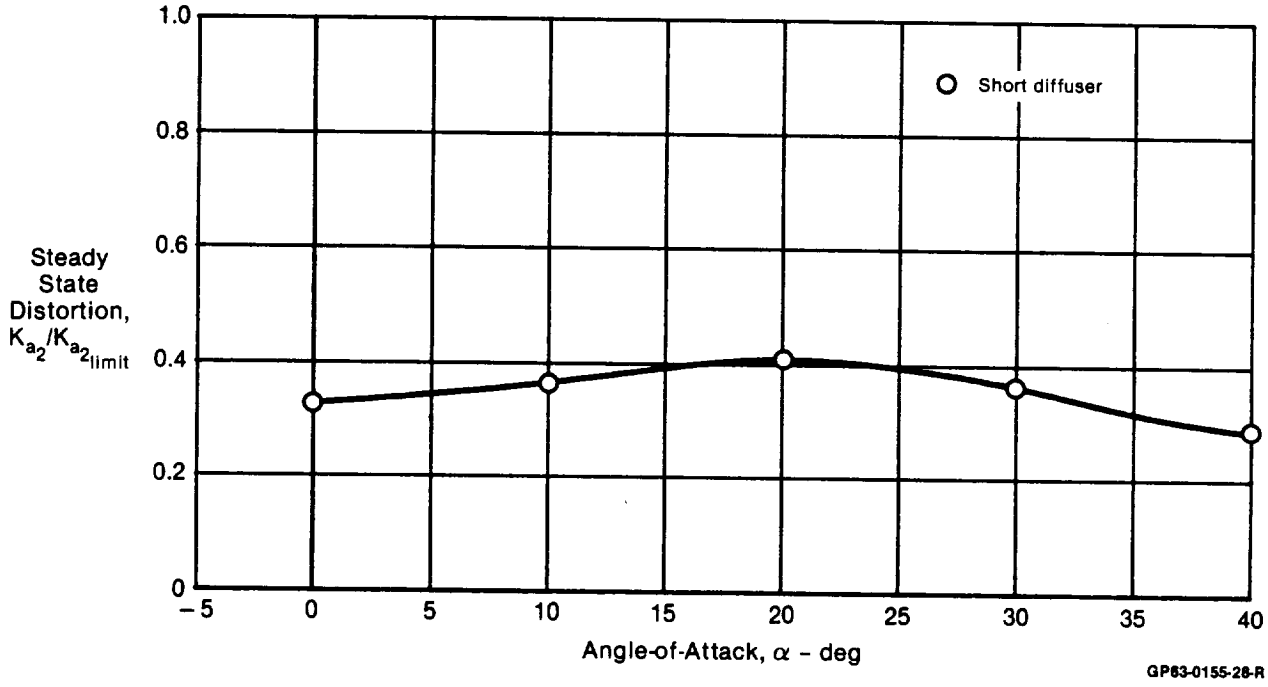

Figure 5-2. Baseline 2-D Inlet Distortion
Mach 0.6

Total pressure contours generated from the engine face rake data provide insight into the pressure loss mechanism within the inlet. These contours are two dimensional topographical maps of the total pressure field, as viewed from upstream of the rake. The engine face contours at Mach 0.6 show that the primary sources of pressure loss are related to the boundary layer. Figure 5-3 shows these contours for angles of attack of 0°, 20°, and 40°. The ramp side is at the top of these contours. At $\alpha = 0°$, most of the engine face displays 98% recovery or better. Boundary layer losses are evident around the outer circumference.

Total pressure loss is greater on the lower (cowl lip) side of the contour plot. This indicates a possible boundary layer separation on the cowl lip. This region grows with increasing angle of attack. At $\alpha = 20°$, it covers the bottom half of the engine face. This region continues to grow, until at 40° it affects the entire duct.

Inlet performance at Mach 0.9 is similar to the Mach 0.6 results. One notable difference, however, is that recovery, turbulence, and distortion remain constant through 20° angle of attack rather than decreasing in this range. These results are evident in Figures 5-4 and 5-5.

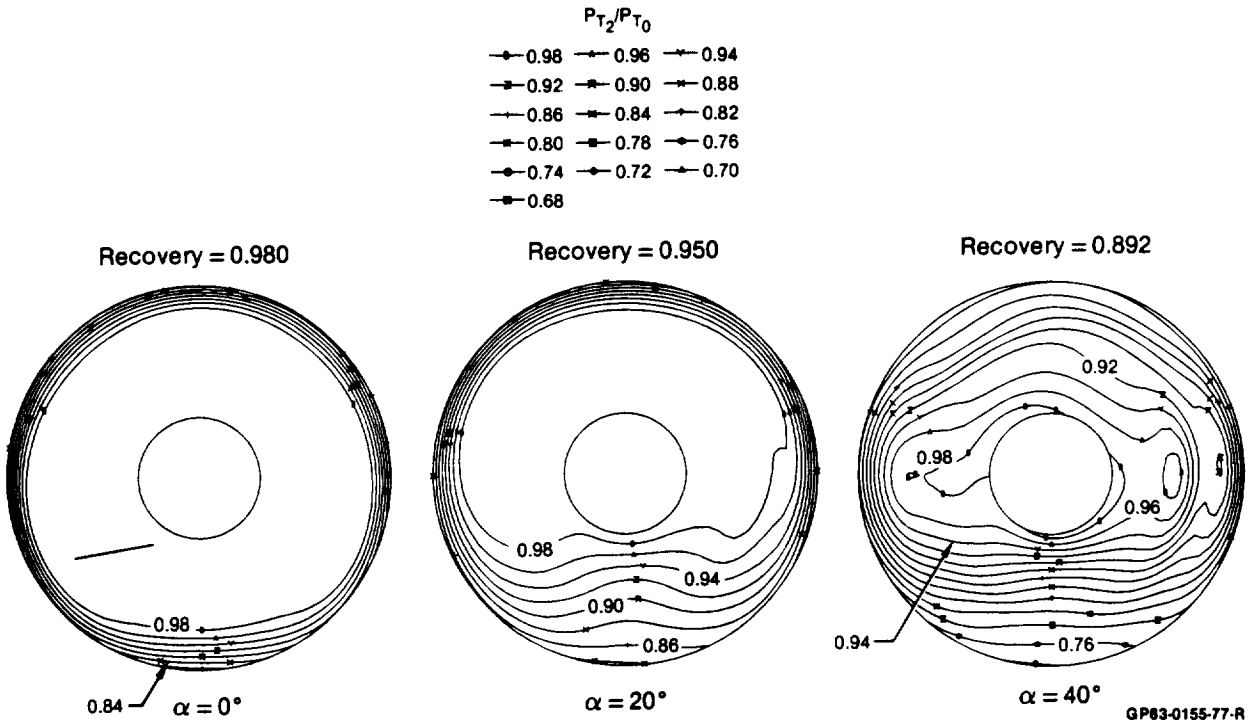

Figure 5-3. Engine Face Pressure Recovery Contours
2-D Inlet Baseline Configuration Short Diffuser
$M_0 = 0.6$

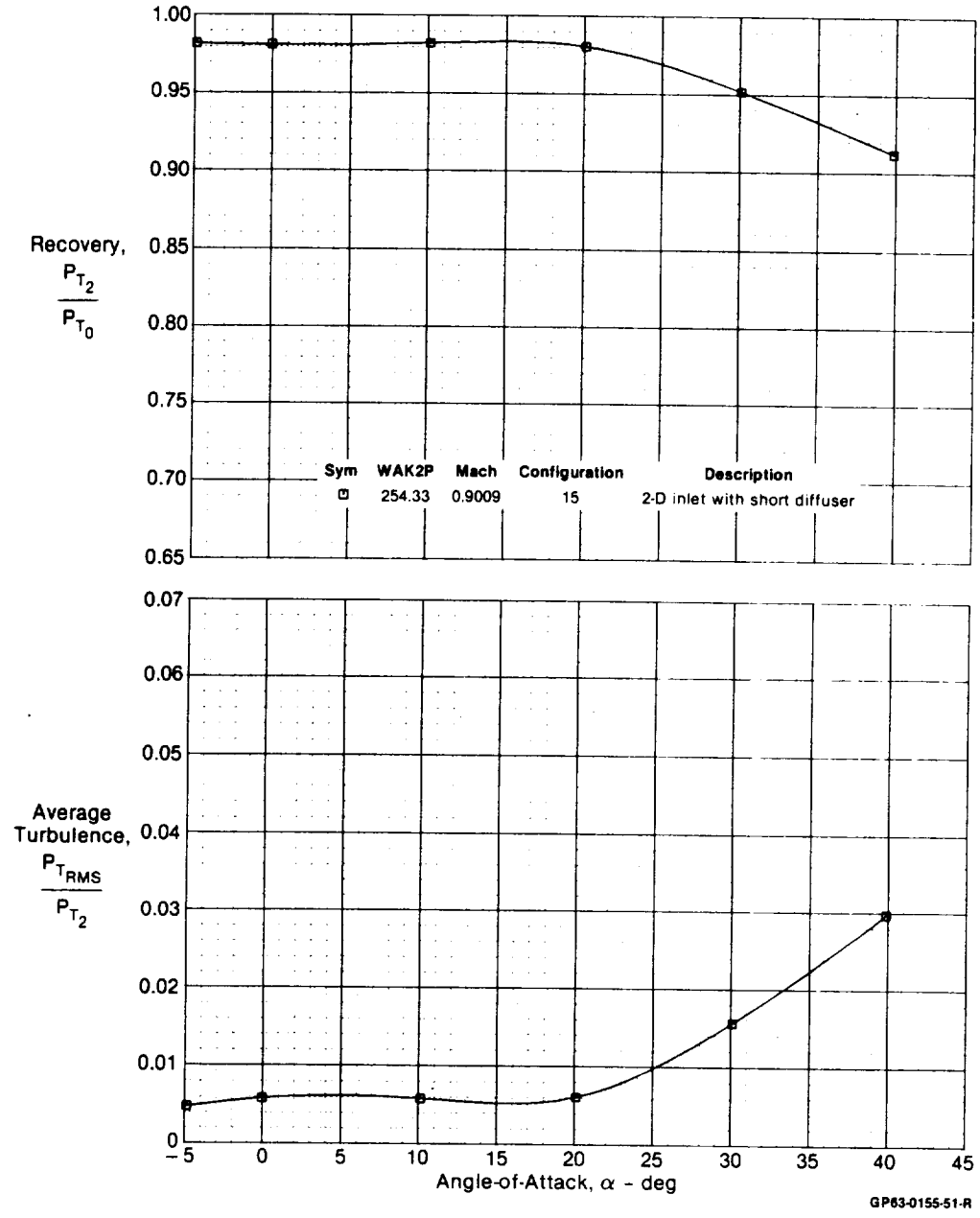

Figure 5-4. Baseline 2-D Inlet Recovery and Average Turbulence vs Angle-of-Attack
$M_0 = 0.9$

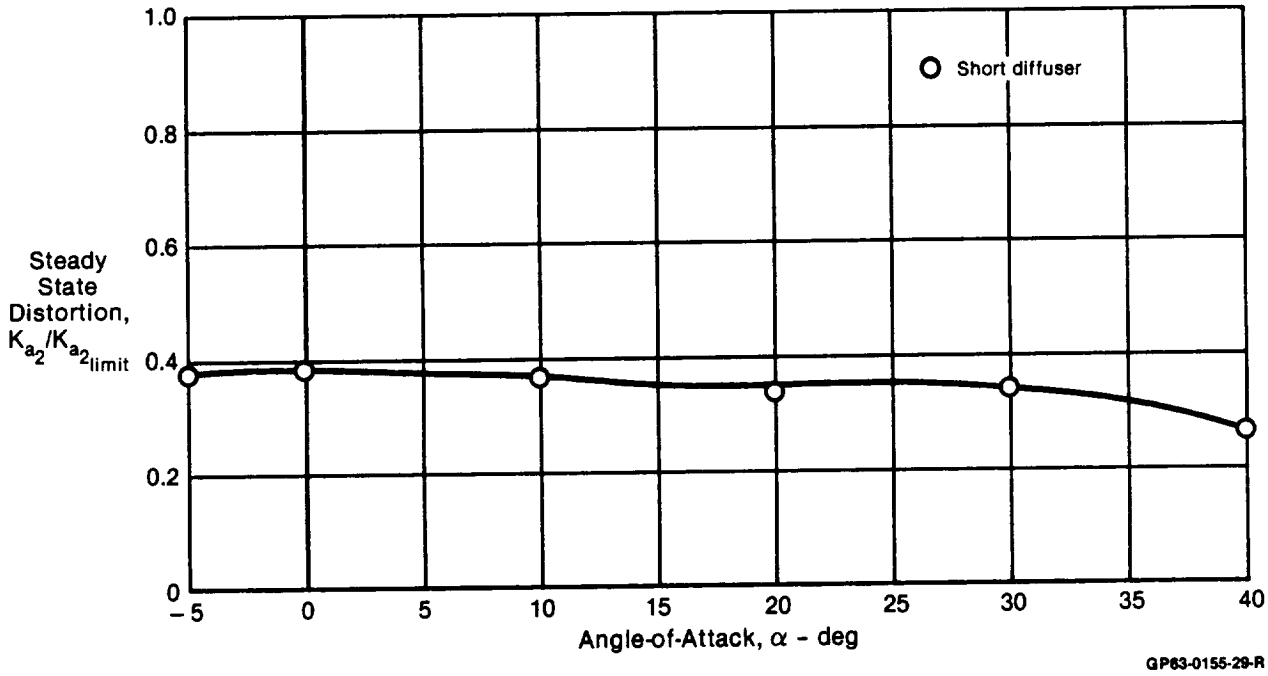

Figure 5-5. Baseline 2-D Inlet Distortion
Mach 0.9

The Mach 0.9 engine face contours shown in Figure 5-6 confirm this trend. There is essentially no change in the contours in the angle of attack range from -5° to 20°. Cowl lip separation occurs between 20° and 30°, as evidenced by the lower recovery levels on the cowl lip side of the engine face contours.

The 2-D inlet also performs well at Mach 1.2. Both recovery and turbulence remain constant at 97%/0.007 up to $\alpha = 25°$, the highest angle of attack tested, Figure 5-7. The distortion screening ratio, $K_{a2}/(K_{a2})_{limit}$, Figure 5-8, was just 50% of the limit value for the complete angles of attack range.

The engine face contours in Figure 5-9 exhibit little evidence of cowl lip separation at Mach 1.2. Only at an angle of attack of 25° is separation indicated by a thickening of the boundary layer on the cowl side of the inlet. A thickening of the boundary layer on the ramp side of the inlet is evident in the engine face contours, indicating that boundary layer bleed should improve the performance slightly at Mach 1.2.

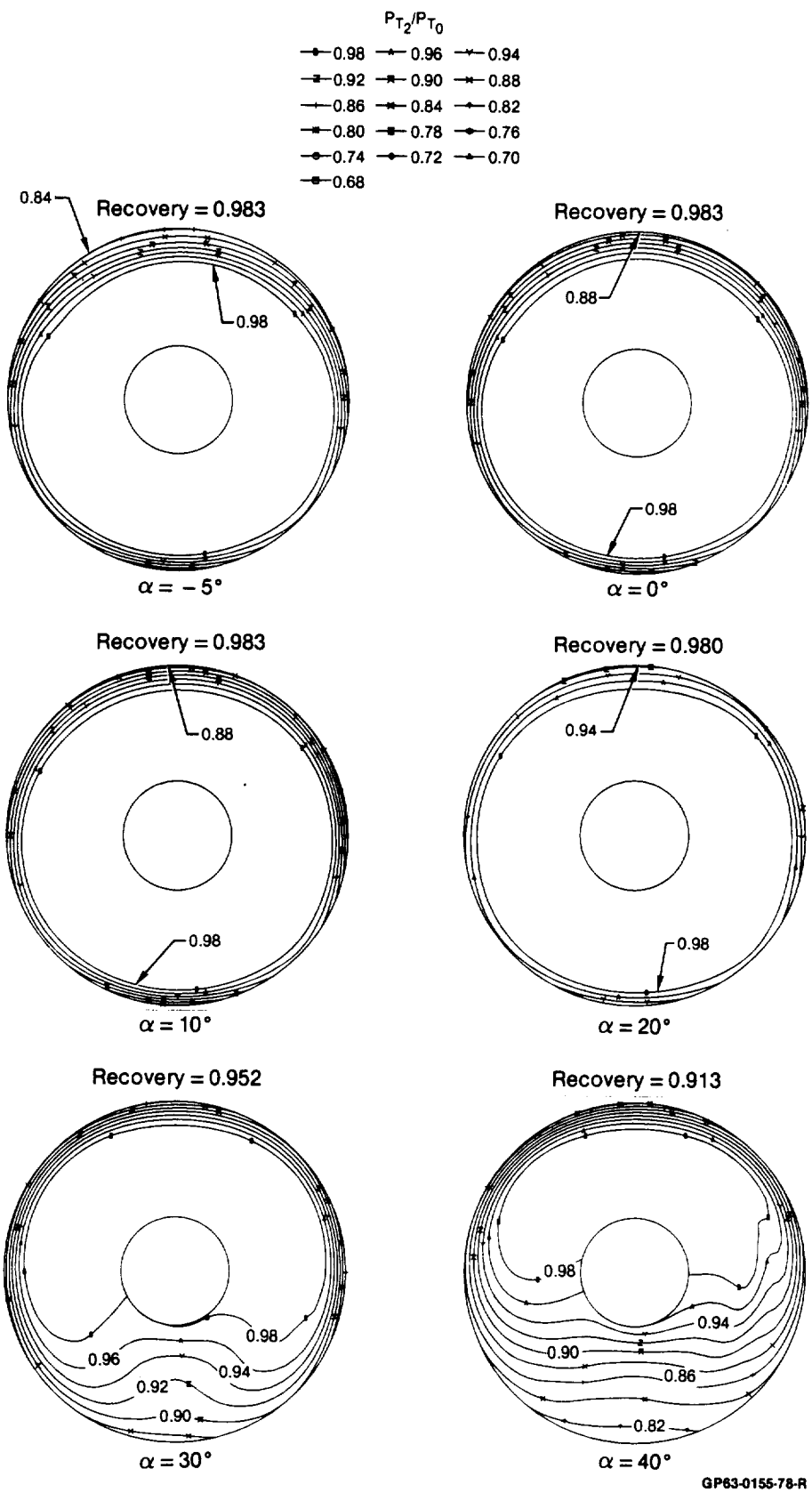

Figure 5-6. Engine Face Pressure Recovery Contours
2-D Inlet Baseline Configuration Short Diffuser
$M_0 = 0.9$

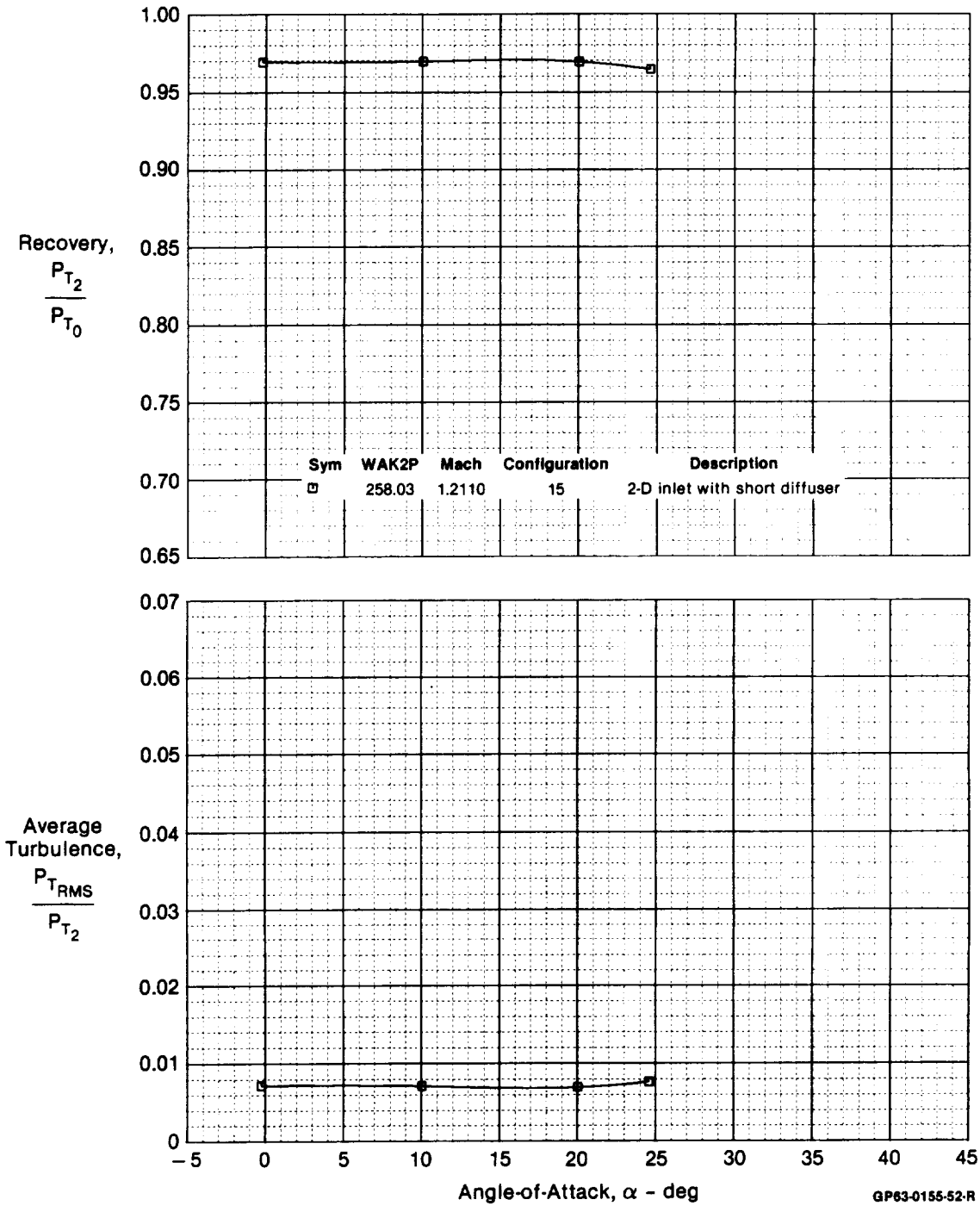

Figure 5-7. Baseline 2-D Inlet Recovery and Average Turbulence vs Angle-of-Attack
$M_0 = 1.2$

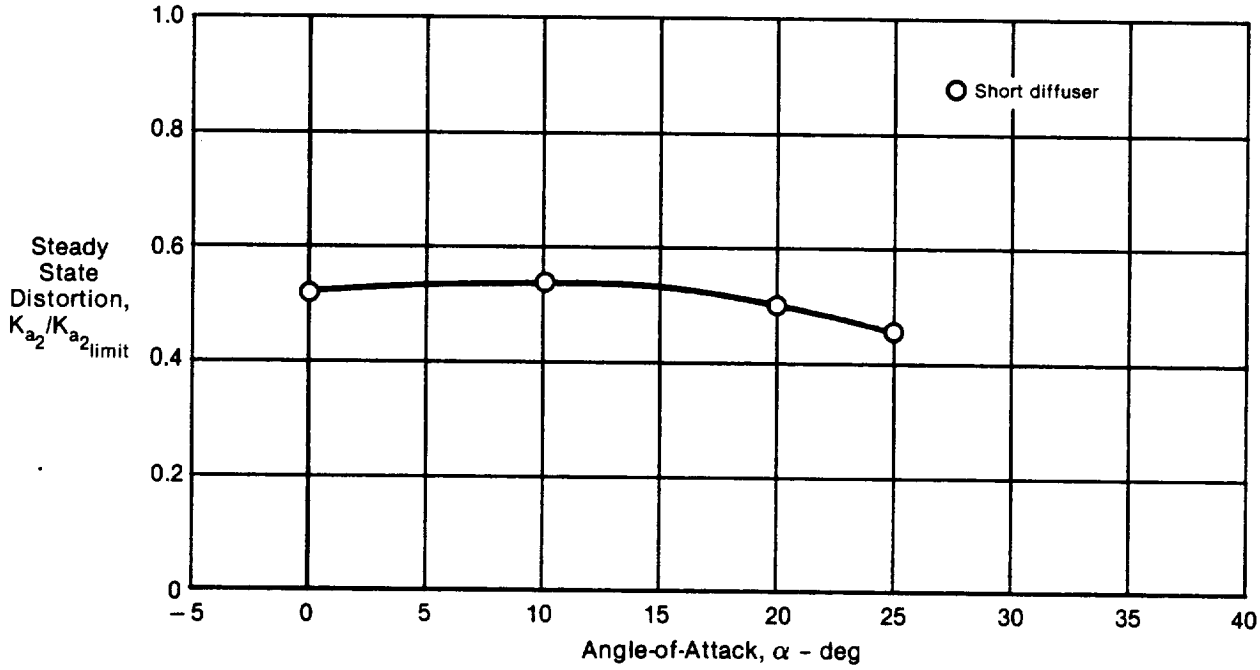

Figure 5-8. Baseline 2-D Inlet Distortion
Mach 1.2

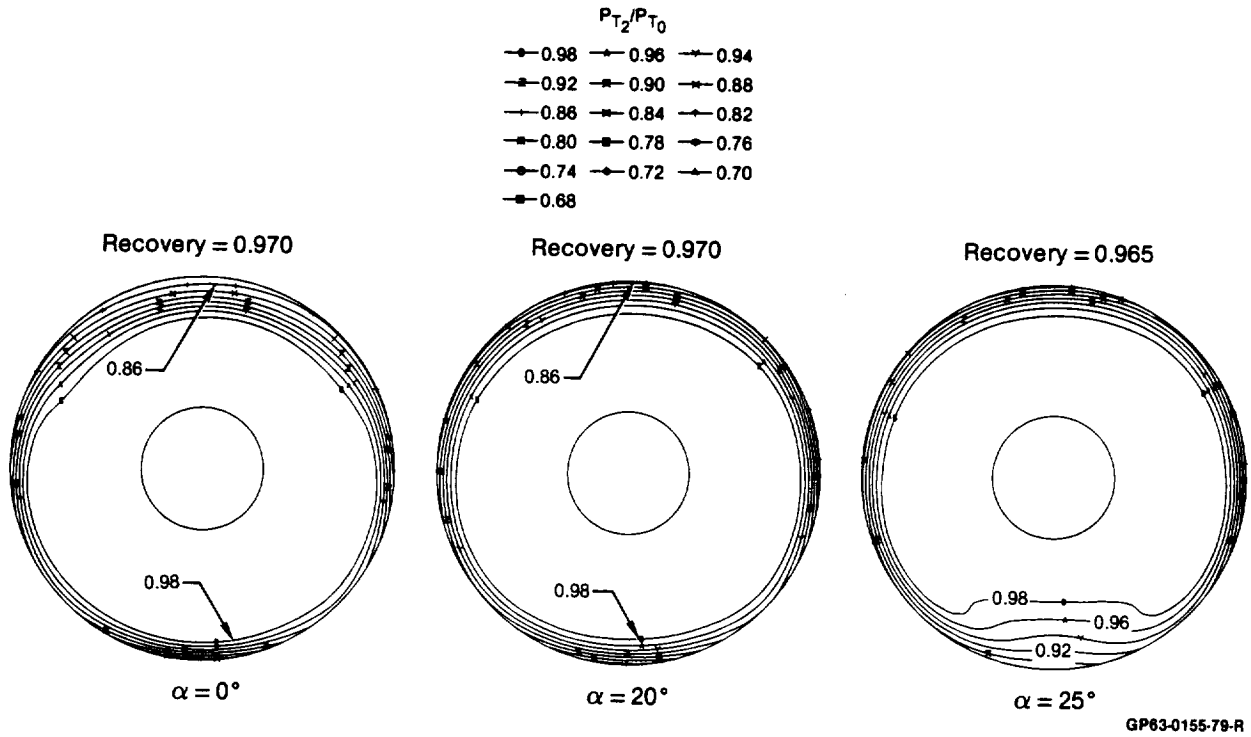

Figure 5-9. Engine Face Pressure Recovery Contours
2-D Inlet Baseline Configuration Short Diffuser
$M_0 = 1.2$

Baseline 2-D Inlet with Long Diffuser - A slight decrease in recovery is expected with the long diffuser configuration. Indeed, at Mach 0.6, the additional boundary layer growth results in a recovery level 1.5% to 2.5% below that of the short diffuser configuration. This effect is illustrated in Figure 5-10. The reason for this loss in recovery is due to additional boundary layer development in the long diffuser duct. The increased boundary layer growth is visable in the engine face contours of Figure 5-11. The addition diffuser length, however, served to attenuate total pressure variations, and therefore distortion for the long diffuser configuration was significantly below that of the short diffuser, Figure 5-12. Note that the distortion data at $\alpha = 40°$ in Figure 5-12 was not available for analysis.

Performance at Mach 0.9 shows a similar change in recovery, turbulence, and distortion with the long diffuser duct. The Mach 0.9 recovery again remains constant out to $\alpha = 20°$ and then begins to show a steady decrease at higher angles of attack, Figure 5-13. While total pressure decreased slightly, average turbulence was lower at angles of attack greater than 30°, indicating attenuation in the time-variant component of total pressure. Distortion also decreased by 10% across the angle of attack range tested, Figure 5-14. The boundary layer build up in the long diffuser is visible in the engine face contours of Figure 5-15.

These same trends occur at Mach 1.2. A recovery loss of 1% relative to the Mach 0.9 results, shown in Figure 5-16, is due to the bow shock in the flow field. Inlet distortion for Mach 1.2 is also less than that of the short diffuser, Figure 5-17.

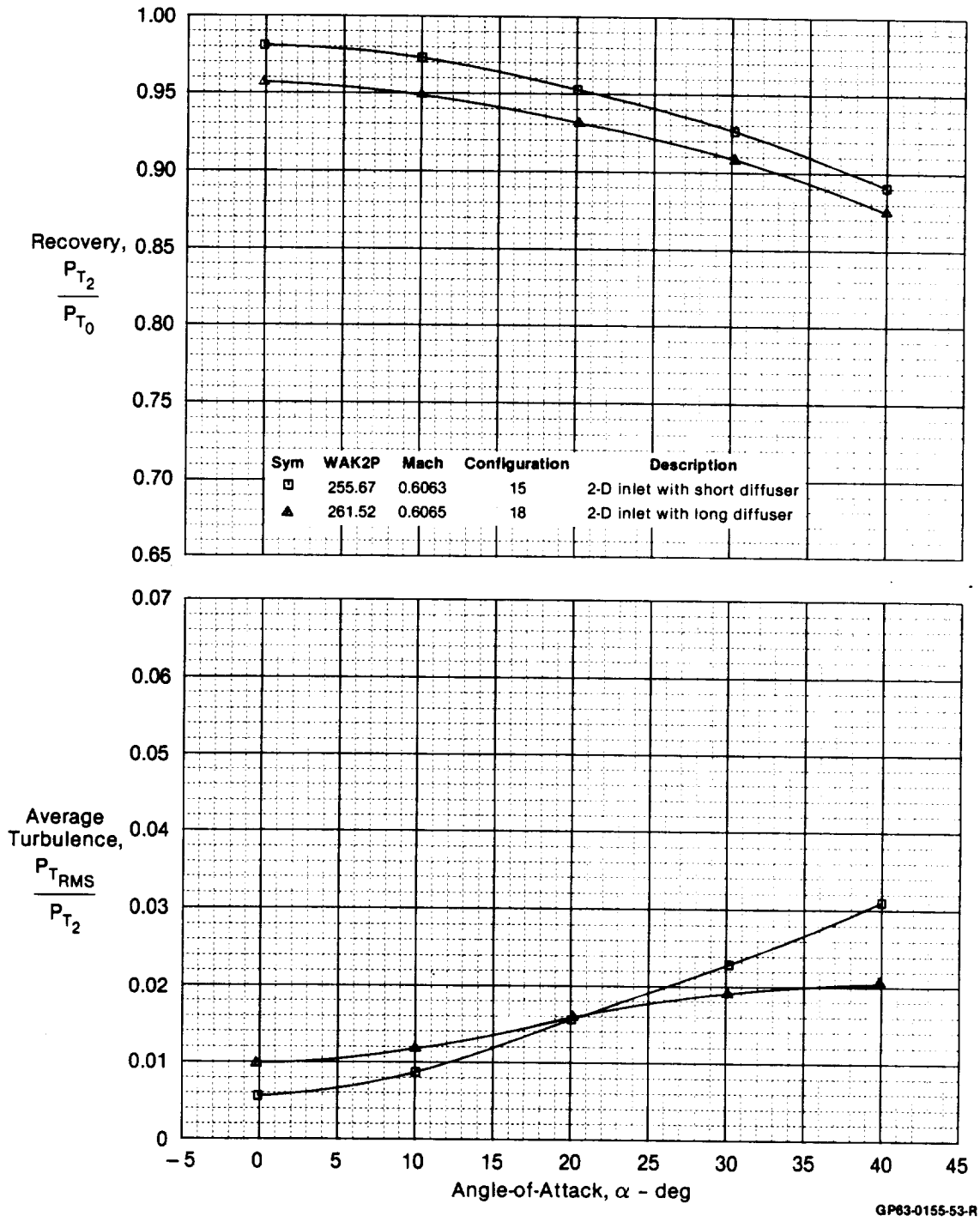

Figure 5-10. Effect of Diffuser Length on 2-D Inlet Recovery and Average Turbulence
$M_0 = 0.6$

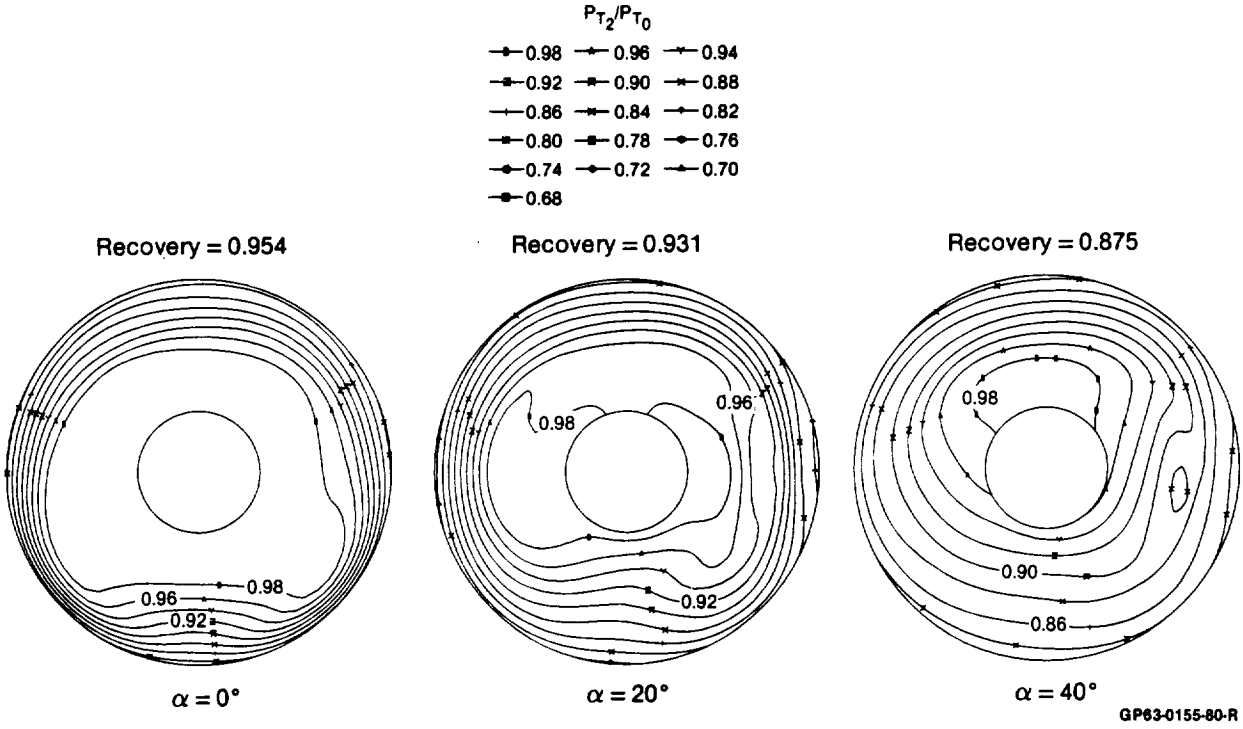

Figure 5-11. Engine Face Pressure Recovery Contours
2-D Inlet Baseline Configuration Long Diffuser
$M_0 = 0.6$

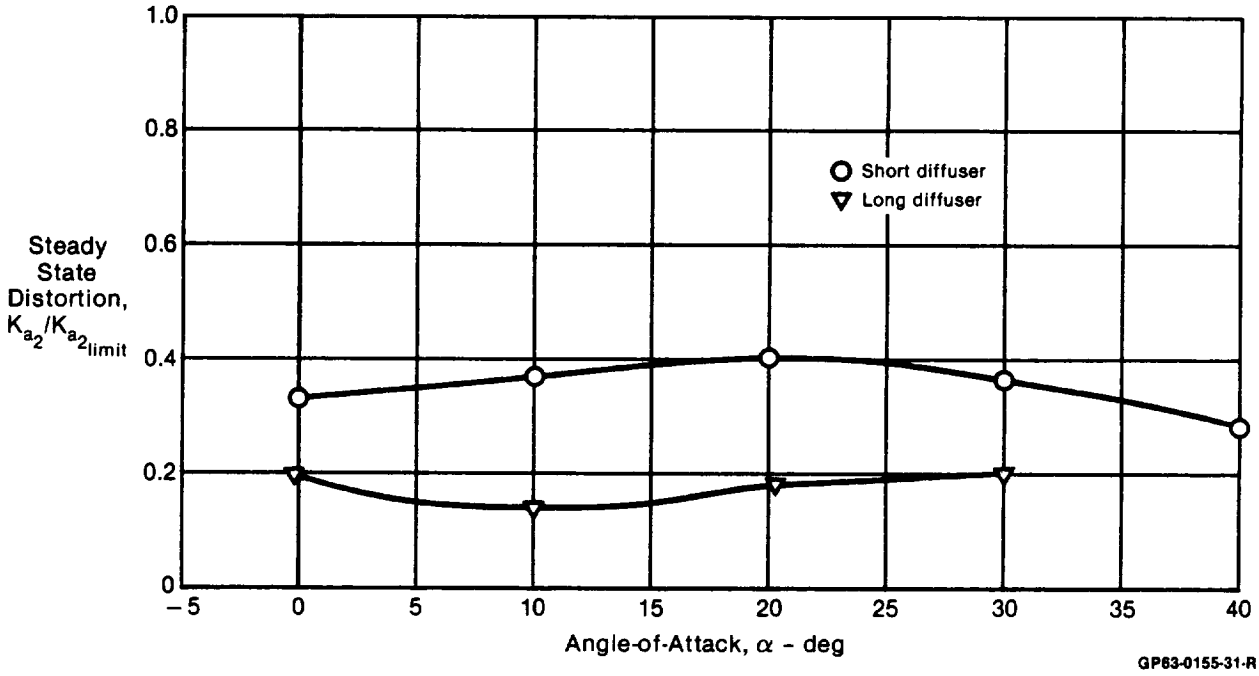

Figure 5-12. Effect of Diffuser Length on 2-D Inlet Distortion
Mach 0.6

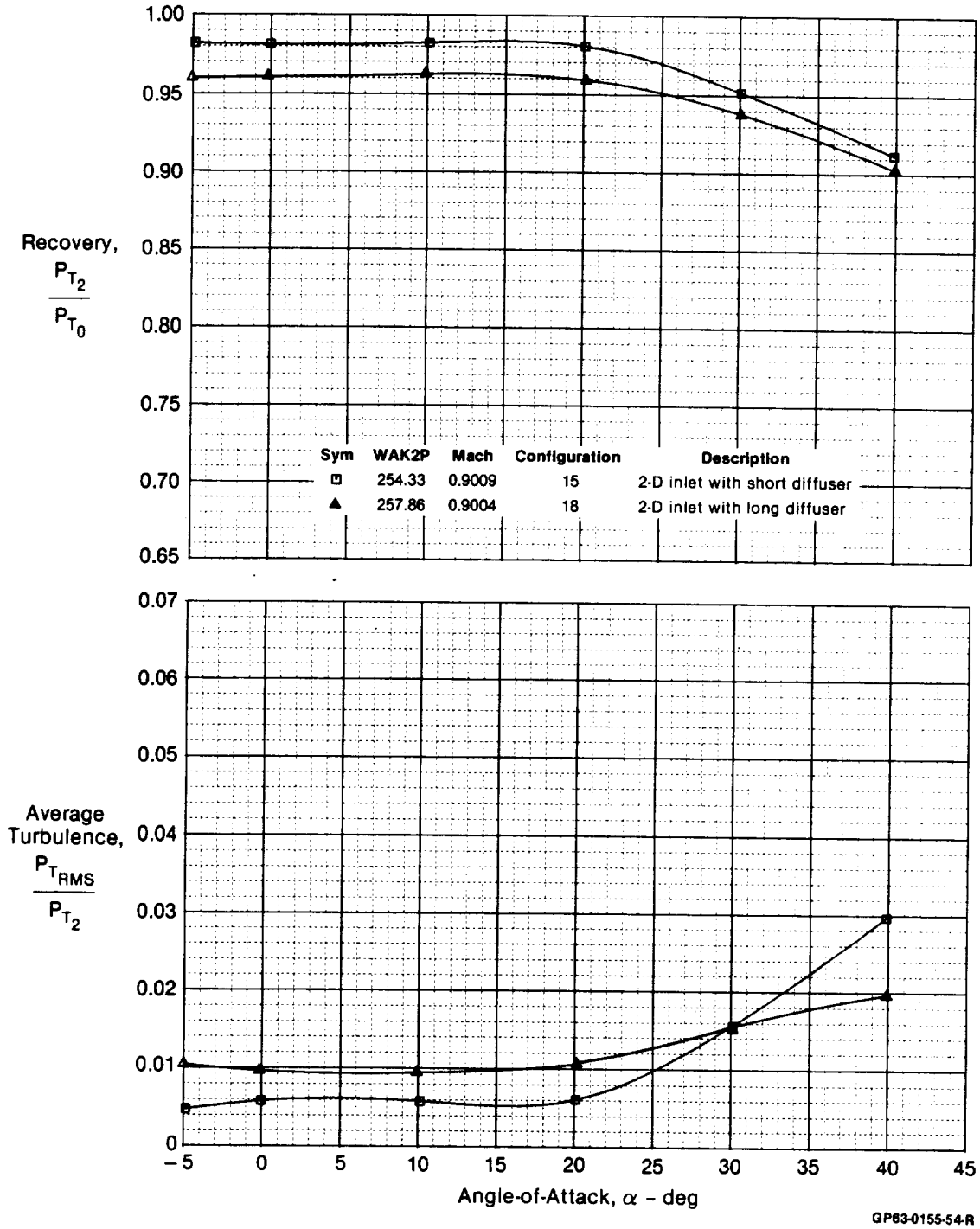

Figure 5-13. Effect of Diffuser Length on 2-D Inlet Recovery and Average Turbulence
$M_0 = 0.9$

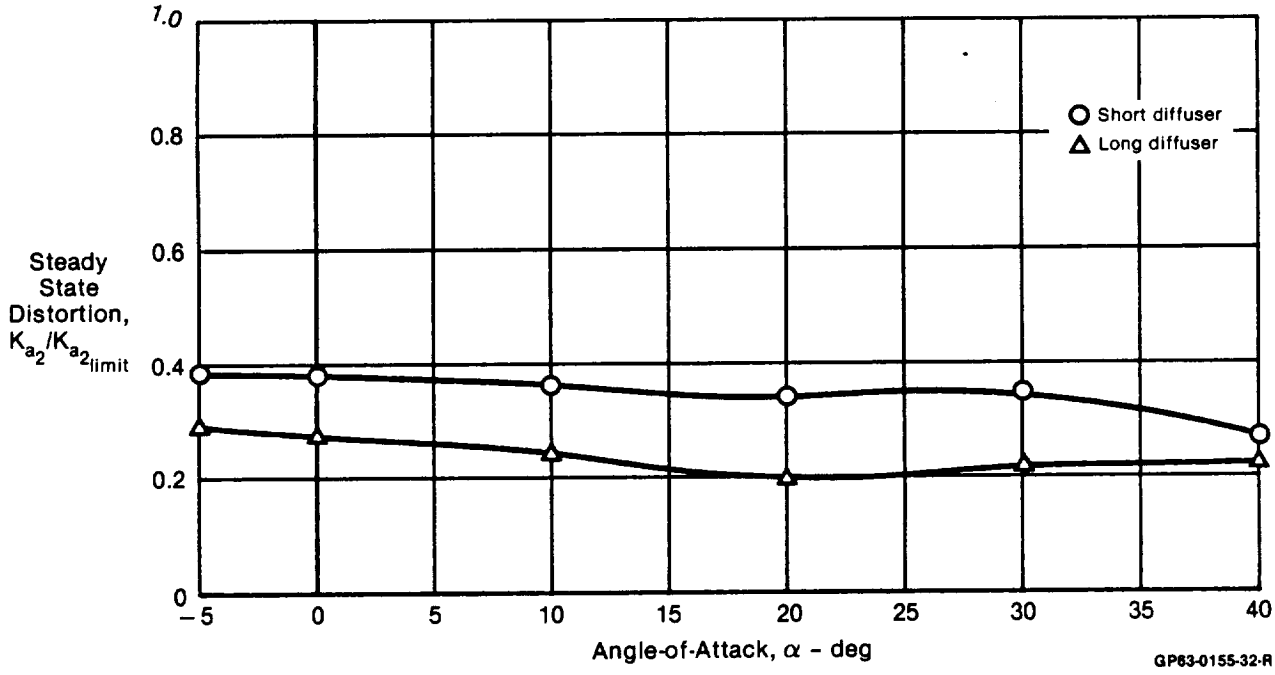

Figure 5-14. Effect of Diffuser Length on 2-D Inlet Distortion
Mach 0.9

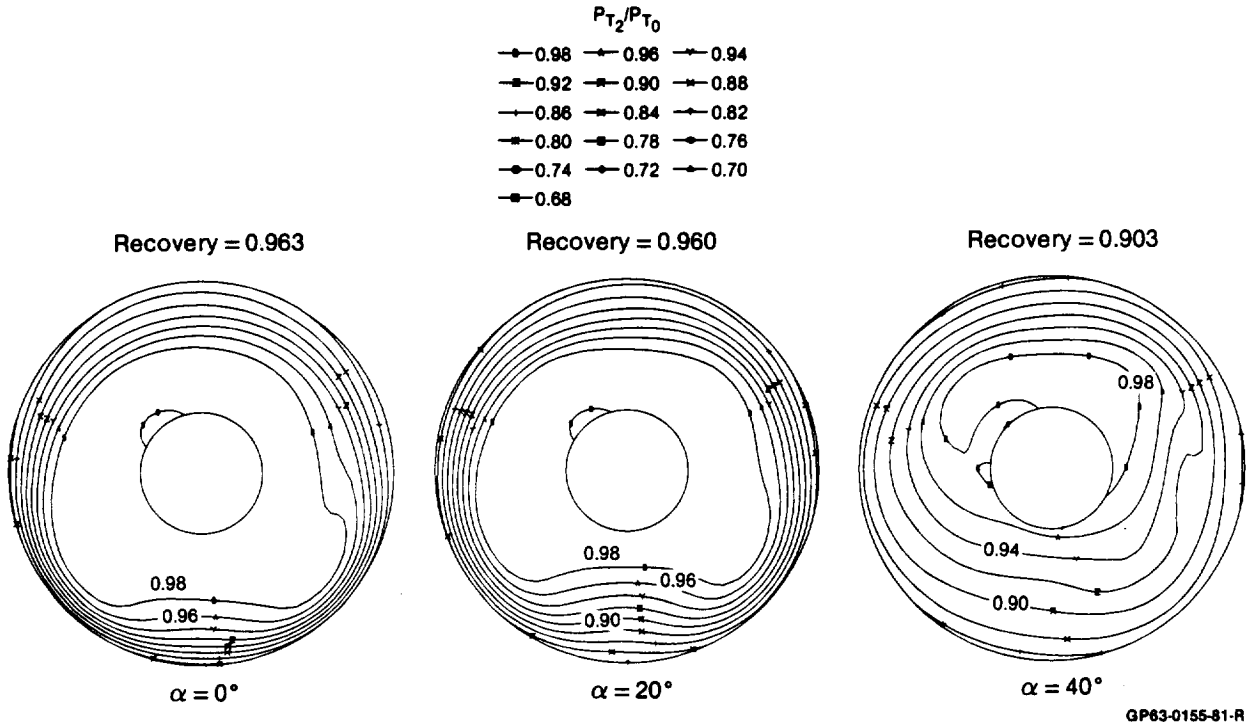

Figure 5-15. Engine Face Pressure Recovery Contours
2-D Inlet Baseline Configuration Long Diffuser
$M_0 = 0.9$

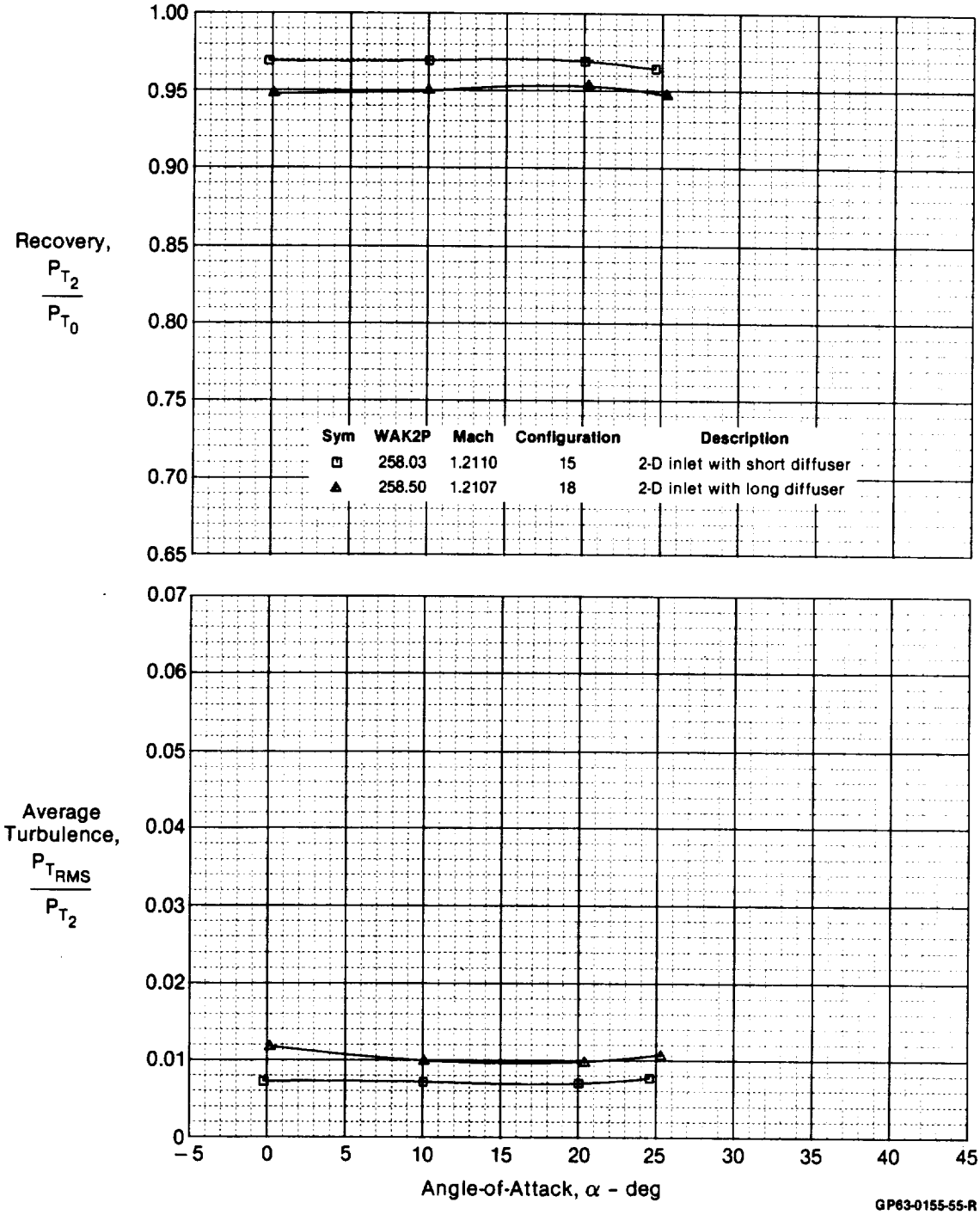

Figure 5-16. Effect of Diffuser Length on 2-D Inlet Recovery and Average Turbulence
$M_0 = 1.2$

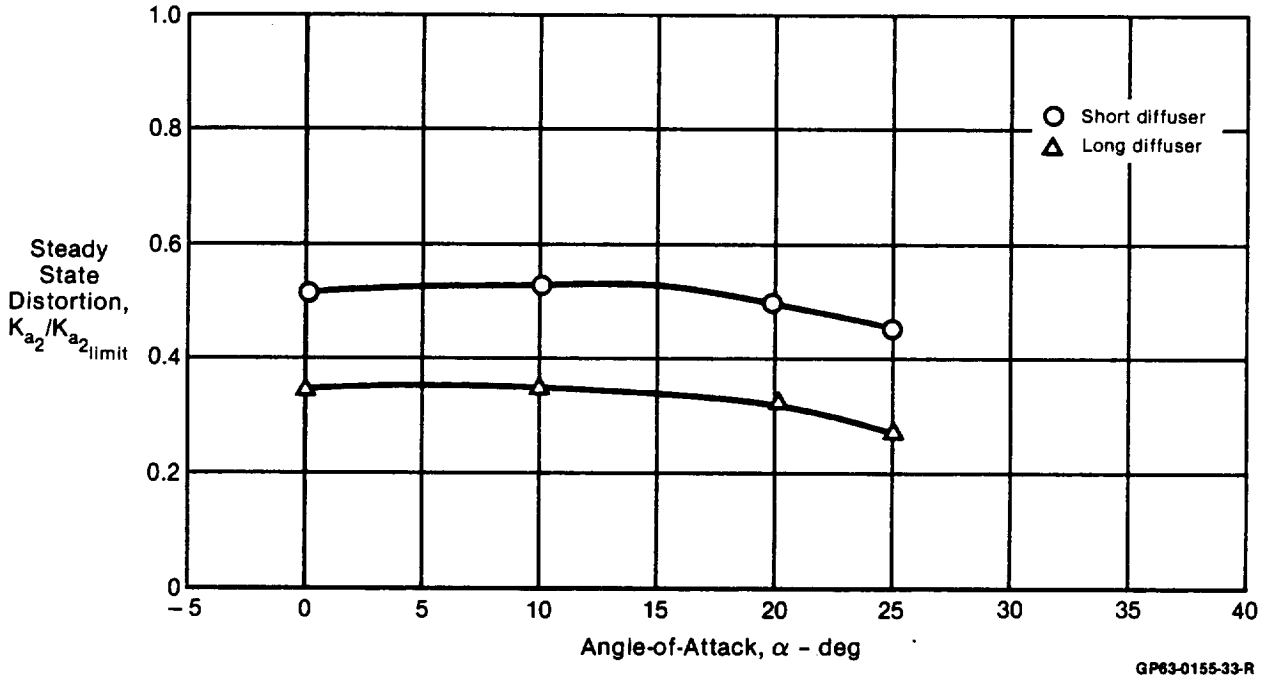

Figure 5-17. Effect of Diffuser Length on 2-D Inlet Distortion
Mach 1.2

5.1.2 Rotating Cowl Lip Performance - Cowl lip rotation angles of 20° and 40° were tested with the short diffuser at Mach 0.6, 0.9, and 1.2. The corresponding angle of attack ranges were 0° to 40° at Mach 0.6, -5° to 40° at Mach 0.9, and 0° to 25° at Mach 1.2.

Mach 0.6 - The rotating cowl lip was effective in increasing recovery and decreasing turbulence at Mach 0.6. A rotation of 20° resulted in a 4% to 8% increase in total pressure recovery at angles of attack of 20° to 40°, Figure 5-18. Turbulence was also reduced by a factor of 4 at α = 40°.

The 40° rotated lip was not as effective as the 20° lip at angle of attack, but still showed a substantial recovery benefit over the baseline at the higher angles of attack. Turbulence was reduced by up to a factor of 2 for this configuration.

The results indicate the 20° rotated lip provides the best recovery at all angles of attack tested.

Lip rotation generally results in little impact on the inlet distortion screening variable. Generally, a small increase occurs at angles of attack exceeding 30°, as shown in the Mach 0.6 data of Figure 5-19. Distortion levels for the 40° rotated lip are generally 5% higher than those for the 20° lip.

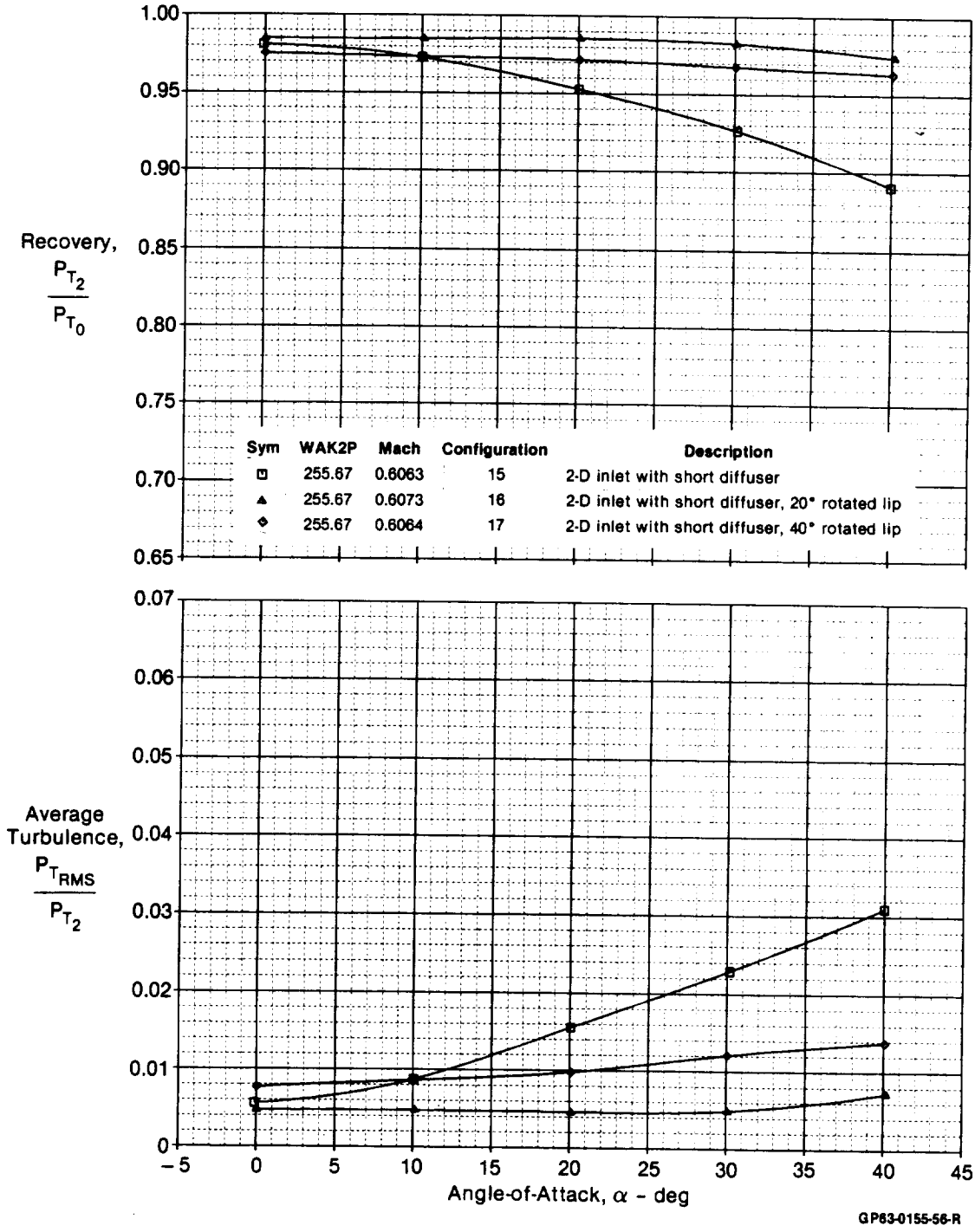

Figure 5-18. Effect of Rotating Cowl Lip on 2-D Inlet Recovery and Average Turbulence $M_0 = 0.6$

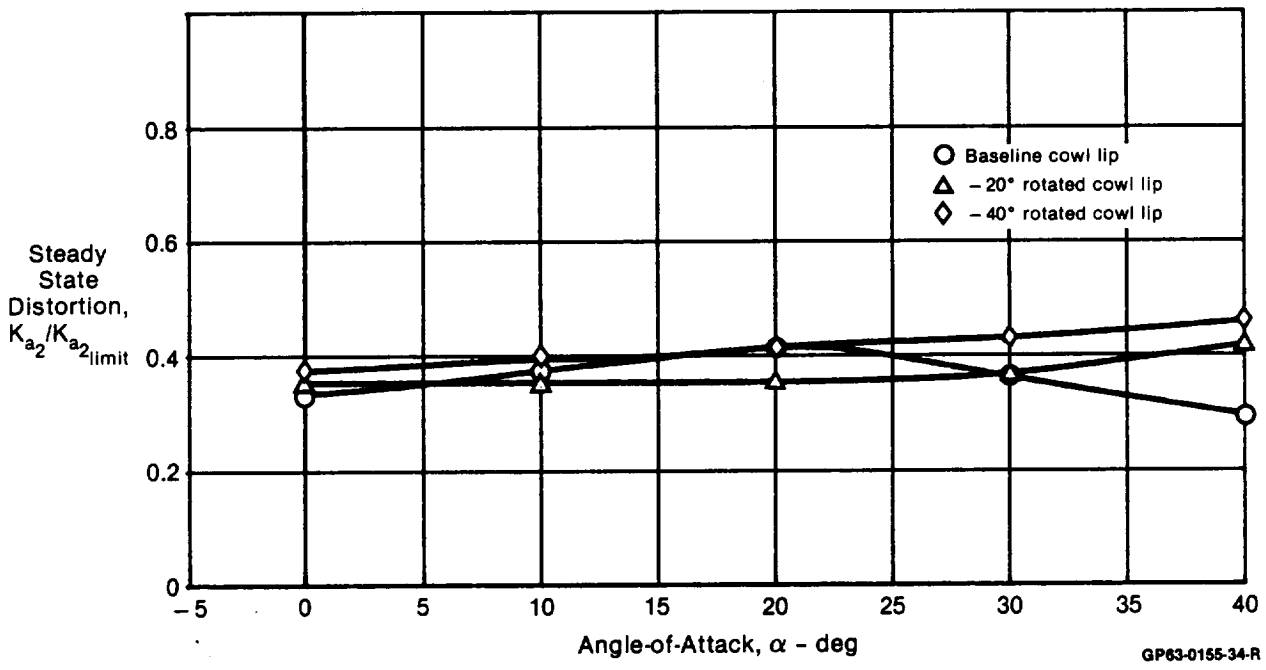

Figure 5-19. Effect of Rotating Cowl Lip on 2-D Inlet Distortion
Mach 0.6

The lower recovery and higher turbulence which occurs when the cowl lip is rotated from 20° to 40° is believed to be due to flow separation in the region of the cowl pivot, as suggested by the contour data in Figures 5-20 and 5-21. This suspected separation on the 40° rotated lip configuration occurred at all angles at attack. The 20° rotated lip, however, showed no evidence of flow separation at the pivot.

Mach 0.9 - The Mach 0.9 data on the rotated cowl lips provides the same trends as observed at Mach 0.6. Recovery, distortion, and turbulence are nearly constant over the angle of attack range for the rotated cowl, Figures 5-22 and 5-23. In addition, the rotated lip performance is nearly identical at both of these two subsonic cases. This information suggests that while lip angle should be scheduled in relation to the local inlet angle of attack to maximize internal performance and compatibility, there is no need to schedule it with Mach number in the high subsonic speed regime of Mach 0.6 to 0.9.

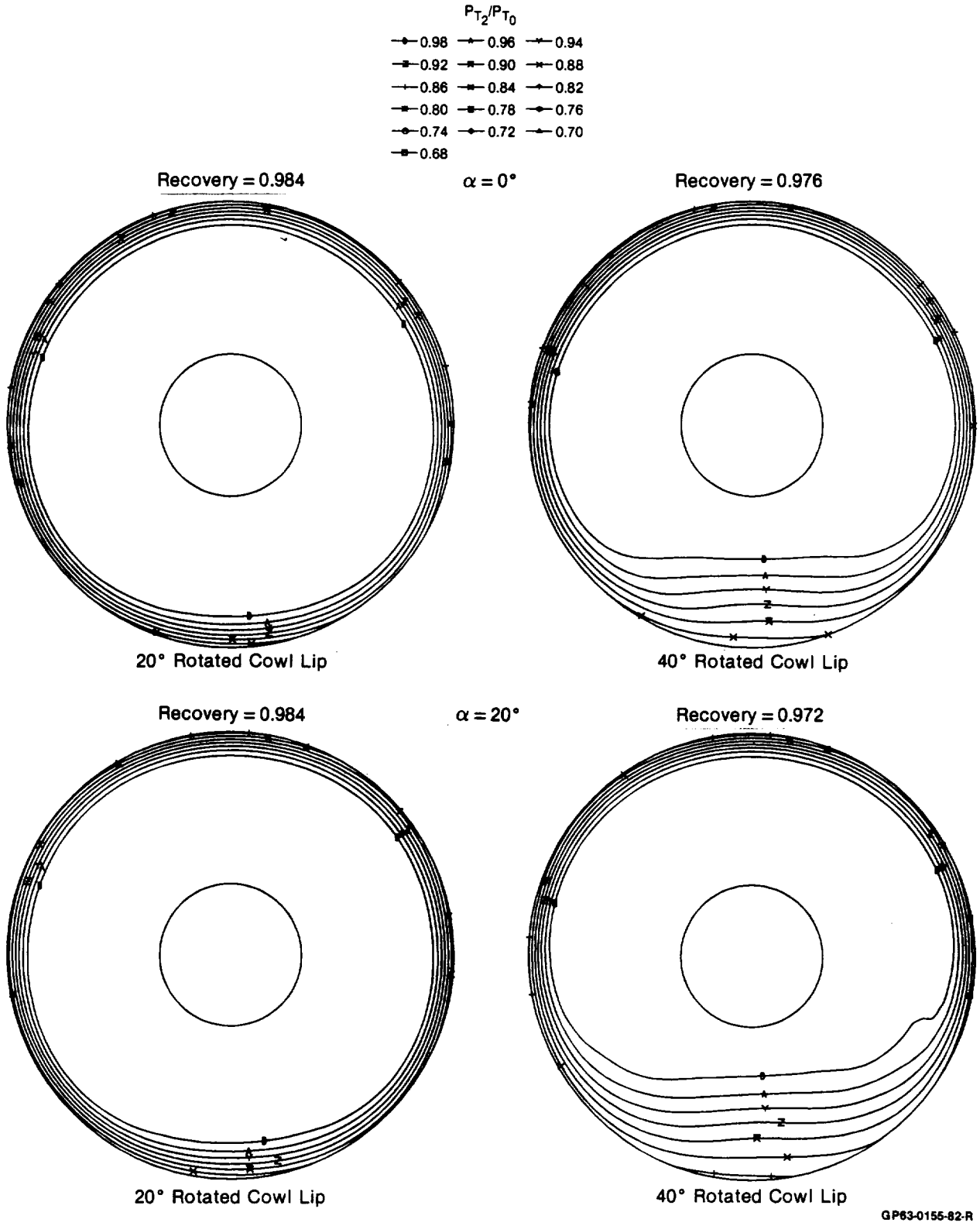

Figure 5-20. Comparison of Engine Face Pressure Recovery Contours
20° and 40° Rotated Cowl Lips 2-D Inlet
$M_0 = 0.6$ $\alpha = 0°, 20°$

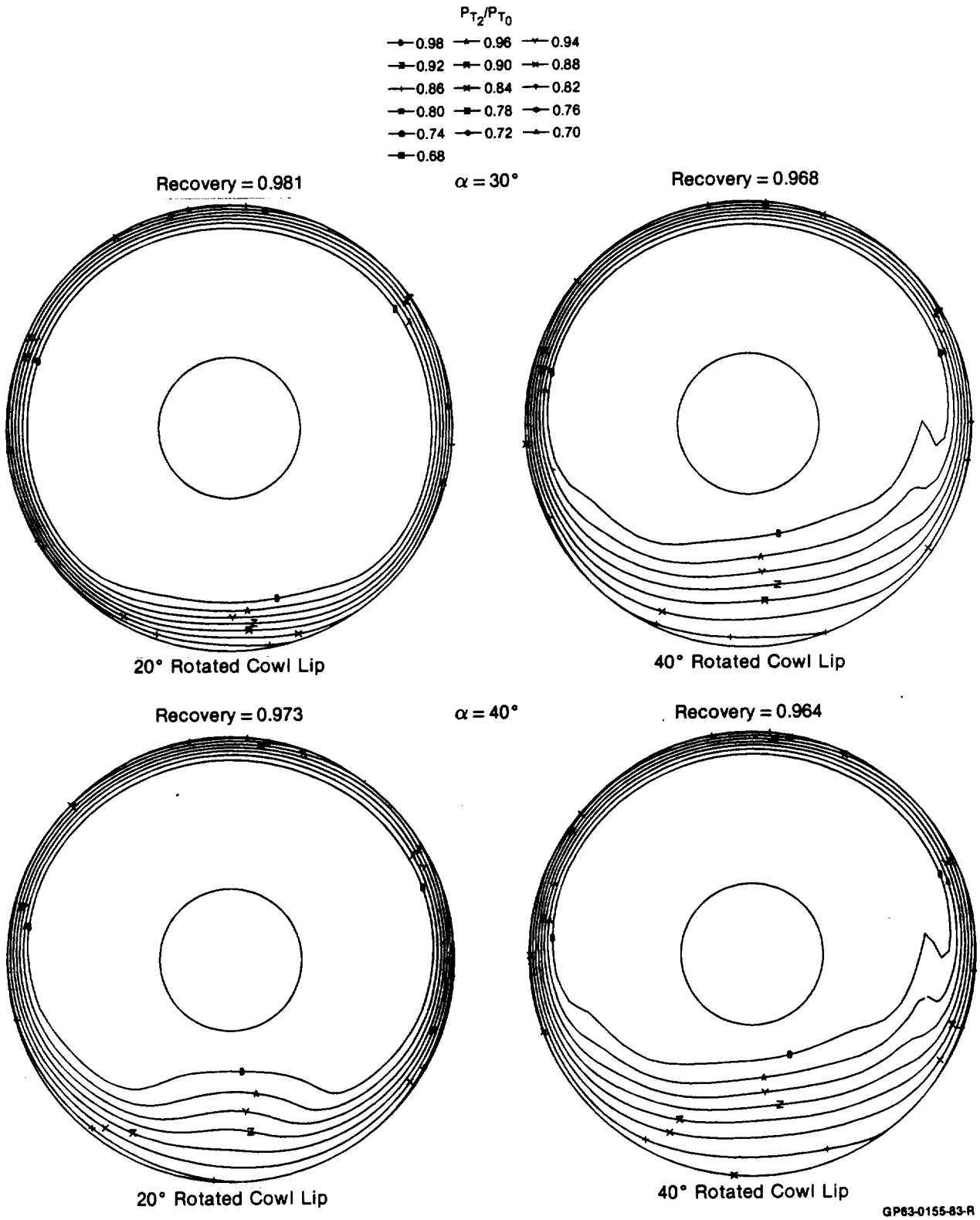

Figure 5-21. Comparison of Engine Face Pressure Recovery Contours
20° and 40° Rotated Cowl Lips 2-D Inlet
$M_0 = 0.6$ $\alpha = 30°, 40°$

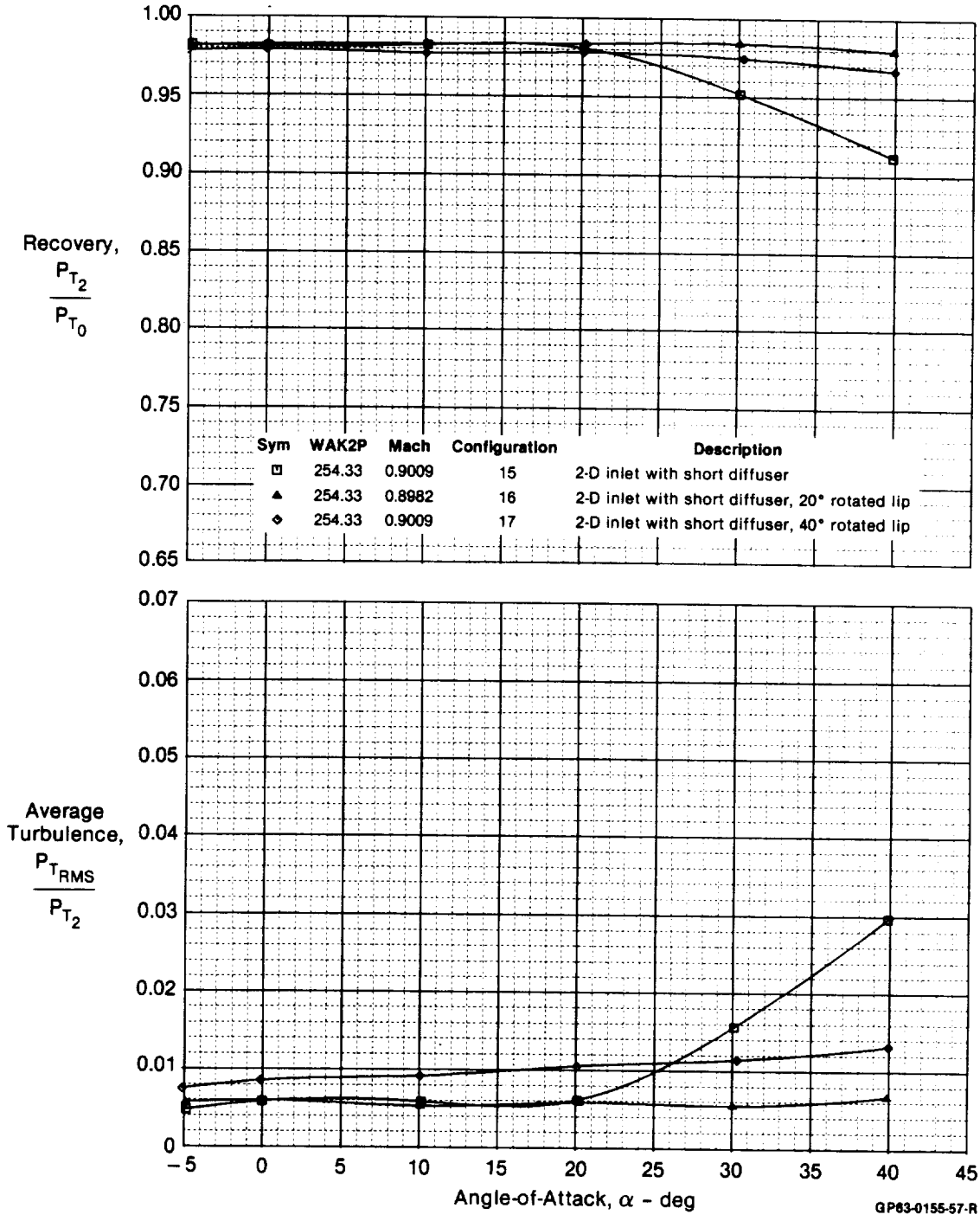

Figure 5-22. Effect of Rotating Cowl Lip on 2-D Inlet Recovery and Average Turbulence
$M_0 = 0.9$

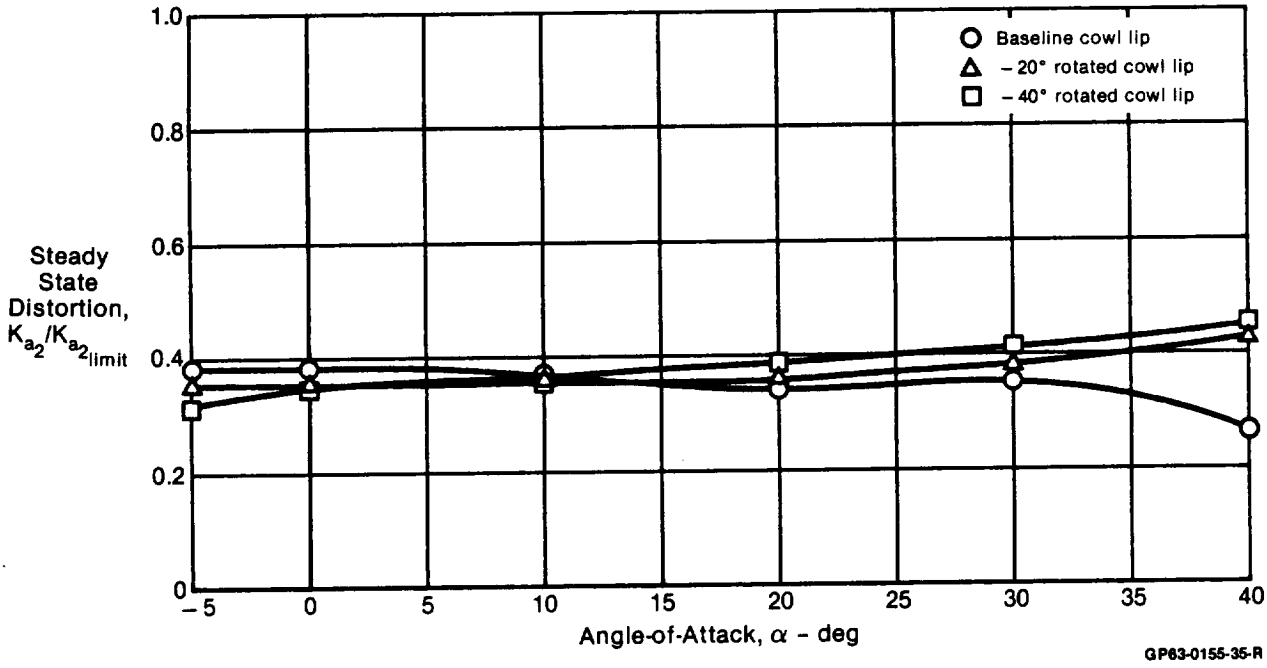

Figure 5-23. Effect of Rotating Cowl Lip on 2-D Inlet Distortion
Mach 0.9

Flow separation on the cowl lip is not as likely at Mach 0.9 as at Mach 0.6, due to the higher Reynolds number. However, the low pressure region in the engine face contours associated with the 40° rotated cowl lip occurs at both Mach numbers. The flowfield of the 40° rotated lip has small regions of flow separation throughout the angle of attack range, as illustrated in the 0°, 30° and 40° angle of attack data of Figure 5-24. However, at 30° and 40°, these are smaller than for the baseline (Figure 5-6). The 20° rotated lip configuration shows virtually no total pressure loss associated with the cowl lip up to $\alpha = 40°$, Figure 5-24.

Mach 1.2 - At Mach 1.2, the rotated cowl lip concept shows no substantial benefit over the baseline inlet. Comparison demonstrates nearly constant recovery and turbulence levels over the angle of attack range, as shown in Figure 5-25. At an angle of attack of 25°, there was a 1% improvement in recovery with a cowl lip rotation angle of 20°. However, the 40° rotated lip resulted in lower performance than the baseline, with a 1% loss in recovery over the entire angle of attack range.

The rotated lip configurations also had only a small effect on turbulence. The 20° rotated lip reduced turbulence by about .002 while the 40° rotated lip increased it by .002.

At a freestream Mach number of 1.2, distortion increases slightly with cowl lip rotation angle, Figure 5-26. However, the baseline and rotated cowl concepts are still substantially below the compatibility screening limit of 1.0.

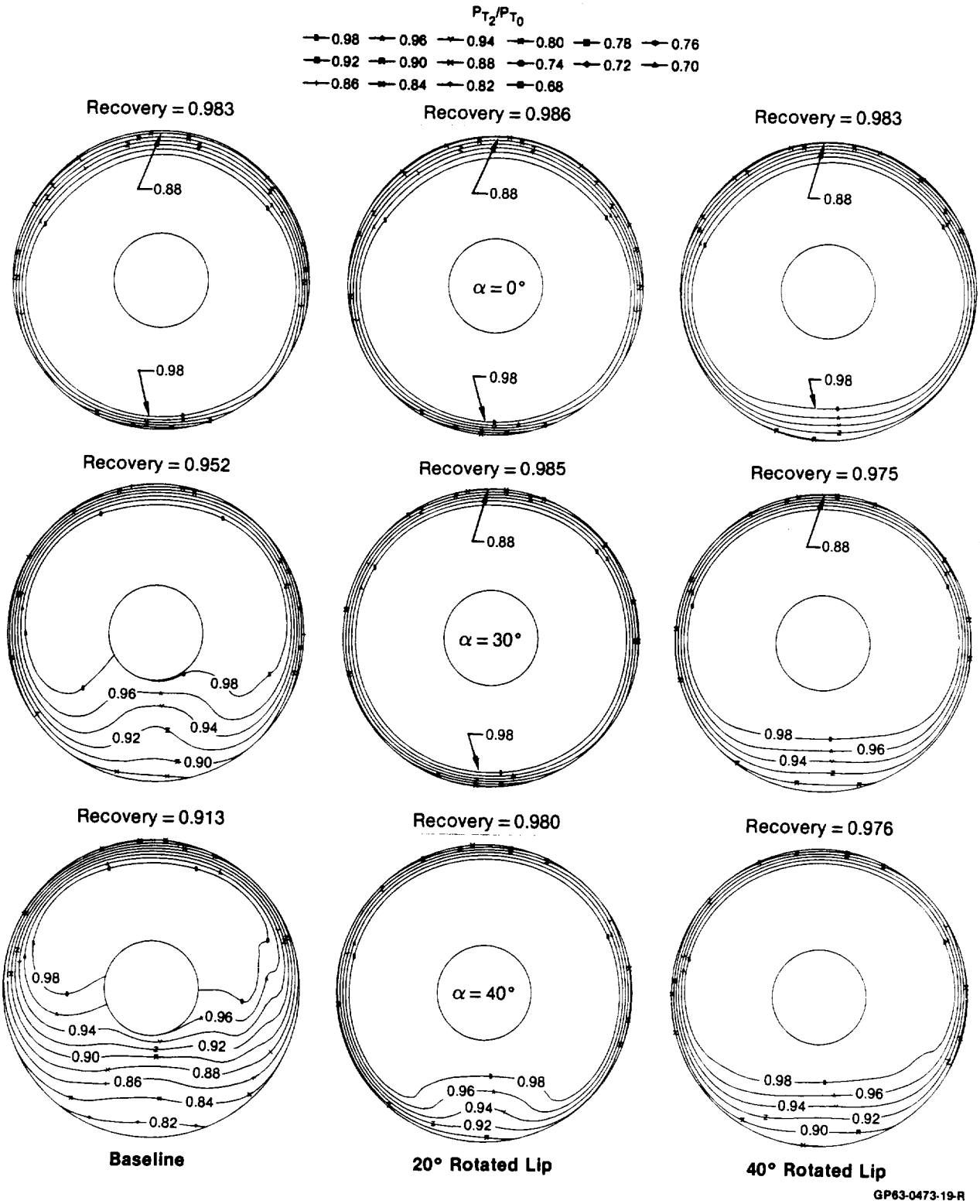

Figure 5-24. Comparison of Engine Face Pressure Recovery Contours
20° and 40° Rotated Cowl Lips
$M_0 = 0.9$ $\alpha = 0°, 30°, 40°$

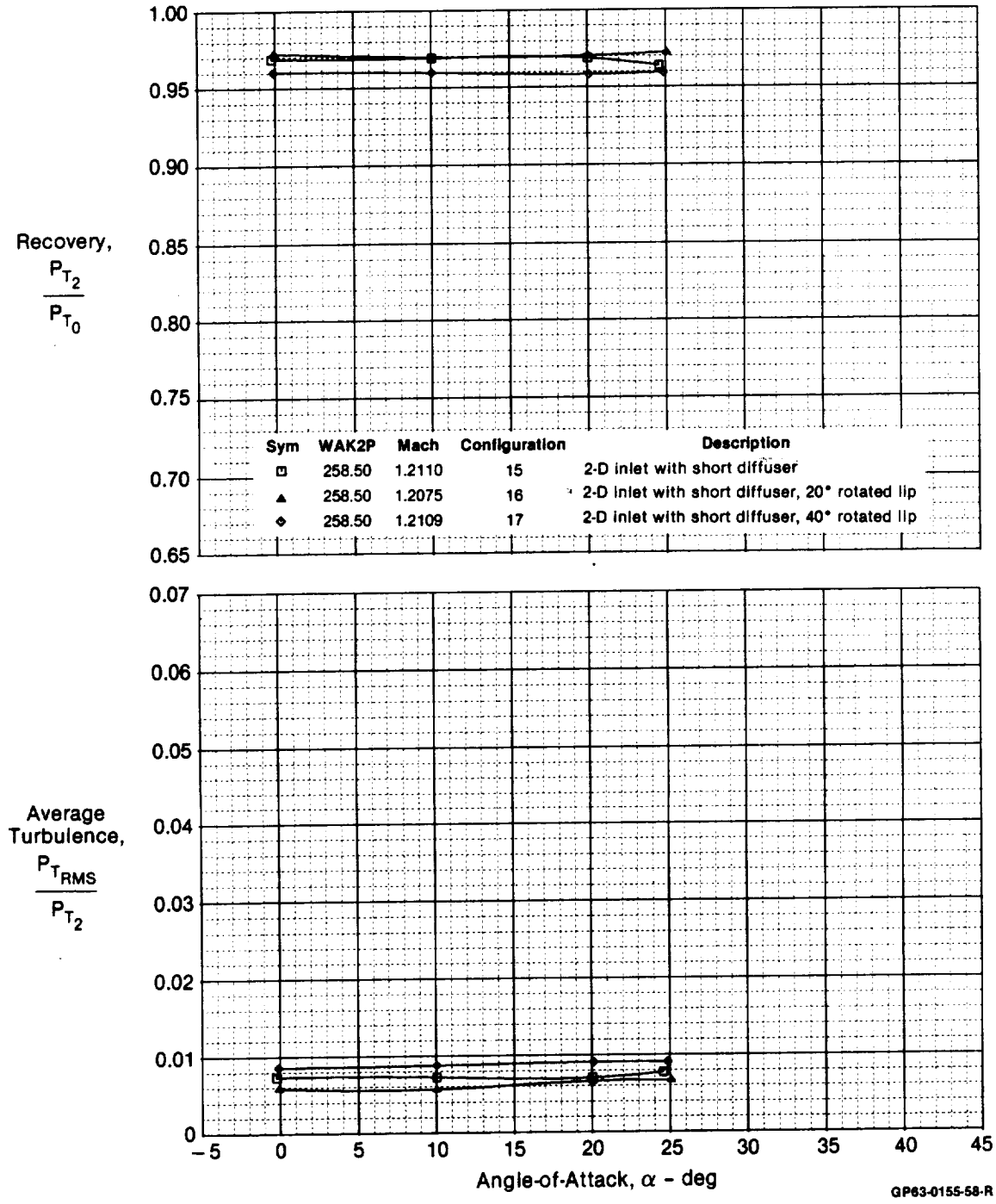

Figure 5-25. Effect of Rotating Cowl Lip on 2-D Inlet Recovery and Average Turbulence
$M_0 = 1.2$

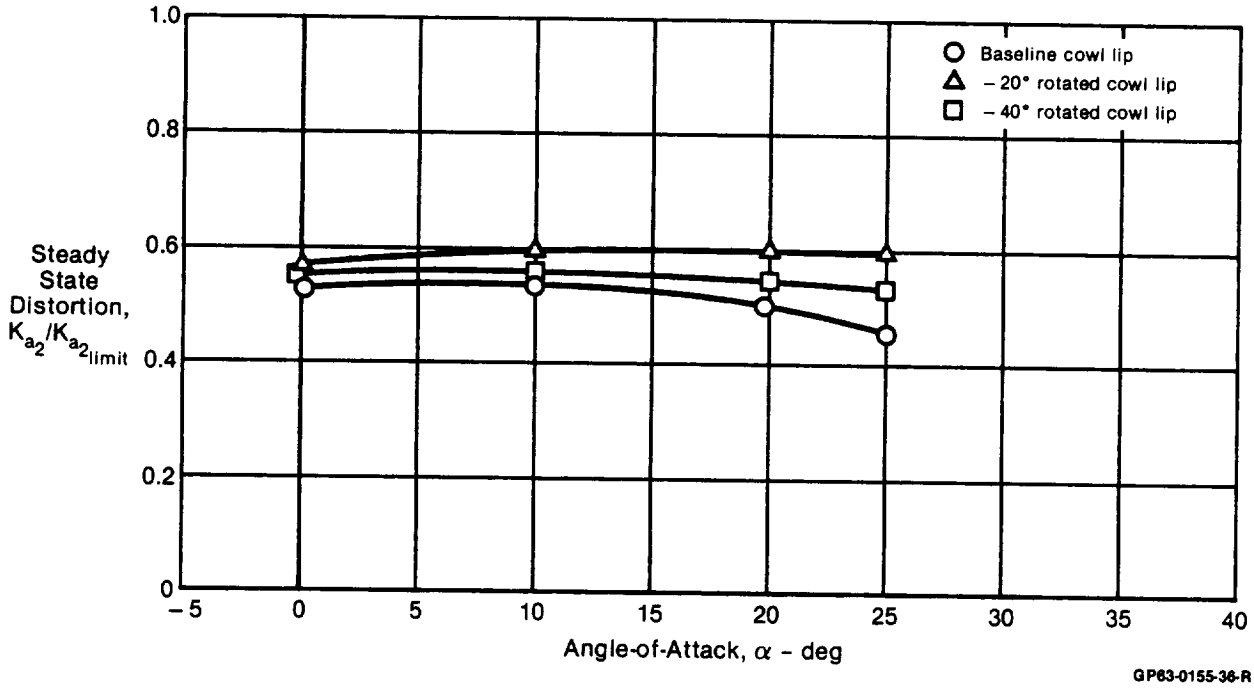

Figure 5-26. Effect of Rotating Cowl Lip on 2-D Inlet Distortion
Mach 1.2

Summary - The rotated cowl lip concept provides one approach to substantial performance improvement during subsonic maneuvering, and is expected to provide increased benefits for concepts with sharper cowl lips. The scheduling of cowl rotation would be independent of the subsonic Mach number in the range 0.6 to 0.9, and would be controlled to return to a baseline cowl orientation at sonic or supersonic speeds. The data from this test also suggests that up to 40° angle of attack, 20° of cowl rotation is sufficient. The scheduling may also have to consider the external cowl drag in addition to internal performance benefits.

If angles of attack beyond 40° are desired, a more gradual curvature in the contour near the theoretical pivot would likely be required to prevent flow separation. A combination of translation and rotation in the cowl position could minimize the local flow turn angle.

Computational Results - As previously mentioned, a 2-D Navier Stokes code was used for analysis of the rotated lip configurations to gain a better understanding of the inlet flowfield. The flow solver uses a multiple zone approach to compute the complete flow field, including the viscous boundary layer region, Reference 2. The zone partitioning for a typical inlet configuration is illustrated in Figure 5-27. The computational space is split into four separate zones. This provides for increased grid resolution in areas of high flow turning, such as the cowl leading edge. Zone boundaries are identified in each figure of computed data.

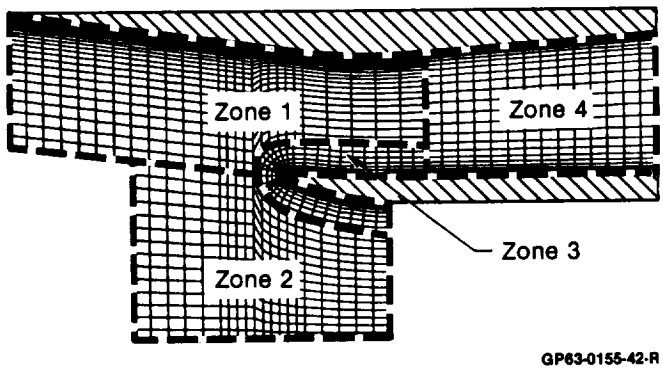

Figure 5-27. Computational Zones for Inlet Analysis

This flow solver was used to obtain solutions for the baseline, 20°, and 40° rotated cowl lip configurations. The short diffuser geometry was used in all three cases. Flow field solutions were obtained for each configuration at 0° and 20° angle of attack at a freestream Mach number of 0.6. The mass flow was specified for each case such that it resulted in a constant corrected airflow equal to the operating point in the test data previously shown. Each case was run using the same freestream conditions tested in the wind tunnel.

Computational Predictions, Baseline Inlet - The experimental contour data at Mach 0.6 (see Figure 5-3) indicated that there may be a region of internal separated flow on the cowl side of the baseline inlet. Analytical predictions of the flow field about the baseline inlet at Mach 0.6 and $\alpha = 0°$ confirm the separation. The analytical results, illustrated in the Mach number contours and flow vector diagram of Figure 5-28, indicate that a separated region does exist in the cowl lip region. The closeup of the cowl lip velocity vectors shows that the separated region is located near the lip leading edge. The stagnation point lies just below the highlight. The flow above the stagnation streamline must therefore turn around the lip leading edge; this turning cannot be supported, and the flow separates immediately after the highlight.

When the angle of attack is increased to 20°, the stagnation streamline moves further downstream on the external cowl surface. This causes increased flow acceleration around the cowl lip, and hence the separation region on the interior surface grows significantly. A thicker boundary layer on the cowl side of the inlet is visible in the Mach contours of Figure 5-29. The increased boundary layer is in the throat region of the inlet, and therefore the effective flow area decreases. There is sufficient boundary layer in the throat such that the flow chokes, and a normal shock forms in the diffuser section. Recovery is further decreased by boundary layer separation on the ramp side due to the presence of this shock.

Hence we can see that separation induced by the flow acceleration around the leading edge of the cowl lip causes a cascade of effects which serve to decrease the overall performance of the inlet. The next step of this analytical study was to determine how the rotated lip affects the inlet flow field to improve performance.

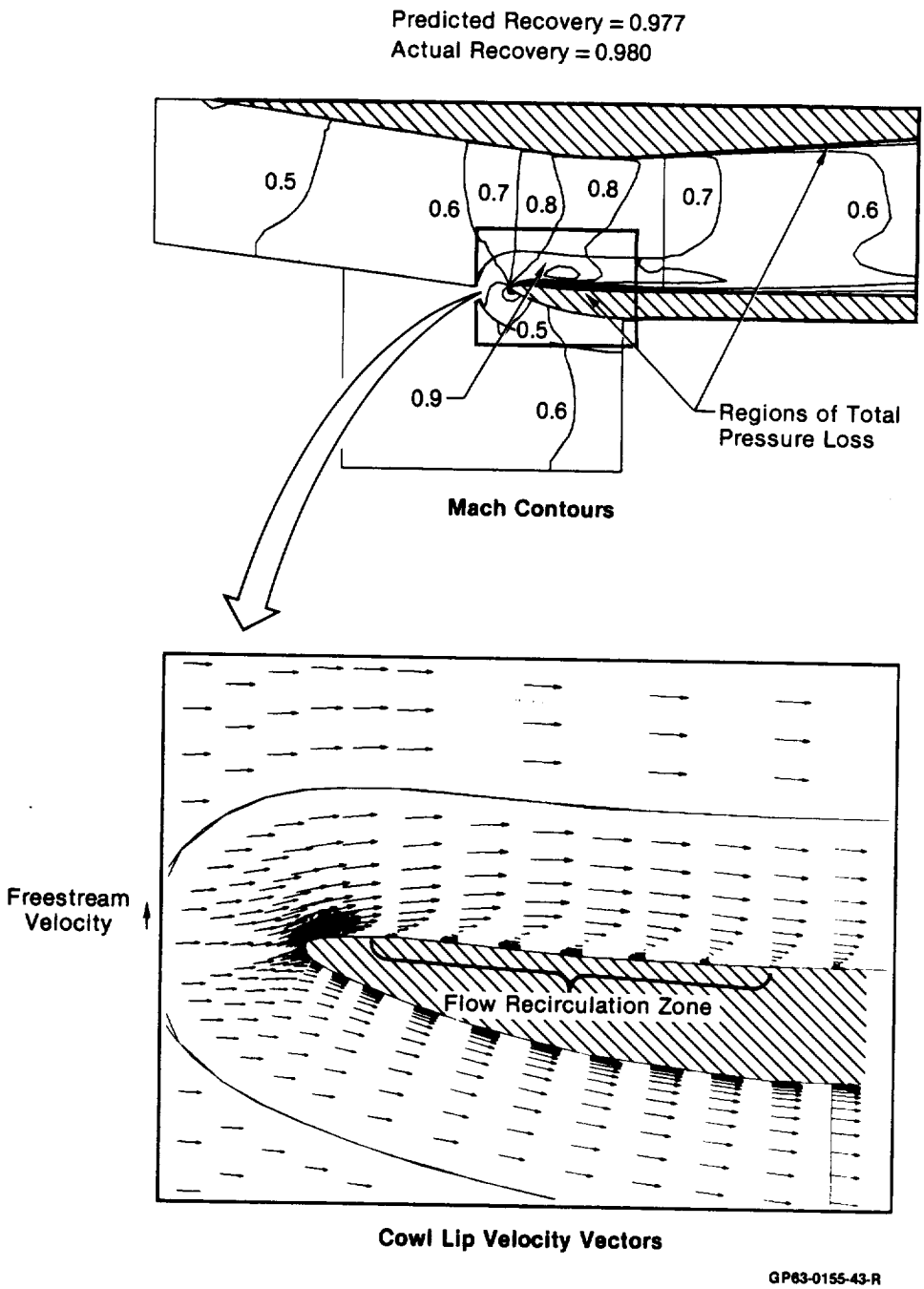

Figure 5-28. Baseline Configuration, Computed Flowfield
$M_0 = 0.6 \quad \alpha = 0°$

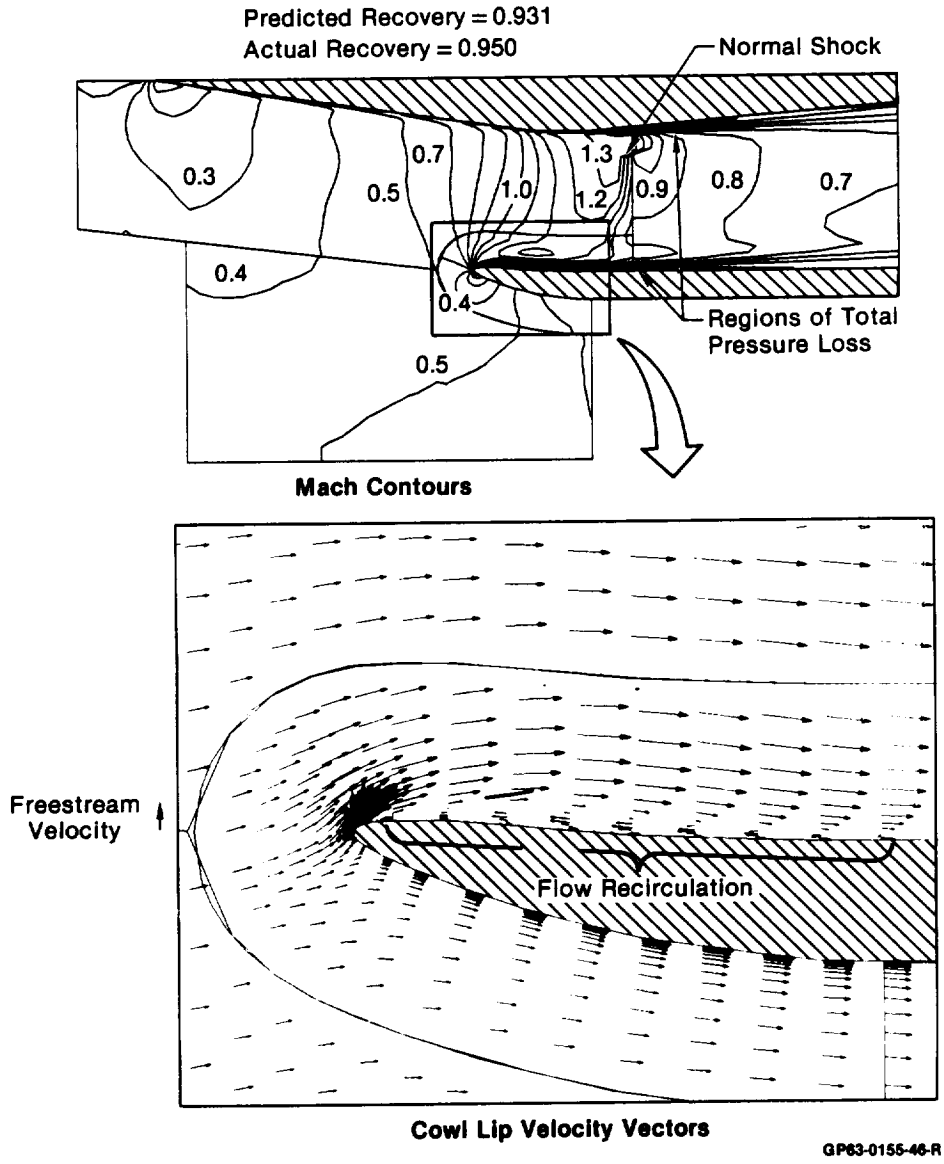

Figure 5-29. Baseline Configuration, Computed Flowfield
$M_0 = 0.6 \quad \alpha = 20°$

Computational Predictions, 20 Rotated Cowl Lip Configuration - Results of the 20° rotated cowl lip calculations show that the small region of separation visible in Figure 5-28 is eliminated by rotating the cowl lip downward and placing the stagnation streamline on the internal side of the cowl. Close inspection of the velocity vector plot in Figure 5-30 reveals that the stagnation point lies just above the highlight. This results in smooth flow on the internal side of the cowl lip with very little boundary layer growth. However, in this $\alpha = 0°$ case, the flow spilling around the leading edge cannot make the turn, resulting in separation outside the inlet. Although this region has no effect on inlet performance, it would affect cowl drag. Very little total pressure loss is indicated inside the inlet however, and the computed recovery compares well with experiment, Figure 5-30.

The flow field solution for the 20° rotated lip at $\alpha = 20°$ indicates that angle of attack performance can be improved through cowl rotation. There is attached flow everywhere on the cowl lip because the stagnation streamline is located on the cowl leading edge, Figure 5-31, and therefore the boundary layer growth present in the baseline case at angle of attack (Figure 5-29) is eliminated. Hence the throat does not choke and a normal shock does not form in the diffuser. These flow improvements are a direct result of the attached flow at the cowl lip. In addition, there is no external spill or separation due to spill, and therefore the drag penalty for the cowl rotation is minimal.

Computational Predictions, 40 Rotated Cowl Lip Configuration - The flow field solution of the 40° rotated lip at $\alpha = 0°$ is similar to that for the 20° lip in that the flow aligns itself with the internal cowl surface without separating near the leading edge, Figure 5-32. However, a new separation region formed at the knee of the rotated lip. The 40° turn from the cowl surface into the inlet throat is too great for the flow to remain attached. It is this excessive flow turning which is responsible for the poor total pressure recovery evident at the bottom of the engine face contour in Figure 5-20.

In addition to this internal separation, a large external region of separated flow is visible behind the rotated cowl, Figure 5-32. This is due to the placement of the stagnation streamline on the interior cowl surface, and the resulting flow expansion around the leading edge. There would be a drag penalty associated with this overrotation at small angles of attack due to this recirculation.

The flow field solution for the 40° rotated cowl lip at $\alpha = 20°$ identifies the same internal separation problem at the knee as in the $\alpha = 0°$ case. This is evident in Figure 5-33. Therefore the radius of curvature at the knee of this cowl lip is too small at any angle of attack.

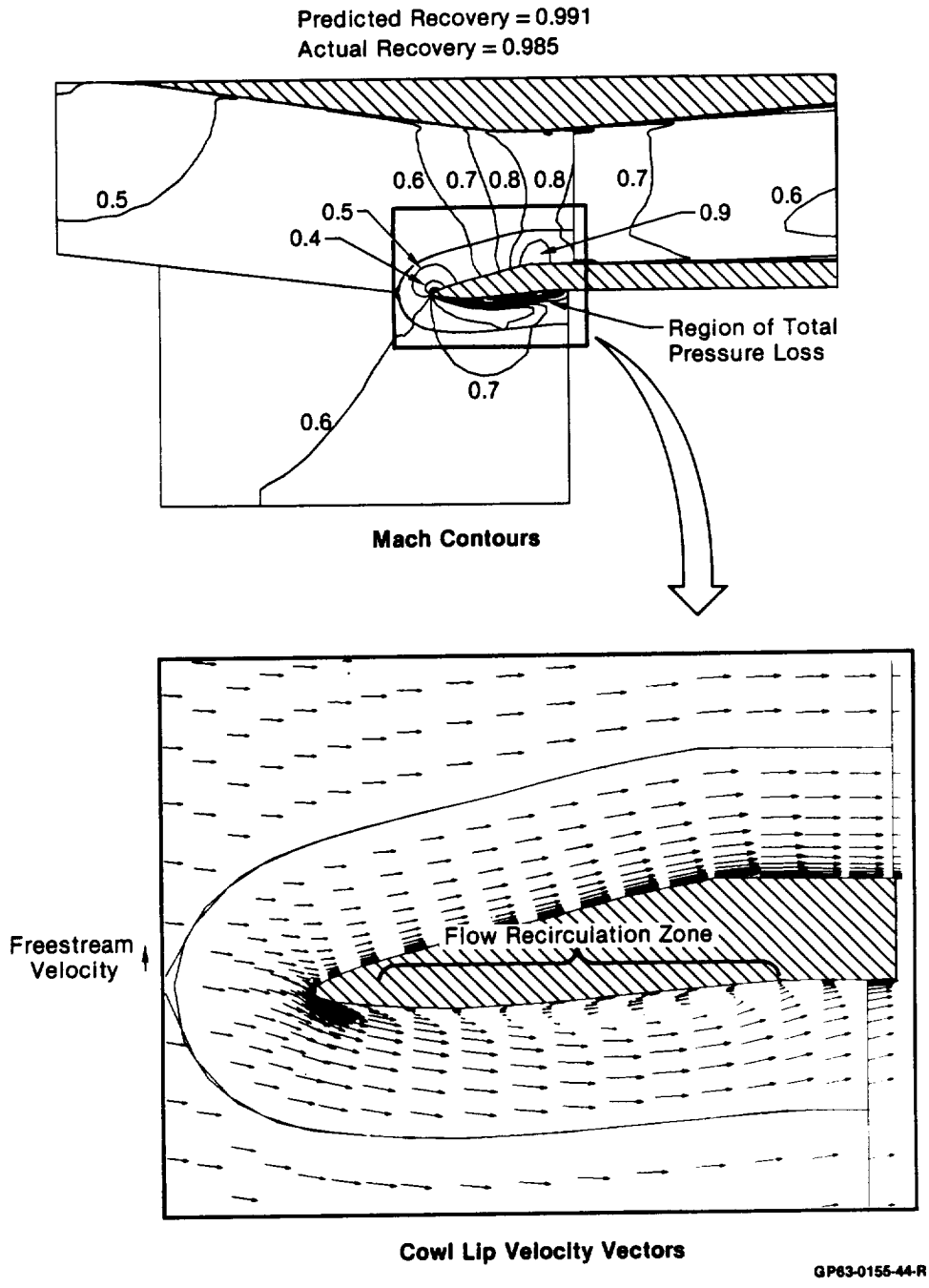

Figure 5-30. 20° Rotated Lip Configuration, Computed Flowfield
$M_0 = 0.6 \quad \alpha = 0°$

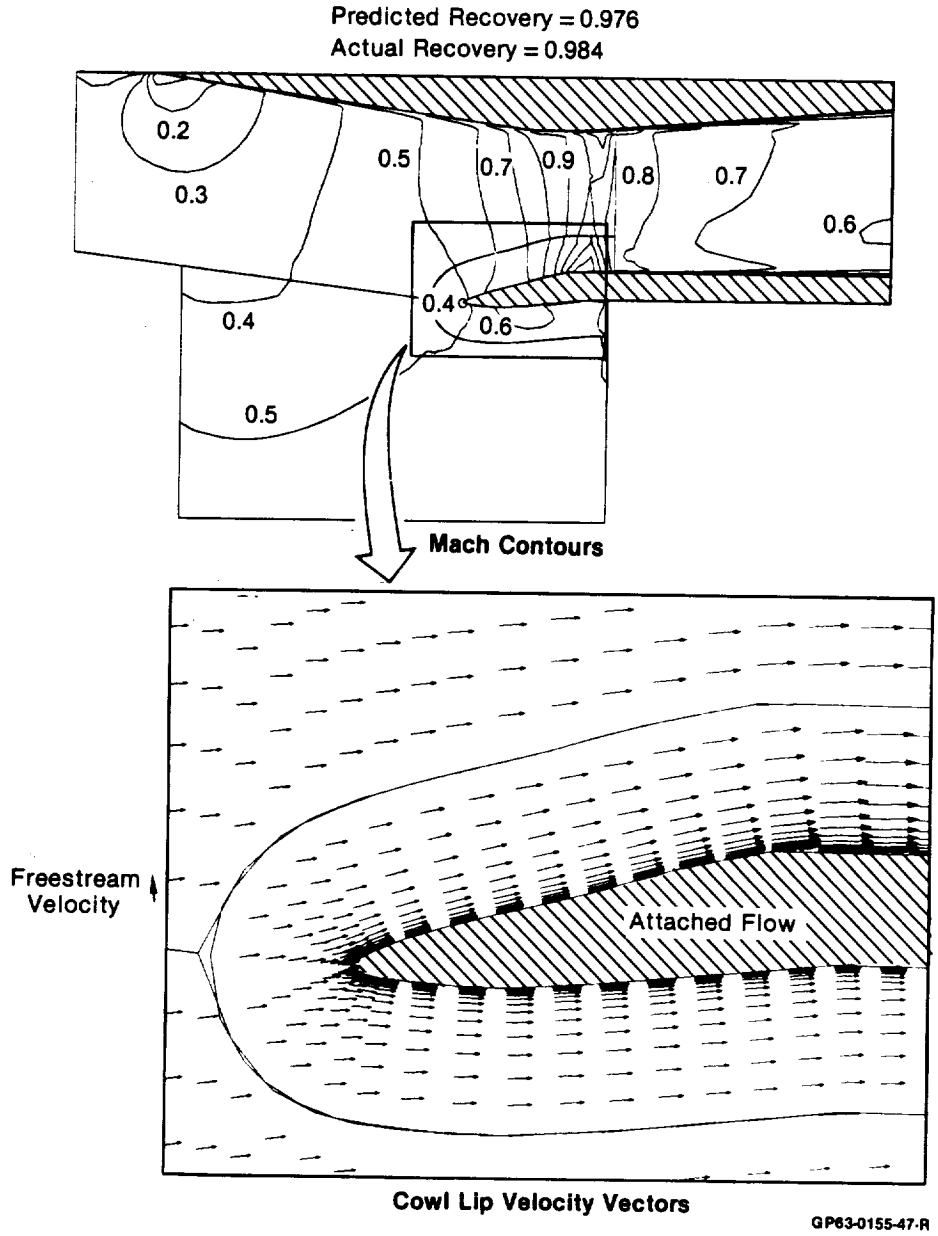

Figure 5-31. 20° Rotated Lip Configuration, Computed Flowfield
$M_0 = 0.6 \quad \alpha = 20°$

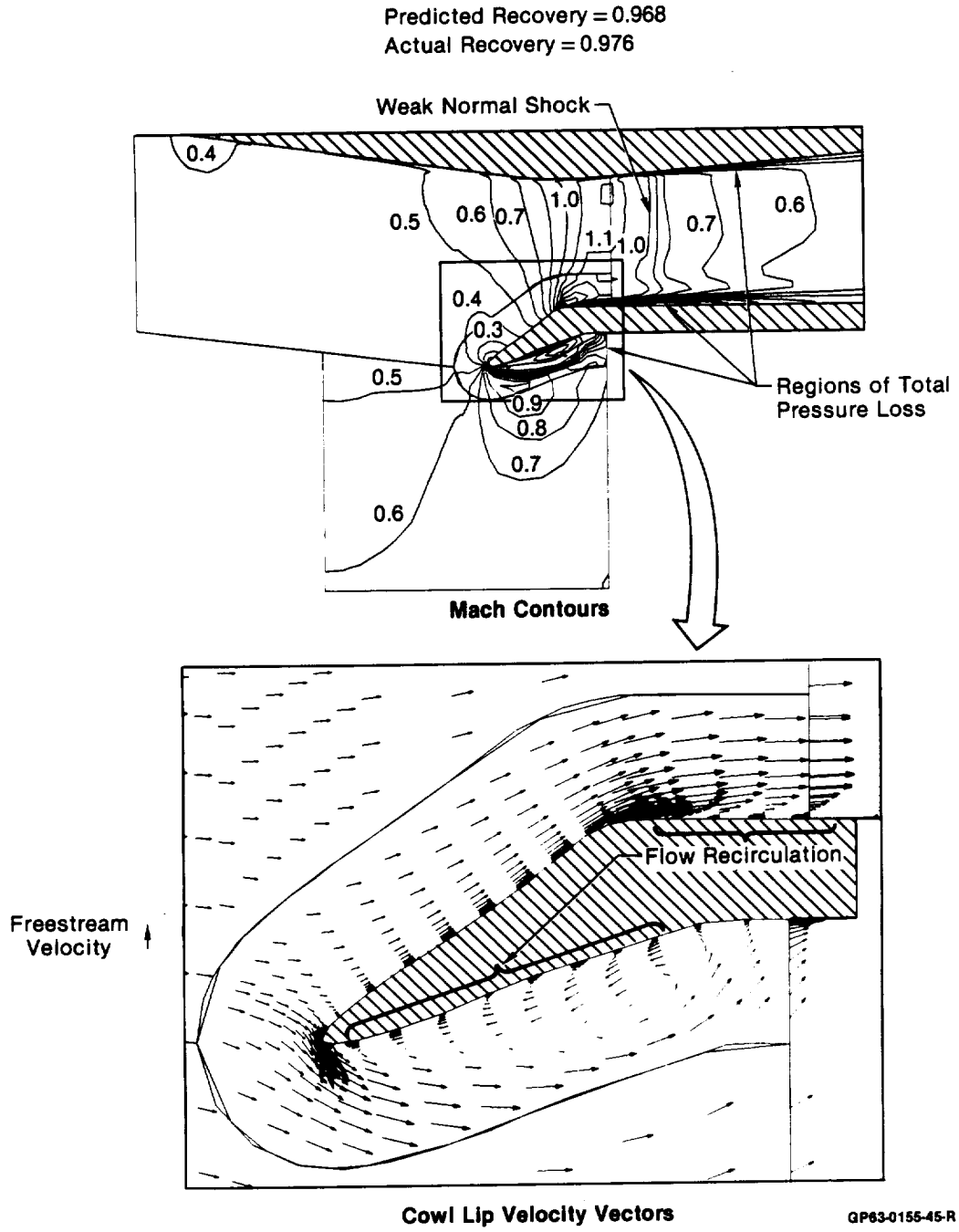

Figure 5-32. 40° Rotated Lip Configuration, Computed Flowfield
$M_0 = 0.6 \quad \alpha = 0°$

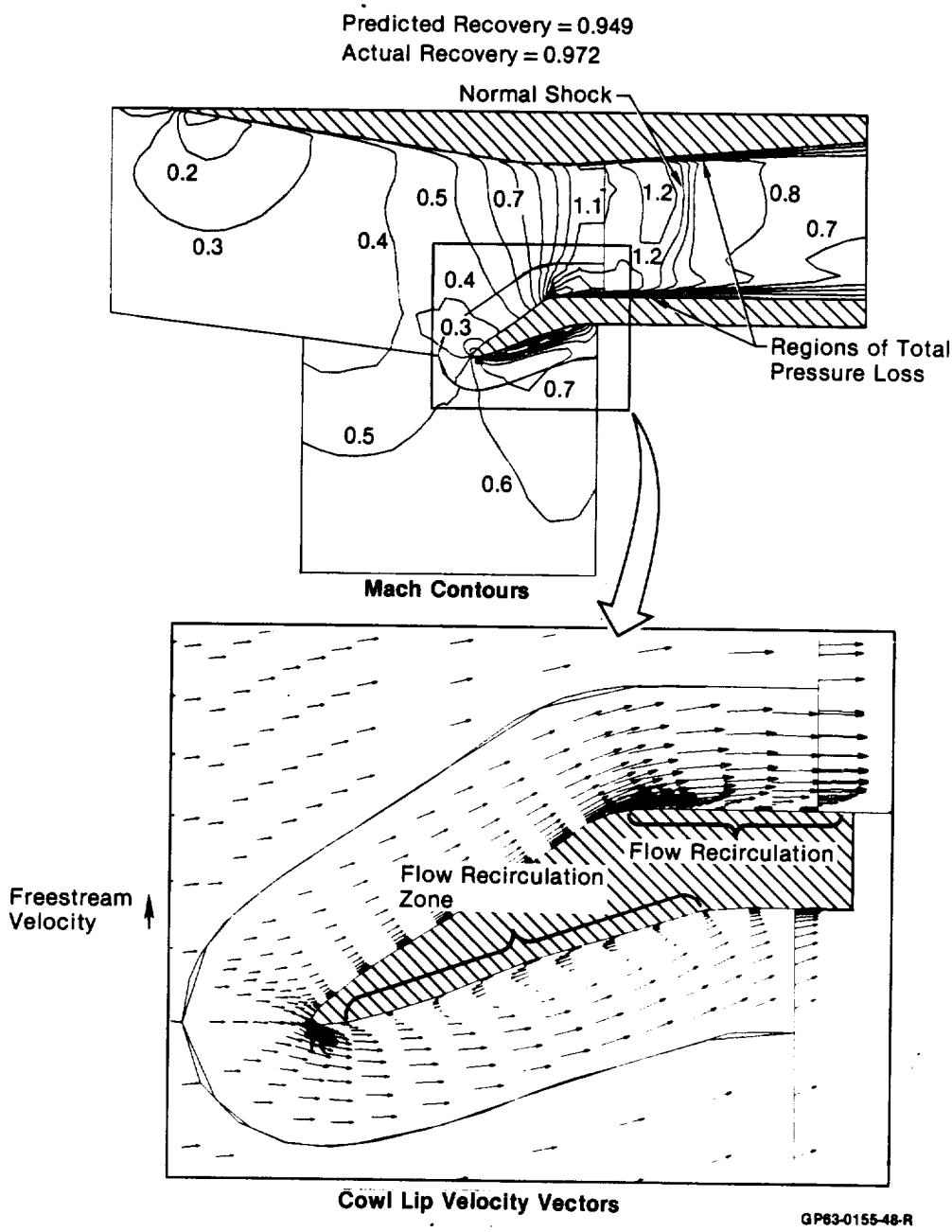

Figure 5-33. 40° Rotated Lip Configuration, Computed Flowfield
$M_0 = 0.6 \quad \alpha = 20°$

Summary of Computational Results - These computations illustrate that close attention must be given to the amount of flow turning at both the cowl highlight and the pivot point of the cowl lip. At supersonic Mach numbers, the cowl lip is usually designed so that it is closely aligned with the last compression ramp. At subsonic Mach numbers, however, the stagnation streamline would fall below the highlight, causing the flow separation seen in Figure 5-29. A fixed cowl lip designed for supersonic operation will therefore be susceptible to performance loss subsonically. This indicates the need for cowl lip rotation at angle of attack. However, overrotation can cause internal flow separation at the knee as seen in Figure 5-33.

For any rotating cowl lip design to aehieve optimum performance, there must be a proper balance between the elimination of lip separation and preventing the onset of separation at the cowl lip knee. This may necessitate a large pivot point radius or a translating/rotating lip design to maximize the flow turning angle. The increased weight associated with the latter would have to be carefully balanced against the resulting performance improvements before making the final design choice.

Verification of Code Accuracy - The accuracy of the flow field solutions was assessed by comparing the analytically predicted pressures on the cowl lips to the experimentally determined surface pressures. Two cases are of particular interest, the Baseline configuration at $\alpha = 20°$, and the 40° rotated lip configuration at $\alpha = 0°$. A comparison of the predicted and experimental cowl lip surface pressures is shown for these two cases in Figure 5-34. In both solutions, note that the code accurately predicted the location and pressure level of the stagnation point. Of particular interest is that the surface pressures on the Baseline cowl, both internally and externally, show excellent agreement with experiment, even though there is significant flow separation internally (see Figure 5-29).

On the 40° rotated cowl lip, the internal predicted pressures also compare well with the wind tunnel data, Figure 5-34. However, there is a significant difference between test and prediction on the external side of the cowl. Recall that there is severe flow recirculation in this region (Figure 5-32). This occurance is predicted by the code, though the actual pressure level is less reliable. The reason for this discrepancy can be understood by a more detailed examination of the surface pressure ratio plotted in Figure 5-34.

The local static pressure divided by the freestream total pressure can be divided up in the following way:

$$\frac{P_{S_{local}}}{P_{T_o}} = \frac{P_{S_{local}}}{P_{T_{local}}} \quad \frac{P_{T_{local}}}{P_{T_o}} \quad .$$

The first factor in the above is only a function of the local Mach number; the second is simply the local total pressure recovery. The lower predicted pressures of Figure 5-34 are due to the tendency of the code to overpredict the local toal pressure loss in regions of highly separated flow. However, the fact that the code is able to predict the occurance and location of these recirculation zones makes it a highly useful design and analysis tool.

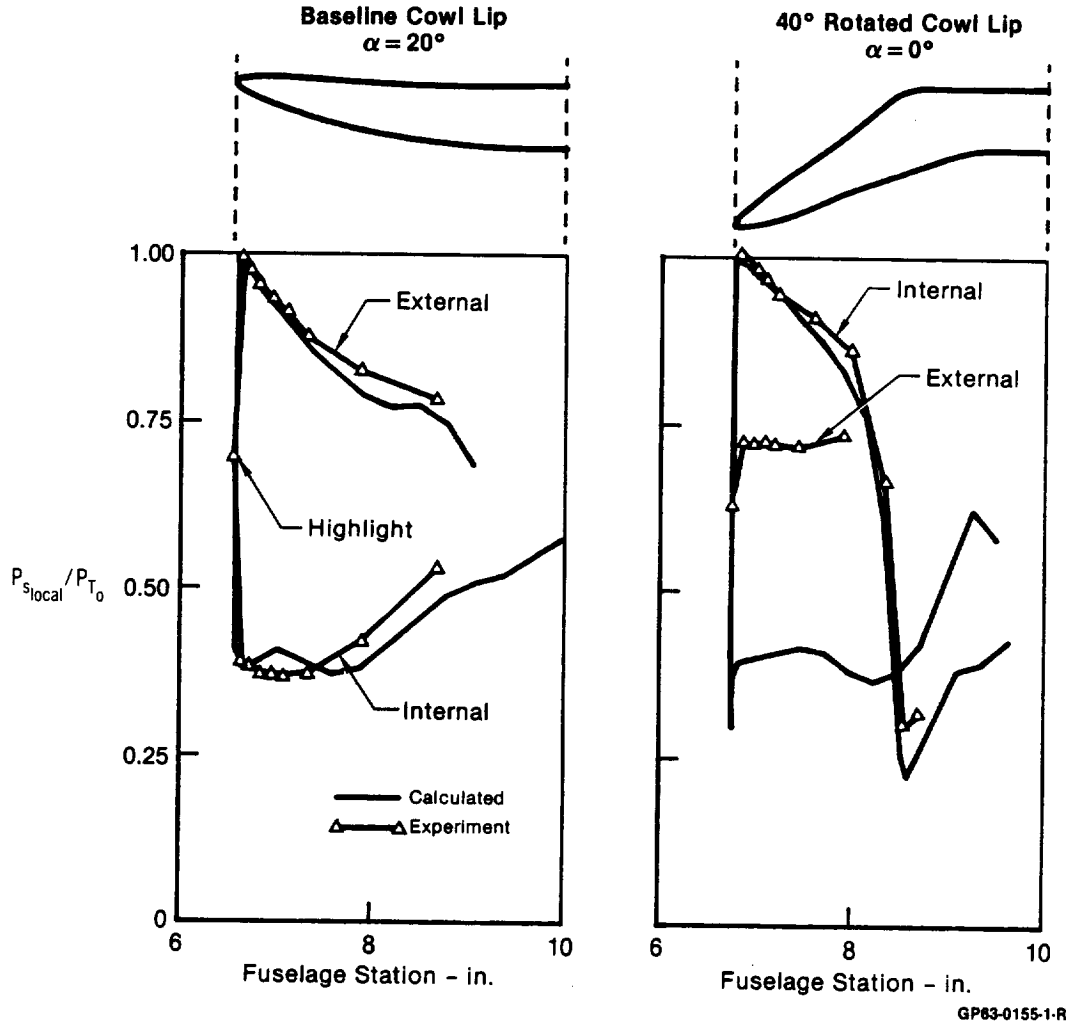

Figure 5-34. Comparison of Predicted and Experimental Cowl Lip Static Pressures
$M_0 = 0.6$

5.1.3 2-D Auxiliary Inlet Performance - Three auxiliary inlet configurations were tested on the lower side of the 2-D inlet model. The first configuration had an auxiliary inlet which was flush with the bottom of the inlet. The second configuration, which was also flush, had a new geometry on the aft ramp of the auxiliary inlet. This was the elliptical ramp mentioned in Section 3.1.2. The final concept included an external scoop. Testing was conducted at Mach numbers of 0.6 and 0.9. Recall that the baseline inlet for these investigations is the long diffuser configuration.

Mach 0.6 - The Mach 0.6 testing shows that auxiliary inlets provide a small performance improvement at very high angles of attack. These results, shown in Figure 5-35, also include the baseline inlet with a bleed system for comparison. The auxiliary inlet with external scoop has the best performance of all the auxiliary inlet concepts. At the highest angles of attack, it increases recovery 4% over the baseline inlet. The flush auxiliary inlets had recovery levels approximately 1% below that of the external scoop. The performance of the two flush auxiliary inlet configurations were nearly identical in both recovery and turbulence, indicating that the aft ramp geometry did not have a great impact on auxiliary inlet performance.

Mach 0.9 - Opening auxiliary inlets at Mach 0.9 reduced 2-D inlet performance. This decreased inlet recovery by 2% and increased turbulence by 30% at all angles of attack, Figure 5-36. The external scoop provided no significant performance benefit over the flush auxiliary inlet configurations.

At Mach 0.9, the external static pressure is less than the internal static pressure, and this may result in reverse flow through the auxiliary inlets. In addition, the baseline 2-D inlet performance is so high that the total pressure losses through the auxiliary inlets may be greater than through the main inlet duct.

Mach 1.2 - A very limited amount of testing was conducted on the external scoop configuration at Mach 1.2, using angles of attack of 20° and 25°. The external scoop decreased inlet performance at this speed as well. No other 2-D auxiliary inlet configurations were tested at Mach 1.2.

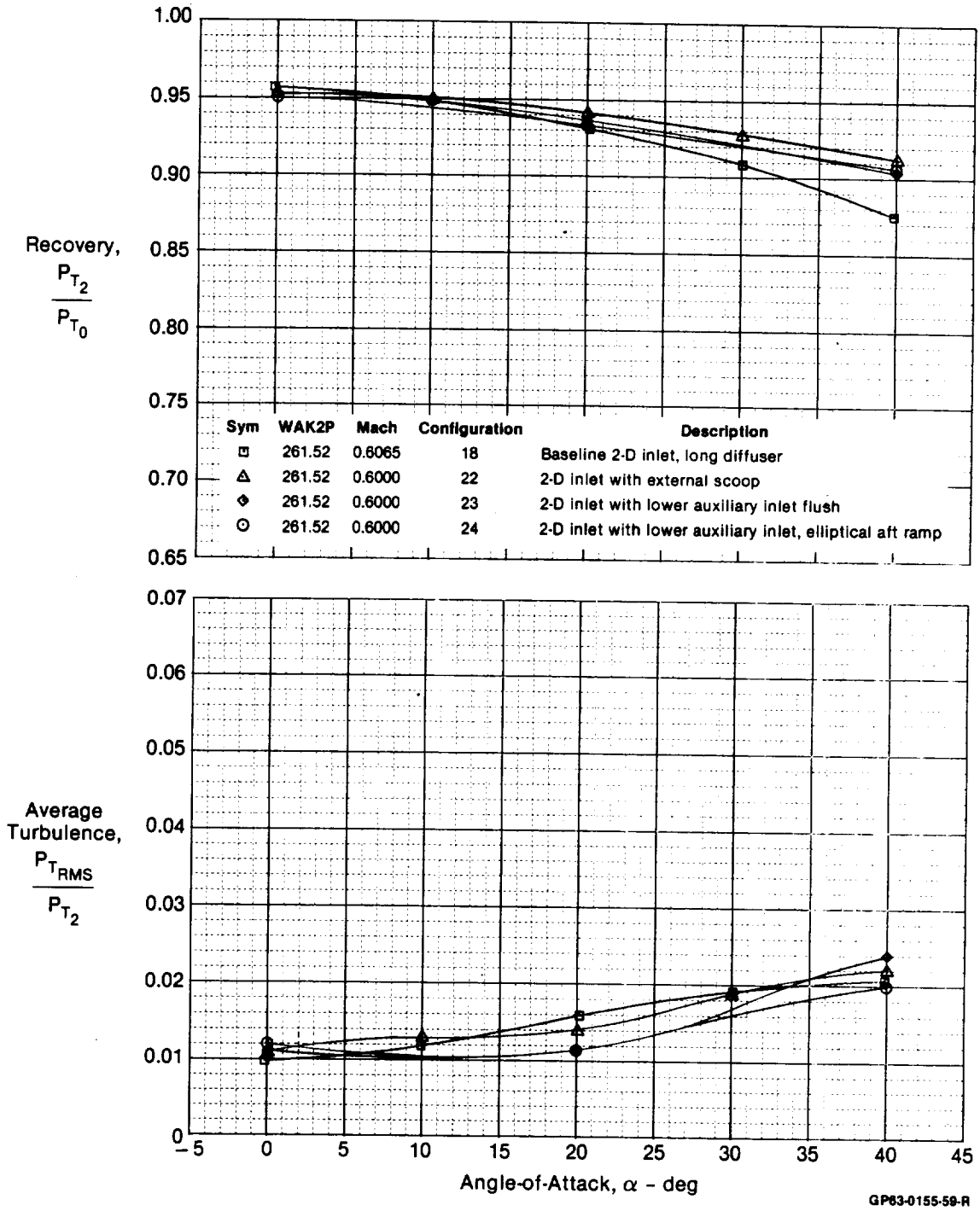

Figure 5-35. Effect of Opening Auxiliary Inlets on 2-D Inlet Recovery and Average Turbulence
$M_0 = 0.6$

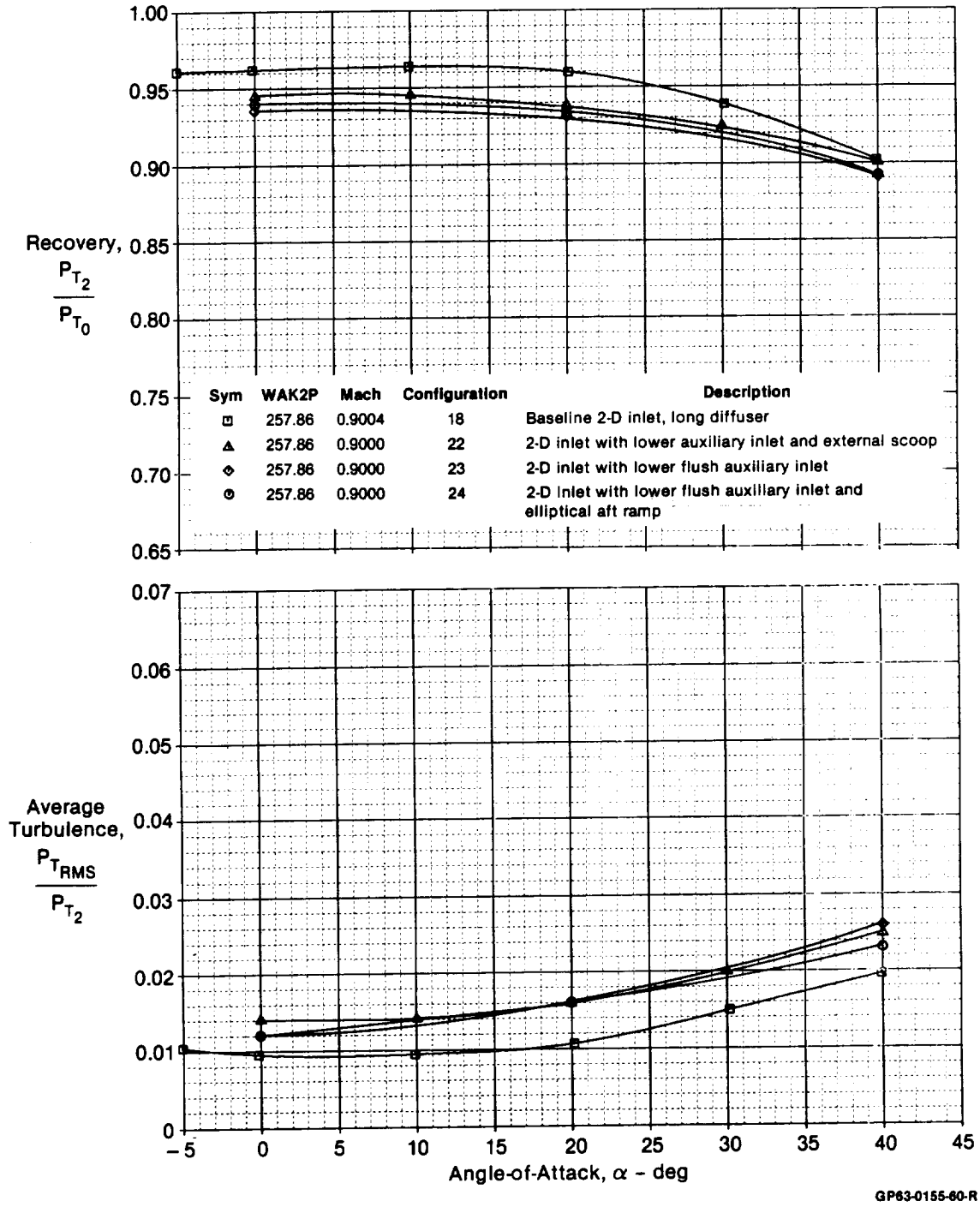

Figure 5-36. Effect of Opening Auxiliary Inlets on 2-D Inlet Recovery and Average Turbulence
$M_0 = 0.9$

5.2 AXISYMMETRIC INLET PERFORMANCE - Rotating cowl lip and auxiliary inlet tests were performed with the MCAIR 10% scale axisymmetric inlet. A retracted centerbody was also investigated. Testing was conducted at Mach numbers of 0.6, 0.9, 1.2, and 1.4.

Performance trends at Mach 0.6 and 0.9 are very similar, as are Mach 1.2 and 1.4 results. Results at Mach 0.9 and 1.4 will therefore be used to summarize typical subsonic and transonic performance trends.

5.2.1 Baseline Axisymmetric Inlet Performance

Mach 0.9 Performance - The baseline configuration performed reasonably well at angles of attack from 0° to 20°. Total pressure recovery varied from 0.965 to 0.935 over this angle of attack range, Figure 5-37. Average turbulence was also relatively low, remaining essentially constant at 0.01. At angles of attack beyond 20° the performance of the axisymmetric inlet decreased rapidly.

Steady state distortion levels were 43% to 65% of the limit over the range as illustrated in Figure 5-38. The distortion levels increased with angle of attack up to 30°. Above 30°, the separated flow completely filled the inlet and distortion reached a maximum, thereafter remaining essentially constant.

The engine face total pressure recovery contour plot for $\alpha = 0°$, shown in Figure 5-39, indicates that the primary sources of inlet distortion were the three struts supporting the centerbody, as well as boundary layer development along the diffuser duct. The locations of the struts are shown in the contour plot at $\alpha = 0°$. The effects of the strut wakes are clearly seen on the pressure contours.

The $\alpha = 0°$ contour plot also shows a large pressure gradient near the outer wall of the duct. This is a result of the boundary layer growth along the duct walls. There is no evidence of a large boundary layer buildup along the inlet centerbody. This is possibly due to the expansion of the flow on the downstream end of the centerbody.

The baseline subsonic performance declined rapidly at angles of attack greater than 20°. The rapid loss in recovery and increase in turbulence at high angles of attack is typical of other axisymmetric inlet test results.

In the 20° to 40° angle of attack range, the flow separated over the cowl lip resulting in large total pressure losses on the lower cowl. The corresponding decrease in total pressure recovery on the lower half of the engine face can be seen in the $\alpha = 20°$ contour of Figure 5-39. However, just above the hub recovery remained in the 98% to 100% range at 20° angle of attack, indicating the absence of separation off the centerbody up to this value.

Decrease in inlet performance up to 20° angle of attack appears to be due solely to cowl lip separation. However, at $\alpha = 40°$, separated flow off the cowl lip and centerbody completely spanned the engine face height.

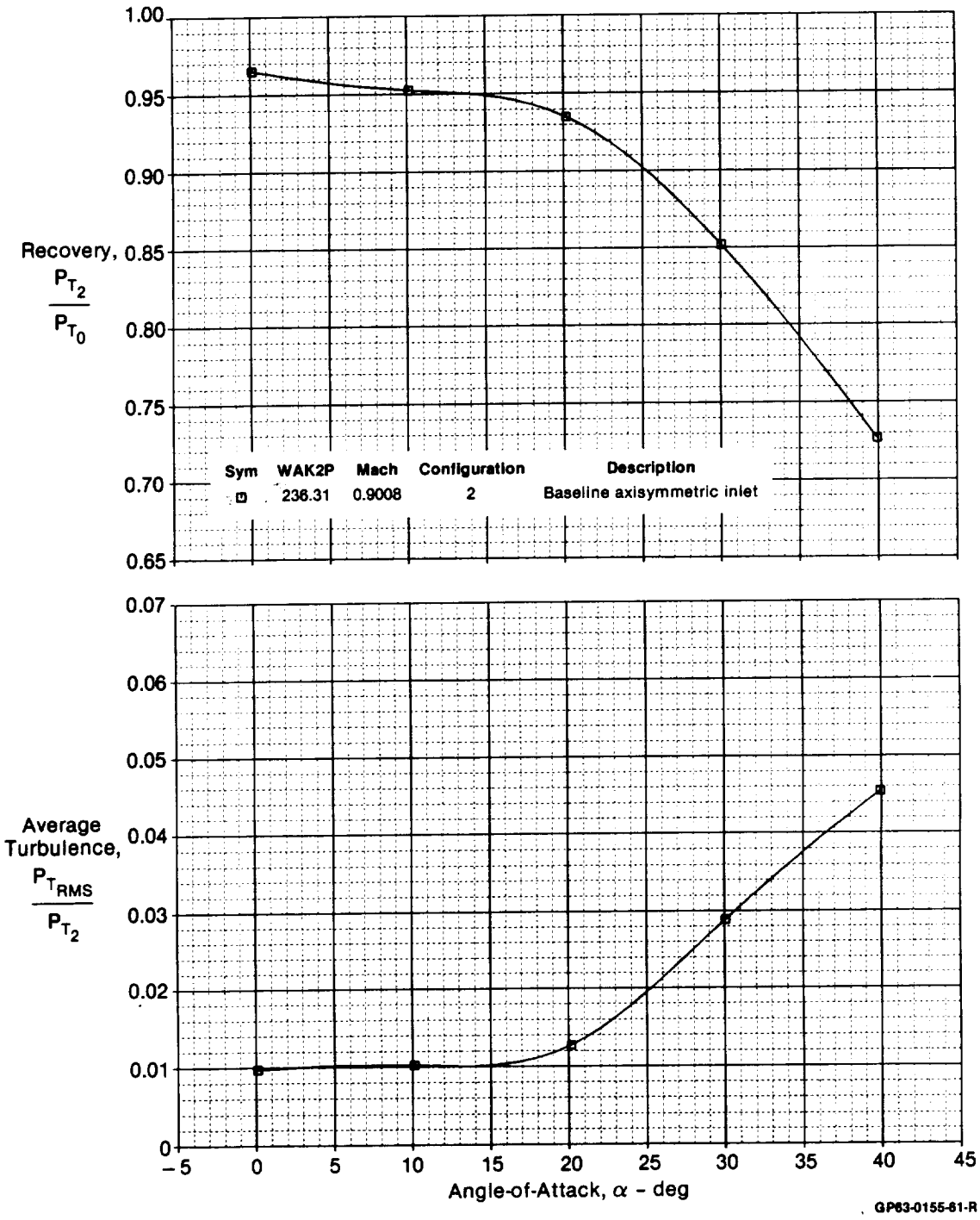

Figure 5-37. Baseline Axisymmetric Inlet Recovery and Average Turbulence vs Angle-of-Attack
$M_0 = 0.9$

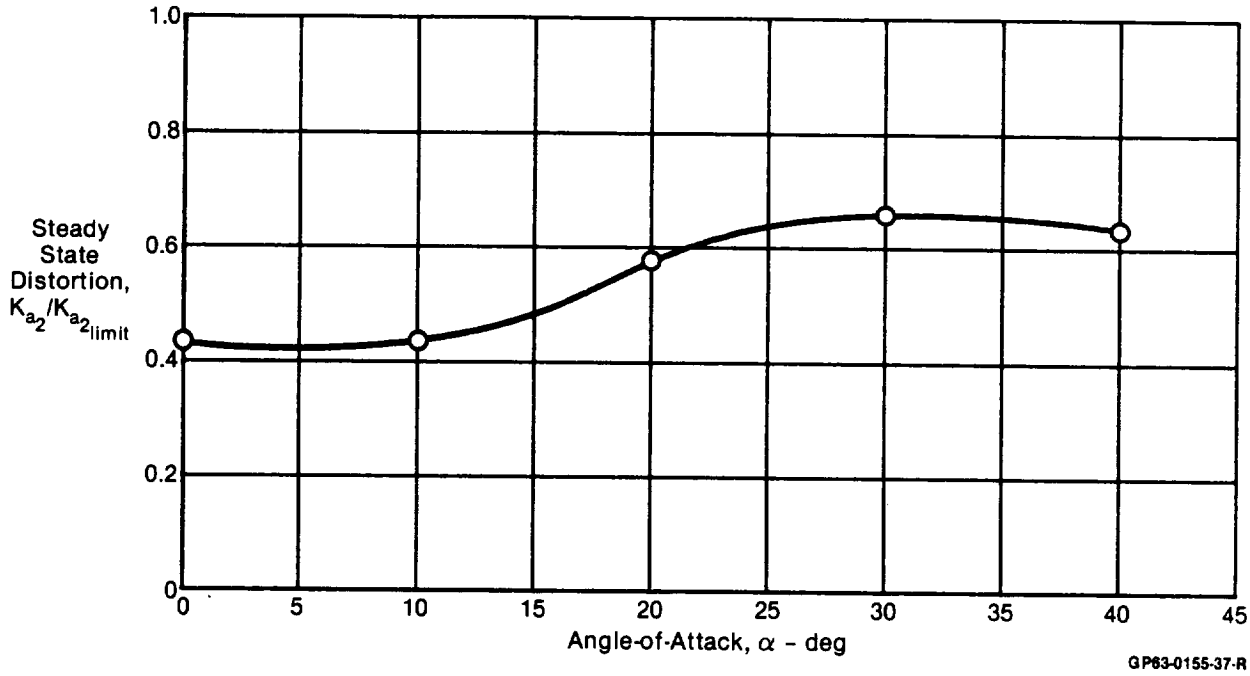

Figure 5-38. Baseline Axisymmetric Inlet Distortion
Mach 0.9

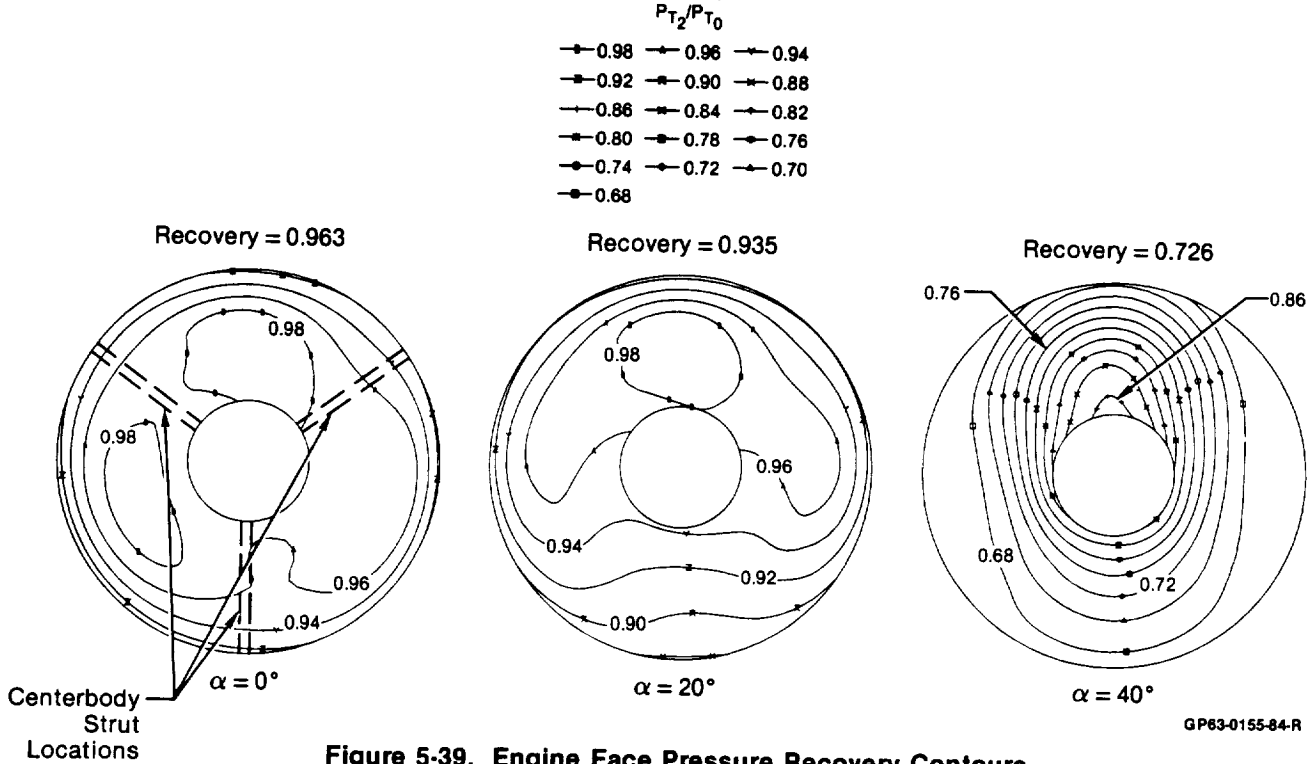

Figure 5-39. Engine Face Pressure Recovery Contours
Baseline Configuration Axisymmetric Inlet
$M_0 = 0.9$

Mach 1.4 Performance - The recovery of the baseline inlet was 0.94 at $\alpha = 0°$, and remained constant up to $\alpha = 15°$, Figure 5-40. There was an additional 2% loss at $\alpha = 20°$. The lower recovery at Mach 1.4 is simply due to the conical shock attached to the centerbody cone. The sonic line downstream of the shock was predicted to lie just inside the cowl lip, and therefore the inlet at Mach 1.4 performs in a similar fashion as in the Mach 0.9 case, except for the additional shock loss.

The total pressure field produced by the inlet at the engine face is very similar to the Mach 0.9 case. The only difference is that the recovery is uniformly decreased over the entire engine face. This becomes evident by comparing the contours of Figure 5-41 to 5-39. This observation is consistent with the above assumption that the only additional pressure loss mechanism is the conical shock attached to the centerbody.

Inlet distortion at Mach 1.4 is a weak function of angle of attack, increasing from 32% to 43% of the limit through an alpha range of 0° to 20°. These results are shown in Figure 5-42.

5.2.2 Rotating Cowl Lip Effects - Cowl lip rotation angles of 20° and 40° were tested over a Mach range of 0.6 to 1.4. Additionally, a configuration simulating the rotated lip in the retracted position was tested. This was to quantify the effects of retracted sideplates on the otherwise baseline configuration arrangement.

Mach 0.9 Results - The 20° rotated lip provided the best performance over the entire angle of attack range tested. Recovery and turbulence characteristics are the same as the baseline inlet out to $\alpha = 15°$, Figure 5-43. However, performance remains constant out to 25° angle of attack, while the baseline performance above 15° angle of attack begins to decline rapidly.

The 20° rotated cowl lip improves performance significantly at angles of attack greater than 20°. The recovery level at $\alpha = 40°$ was increased 20%, Figure 5-43. Turbulence was also reduced by 50%.

Rotating the lip 40° degrades inlet performance at low angles of attack. From 0° to 25°, recovery is 2% to 4% lower than the baseline. Turbulence is 60% to 80% higher than the baseline level. Thus, overrotation of the lip at low angles of attack decreases inlet performance.

The 40° rotated cowl lip has higher recovery and lower turbulence than the baseline inlet above 25° angle of attack. However, the 40° cowl lip performance is lower than the 20° lip at all angles of attack. At angles of attack above 30°, the rate of recovery loss is less. Based upon the data trends in Figure 5-43, the 40° lip would outperform the 20° lip above 40° angle of attack. These results indicate that optimum performance is achieved by setting the lip rotation angle to values substantially less than the inlet angle of attack.

Steady state distortion is reduced at high angles of attack by rotating the cowl lip. Distortion was reduced nearly 20% at $\alpha = 40°$ with the 20° and 40° rotated lip, Figure 5-44. The decrease in distortion is mainly a result of reduced flow separation around the cowl lip and centerbody. At low angles of attack, where there is no lip separation problem, the rotated lip tends to destroy the flow symmetry of the baseline inlet, Figure 5-45.

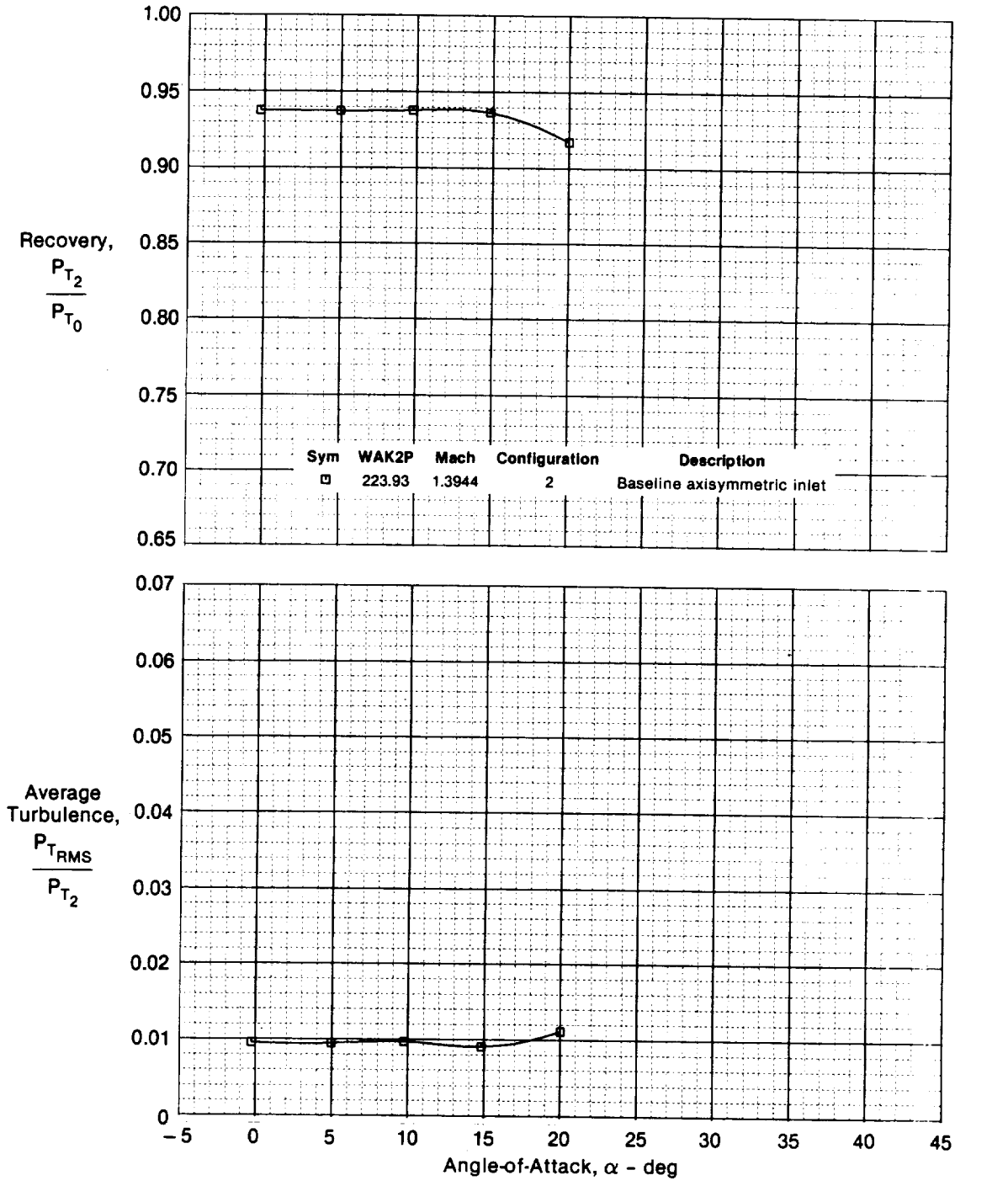

Figure 5-40. Baseline Axisymmetric Inlet Recovery and Average Turbulence vs Angle-of-Attack
$M_0 = 1.4$

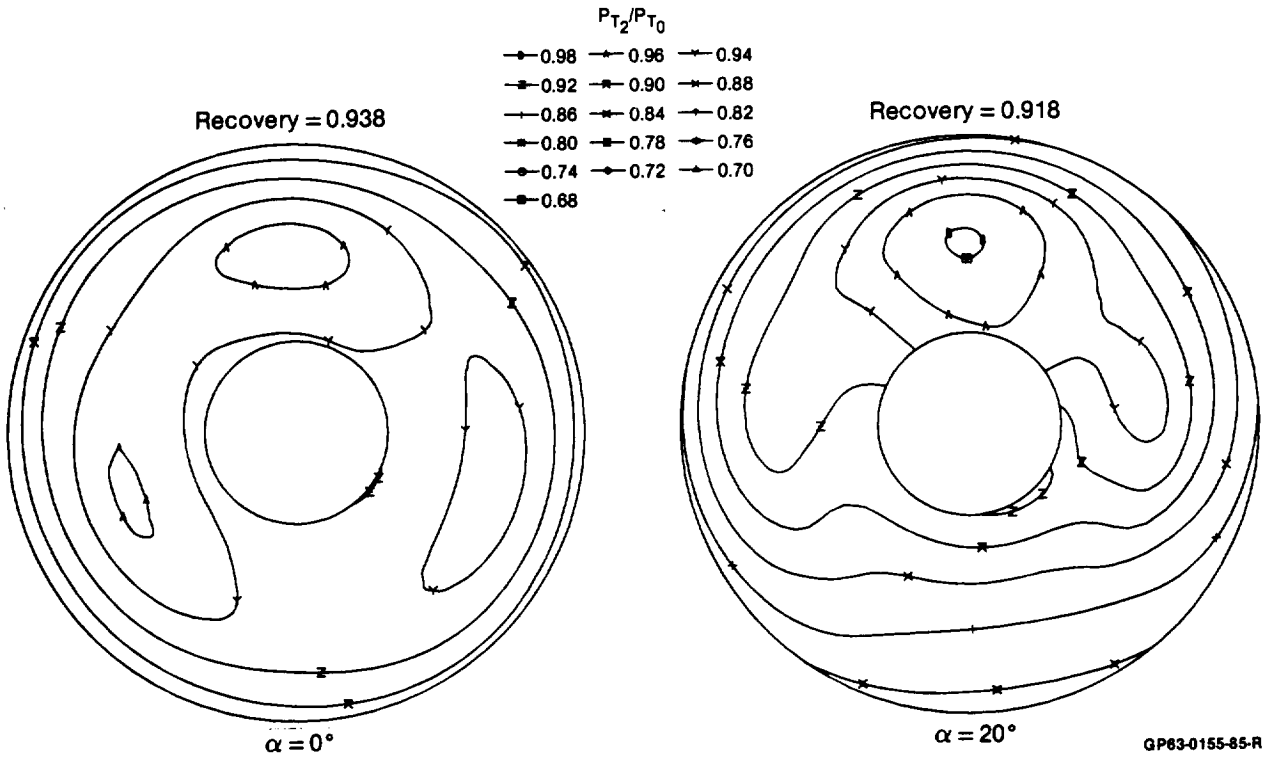

Figure 5-41. Axisymmetric Inlet Engine Face Pressure Recovery Contours
Baseline Configuration $M_0 = 1.4$

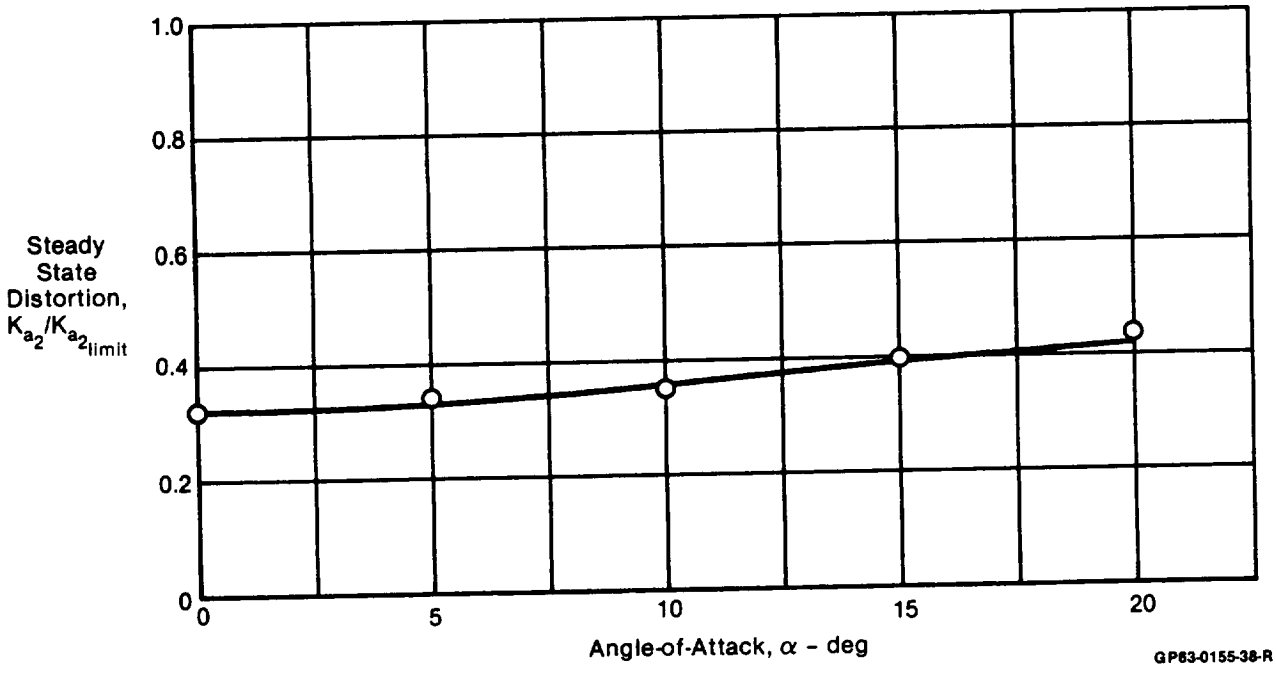

Figure 5-42. Baseline Axisymmetric Inlet Distortion
Mach 1.4

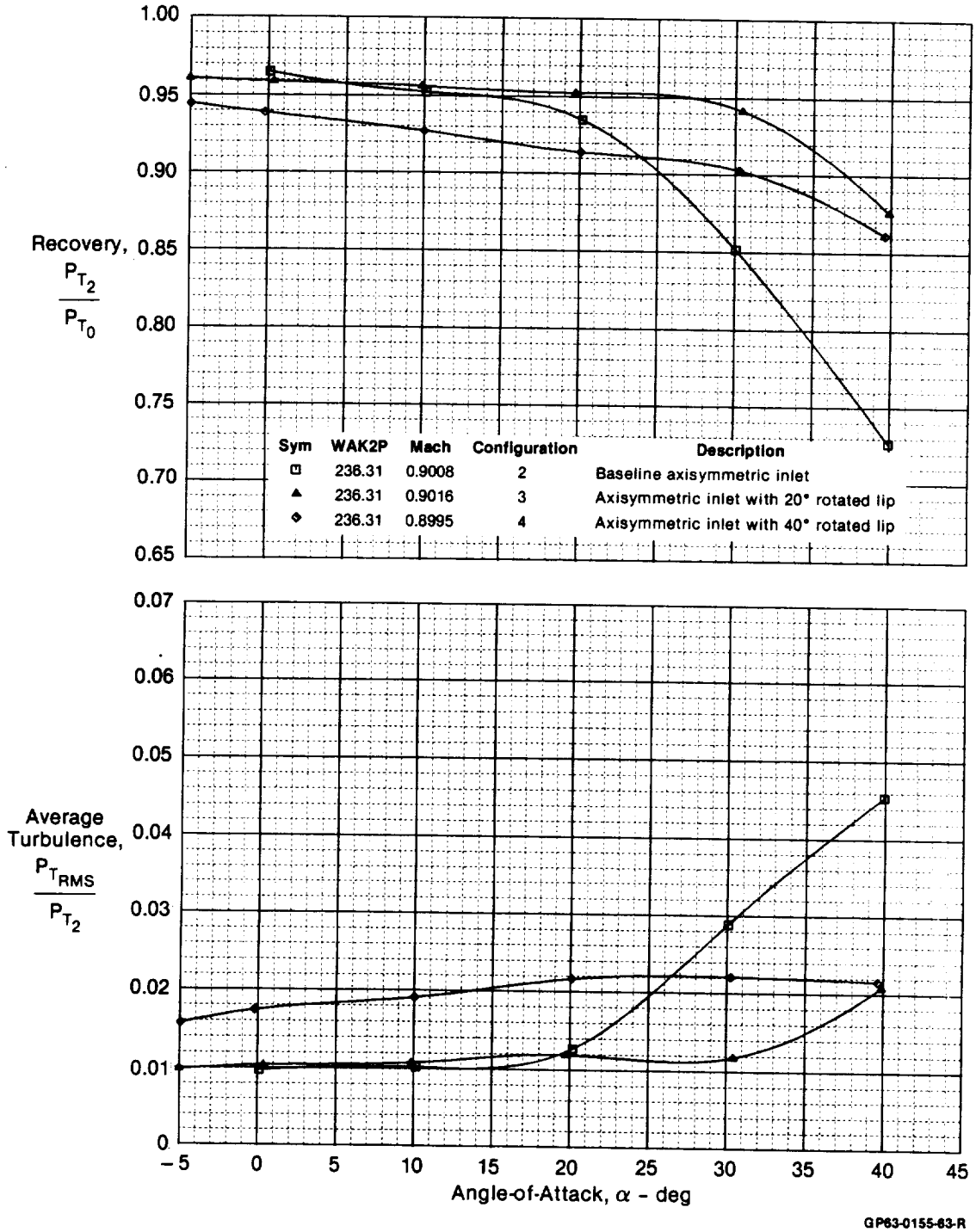

Figure 5-43. Effect of Rotating Cowl Lip on Axisymmetric Inlet Recovery and Average Turbulence
$M_0 = 0.9$

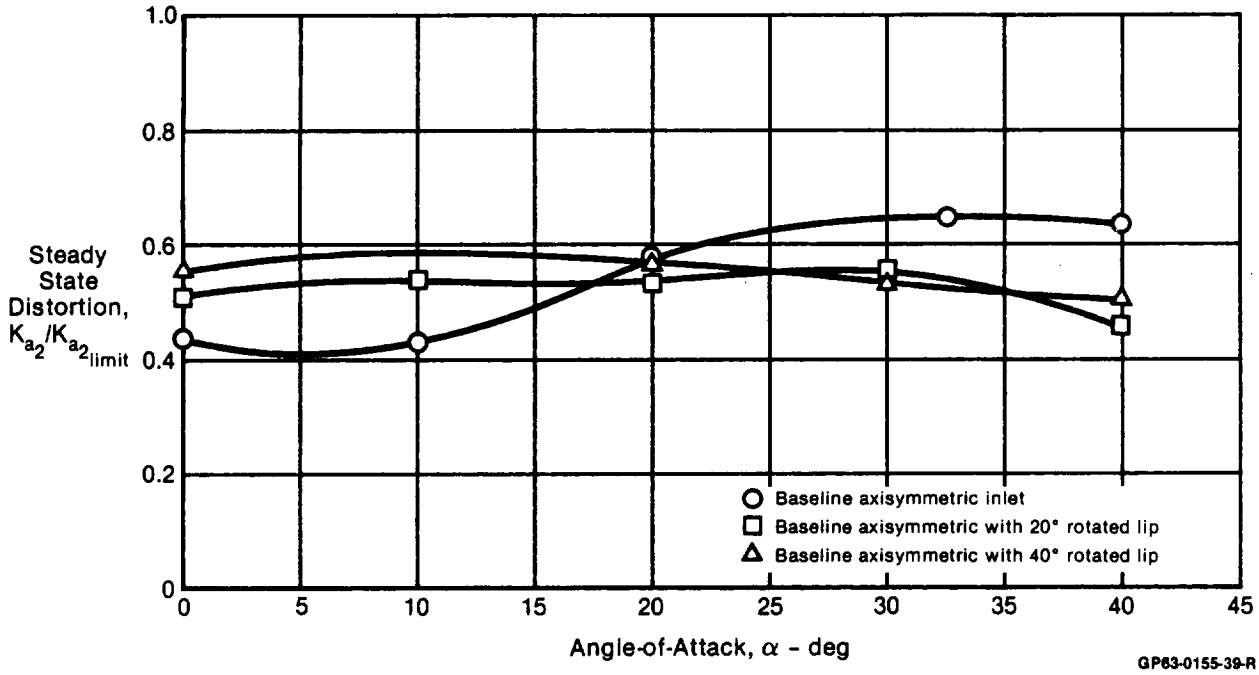

Figure 5-44. Effect of Rotating the Cowl Lip on Axisymmetric Inlet Distortion
Mach 0.9

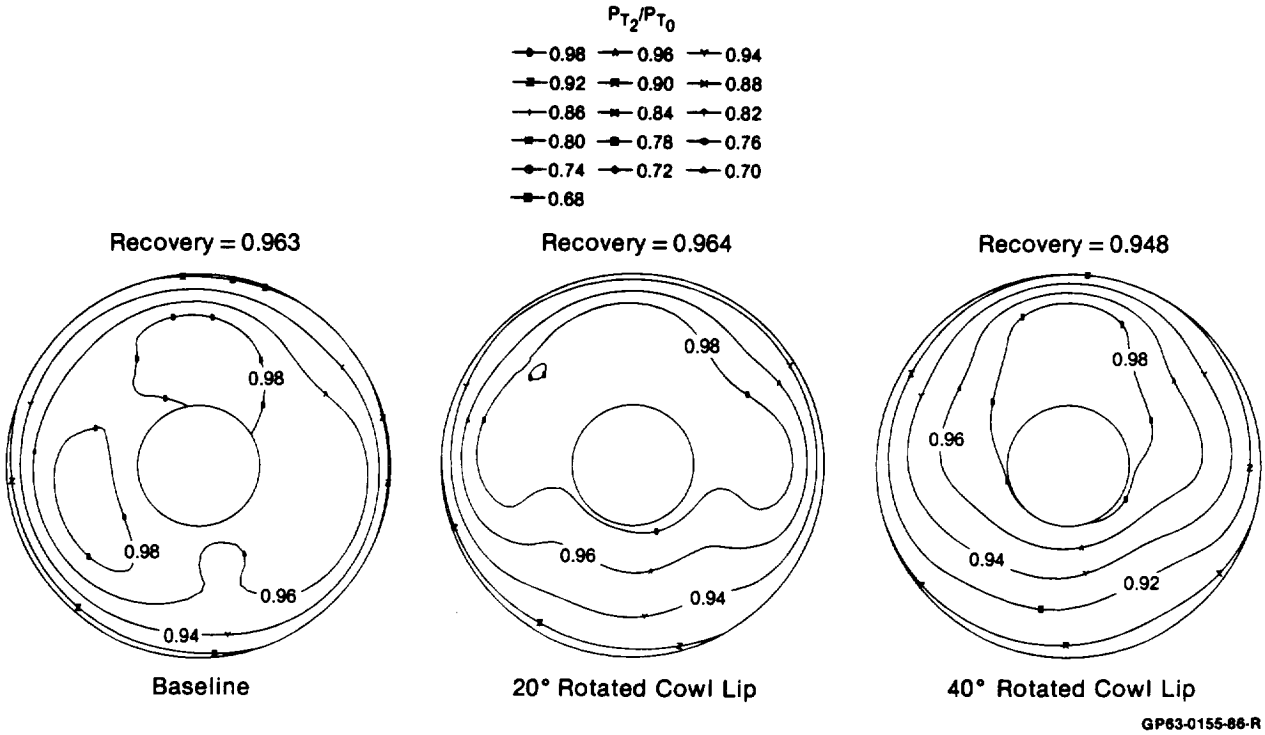

Figure 5-45. Comparison of Axisymmetric Inlet Engine Face Pressure Recovery Contours
Baseline and Rotated Cowl Configurations $M_0 = 0.9$ $\alpha = 0°$

Engine face total pressure contours indicate that the rotated lips may induce flow separation at small angles of attack and reduce it at high angles of attack. Figure 5-45 shows pressure contours for the baseline, 20°, and 40° lips at $\alpha = 0°$. Lower total pressures prevail on the lower half of the engine face of the rotated lips. Average recovery levels are correspondingly lower. This indicates separation at the knee of the rotated cowl, similar to that encountered in the 2-D inlet. As illustrated by the pressure contours in Figure 5-46, the cowl lip of the baseline inlet at $\alpha = 40°$ is completely separated. The rotated lips, however, do not show this severe separation.

The 20° and 40° rotated lips discussed thus far had a slightly blunter cowl lip than the baseline. In order to determine the effect of this cowl lip geometry, the 40° rotated lip was tested using the sharper contour of the baseline axisymmetric inlet at 0°, 20°, and 40° angles of attack and a free-stream Mach number of 0.9. Figure 5-47 indicates nearly identical recovery and turbulence levels between the two lip contours. The shape of the lip therefore does not have a great impact on inlet performance within the range of these tests.

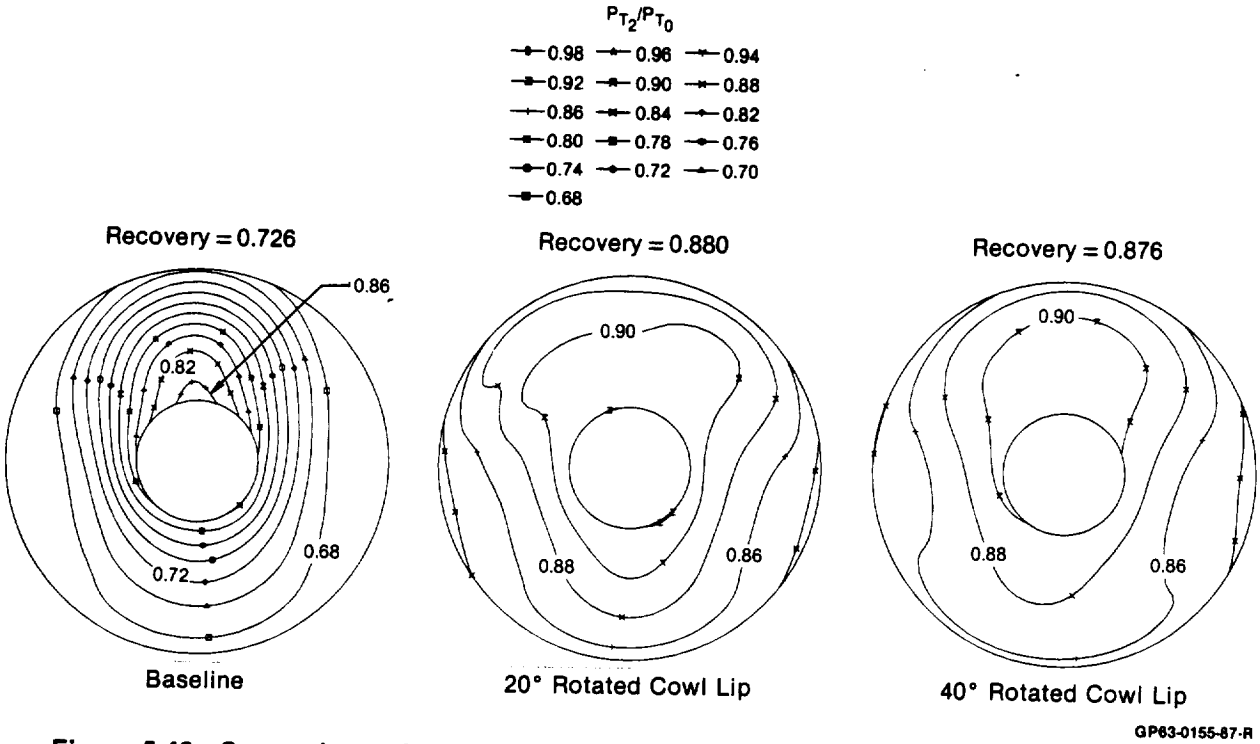

Figure 5-46. Comparison of Axisymmetric Inlet Engine Face Pressure Recovery Contours
Baseline and Rotated Cowl Configurations $M_0 = 0.9$ $\alpha = 40°$

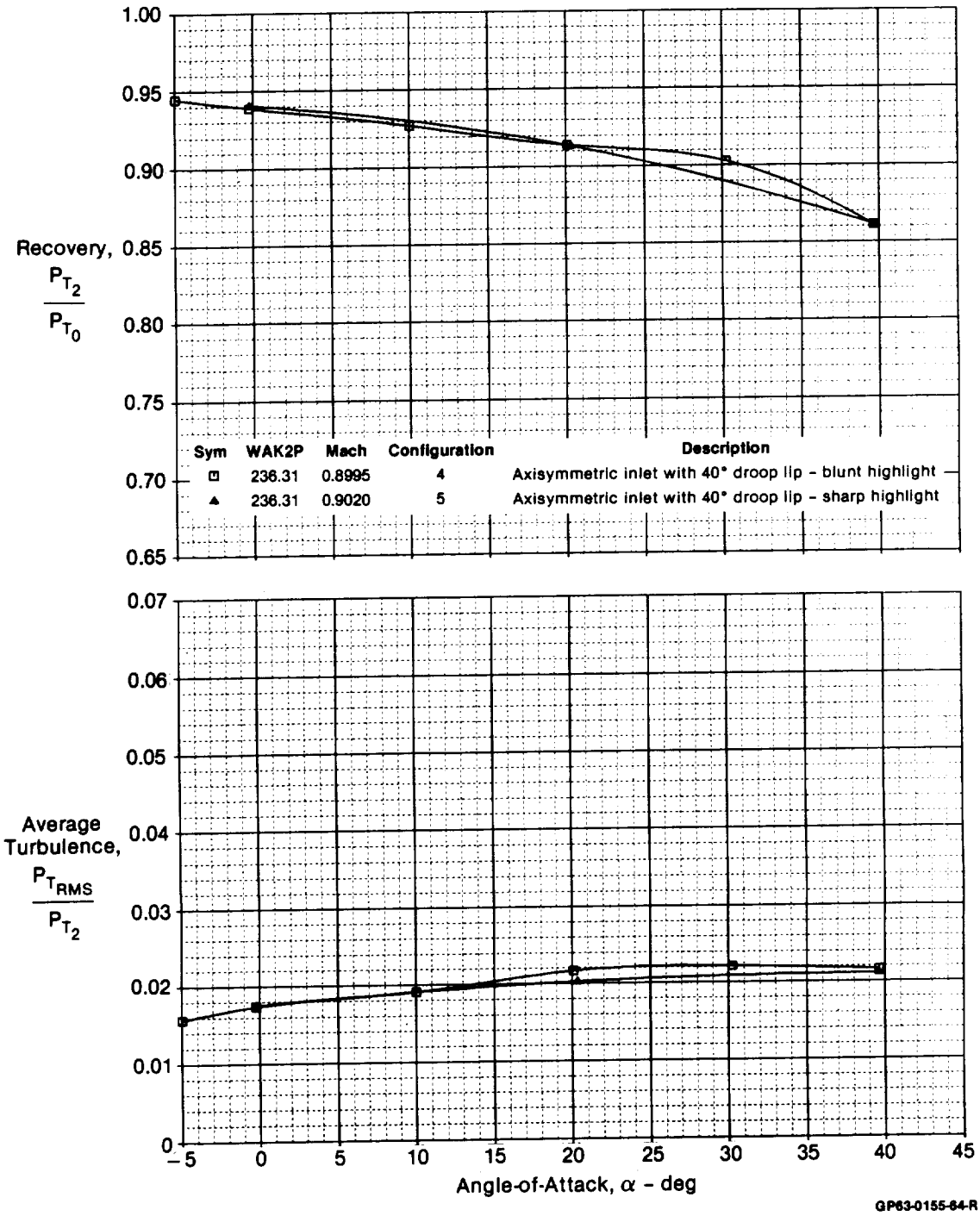

Figure 5-47. Effect of Blunt and Sharp Highlights on 40° Rotated Lip Recovery and Average Turbulence
$M_0 = 0.9$

Mach 1.4 Results - The rotated lip was not effective in improving the angle of attack performance of the axisymmetric inlet at Mach 1.4. The recovery of the 20° rotated lip was generally 1% to 2% below that of the baseline inlet, Figure 5-48. Turbulence, however, was not increased with this configuration. At a 20° angle of attack, the recovery levels of the baseline and 20° rotation configurations were nearly equal. Based on the slopes of the recovery curves at $\alpha = 20°$, the 20° rotated lip may outperform the baseline inlet at higher angles of attack.

A cowl lip rotation angle of 40° decreased the baseline inlet recovery by 5% across the angle of attack range tested. Turbulence also increased significantly, Figure 5-48.

The suspected reasons for the decrease in performance are increased shock losses. The 40° rotated lip would penetrate the conical shock. Therefore, a bow shock is generated from the rotated cowl lip, which accounts for the sharp decrease in total pressure recovery and increase in turbulence. Higher Mach numbers would result in a continual decrease in recovery. Hence, at supersonic speeds, bow shocks generated by the rotated cowl eliminate any benefits of this particular rotated lip design.

Retracted Sideplates Results - Mach 0.9 - Rotating the cowl lip does not improve performance at low angles of attack and may increase inlet drag. Therefore, the rotated lip should not be deployed at low angles of attack. The intent of the retracted sideplates configuration was to determine the effect of retracting the rotating cowl lip sideplates into the throat region of the inlet at low angles of attack.

Retracting the sideplates reduces the inlet throat area, due to physical blockage and the effects of boundary layer buildup on the retracted sideplates. In addition, the centerbody cone acts to turn the flow radially outward. However, the sideplates are located such that they contain the flow on the lower half of the centerbody. This gives a smaller effective throat area, resulting in a choked throat condition at a lower mass flow than anticipated from the blockage calculations. While the actual throat area decreased only 1.5%, the actual choking mass flow was reduced 2.5%.

The recovery loss with the retracted sideplates in the throat region is 3% at small angles of attack. This is illustrated in Figure 5-49. The viscous wake of the retracted sideplates is a significant contributor to this loss. The wake is clearly visible in the engine face contour, Figure 5-50.

The sideplate effect diminishes with increasing angle of attack, due to flow separation off the cowl lip. At $\alpha = 40°$, the separation effectively masks the sideplate losses, Figure 5-50.

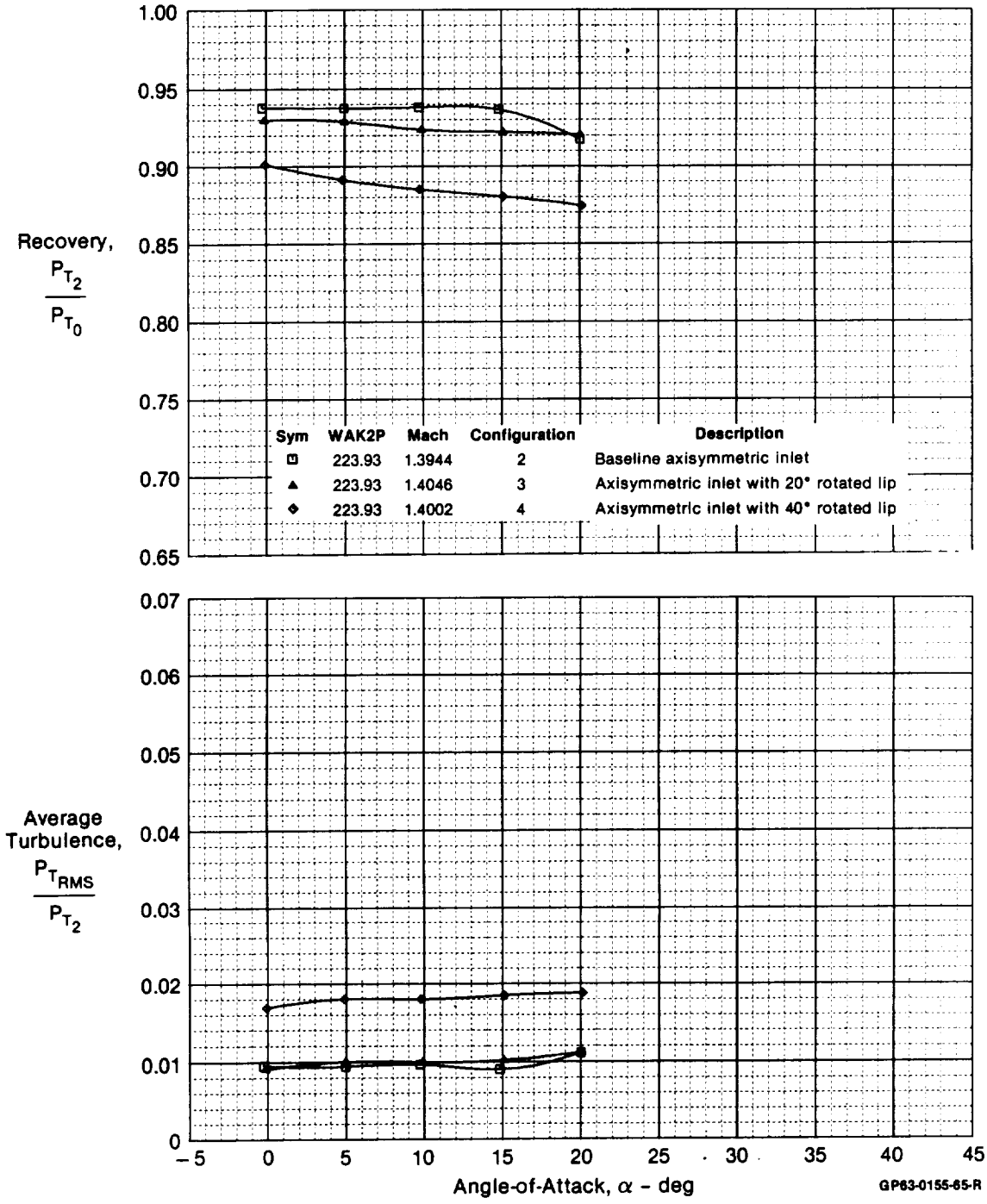

Figure 5-48. Effect of Rotating Cowl Lip on Axisymmetric Inlet Recovery and Average Turbulence
$M_0 = 1.4$

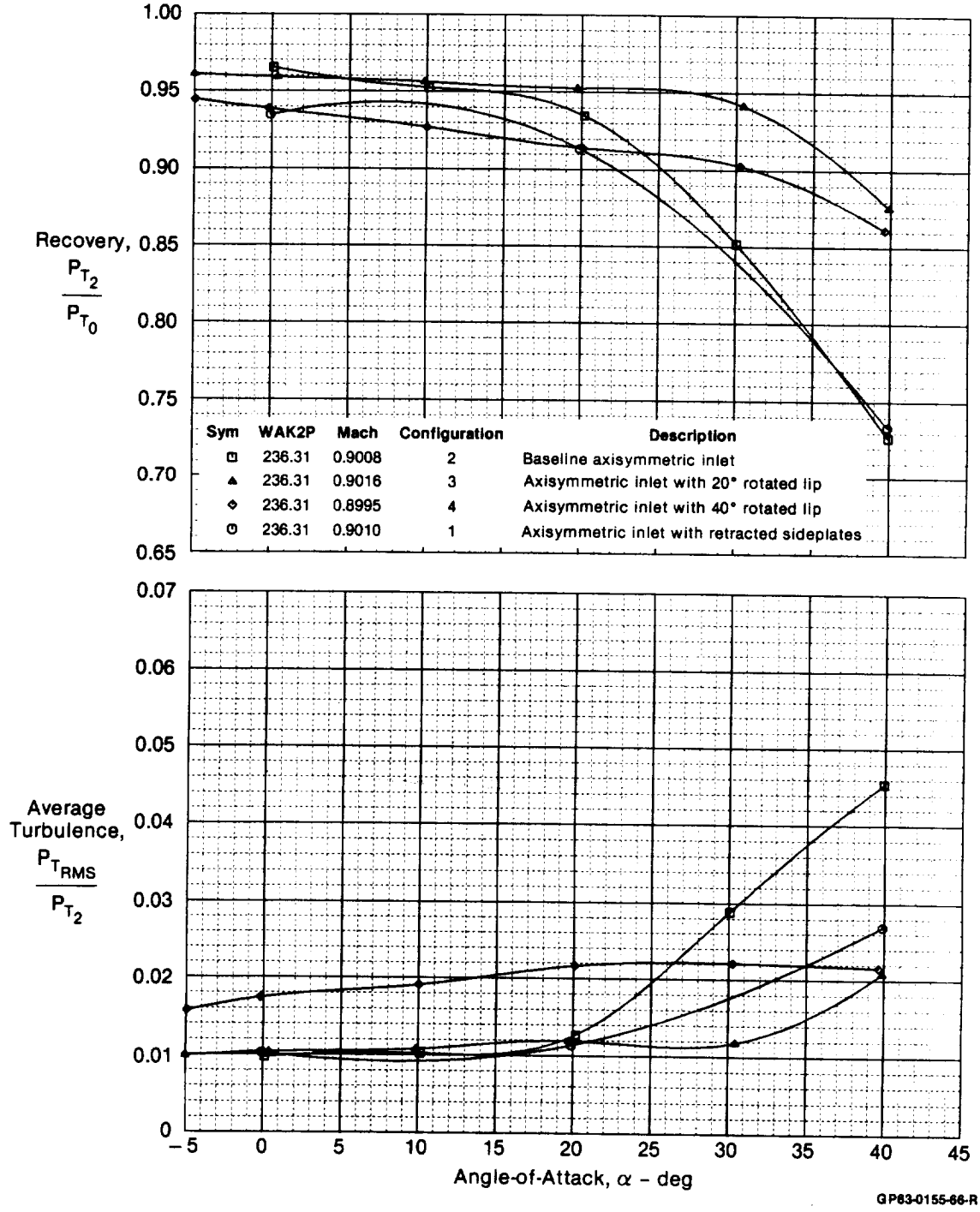

Figure 5-49. Effect of Retracting Sideplates Into the Axisymmetric Inlet Throat
$M_0 = 0.9$

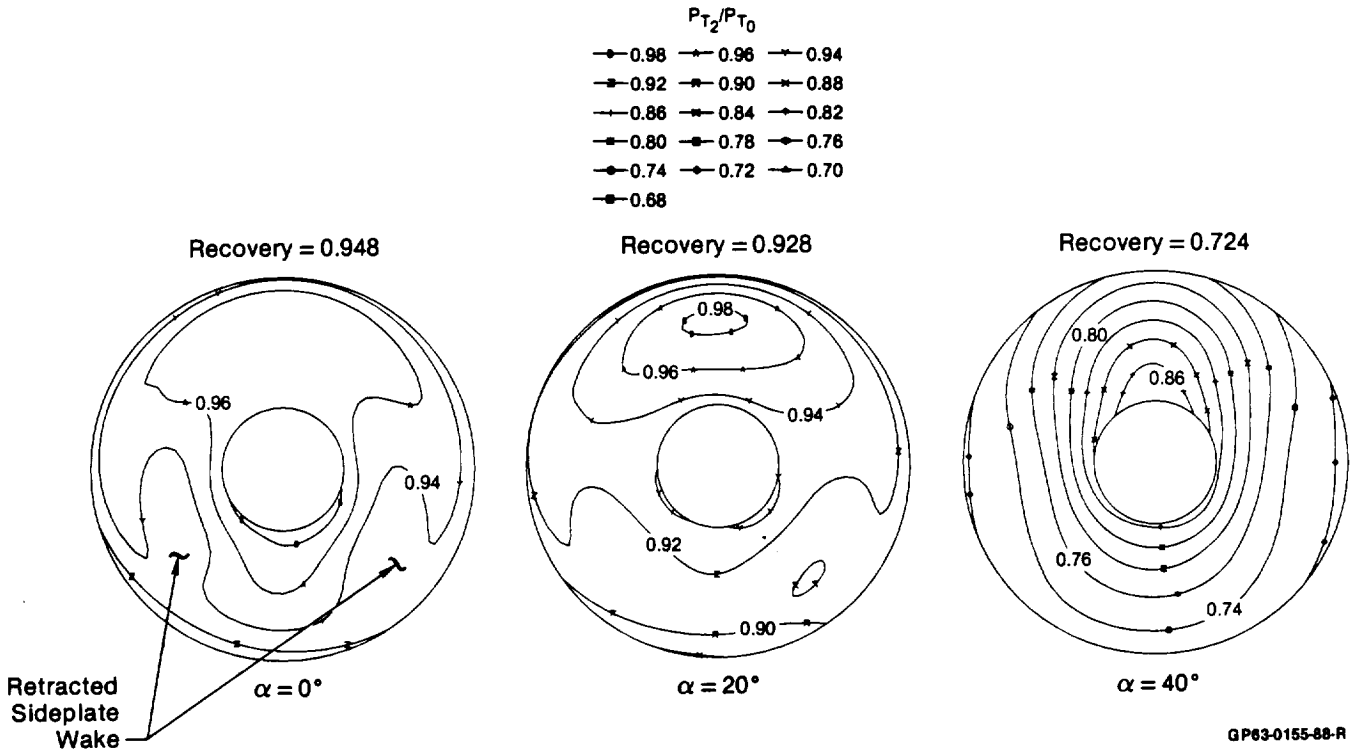

Figure 5-50. Axisymmetric Inlet Engine Face Pressure Recovery Contours
Retracted Sideplates Configuration $M_0 = 0.9$

Mach 1.4 Performance - The performance of the axisymmetric inlet with retracted sideplates was much lower at Mach 1.4 than at Mach 0.9. Figure 5-51 shows a 5% drop in recovery, as opposed to only a 3% loss at Mach 0.9. The reason is a change in the centerbody position at Mach 1.4. At subsonic Mach numbers, the centerbody is in the Mach 0.0 (aft) position. The sideplates are approximately triangular, as shown in Figure 5-52. The point where the centerbody first reaches its maximum radius is well aft of the height of the sideplates. The cross section at this point (AA) has a blockage ratio of 0.418, where the ratio is defined as the cross sectional area of the centerbody and sideplates divided by the area enclosed by the outer circumference of the duct. This provides ample room for the viscous wake of the sideplates to travel past the centerbody.

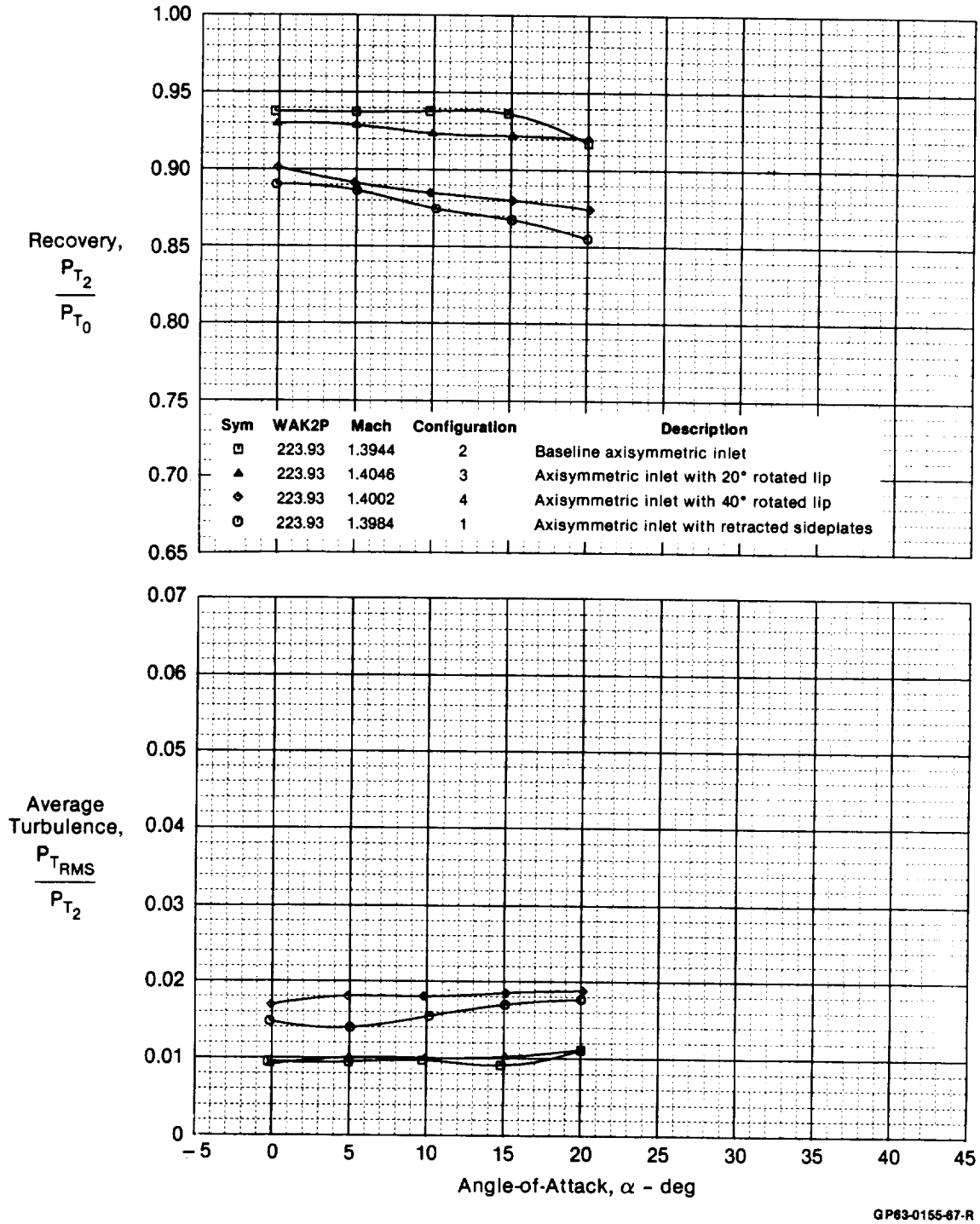

Figure 5-51. Effect of Retracting Sideplates Into the Axisymmetric Inlet Throat
$M_0 = 1.4$

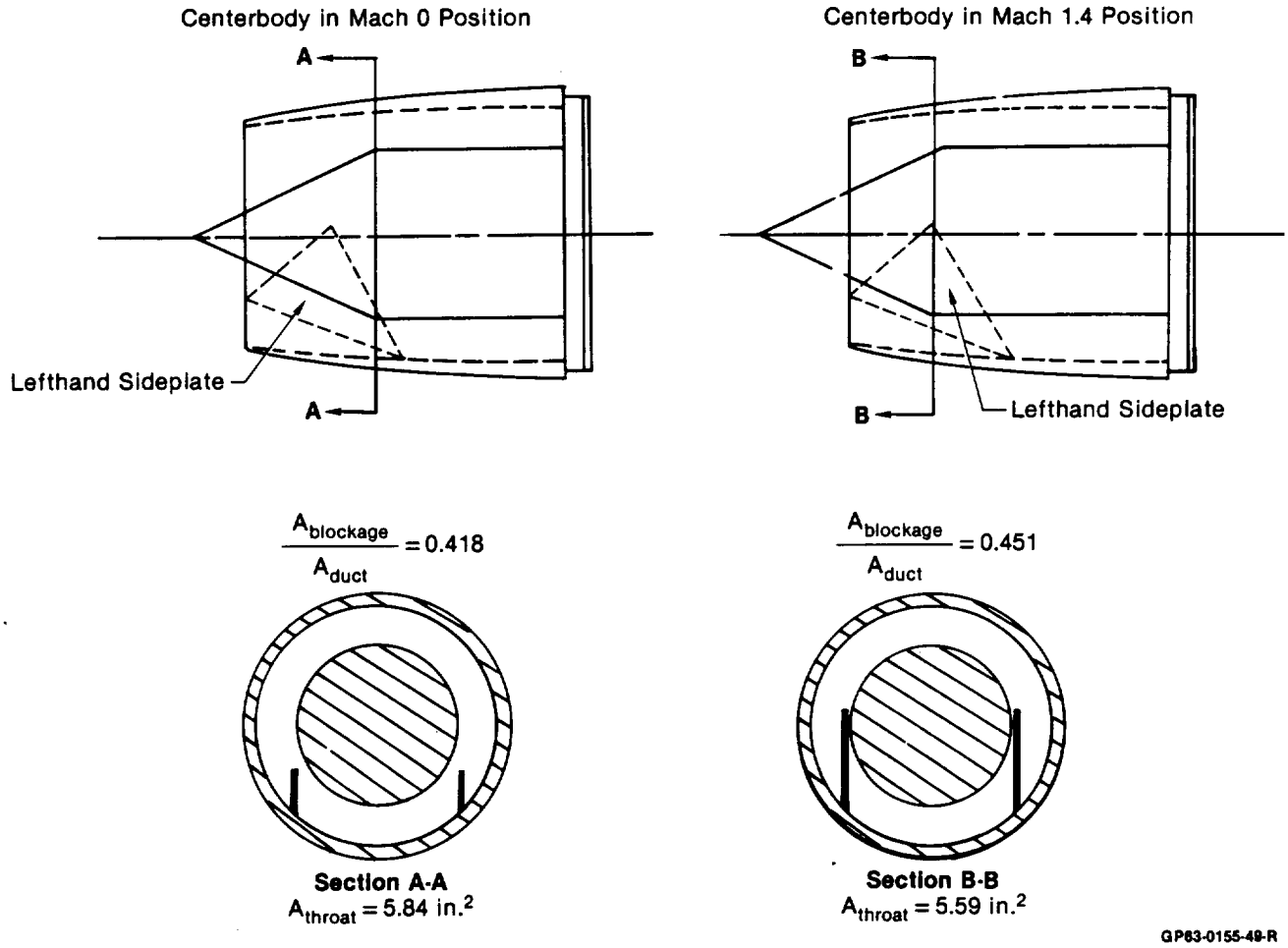

Figure 5-52. Blockage Ratios for the Two Axisymmetric Inlet Centerbody Positions With Retracted Sideplates

At Mach 1.4, the centerbody is moved forward. The point where the centerbody first reaches its maximum radius roughly coincides with the point of maximum height of the sideplates (BB). This results in a maximum sideplate blockage ratio of 0.451. Boundary layers consume the area between the centerbody and the sideplates.

Consequently, the wake of the sideplates is not seen on the engine face contour, Figure 5-53. The area of poor pressure recovery has increased, leaving a small high pressure region just below the hub, between the sideplates. These effects tend to isolate flow on the lower half from the upper half of the inlet. As a result, there are two high pressure pockets, one above and one below the hub.

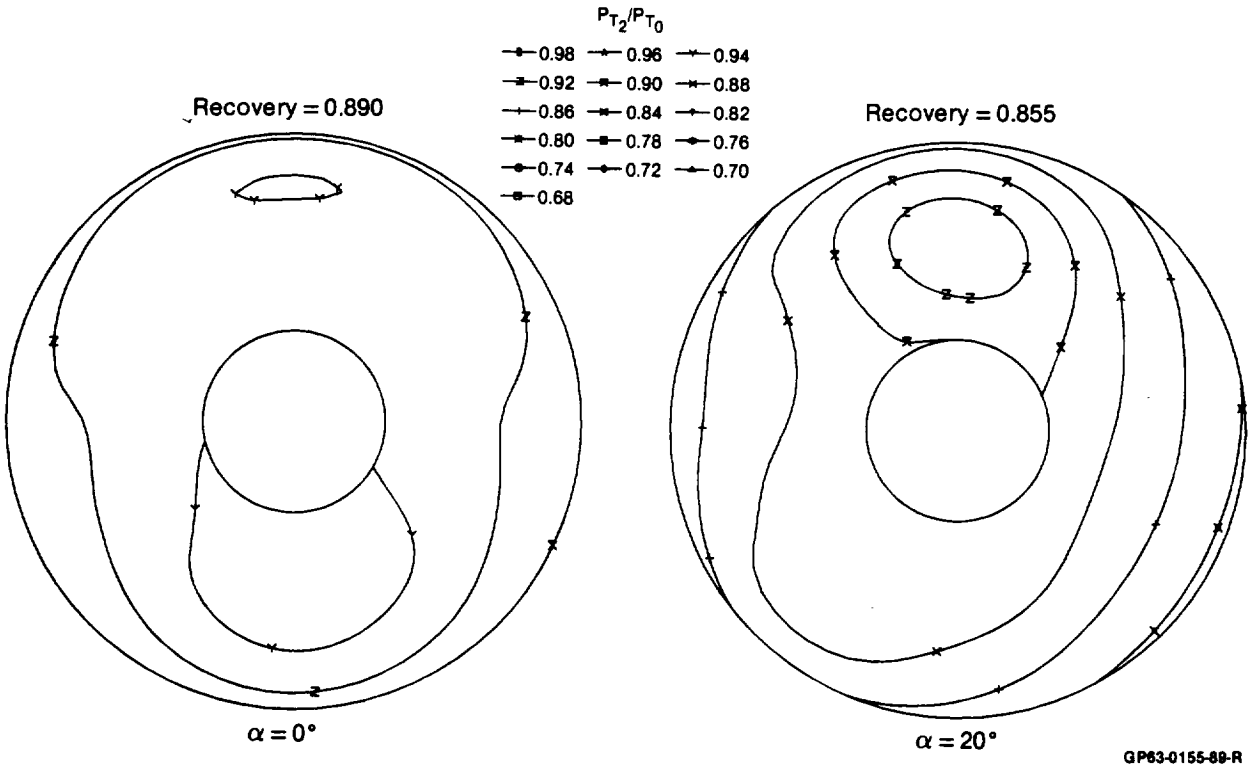

Figure 5-53. Axisymmetric Inlet Engine Face Pressure Recovery Contours
Retracted Sideplates Configuration $M_0 = 1.4$

5.2.3 Auxiliary Inlet Effects - The purpose of the auxiliary inlets is to reduce the mass flow through the main inlet. This would reduce the flow velocity about the cowl lip. If this effect were achieved, it would decrease the severity of cowl lip separation, improving inlet angle of attack performance.

Several axiliary inlet configurations were evaluated to improve the angle of attack performance of the axisymmetric inlet. Auxiliary inlet location and throat area were varied to determine the effect of these parameters.

Three configurations were tested: (1) lower auxiliary inlets open 100%, (2) upper auxiliary inlets open 100%, and (3) upper and lower auxiliary inlets each open 50%. The configurations were screened at Mach 0.9 and Mach 1.4.

Lower Auxiliary Inlets Open 100% - Mach 0.9 - Performance of this auxiliary inlet concept below 30° angle of attack is generally below that of the baseline configuration. At the highest angle of attack, only the lower auxiliary inlet configuration provides more than a 5% improvement in recovery, as shown in Figure 5-54. However in the 30° to 40° range, distortion increases, indicating a potential engine compatibility problem at high angles of attack, Figure 5-55.

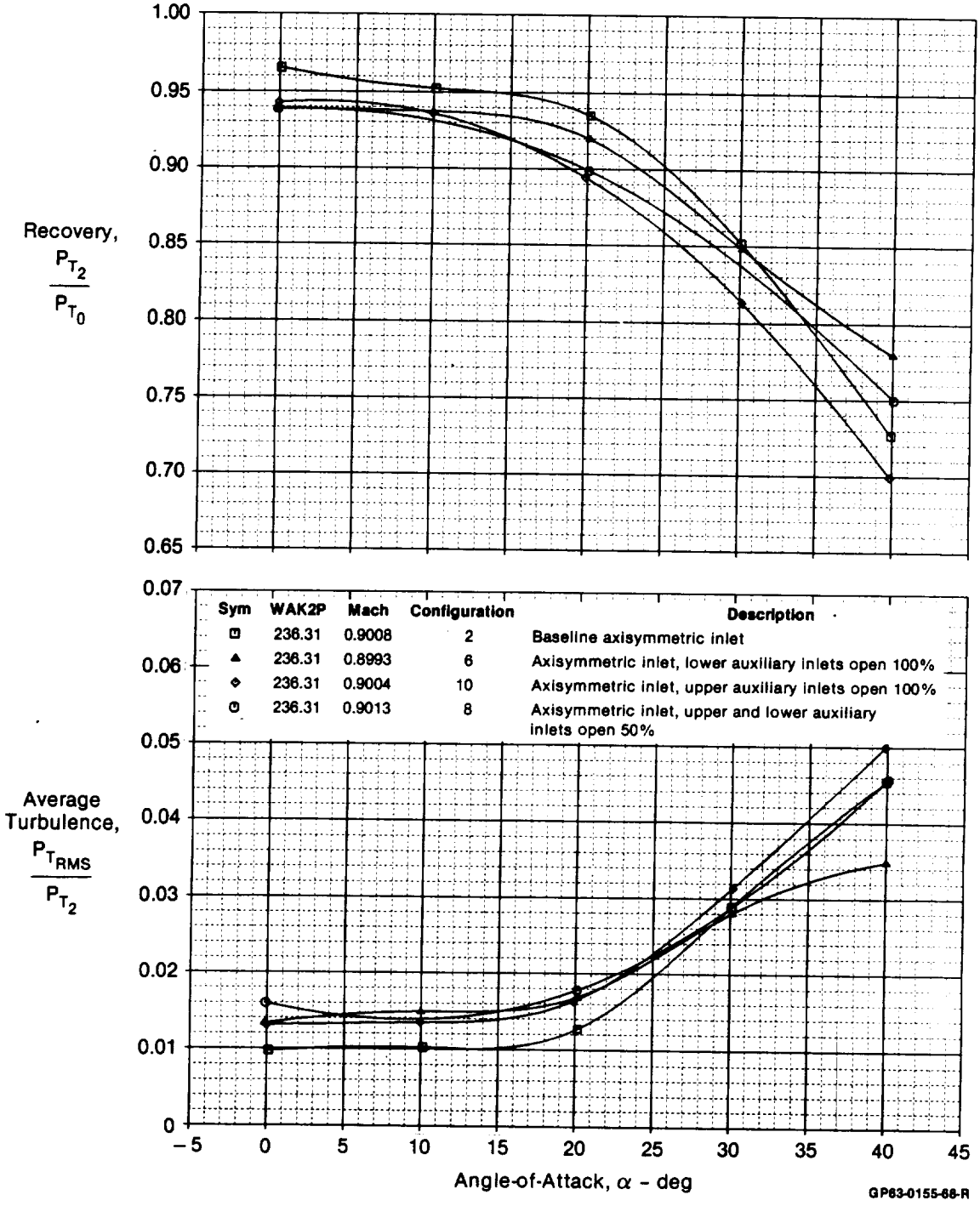

Figure 5-54. Effect of Opening Auxiliary Inlets on Axisymmetric Inlet Recovery and Average Turbulence
$M_0 = 0.9$

C-2

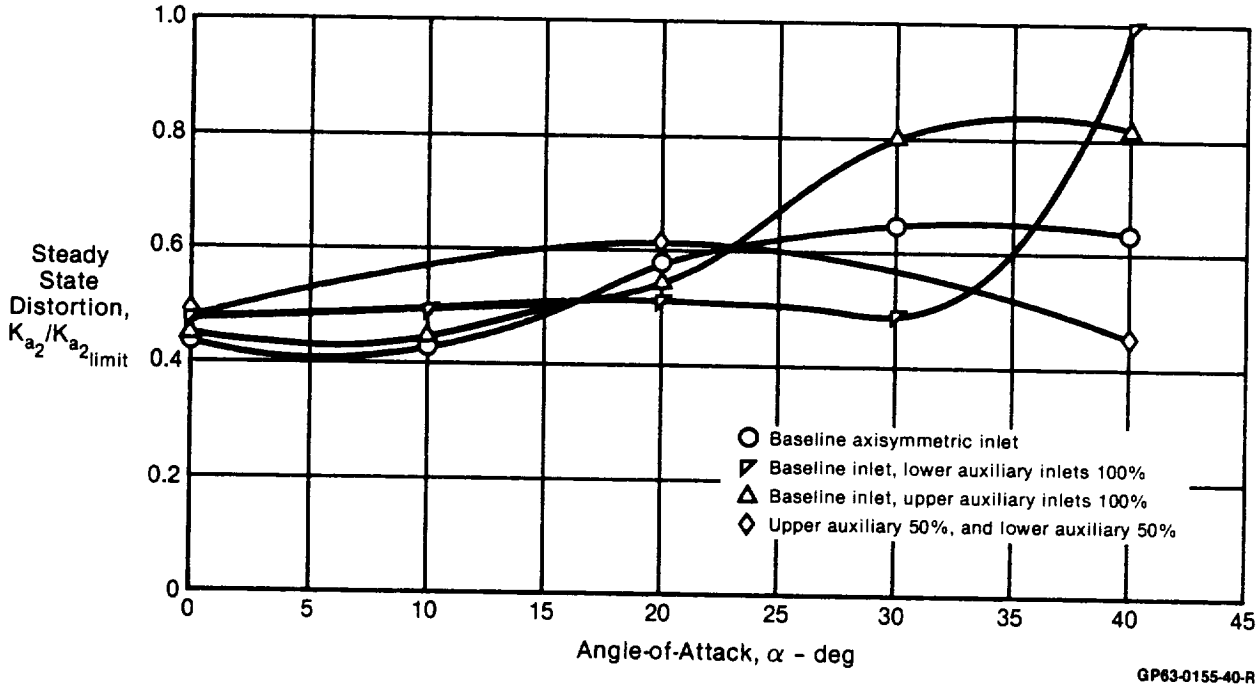

Figure 5-55. Effect of Opening Lower Auxiliary Inlets 100% on Axisymmetric Inlet Distortion
Mach 0.9

The engine face contour provides insight into the operation of this inlet with lower auxiliary inlets. The contour for the auxiliary inlets open 100% at 0° angle of attack, Figure 5-56(b), is very similar to the baseline inlet, Figure 5-56(a). The three low pressure wakes off the centerbody struts are visible as in the baseline. The engine face contour at α = 20°, shown in Figure 5-57(b), is also very similar to the baseline contour. This indicates that there isn't a significant benefit for the auxiliary inlet up to 20° angle of attack.

The lower auxiliary inlets improve recovery performance at α = 40°. Recovery is increased by the high energy air entering the inlet through the auxiliary inlets. This results in the high total pressure evident on the lower half of the pressure contour in Figure 5-58(b). The upper half of the engine face has a relatively lower total pressure level; this is caused by separation on the leeward side of the centerbody. The combined effect of this imbalance is to produce the high distortion for lower auxiliary inlets, which is evident in Figure 5-55.

Upper Auxiliary Inlets Open 100%, Mach 0.9 - The upper auxiliary inlet configuration has the lowest recovery performance of all the axisymmetric auxiliary inlet concepts. Total pressure recovery was 3 to 5% below baseline levels across the angle of attack range tested, Figure 5-54.

The engine face contour, Figure 5-56(c), identifies the upper half of the engine face as the region of decreased recovery. At angle of attack, the external flow separates from the inlet nacelle rather than enter the upper auxiliary inlets. This renders upper auxiliary inlets ineffective for high angle of attack.

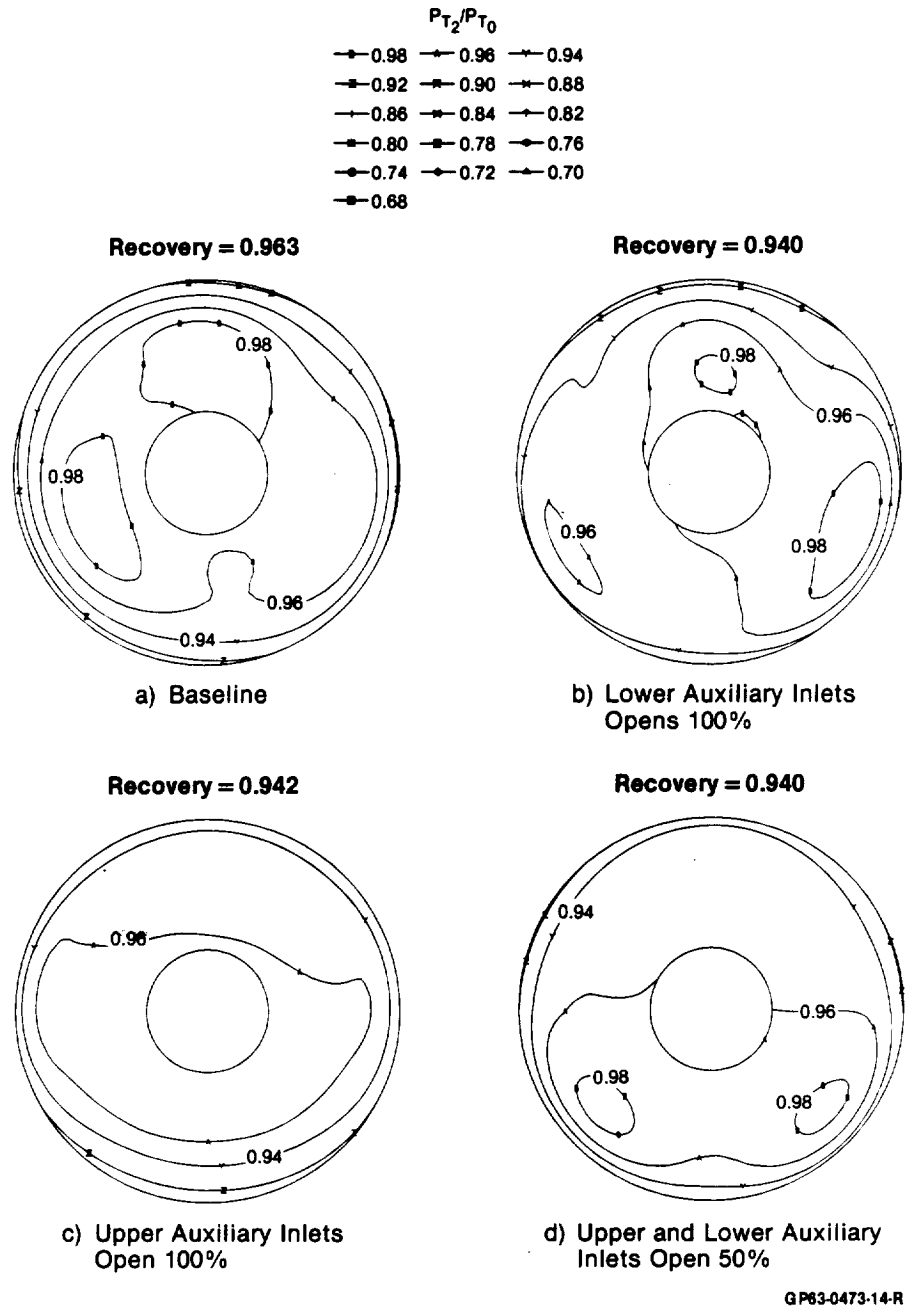

a) Baseline

b) Lower Auxiliary Inlets Opens 100%

c) Upper Auxiliary Inlets Open 100%

d) Upper and Lower Auxiliary Inlets Open 50%

Figure 5-56. Comparison of Axisymmetric Inlet Engine Face Pressure Recovery Contours
Auxiliary Inlet Configurations $M_0 = 0.9$ $\alpha = 0°$

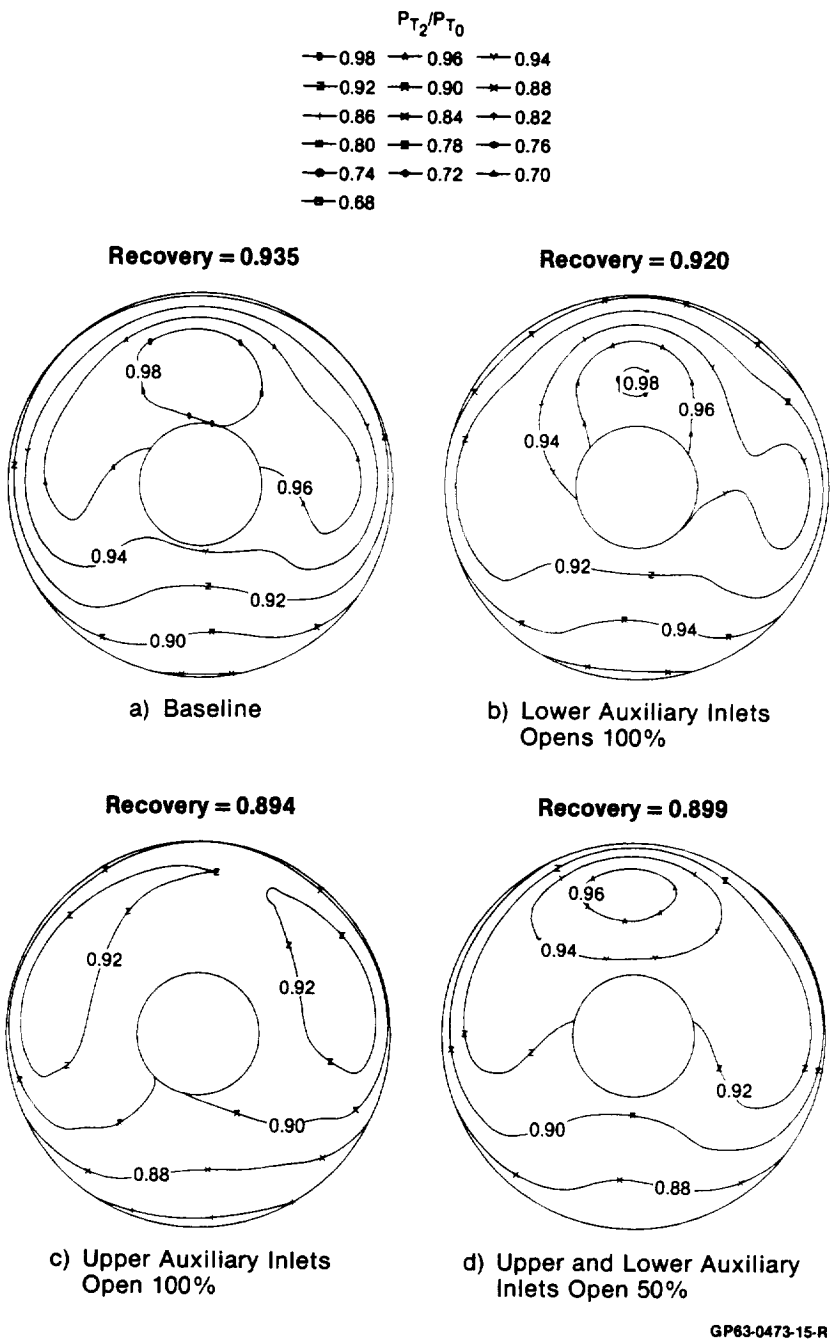

a) Baseline

b) Lower Auxiliary Inlets Opens 100%

c) Upper Auxiliary Inlets Open 100%

d) Upper and Lower Auxiliary Inlets Open 50%

GP63-0473-15-R

Figure 5-57. Comparison of Axisymmetric Inlet Engine Face Pressure Recovery Contours
Auxiliary Inlet Configurations $M_0 = 0.9$ $\alpha = 20°$

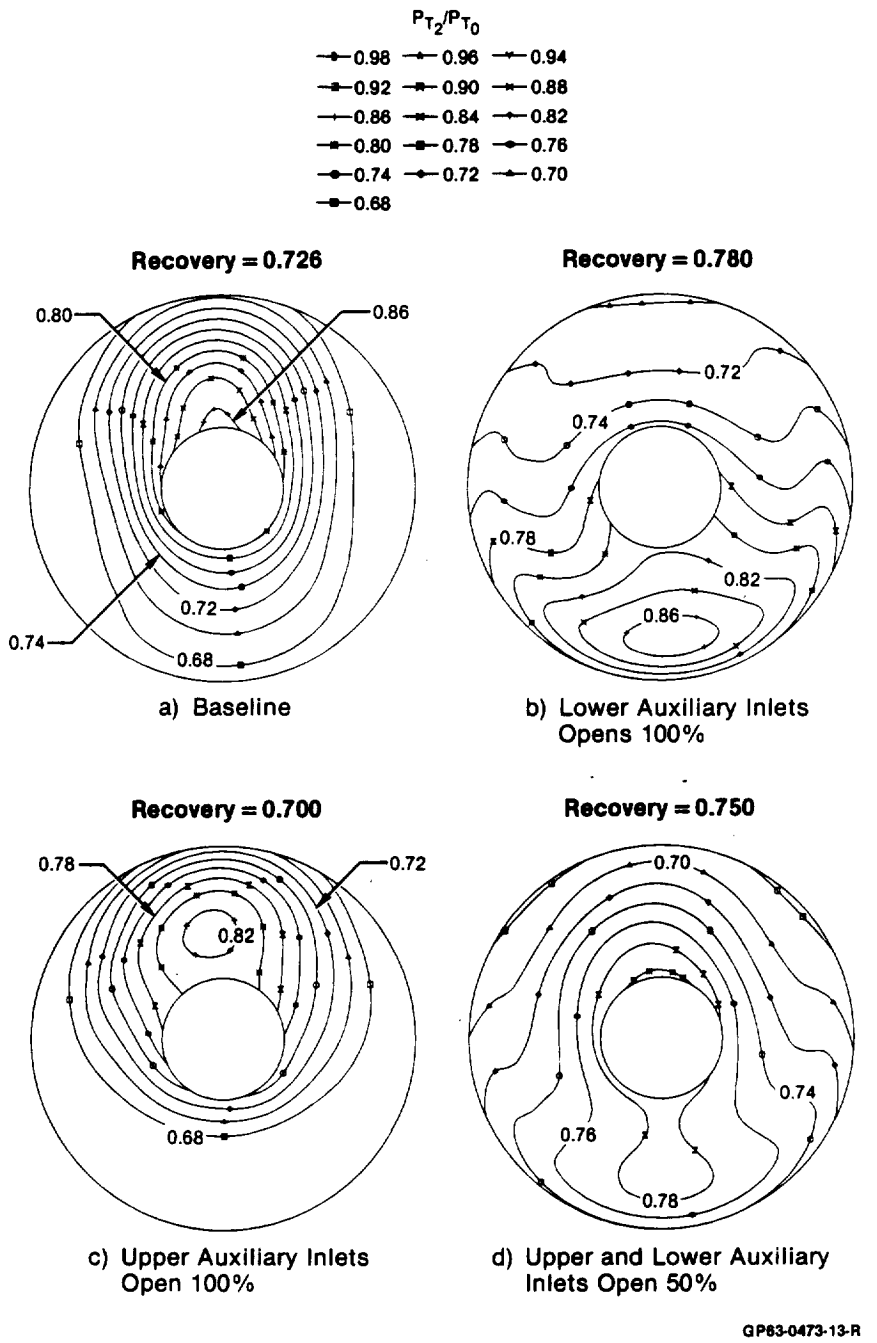

a) Baseline

b) Lower Auxiliary Inlets Opens 100%

c) Upper Auxiliary Inlets Open 100%

d) Upper and Lower Auxiliary Inlets Open 50%

Figure 5-58. Comparison of Axisymmetric Inlet Engine Face Pressure Recovery Contours
Auxiliary Inlet Configurations $M_0 = 0.9$ $\alpha = 40°$

Upper and Lower Auxiliary Inlets Open 50%, Mach 0.9 - The performance of this configuration fell between the upper auxiliary inlet and lower auxiliary inlet configurations. All performance parameters, with the exception of inlet distortion, indicate that the effects of each auxiliary inlet location are averaged when all inlets are open. At $\alpha = 0°$, the viscous wake of the lower strut is visible in Figure 5-56(d). This is similar to the case with lower auxiliary inlets open 100%, see Figure 5-56(b).

The ram effect of the lower inlets is visible at $\alpha = 40°$, Figure 5-58(d). This, however, does not offset losses from the upper inlets, so that overall recovery is still lower than the baseline.

Lower Auxiliary Inlets Open 100%, Mach 1.4 - As in the case of the rotating cowl designs, supersonic Mach numbers tend to complicate the flowfield so that auxiliary inlets substantially decrease the overall performance of the inlet. There was no performance benefit of auxiliary inlets at any angles of attack tested at Mach 1.4. Recovery decreased 9% at most angles of attack, as shown in Figure 5-59. Distortion was also increased at this condition. The engine face pressure contours were similar to those of the baseline at angle of attack.

Upper Auxiliary Inlets Open 100%, Mach 1.4 - In the supersonic case, recovery is decreased substantially with the upper auxiliary inlets open. There is no ram effect with this configuration, so performance drops off rapidly with angle of attack, Figure 5-59. The engine rake contour indicates some separation off the lower cowl lip. Hence, the velocity of the mass flow at the inlet plane was not low enough to avoid the lip separation observed in the baseline case.

5.2.4 Retracted Centerbody Results - Flow separation from the centerbody cone was identified earlier as a potential inlet loss mechanism at very high angles of attack. The axisymmetric inlet model was tested at Mach 0.9 with a retracted centerbody to determine if it would delay flow separation. It was tested at 0°, 20°, and 40° angles of attack.

Test data shows this concept does improve inlet performance at angles of attack greater than 20°. Recovery levels, shown in Figure 5-60, are 3% higher than those of the baseline at $\alpha = 40°$. Average turbulence was also reduced by 33%. However, this concept increases inlet distortion above $\alpha = 20°$, where recovery and turbulence characteristics are improved, Figure 5-61.

With the retracted centerbody configuration at $\alpha = 40°$, the distortion level rose from 64% to 84% of the limit value. This increase is due primarily to an increase in the circumferential component of distortion. The engine face contour plot for the retracted centerbody, Figure 5-62, indicates that while the radial component may have decreased, circumferential distortion is large enough to result in a total distortion increase.

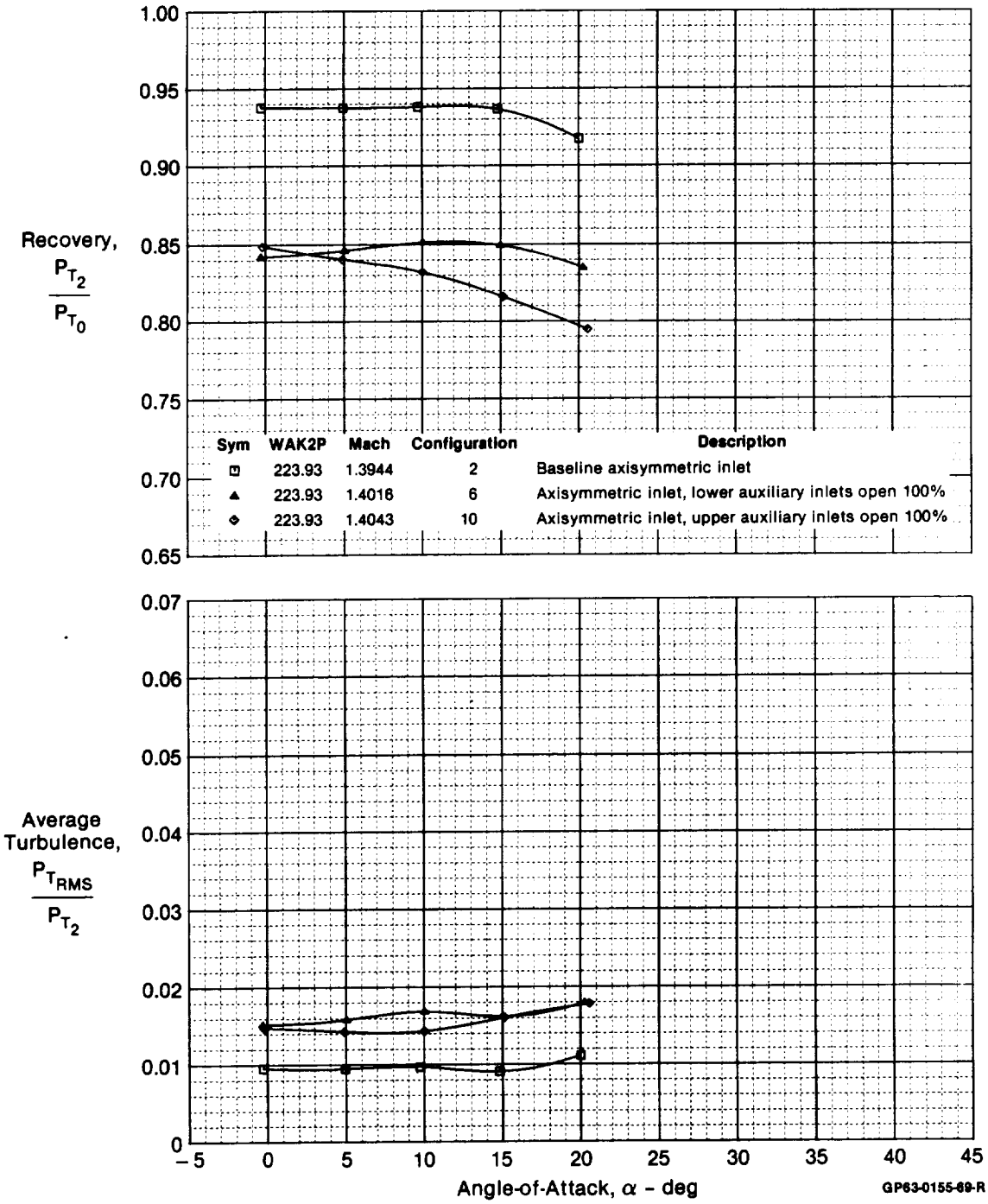

Figure 5-59. Effect of Opening Auxiliary Inlets on Axisymmetric Inlet Recovery and Average Turbulence
$M_0 = 1.4$

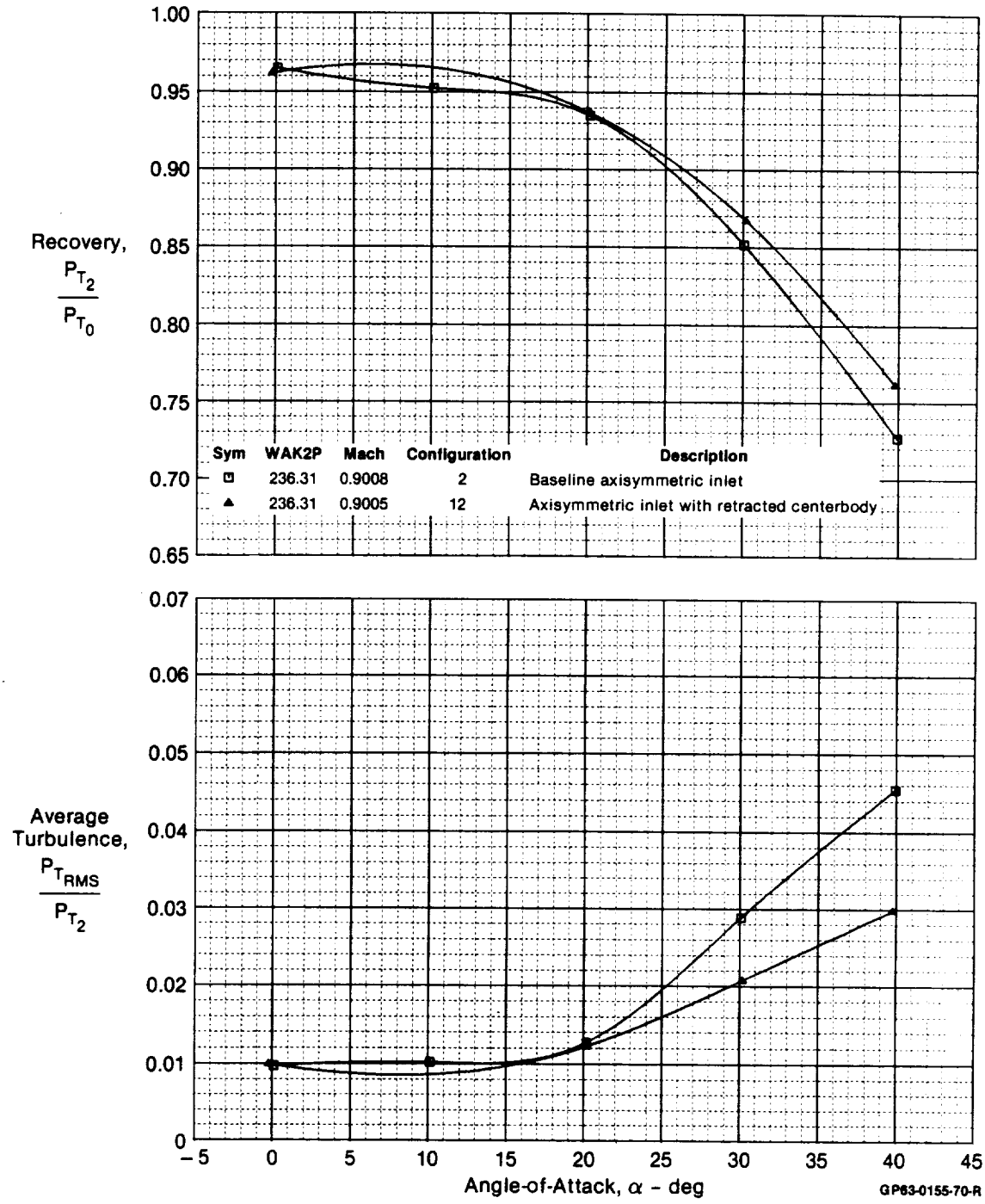

Figure 5-60. Effect of Retracting Centerbody on Axisymmetric Inlet Recovery and Average Turbulence
$M_0 = 0.9$

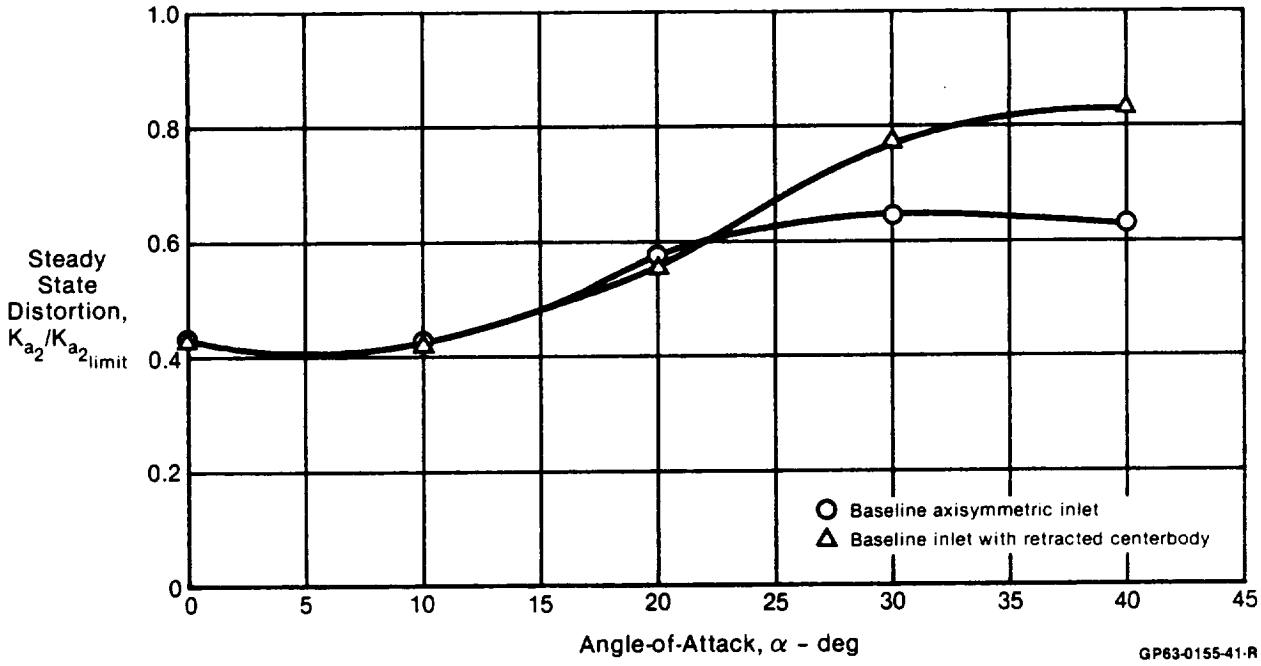

Figure 5-61. Effect of Retracting Centerbody on Axisymmetric Inlet Distortion
Mach 0.9

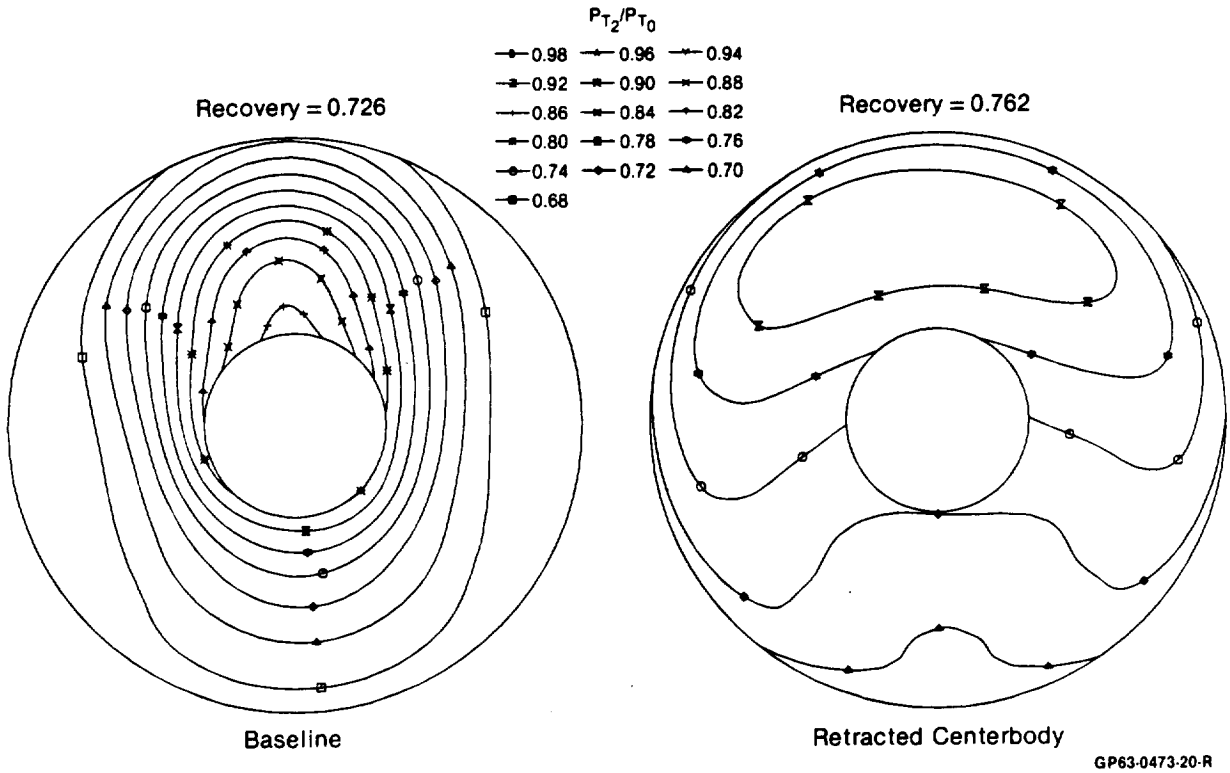

Figure 5-62. Comparison of Baseline and Retracted Centerbody Axisymmetric Inlet Configuration Total Pressure Recovery Contours
$M_0 = 0.9 \quad \alpha = 40°$

5.3 COMPARISON OF COMPETING CONCEPTS - The test results presented in Sections 5.1 and 5.2 suggest that of the two primary flow improvement concepts tested, the rotating cowl lip is superior to the auxiliary inlet design for both 2-D and axisymmetric inlets. The auxiliary inlets tested in this program provided marginal performance improvement only at very high angles of attack and Mach numbers 0.6 and 0.9. Conversely, cowl lip rotation was found to be an effective means to improve inlet performance at all subsonic Mach numbers tested. In fact, the test data indicates that it may be possible to attain a constant total pressure recovery performance across the angle of attack range from 0° to 40°.

The 2-D inlet model displayed higher performance characteristics than the axisymmetric inlet at all angles of attack and Mach numbers. A comparison between the baseline axisymmetric and 2-D inlets is shown in Figures 5-63, 5-64 and 5-65 for Mach numbers of 0.6, 0.9, and 1.2, respectively. The recovery for both inlets begins to decrease at an angle of attack of approximately 20°. However, the loss in the 2-D inlet recovery is more gradual than that of the axisymmetric inlet.

This recovery benefit is inherent in the inlet design by virtue of the overhead compression ramps and the 2-D cowl lip. The 2-D overhead ramp serves to turn the flow into the inlet plane, while the centerbody cone of the axisymmetric inlet may be separated on its leeward side, thus causing reduced angle of attack performance. Also, the cowl lip of the 2-D inlet is more contoured than the axisymmetric cowl, thus reducing the potential for separation on the cowl surface.

At small angles of attack, the recovery of the 2-D inlet is 1 to 2% higher than that of the axisymmetric inlet. The cause is most likely the greater duct length of the axisymmetric inlet. The recovery values of the 2-D inlet with the long diffuser at small angles of attack are comparable to those of the axisymmetric inlet, Figures 5-13 and 5-37. However, the angle of attack performance of the 2-D inlet with the long diffuser remains significantly higher than that of the axisymmetric inlet.

The 2-D inlet with 20° rotated lip has superior performance compared to the axisymmetric inlet with the same lip rotation. Figures 5-66, 5-67, and 5-68 compare the axisymmetric and 2-D inlets with the 20° rotated cowl lip for Mach numbers of 0.6, 0.9, and 1.2.

In addition to increased recovery and turbulence performance, the 20° rotated cowl lip reduced peak dynamic distortion by 50% at α = 40°, Figure 5-69. While the baseline inlet displayed a compatibility problem in the higher angle of attack range, the 20° rotated lip configuration achieved a constant peak dynamic distortion level of 0.35.

The rotated cowl lip concept has considerable appeal with respect to axiymmetric inlets because the performance is so dramatically improved at angle of attack. However, this concept on the axisymmetric inlet does have the disadvantage of requiring that the sideplates retract into the inlet duct.

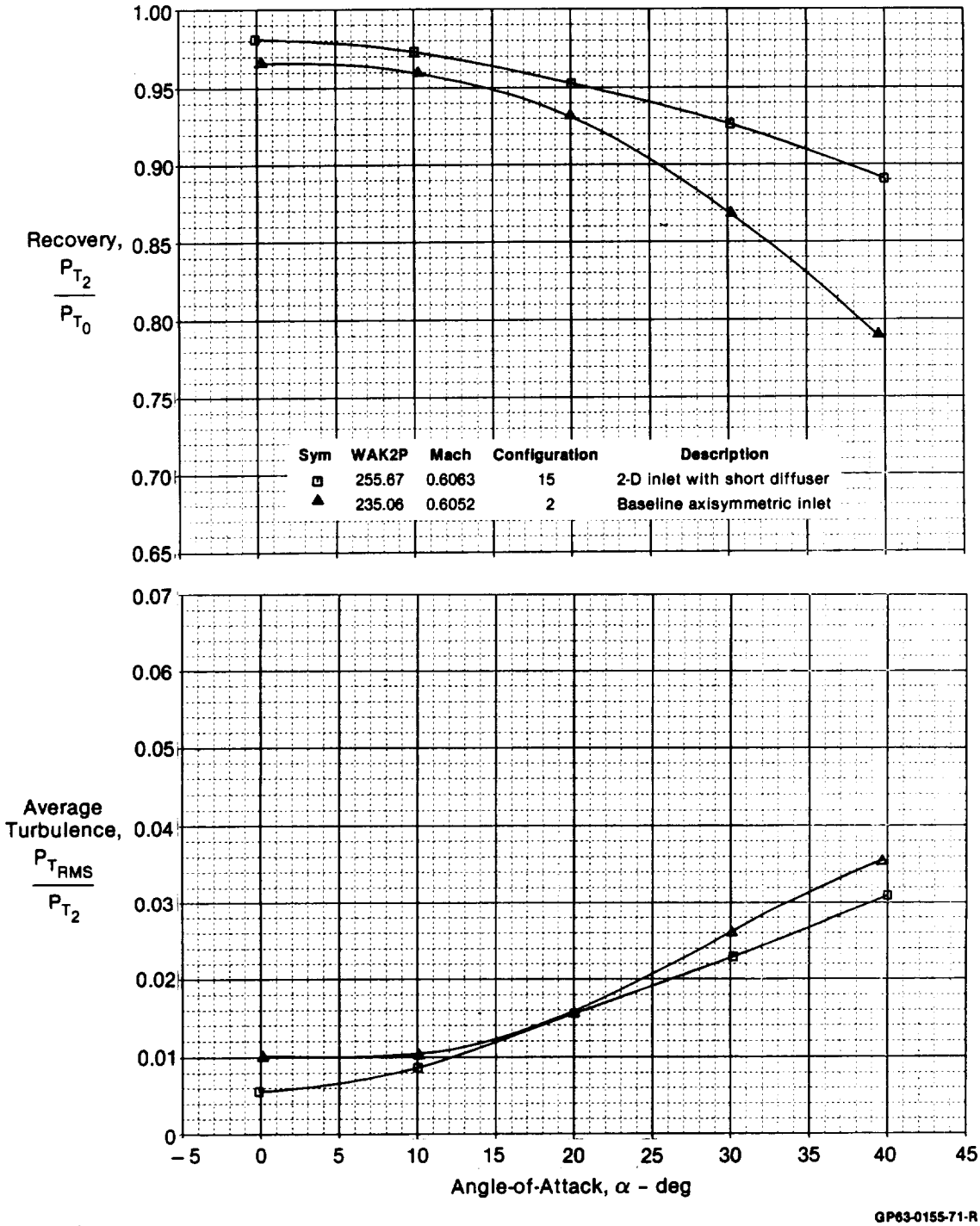

Figure 5-63. Comparison of 2-D and Axisymmetric Inlets
$M_0 = 0.6$

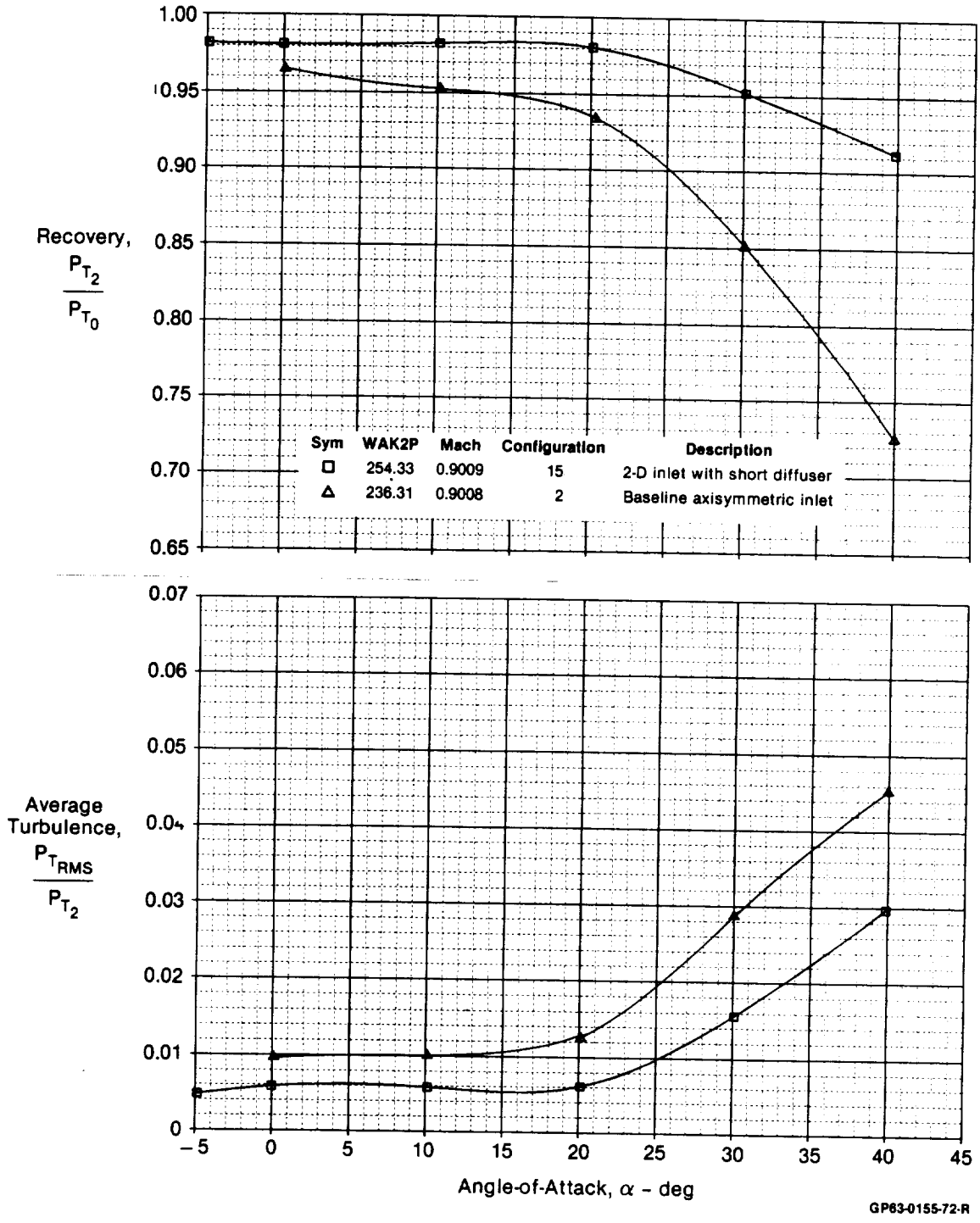

Figure 5-64. Comparison of 2-D and Axisymmetric Inlets
$M_0 = 0.9$

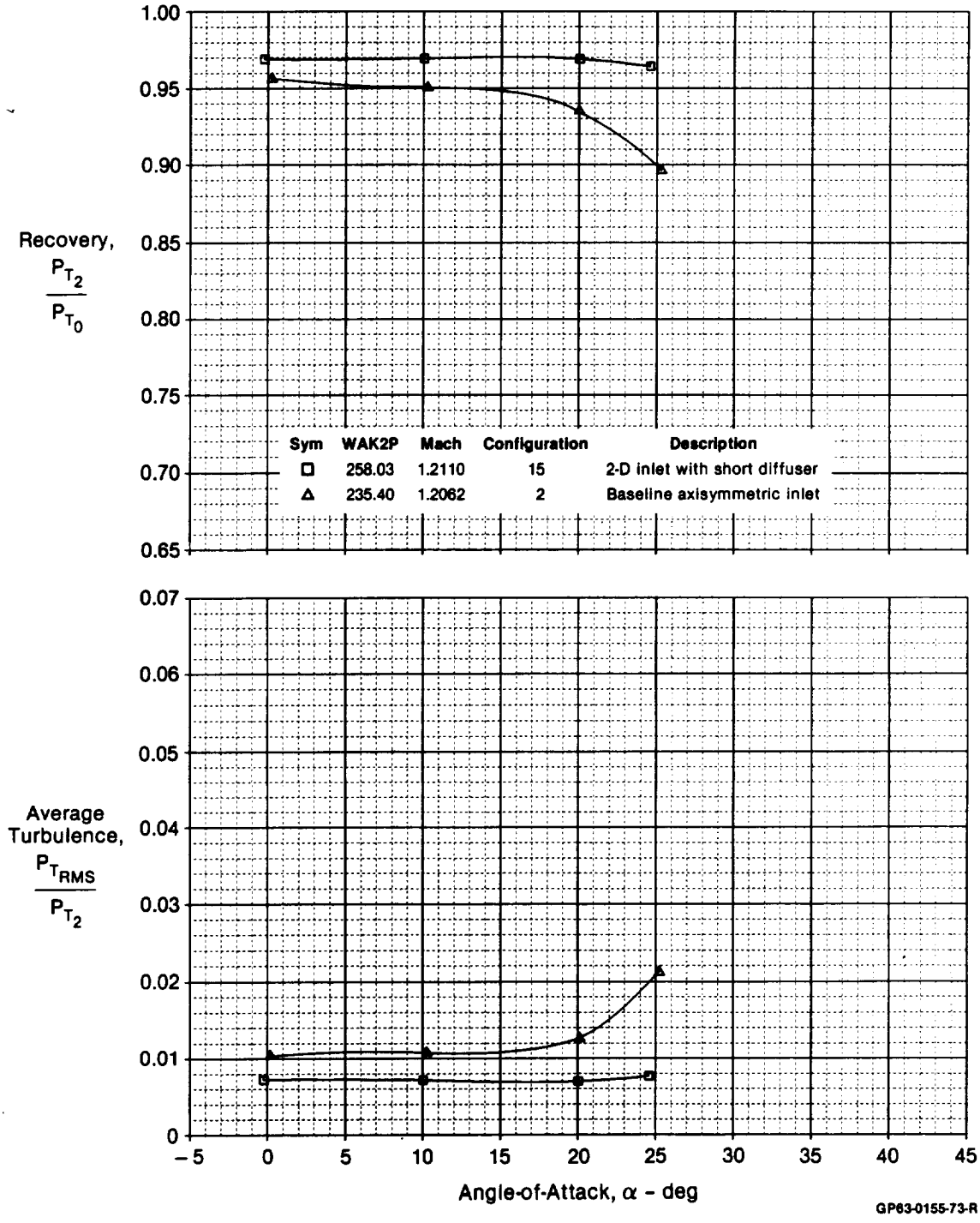

Figure 5-65. Comparison of 2-D and Axisymmetric Inlets
$M_0 = 1.2$

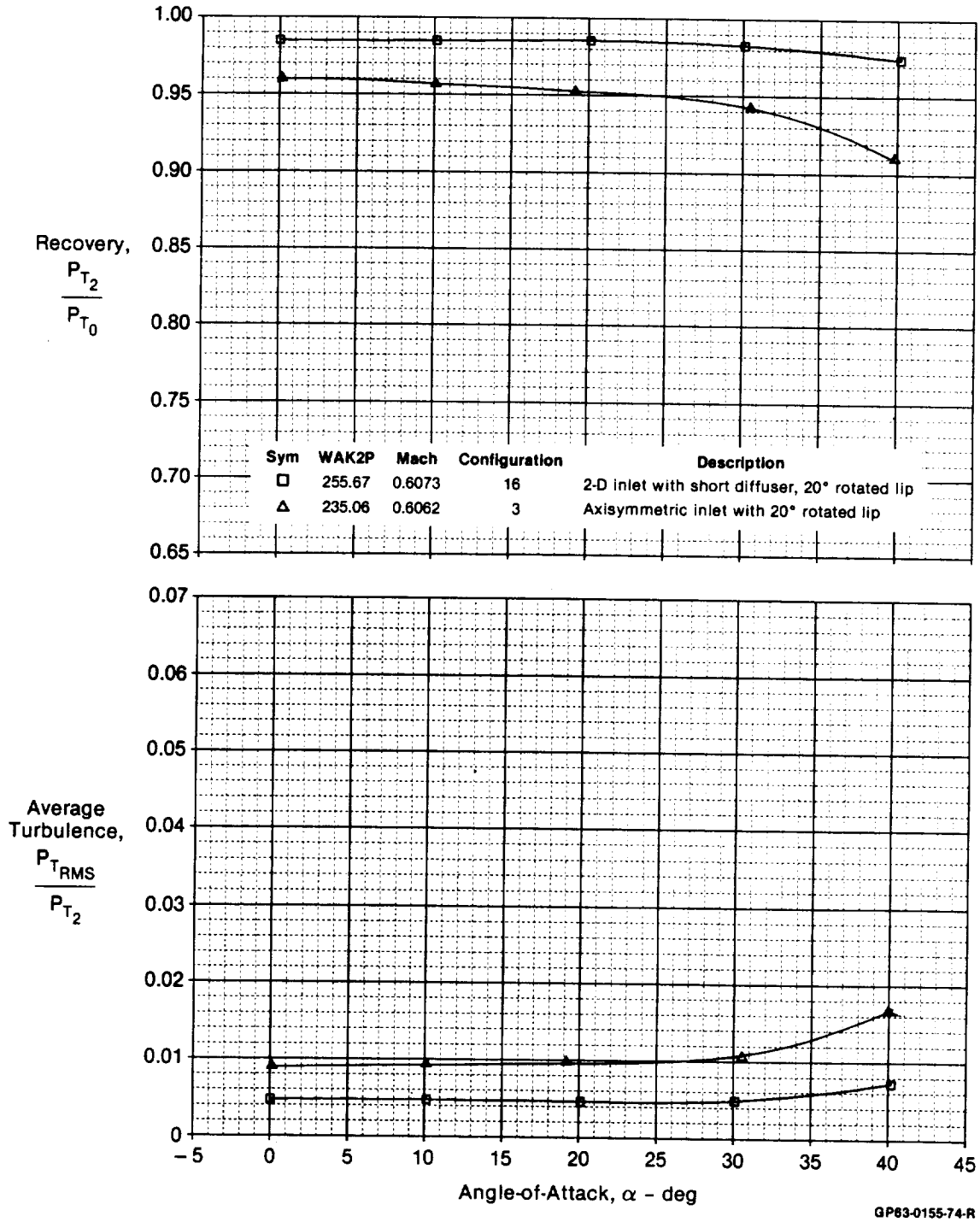

Figure 5-66. Comparison of 2-D and Axisymmetric Inlets
20° Rotated Cowl Lip Configurations $M_0 = 0.6$

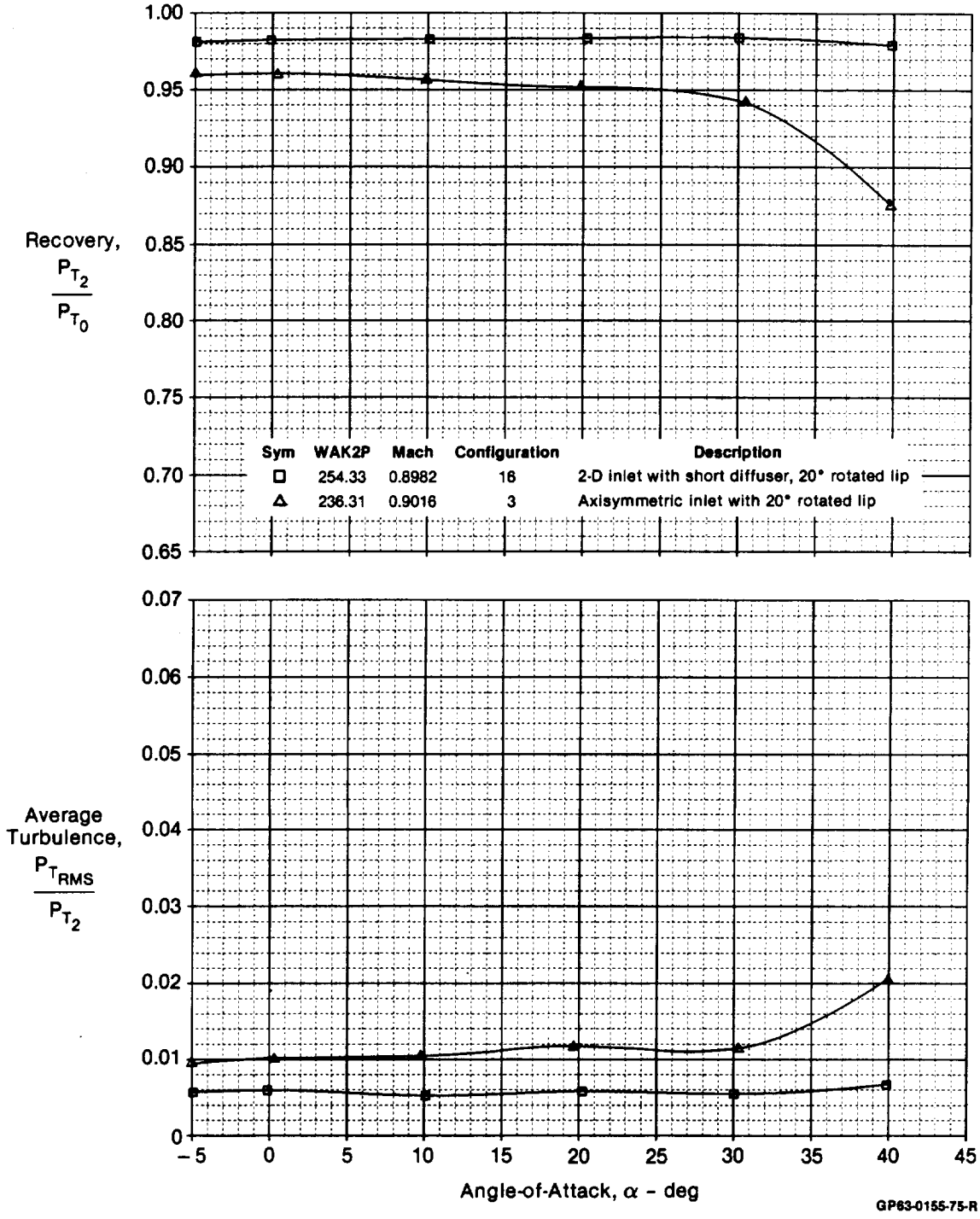

Figure 5-67. Comparison of 2-D and Axisymmetric Inlets
20° Rotated Cowl Lip Configurations $M_0 = 0.9$

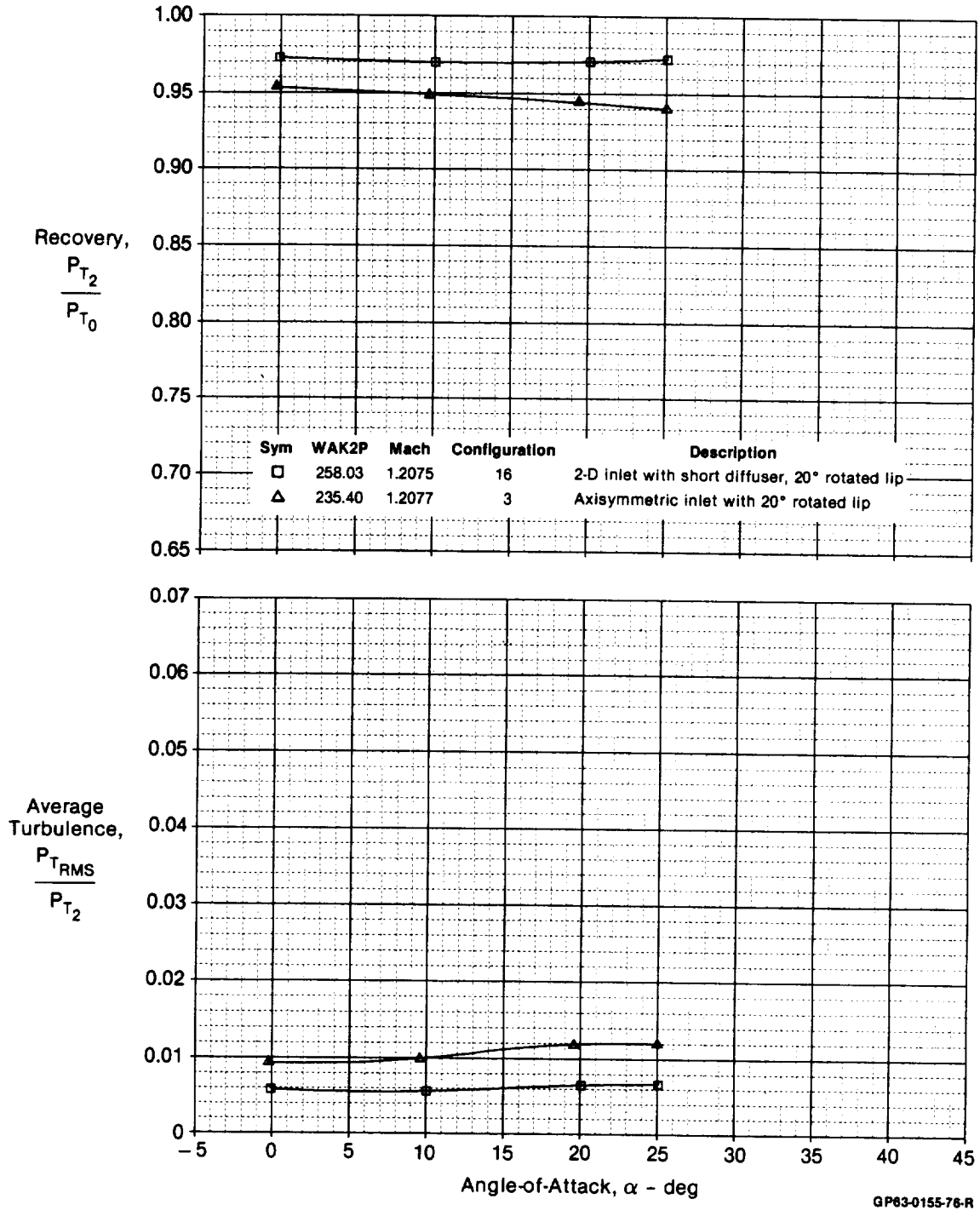

Figure 5-68. Comparison of 2-D and Axisymmetric Inlets
20° Rotated Cowl Lip Configurations $M_0 = 1.2$

The rotated lip does not seem as beneficial on the 2-D inlet only because its baseline performance was already high relative to axisymmetric inlets. With the 20° rotated cowl lip, the 2-D inlet recovery and turbulence levels were invariant with model angle of attack from Mach 0.6 to 1.2. This is in contrast to the axisymmetric case, where the break in recovery was only delayed to $\alpha = 30°$. The 2-D inlet also has the considerable benefit of easy mechanical implementation.

The exceptional performance of the 2-D inlet with the blunt rotating cowl lip suggests that it may be possible to design an inlet with a sharp cowl lip for low drag at supersonic speeds, and yet maintain the required maneuvering performance in the subsonic/transonic regime.

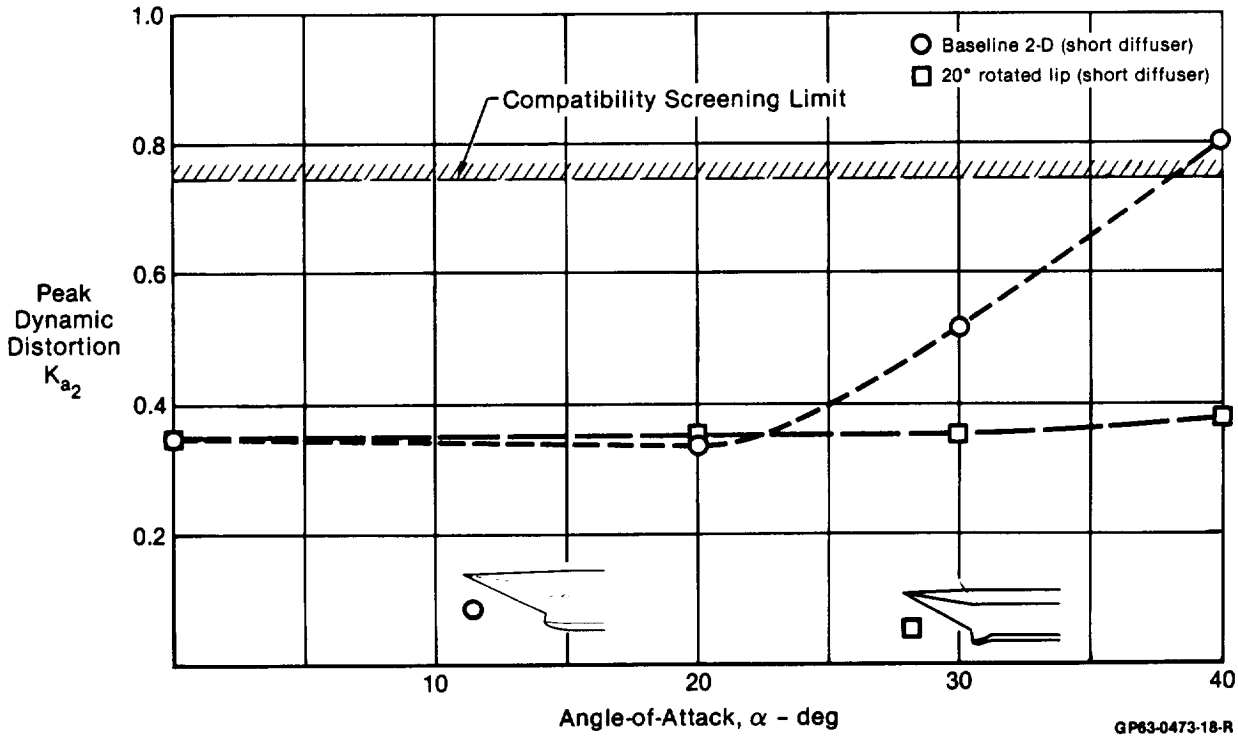

Figure 5-69. Peak Dynamic Distortion for the Baseline and 20° Rotated Lip Configurations
Mach 0.9

6. CONCLUSIONS

The purpose of this test program was to evaluate flow improvement concepts designed to improve the subsonic/transonic maneuvering performance of 2-D and axisymmetric inlets. Two methods were tested extensively: a rotating cowl lip design and auxiliary inlets. A retracting centerbody was also tested on the axisymmetric inlet. Testing was conducted over a Mach number range of 0.6 to 1.4. Conclusions and recommendations can be summarized as follows:

1. Of the two concepts tested, the rotated lip design was superior. It was effective for both 2-D and axisymmetric inlets.

2. Tests were conducted on 20° and 40° cowl lip rotation angles. The 20° angle provided the best performance for both the 2-D and axisymmetric inlets. Recovery levels at 40° angle of attack were improved with the 20° rotated lip by 7.5% for the 2-D inlet and 20% for the axisymmetric inlet. Turbulence levels were reduced by a factor of 4.5 and 2.3 respectively.

3. The rotating cowl lip design tested on the axisymmetric inlet in this program requires that the sideplates retract into the inlet throat. This decreased recovery by 3% at Mach 0.9 and $\alpha = 0°$.

4. The cowl lip contour did not have a great impact on the 40° rotated lip configuration. The location of the stagnation point on the cowl was the principle variable effecting inlet performance.

5. The auxiliary inlet concepts were not effective in improving inlet angle of attack performance in the Mach 0.6 to 0.9 range. This was the case for both the 2-D and axisymmetric inlets. Auxiliary inlets on the lower side of the inlet provided marginal performance improvement at very high angles of attack.

6. An external scoop provided a small performance improvement over the flush auxiliary inlet on the 2-D inlet.

7. Neither of the two flow improvement concepts were effective at supersonic Mach numbers.

8. Retracting the centerbody on the axisymmetric inlet provided slightly better inlet performance at angles of attack above 20°.

Analysis of the test data, and also computational results on the 2-D inlet, indicate that cowl rotation can eliminate flow separation on the cowl lip. Over-rotation, however, can result in separation at the pivot point of the cowl lip. The condition defining the optimum rotation angle at each Mach number and angle of attack combination can be considered to be that rotation which places the stagnation streamline on the cowl lip highlight.

The auxiliary inlet configurations did not provide significant recovery advantages over the Mach number range tested. It may be possible, however, with alternate designs, to improve their performance.

7. REFERENCES

1. Aiello, R. A., and Swallow, R. J., "NASA Lewis 8-by-6-Foot Supersonic Wind Tunnel," NASA TM X-71542, May 1974.

2. Bush, R. H., "External Compression Inlet Predictions Using an Implicit, Upwind, Multiple Zone Approach", AIAA Paper 85-1521, AIAA 7th Computational Fluid Dynamics Conference, July 1985.

APPENDIX A
NASA LEWIS HIMAT MASS FLOW PLUG CALIBRATION RESULTS

The mass flow plug used in this test program was calibrated in April 1982 in the NASA Lewis 8x6 foot wind tunnel. The calibration was performed just prior to the inlet test program to provide accurate computation of the inlet mass flow. This appendix presents a brief description of the calibration procedure and documents the results of the calibration. Calibration results given in terms of the plug airflow corrected to sea level standard conditions as a function of the mass flow plug position and static to total pressure ratio.

The mass flow plug was calibrated over a corrected airflow range from 0.5 to 5.0 lbm/sec. High pressure air was metered through the mass flow plug and exhausted to ambient air in the wind tunnel test section. The calibration setup is illustrated in Figure A-1. Calibrated choked flow venturi flowmeters were used to measure the flow rate to the mass flow plug. A 1.00 inch diameter venturi was used in the calibration for the larger plug positions. At the smaller plug positions, where the 1.0 inch diameter venturi would unchoke, a 0.67 inch diameter venturi was used to measure massflow. Flow from the venturi flowmeters passed through a perforated plate to dissipate any flow distortion entering the mass flow plug.

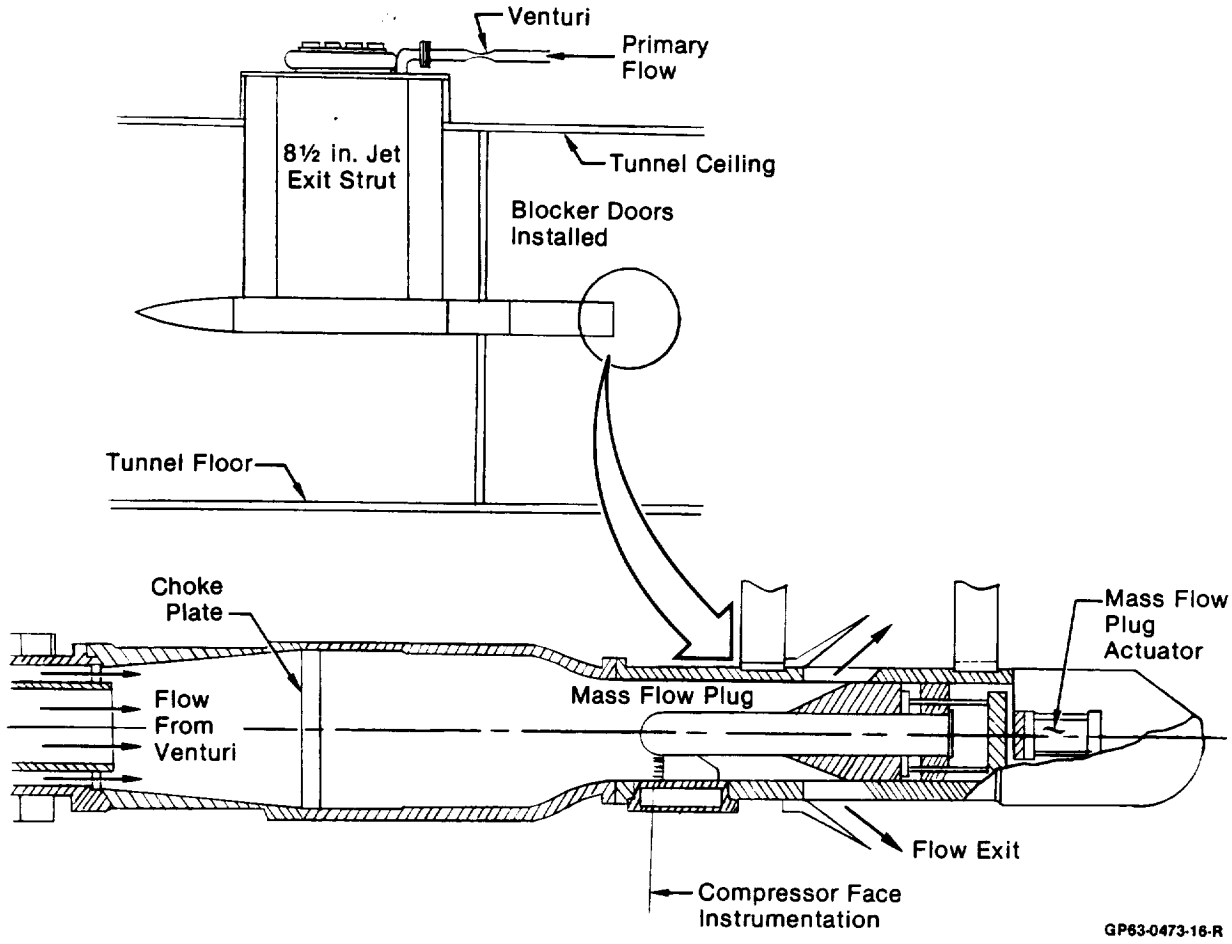

Figure A-1. Mass Flow Plug Calibration Setup in 8 x 6 Ft Wind Tunnel

The mass flow plug pressure ratio is defined as the average exit static pressure divided by the average total pressure at the plug entrance. The mass flow plug instrumentation is detailed in Section 3.3. The average of the 40 total pressure measurements at the plug entrance rake gives the plug total pressure. Eight static pressure measurements near the plug housing exit were averaged to determine the exit static pressure. The mass flow through plug was computed from the measured static pressures on the calibrated choked flow venturi. Airflow values were corrected using the mass flow plug average total pressure and venturi total temperature.

The mass flow plug was calibrated by varying the plug pressure ratio at a fixed plug position. The plug position was set and the supply pressure at the calibrated venturi was varied to provide a static to total pressure ratio at the mass flow plug between 0.95 and 0.99. The plug average static and total pressure were recorded along with the computed mass flow through the venturi. The supply pressure was then raised to increase the Mach number (reduce (PS/PT) plug) at the mass flow plug exit. The mass flow plug static to total pressure ratio was reduced in increments of .02 to .05 until the ratio could not be further reduced, indicating the flow was choked. The mass flow plug position was set to the next desired position and the pressure ratio sweep repeated. The largest plug positions were calibrated using the larger calibrated choked flow venturi. Plug position is defined to be the distance from the base of the mass flow plug housing to the shoulder of the conical plug, Figure A-2. Limits on plug position were 0.2 to 2.5 inches. The plug positions tested are also shown in Figure A-2.

The calibration results give the mass flow plug corrected airflow values as a function of the measured static to total pressure ratio for 13 plug positions. Figure A-3 presents the results of the mass flow plug calibration for plug positions from 0.21 to 2.5 inches. At mass flow plug positions of 2.2 and 2.5, flow choked at the plug rake rather than at the plug exit. A calibration summary plot containing the calibration curves for plug positions of 0.21 to 2.0 is presented in Figure A-4. Figure A-5 shows the variation in choked corrected flow with mass flow plug position.

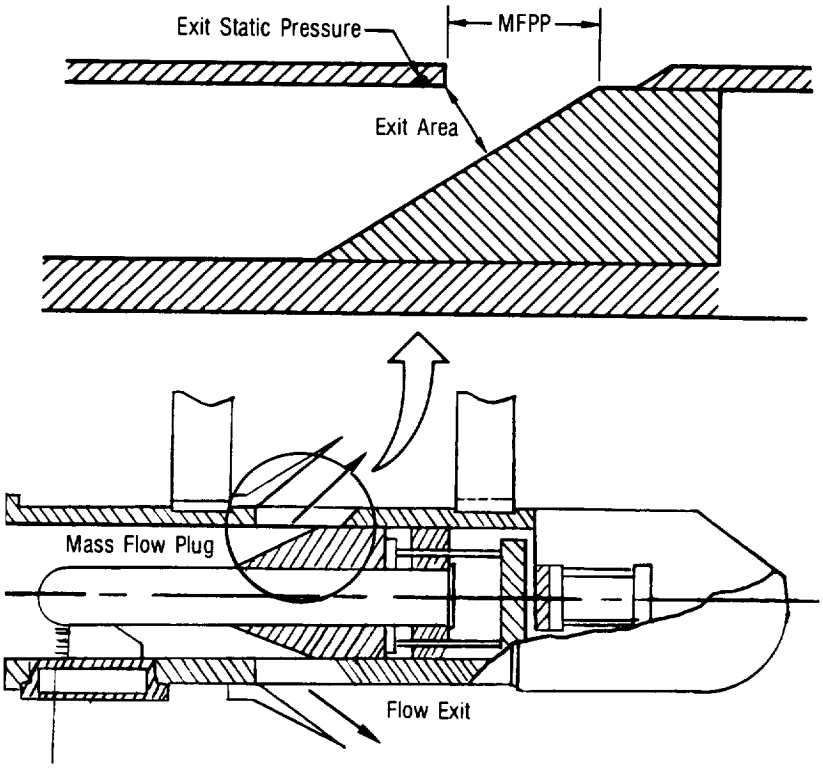

Mass Flow Plug Position (MFPP)	(in.)	0.21	0.31	0.41	0.63	0.80	1.00	1.20	1.40	1.60	1.80	2.00	2.20	2.50
Choked Corrected Flow Rate, $\dot{W}\sqrt{\theta}/\delta$	(lbm/sec)	0.53	0.77	1.10	1.71	2.19	2.71	3.22	3.73	4.19	4.55	4.83	4.94	4.97

GP63-0473-17-R

Figure A-2. Mass Flow Plug Positions and Corresponding Choked Corrected Airflow Rates

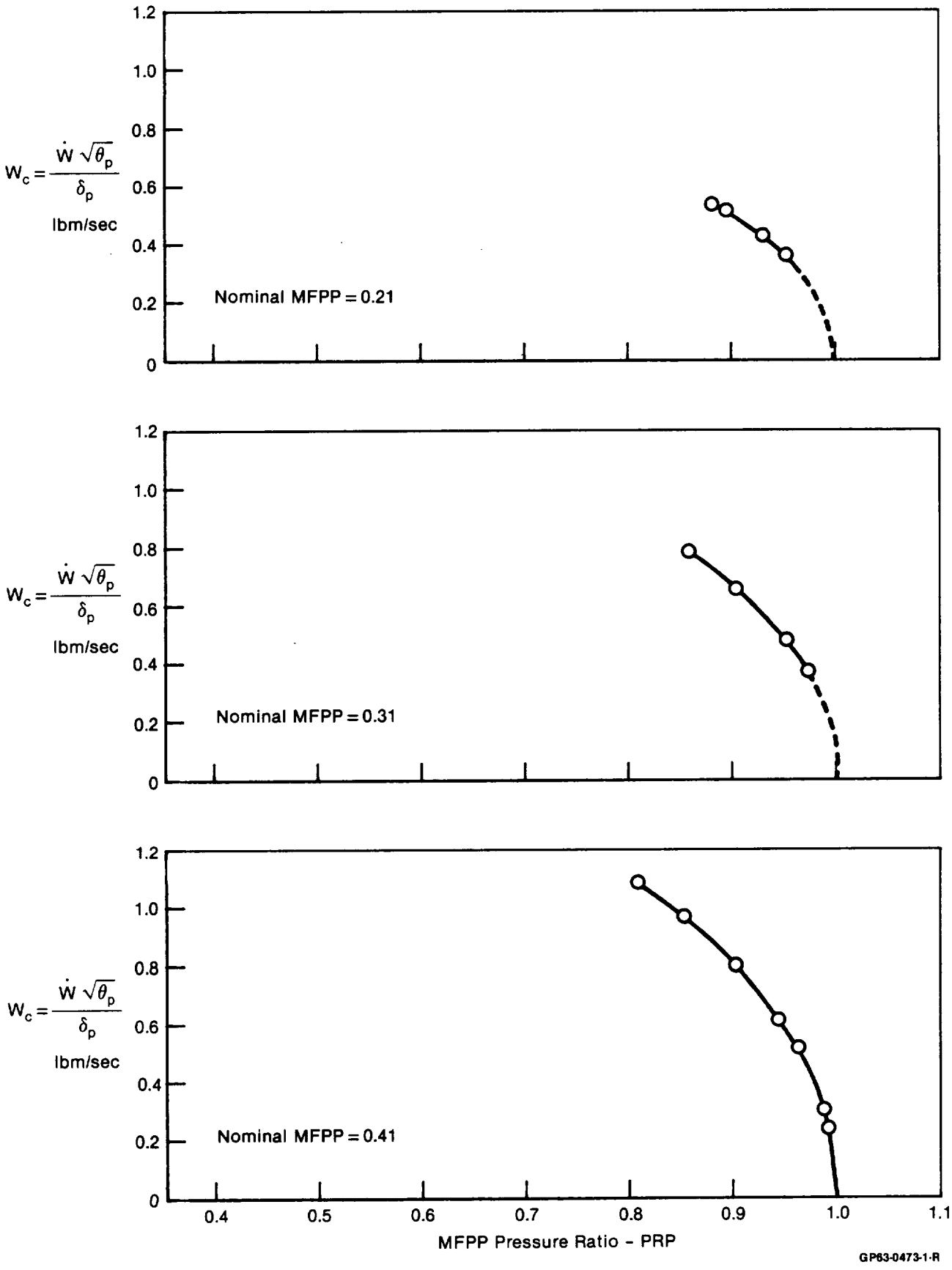

Figure A-3. NASA-Lewis HIMAT Mass Flow Plug Calibration Curves

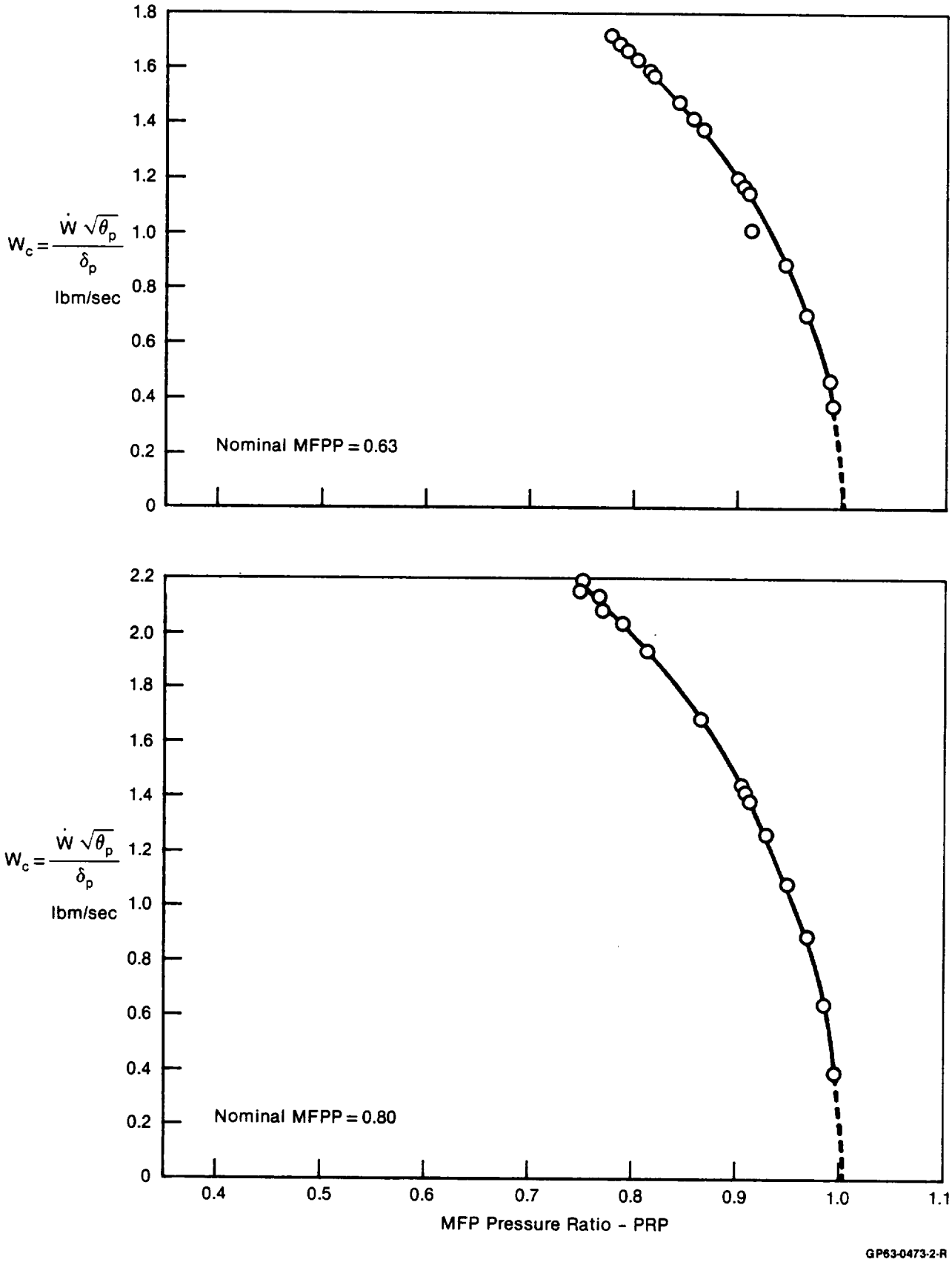

Figure A-3. (Continued) NASA-Lewis HIMAT Mass Flow Plug Calibration Curves

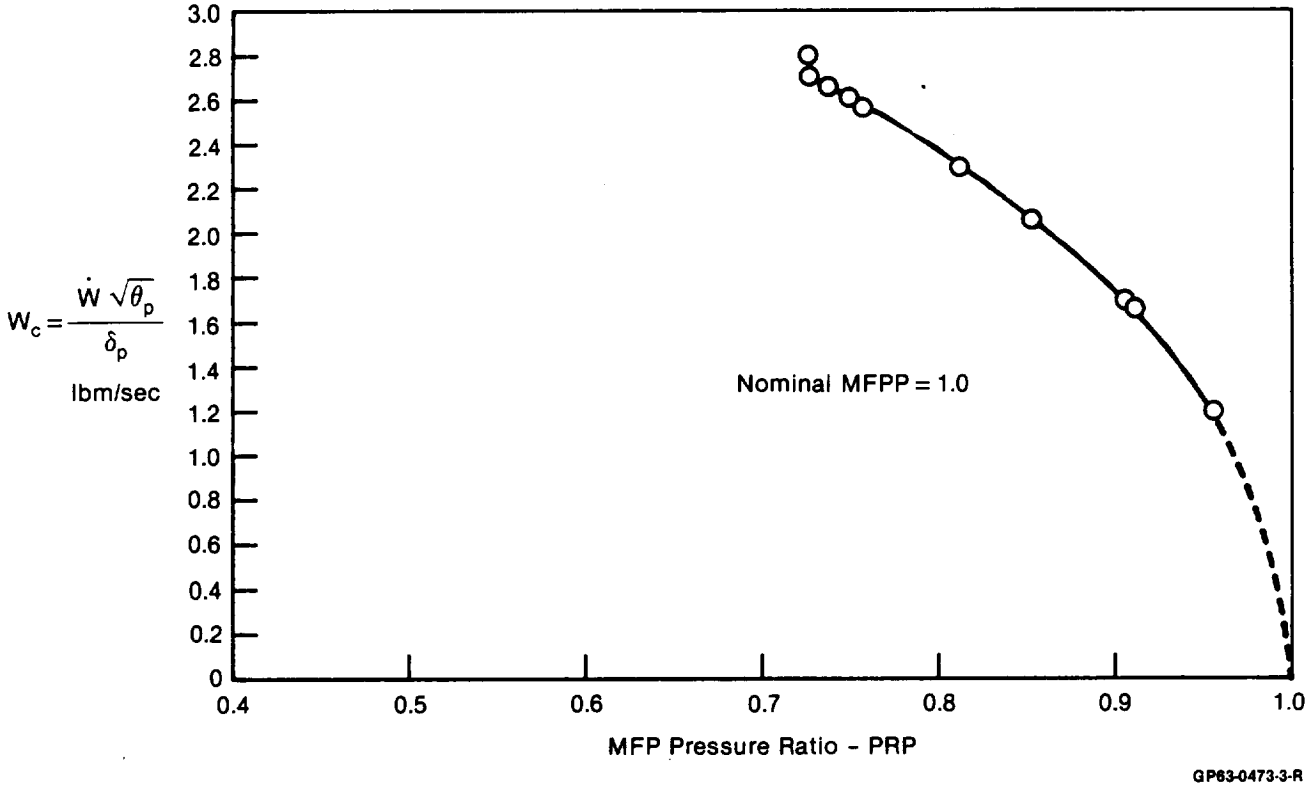

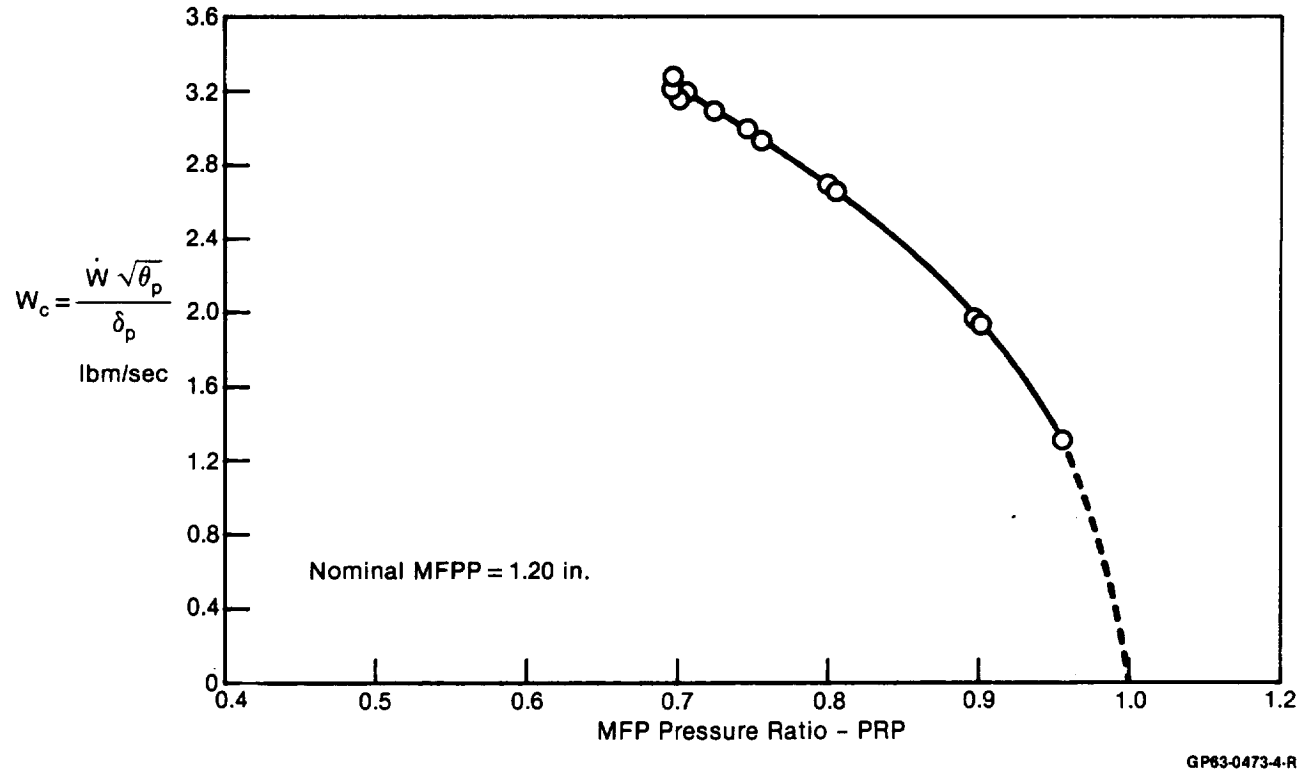

Figure A-3. (Continued) NASA-Lewis HIMAT Mass Flow Plug Calibration Curves

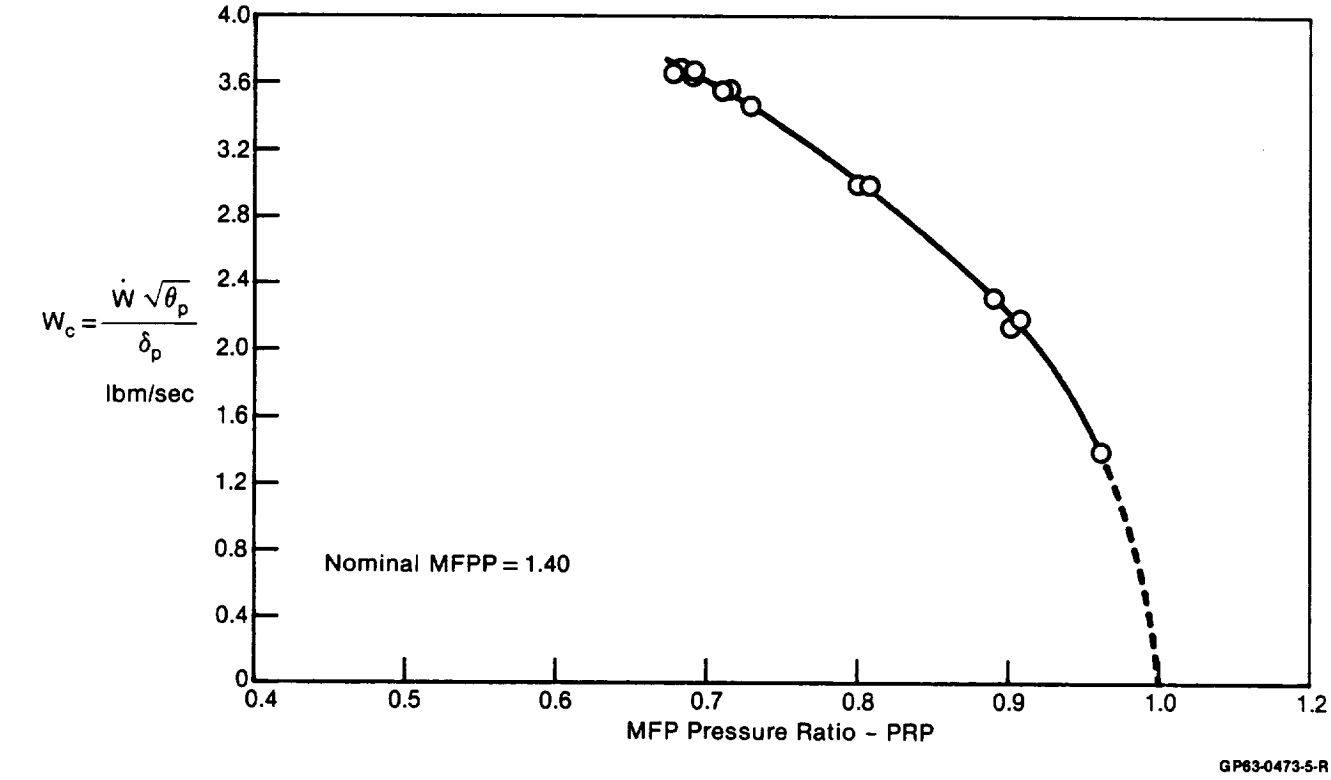

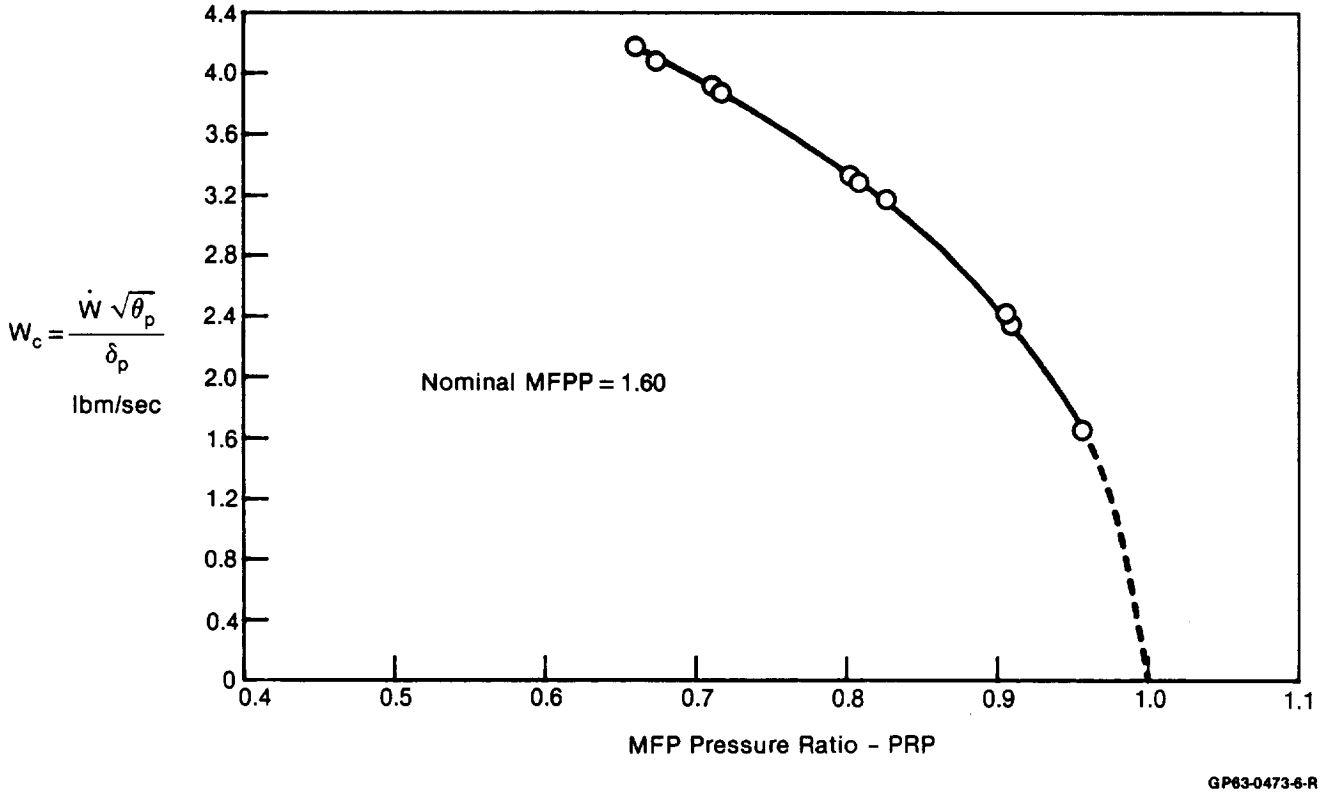

Figure A-3. (Continued) NASA-Lewis HIMAT Mass Flow Plug Calibration Curves

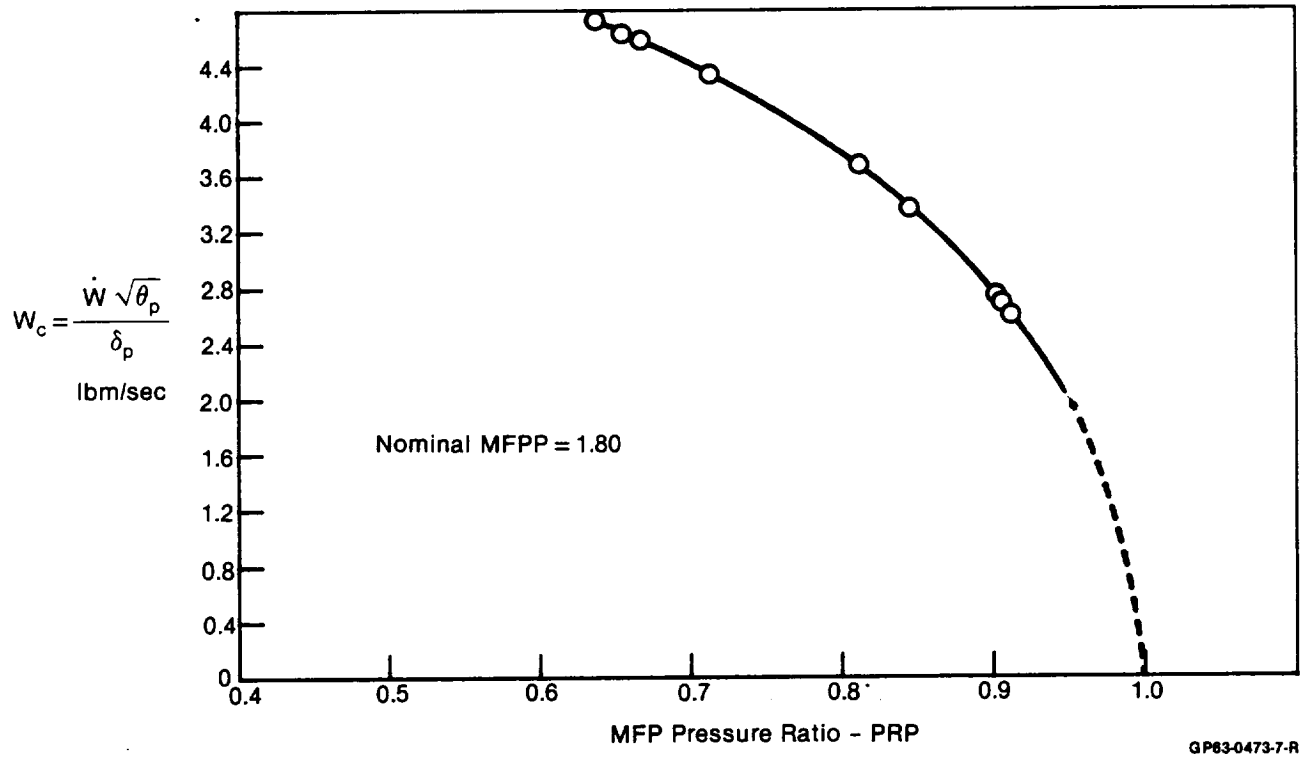

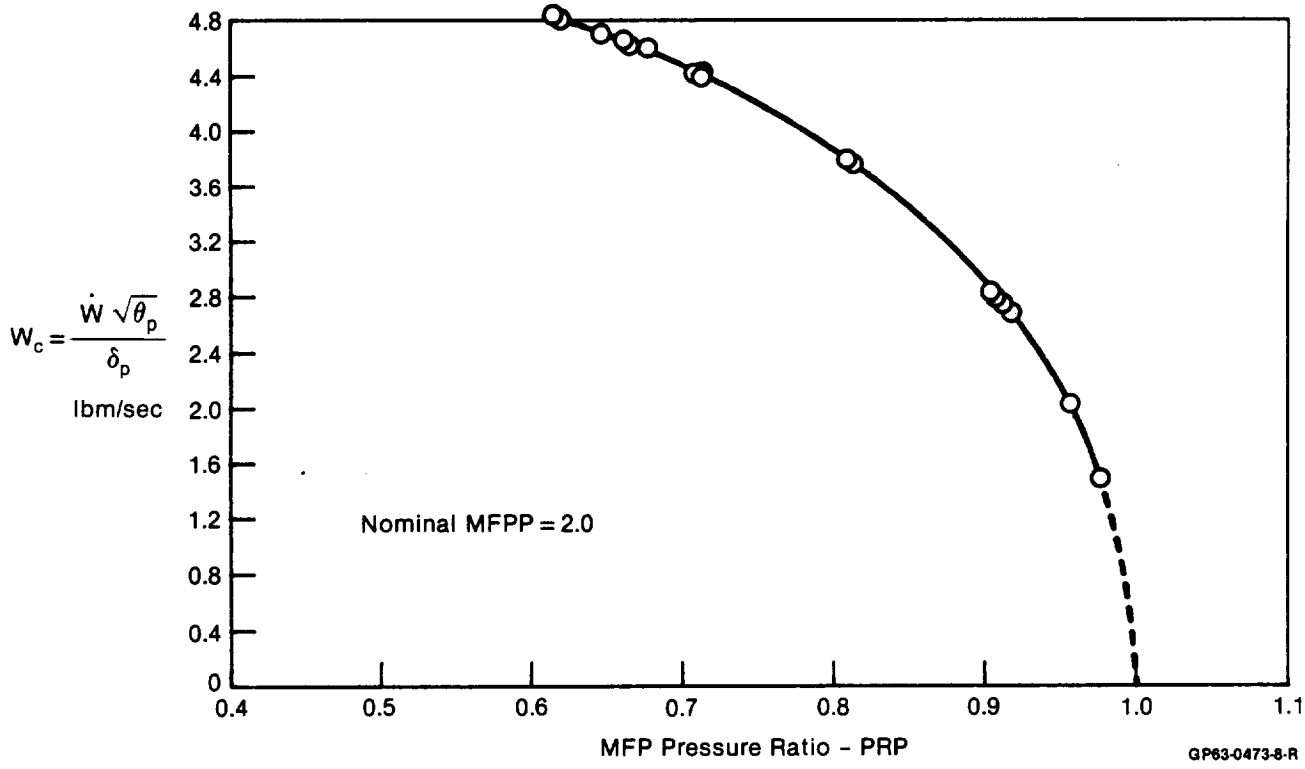

Figure A-3. (Continued) NASA-Lewis HIMAT Mass Flow Plug Calibration Curves

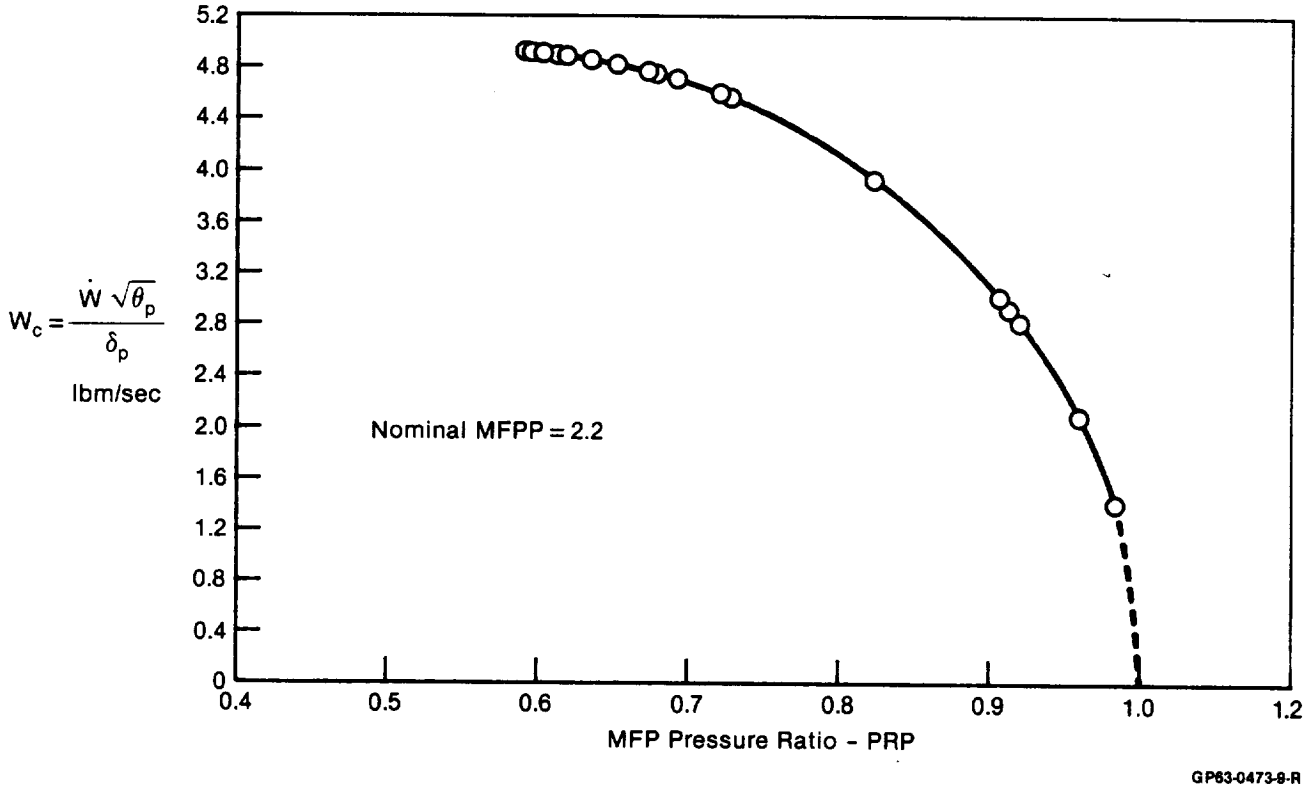

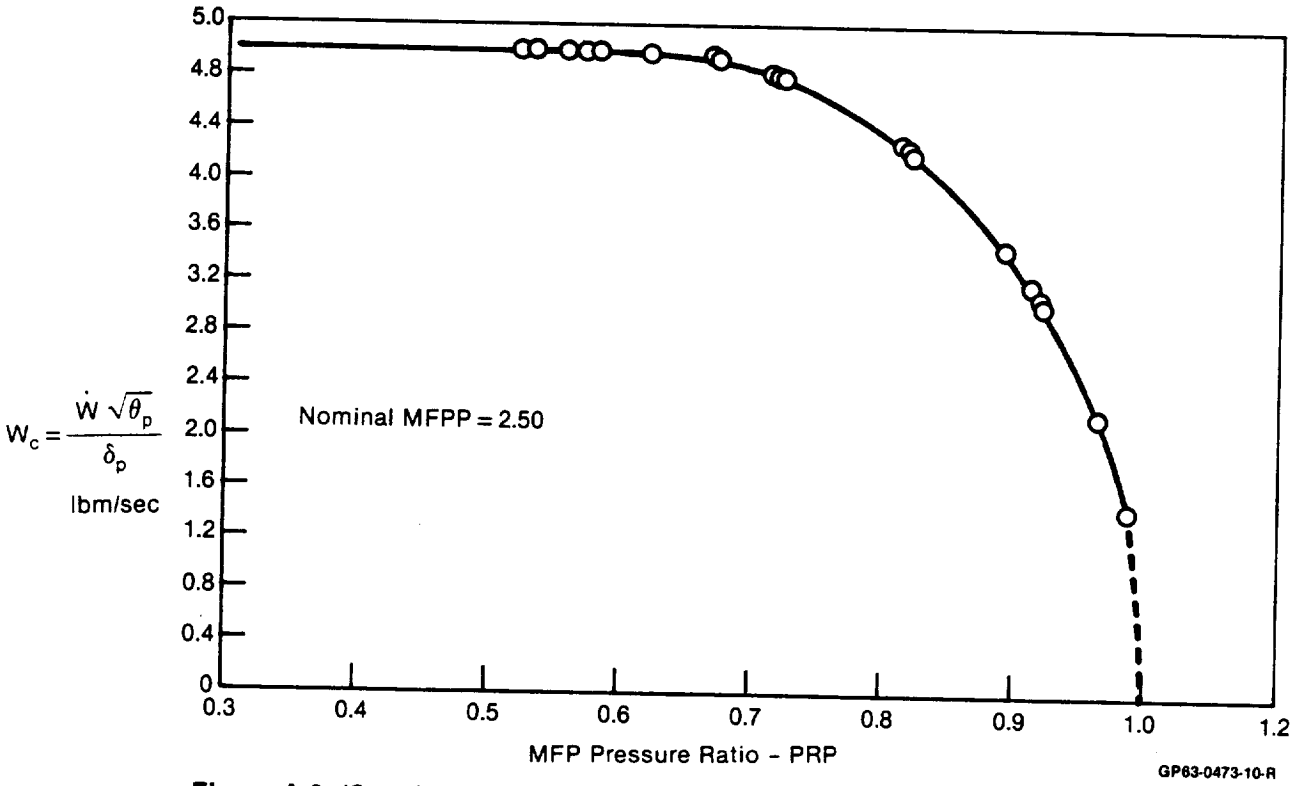

Figure A-3. (Concluded) NASA-Lewis HIMAT Mass Flow Plug Calibration Curves

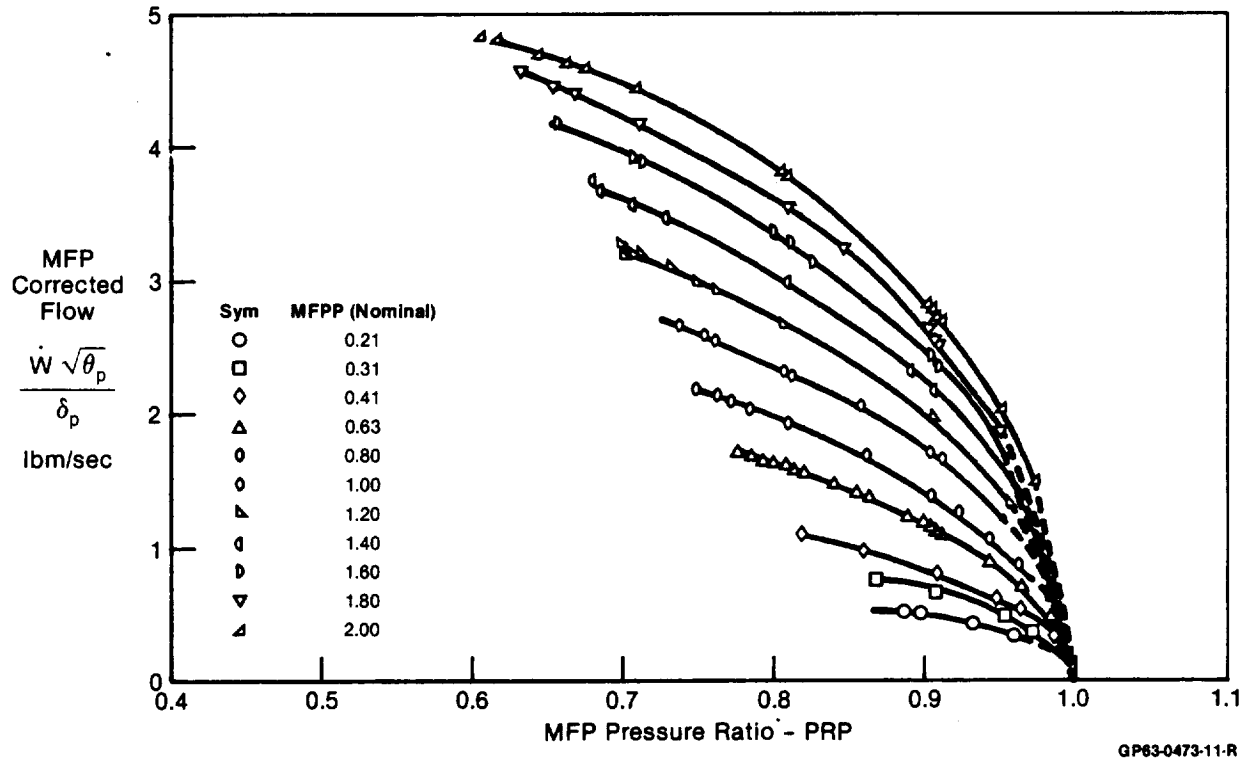

Figure A-4. Summary of NASA-Lewis HIMAT Mass Flow Plug Calibration

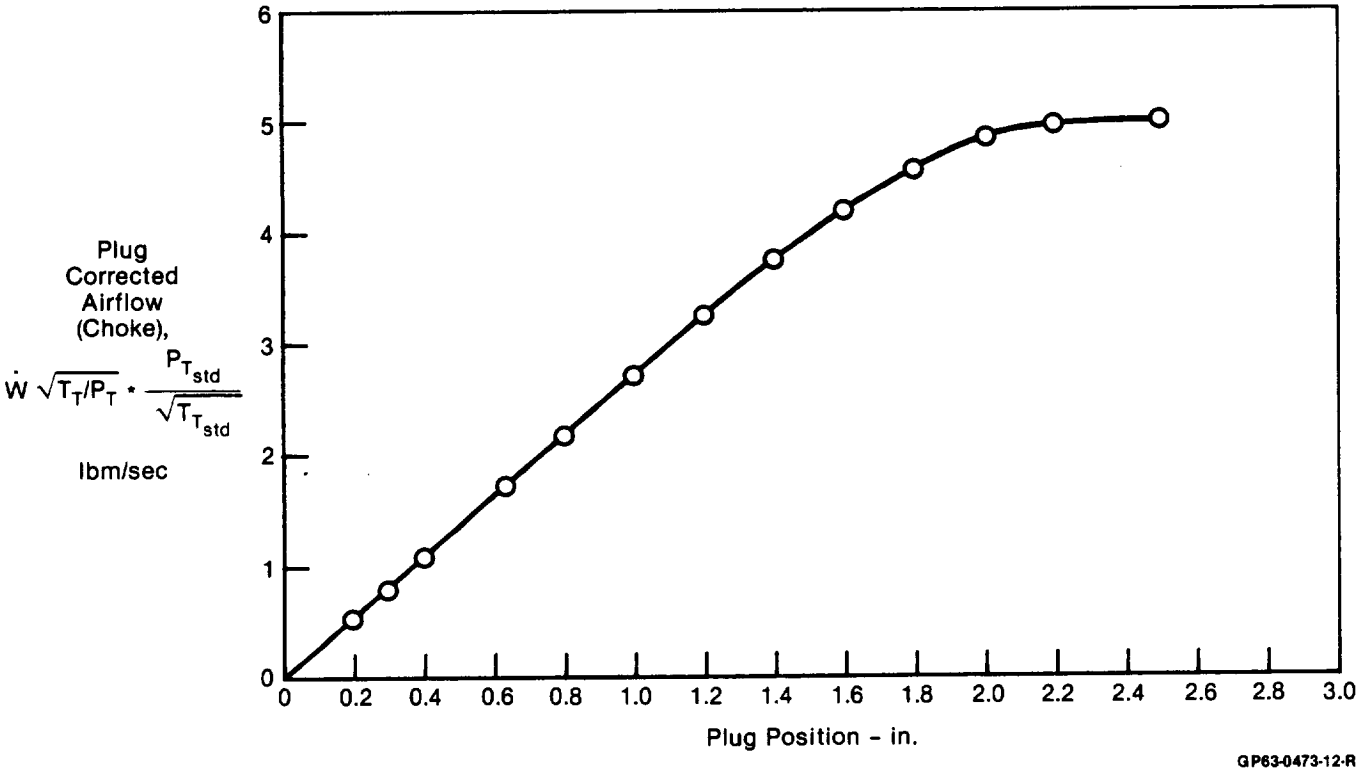

Figure A-5. Curve of Choked Corrected Airflow Values for the NASA-Lewis HIMAT Mass Flow Plug

APPENDIX B
INLET PERFORMANCE AS A FUNCTION OF MASS FLOW

This Appendix presents the recovery and average turbulence data as a function of mass flow ratio for all the Mach numbers and angles of attack tested. Each figure contains data for one configuration at a particular test Mach number, while each curve on a Figure represents a different angle of attack. Table B-1 indexes the data contained in this Appendix. It shows the figure numbers for each configuration, Mach number, and angle of attack combination. The angle of attack schedules referred to in Table B-1 are given below:

Schedule	Angles of Attack (degrees)
A	0, 10, 20, 30, 40
B	0, 10, 20, 25
C	0, 5, 10, 15, 20
D	-5, 0, 10, 20, 30, 40
E	0, 20, 40
F	-5, 0, 5, 10, 15, 20

Table B-1. Index for Appendix B

Configuration	Mach Number	Angle-of-Attack Schedule	Figure
Baseline Axisymmetric Inlet	0.6	A	B-1
	0.9	A	B-2
	1.2	B	B-3
	1.4	C	B-4
Axisymmetric Inlet, 20° Rotated Lip	0.6	A	B-5
	0.9	D	B-6
	1.2	B	B-7
	1.4	C	B-8
Axisymmetric Inlet, 40° Rotated Lip	0.6	A	B-9
	0.9	D	B-10
	1.2	B	B-11
	1.4	C	B-12
Axisymmetric Inlet With Retracted Sideplates	0.6	E	B-13
	0.9	E	B-14
	1.4	C	B-15
Axisymmetric Inlet, Lower Auxiliary Inlets Open 100%	0.6	A	B-16
	0.9	A	B-17
	1.2	B	B-18
	1.4	B	B-19
Axisymmetric Inlet, Lower Auxiliary Inlets Open 50%	0.6	E	B-20
	0.9	E	B-21
Axisymmetric Inlet, Upper and Lower Auxiliary Inlets Open 50%	0.6	E	B-22
	0.9	E	B-23
Axisymmetric Inlet, Upper and Lower Auxiliary Inlets Open 100%	0.6	A	B-24
	0.9	A	B-25
	1.2	E	B-26
	1.4	C	B-27
Axisymmetric Inlet, Upper Auxiliary Inlets Open 100%	0.6	A	B-28
	0.9	A	B-29
	1.2	B	B-30
	1.4	C	B-31
Axisymmetric Inlet, Upper Auxiliary Inlets Open 50%	0.6	E	B-32
	0.9	E	B-33
Axisymmetric Inlet With Retracted Centerbody	0.6	E	B-34
	0.9	A	B-35
Axisymmetric Inlet, 20° Rotated Lip, Lower Auxiliary Inlets Open 100%	0.6	A	B-36
	0.9	D	B-37
	1.2	B	B-38
Axisymmetric Inlet, 20° Rotated Lip, Lower Auxiliary Inlets Open 100%, Retracted Centerbody	0.6	A	B-39
	0.9	D	B-40
2-D Inlet With Short Diffuser	0.6	A	B-41
	0.9	D	B-42
	1.2	B	B-43
2-D Inlet, 20° Rotated Lip	0.6	A	B-44
	0.9	D	B-45
	1.2	B	B-46
2-D Inlet, 40° Rotated Lip	0.6	A	B-47
	0.9	D	B-48
	1.2	B	B-49
2-D Inlet, Long Diffuser	0.6	A	B-50
	0.9	D	B-51
	1.2	B	B-52
	1.4	F	B-53

GP63-0155-97-R

SYM	TEST	RUN	RMACH	RALPHA	RBETA	CONFIG	DESCRIPTION
□	41	1	0.6035	0.1932	0.1328	2.0000	BASELINE AXI INLET
△	41	2	0.6053	10.155	0.0978	2.0000	BASELINE AXI INLET
◇	41	3	0.6056	20.052	0.1321	2.0000	BASELINE AXI INLET
○	41	4	0.6050	30.198	-0.0340	2.0000	BASELINE AXI INLET
✱	41	5	0.6064	38.627	-0.0210	2.0000	BASELINE AXI INLET

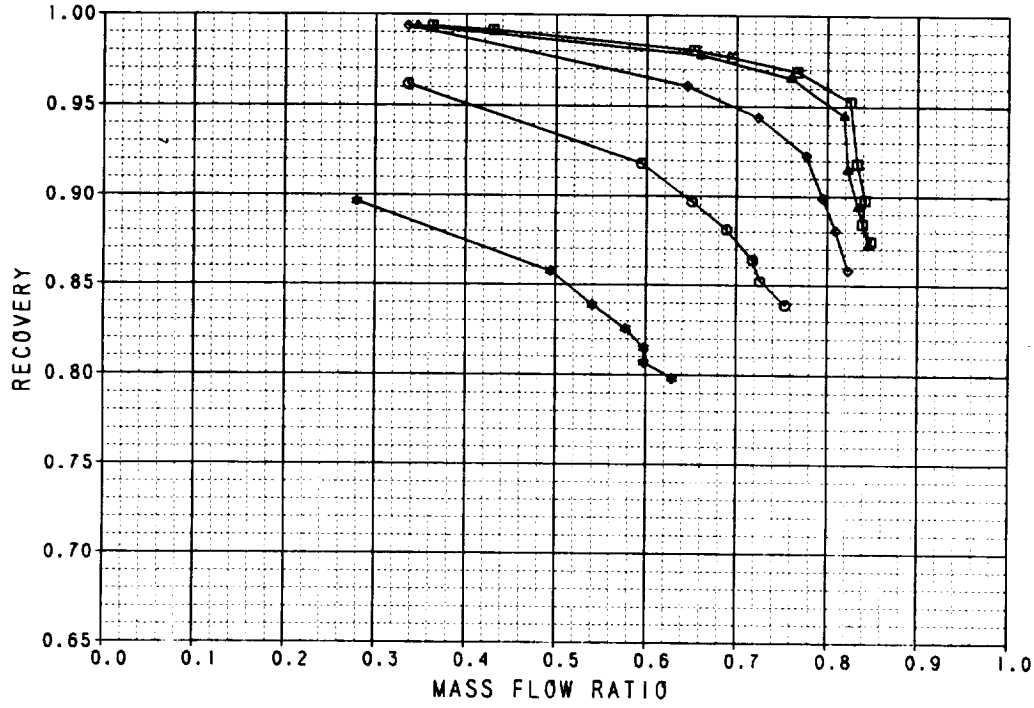

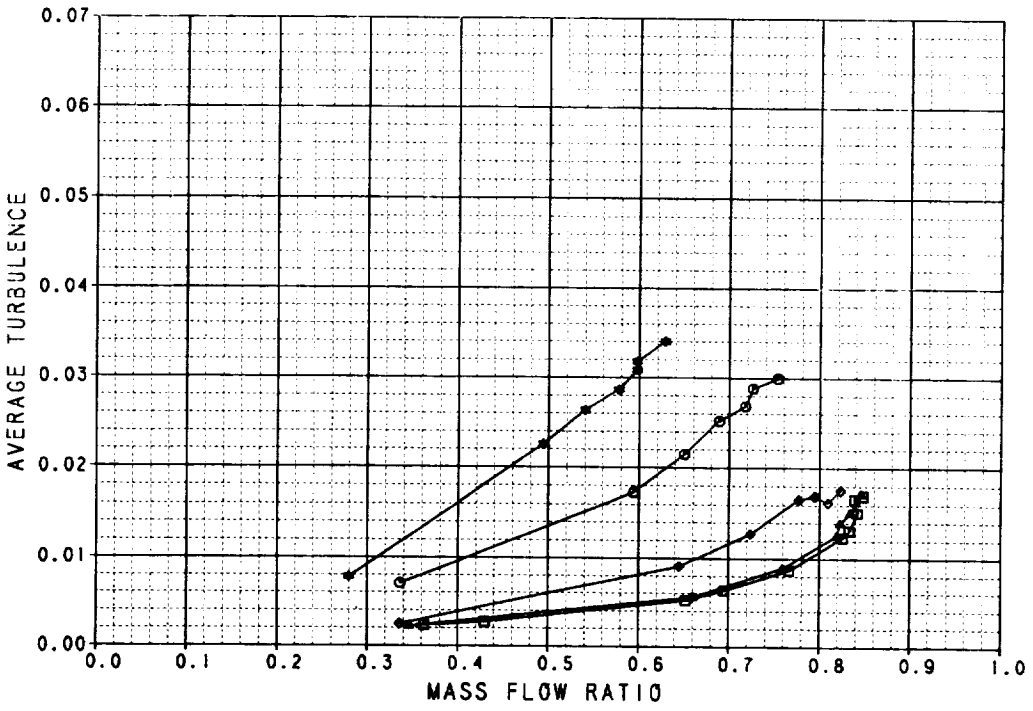

Figure B-1. Performance Data
Baseline Axisymmetric Inlet
$M_0 = 0.6$

SYM	TEST	RUN	RMACH	RALPHA	RBETA	CONFIG	DESCRIPTION
□	41	5	0.9009	0.0654	-0.1005	2.0000	BASELINE AXI INLET
▲	41	9	0.9008	10.096	0.0655	2.0000	BASELINE AXI INLET
◇	41	10	0.9007	20.157	-9.0E-4	2.0000	BASELINE AXI INLET
○	41	13	0.8999	30.048	0.0789	2.0000	BASELINE AXI INLET
✱	41	14	0.9018	39.918	0.0871	2.0000	BASELINE AXI INLET

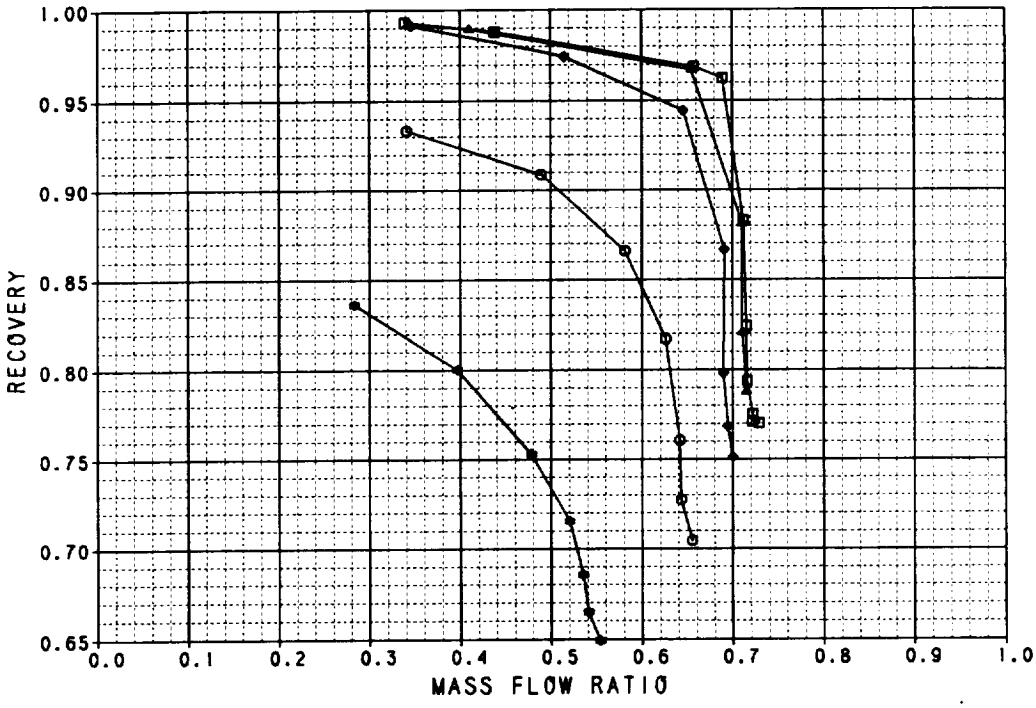

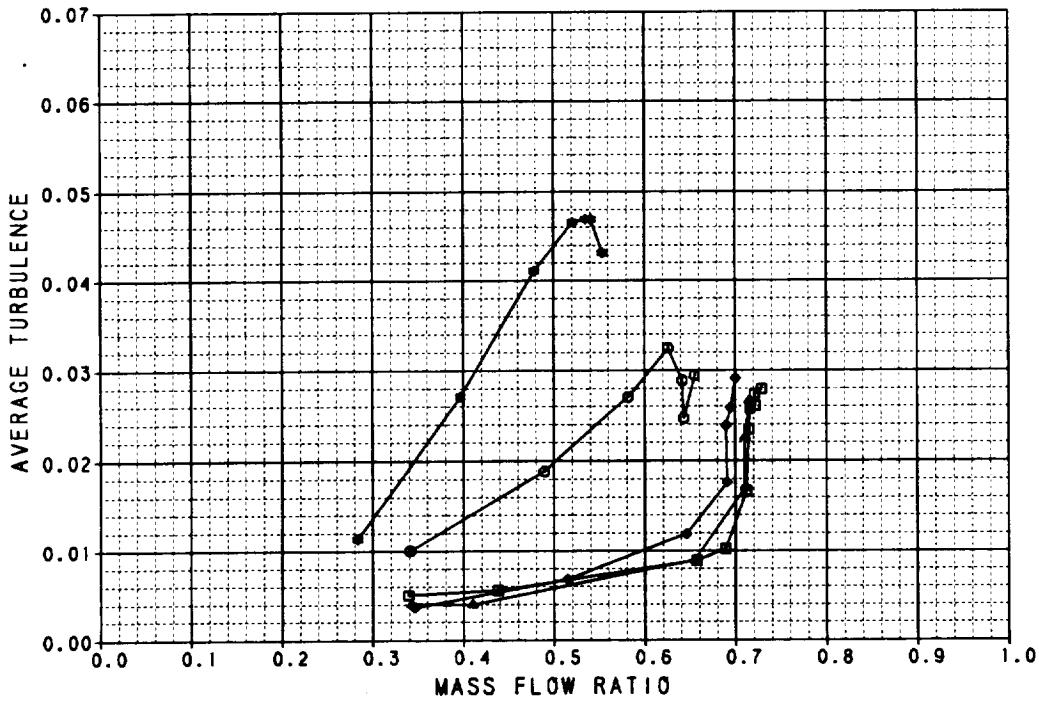

Figure B-2. Performance Data
Baseline Axisymmetric Inlet
$M_0 = 0.9$

SYM	TEST	RUN	RMACH	RALPHA	RBETA	CONFIG	DESCRIPTION
□	41	15	1.2075	0.1941	-0.0233	2.0000	BASELINE AXI INLET
▲	41	16	1.2099	10.234	0.0136	2.0000	BASELINE AXI INLET
◇	41	17	1.2029	20.005	0.0351	2.0000	BASELINE AXI INLET
○	41	18	1.2047	25.306	0.0857	2.0000	BASELINE AXI INLET

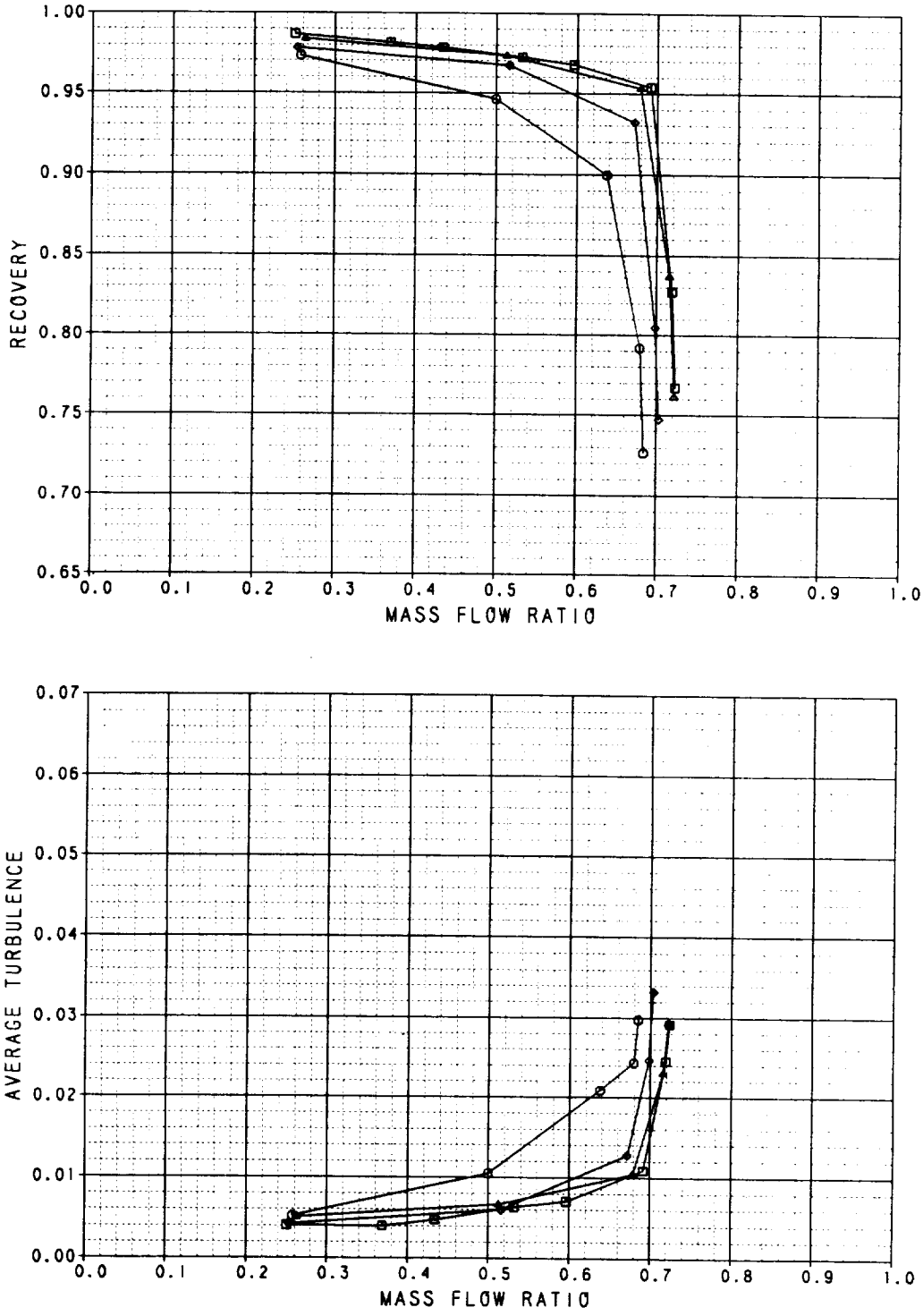

Figure B-3. Performance Data
Baseline Axisymmetric Inlet
$M_0 = 1.2$

SYM	TEST	RUN	RMACH	RALPHA	RBETA	CONFIG	DESCRIPTION
□	41	98	1.3962	-0.2637	0.0682	2.0000	BASELINE AXI INLET
▲	41	99	1.3959	4.9530	0.0620	2.0000	BASELINE AXI INLET
◇	41	100	1.3937	9.7108	0.0627	2.0000	BASELINE AXI INLET
○	41	101	1.3948	14.815	0.0689	2.0000	BASELINE AXI INLET
✱	41	102	1.3956	19.996	0.0779	2.0000	BASELINE AXI INLET

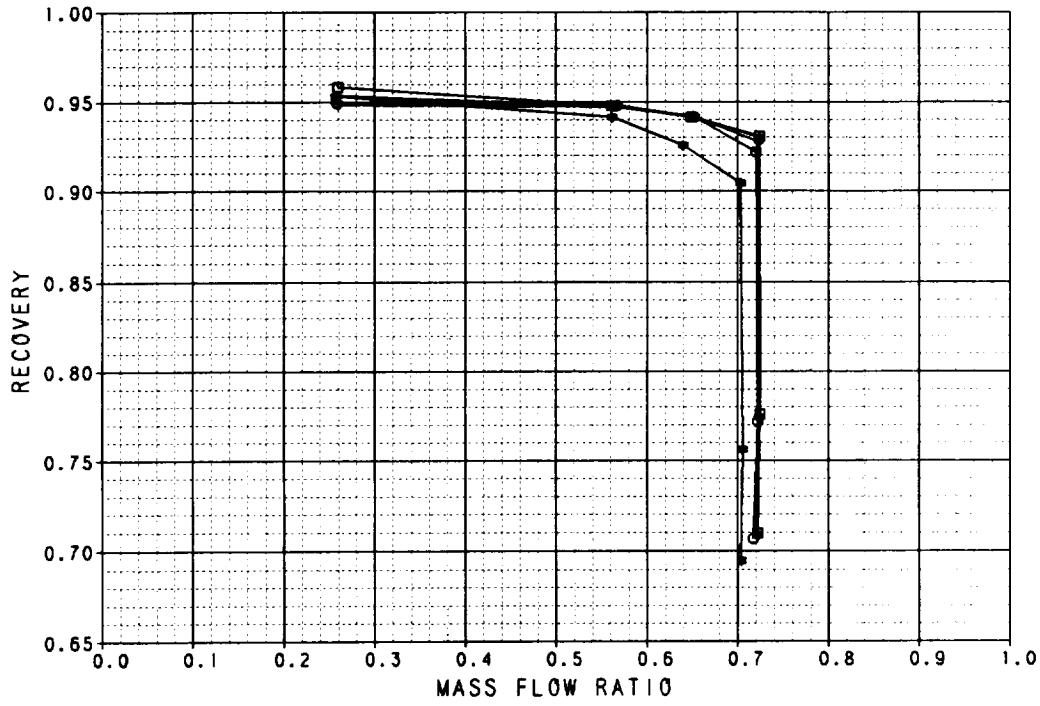

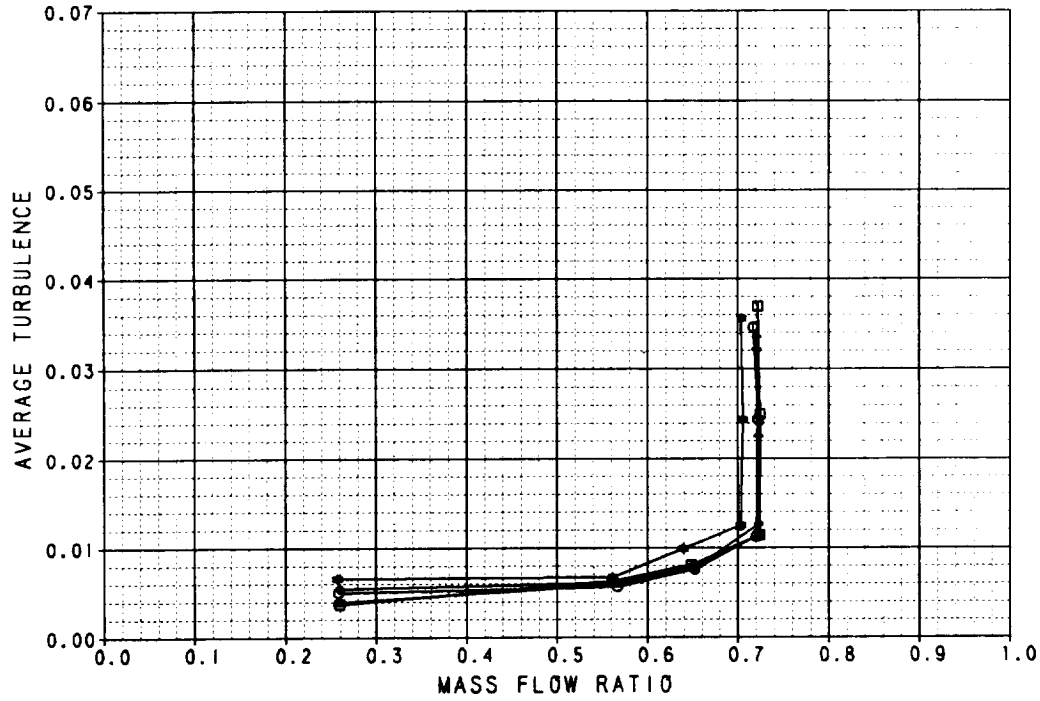

Figure B-4. Performance Data
Baseline Axisymmetric Inlet
$M_0 = 1.4$

SYM	TEST	RUN	RMACH	RALPHA	RBETA	CONFIG	DESCRIPTION
□	41	29	0.6071	0.0481	-0.0847	3.0000	AXI INLET WITH 20 DEG DROOP LIP
▲	41	30	0.6034	10.096	-0.0841	3.0000	AXI INLET WITH 20 DEG DROOP LIP
◇	41	31	0.6060	19.081	-0.0903	3.0000	AXI INLET WITH 20 DEG DROOP LIP
○	41	32	0.6069	30.522	-0.0958	3.0000	AXI INLET WITH 20 DEG DROOP LIP
●	41	33	0.6075	39.807	-0.0923	3.0000	AXI INLET WITH 20 DEG DROOP LIP

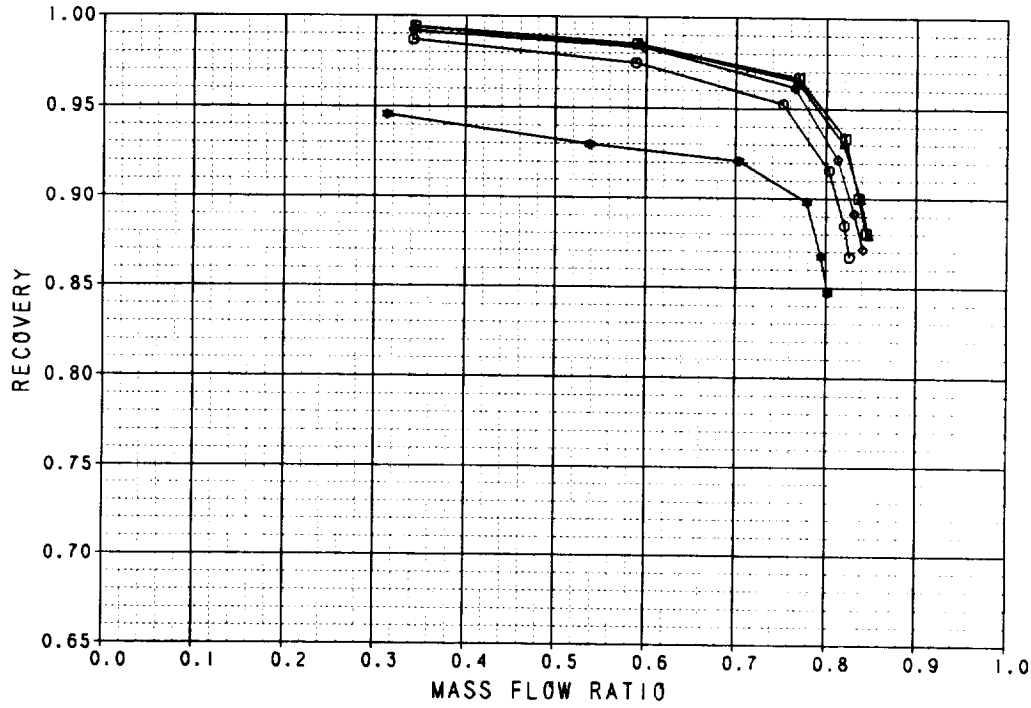

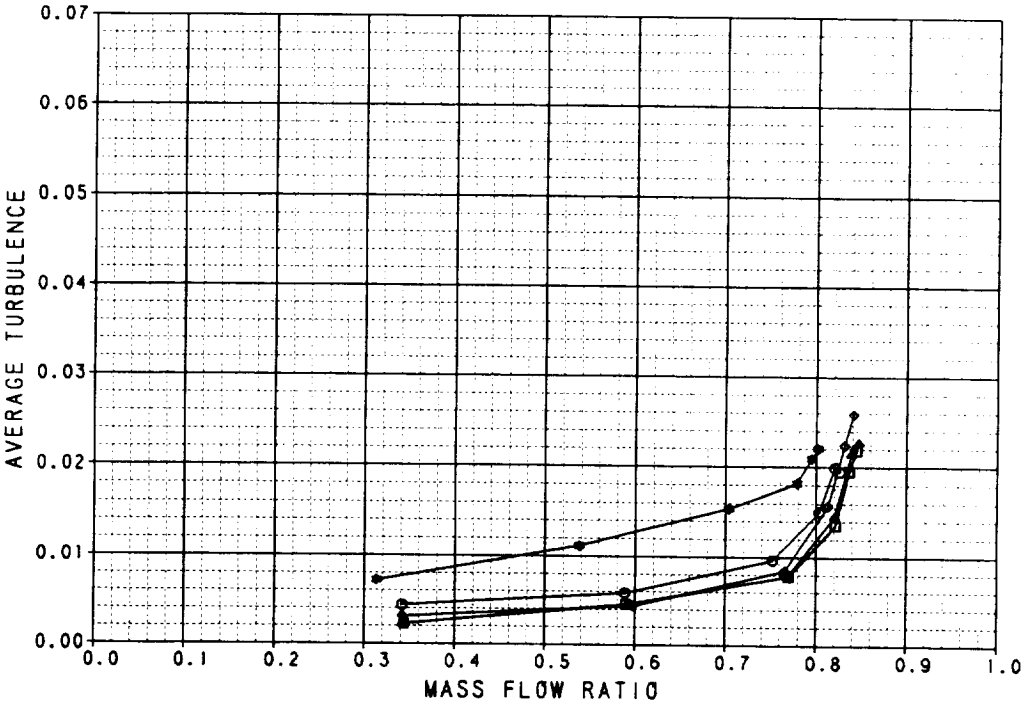

Figure B-5. Performance Data
Axisymmetric Inlet With 20° Cowl Lip
$M_0 = 0.6$

SYM	TEST	RUN	RMACH	RALPHA	RBETA	CONFIG	DESCRIPTION
□	41	37	0.9021	-5.0324	0.0544	3.0000	AXI INLET WITH 20 DEG DROOP LIP
△	41	34	0.9003	0.3480	-0.1042	3.0000	AXI INLET WITH 20 DEG DROOP LIP
◇	41	38	0.9014	9.8146	0.0455	3.0000	AXI INLET WITH 20 DEG DROOP LIP
○	41	39	0.9017	19.707	0.0124	3.0000	AXI INLET WITH 20 DEG DROOP LIP
✱	41	42	0.9034	30.435	-0.0289	3.0000	AXI INLET WITH 20 DEG DROOP LIP
✕	41	43	0.9009	39.852	-0.0420	3.0000	AXI INLET WITH 20 DEG DROOP LIP

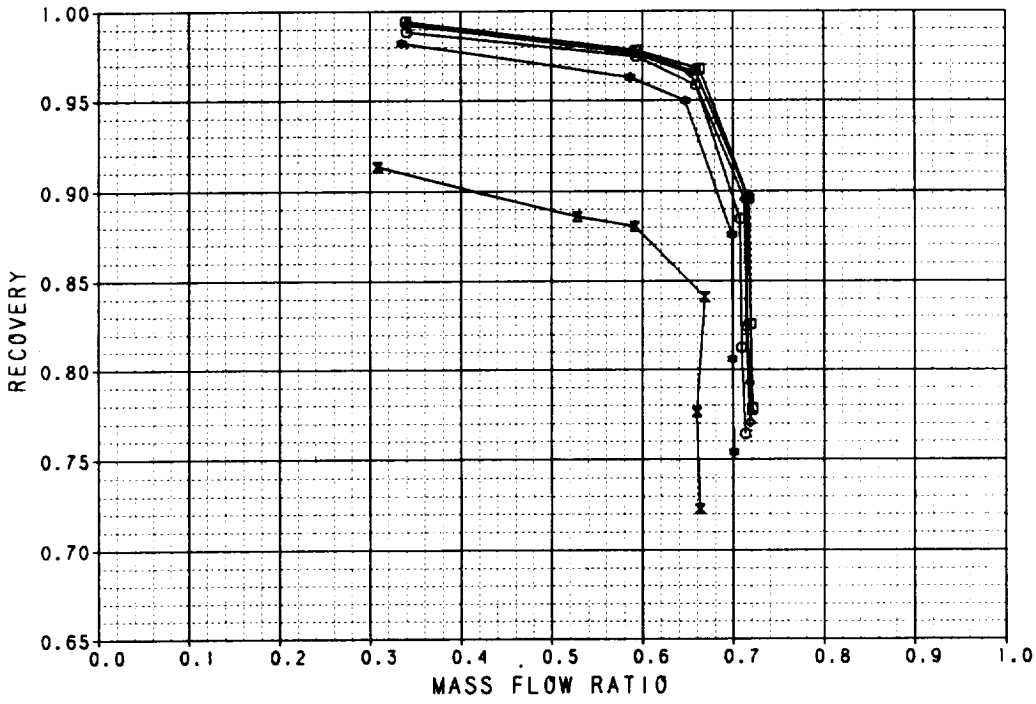

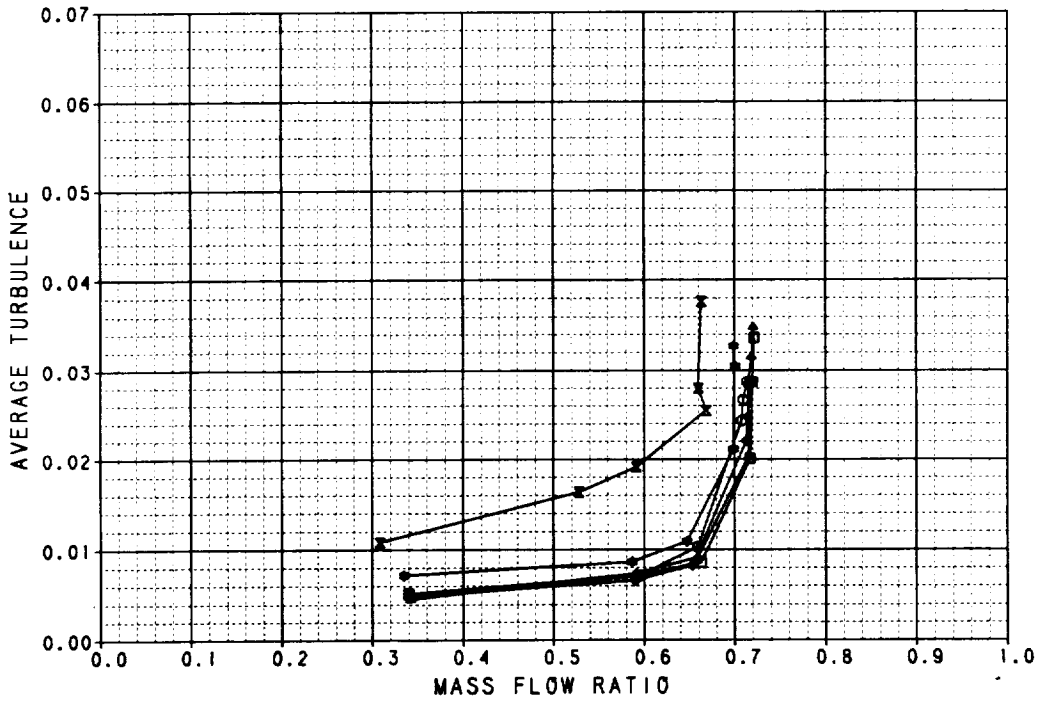

Figure B-6. Performance Data
Axisymmetric Inlet With 20° Cowl Lip
$M_0 = 0.9$

SYM	TEST	RUN	RMACH	RALPHA	RBETA	CONFIG	DESCRIPTION
□	41	44	1.2065	-0.2989	-0.0173	3.0000	AXI INLET WITH 20 DEG DROOP LIP
▲	41	45	1.2045	9.4687	-0.0338	3.0000	AXI INLET WITH 20 DEG DROOP LIP
◆	41	46	1.2068	19.365	-0.0379	3.0000	AXI INLET WITH 20 DEG DROOP LIP
○	41	47	1.2129	24.990	-0.0441	3.0000	AXI INLET WITH 20 DEG DROOP LIP

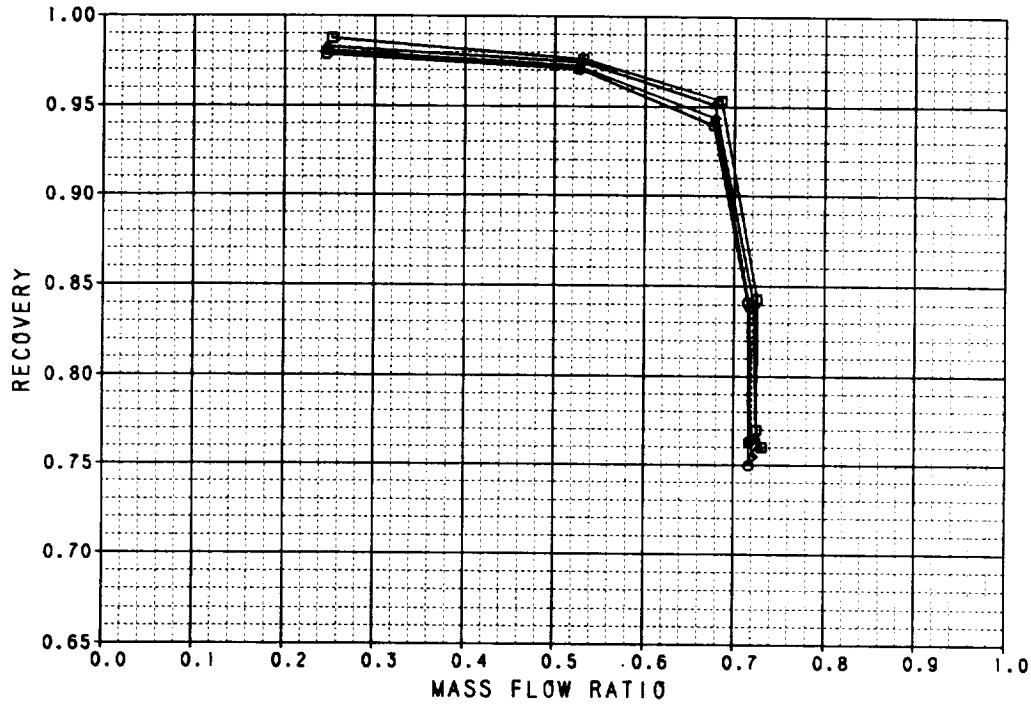

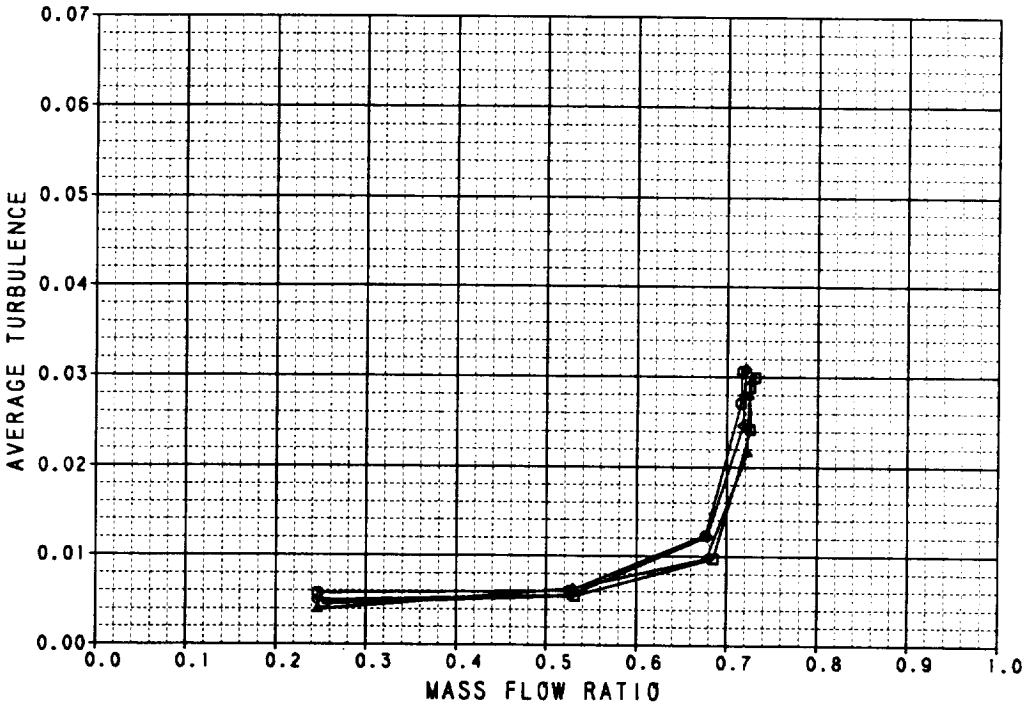

Figure B-7. Performance Data
Axisymmetric Inlet With 20° Cowl Lip
$M_0 = 1.2$

SYM	TEST	RUN	RMACH	RALPHA	RBETA	CONFIG	DESCRIPTION
□	41	78	1.4059	-0.1494	0.0798	3.0000	AXI INLET WITH 20 DEG DROOP LIP
▲	41	79	1.4065	4.9894	0.0782	3.0000	AXI INLET WITH 20 DEG DROOP LIP
◆	41	80	1.4051	9.8798	0.0757	3.0000	AXI INLET WITH 20 DEG DROOP LIP
⊙	41	81	1.4036	15.088	0.0815	3.0000	AXI INLET WITH 20 DEG DROOP LIP
✱	41	82	1.4019	20.018	0.0866	3.0000	AXI INLET WITH 20 DEG DROOP LIP

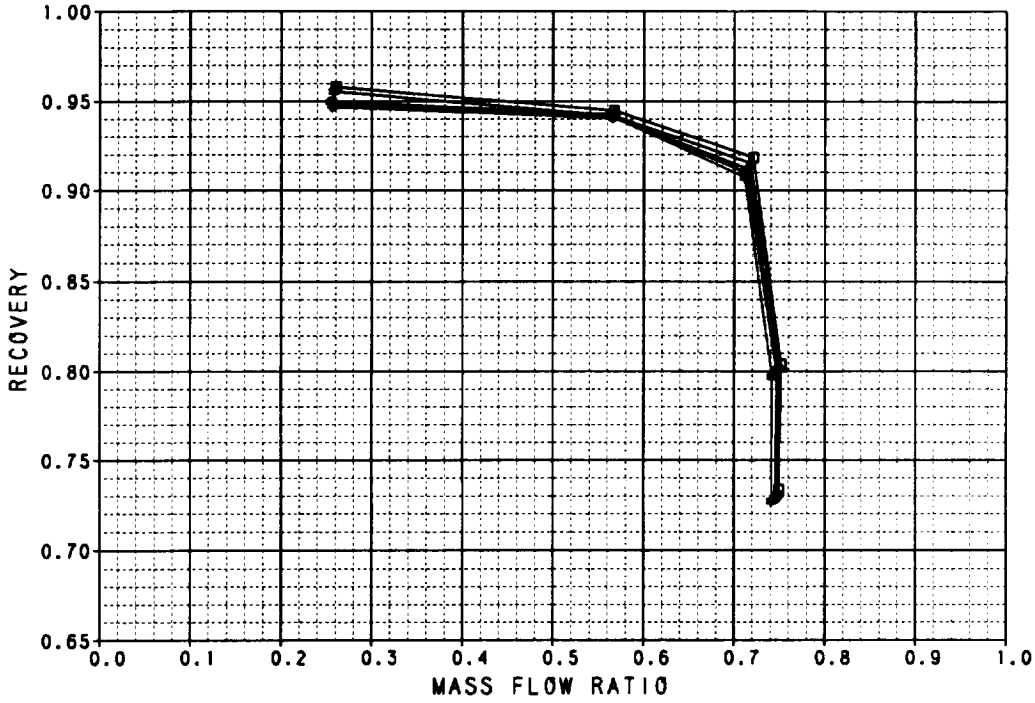

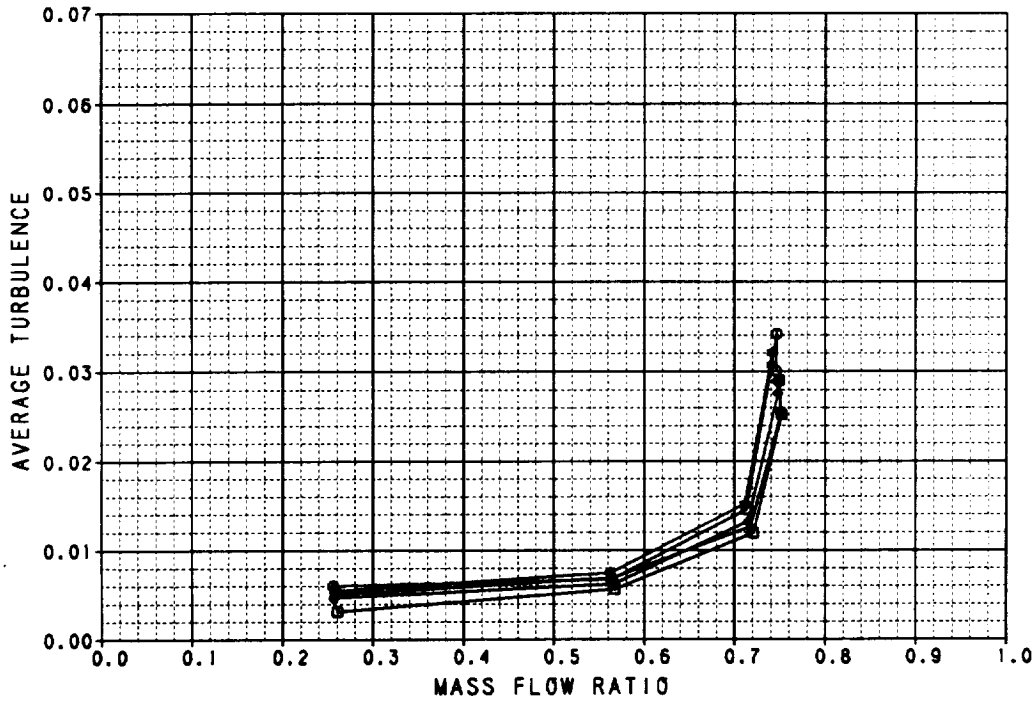

Figure B-8. Performance Data
Axisymmetric Inlet With 20° Cowl Lip
$M_0 = 1.4$

SYM	TEST	RUN	RMACH	RALPHA	RBETA	CONFIG	DESCRIPTION
□	41	68	0.6074	-0.1507	0.0675	4.0000	AXI INLET WITH 40 DEG DROOP LIP
▲	41	69	0.6058	9.8715	0.0655	4.0000	AXI INLET WITH 40 DEG DROOP LIP
◆	41	70	0.6049	19.940	0.0675	4.0000	AXI INLET WITH 40 DEG DROOP LIP
⊙	41	71	0.6056	30.039	0.0765	4.0000	AXI INLET WITH 40 DEG DROOP LIP
●	41	72	0.6073	39.745	0.0786	4.0000	AXI INLET WITH 40 DEG DROOP LIP

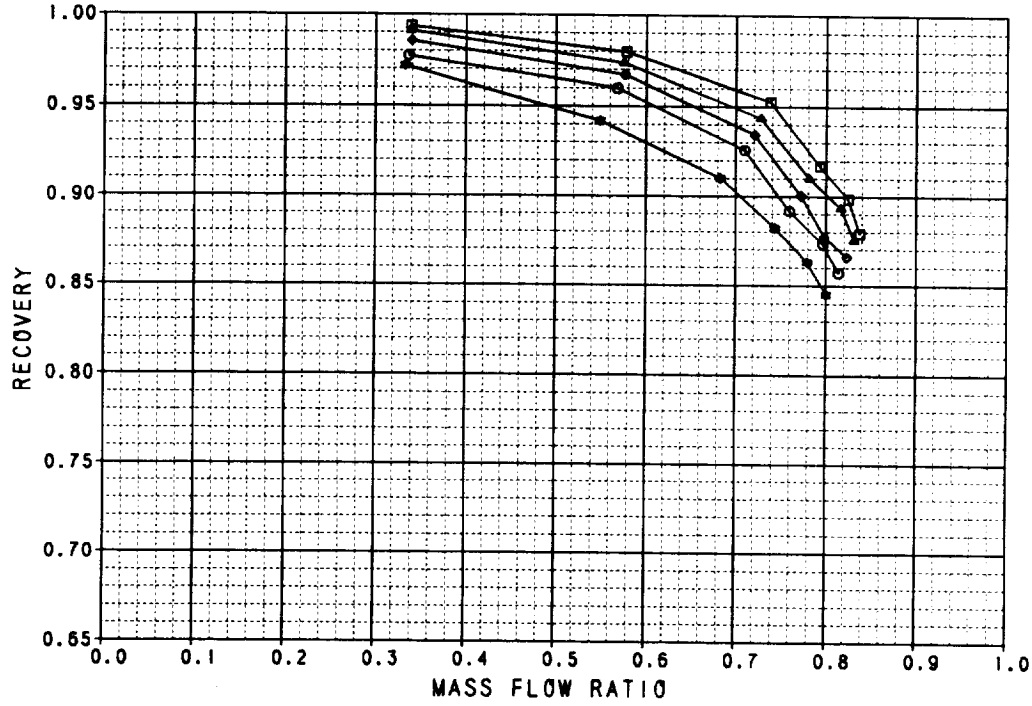

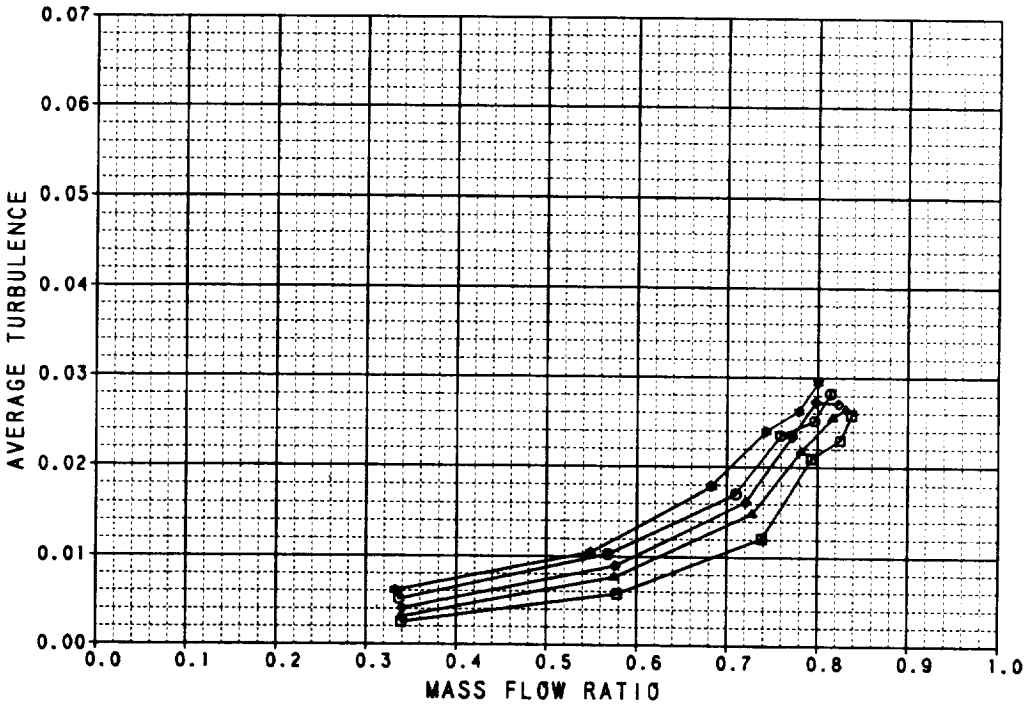

Figure B-9. Performance Data
Axisymmetric Inlet With 40° Cowl Lip
$M_0 = 0.6$

SYM	TEST	RUN	RMACH	RALPHA	RBETA	CONFIG	DESCRIPTION
□	41	57	0.8978	-4.9658	0.0131	4.0000	AXI INLET WITH 40 DEG DROOP LIP
△	41	54	0.8984	-0.2344	0.0827	4.0000	AXI INLET WITH 40 DEG DROOP LIP
◇	41	58	0.8980	10.000	.00825	4.0000	AXI INLET WITH 40 DEG DROOP LIP
○	41	59	0.9010	20.068	-0.0138	4.0000	AXI INLET WITH 40 DEG DROOP LIP
⊕	41	62	0.8997	30.240	0.0799	4.0000	AXI INLET WITH 40 DEG DROOP LIP
⊠	41	63	0.9020	39.618	0.0634	4.0000	AXI INLET WITH 40 DEG DROOP LIP

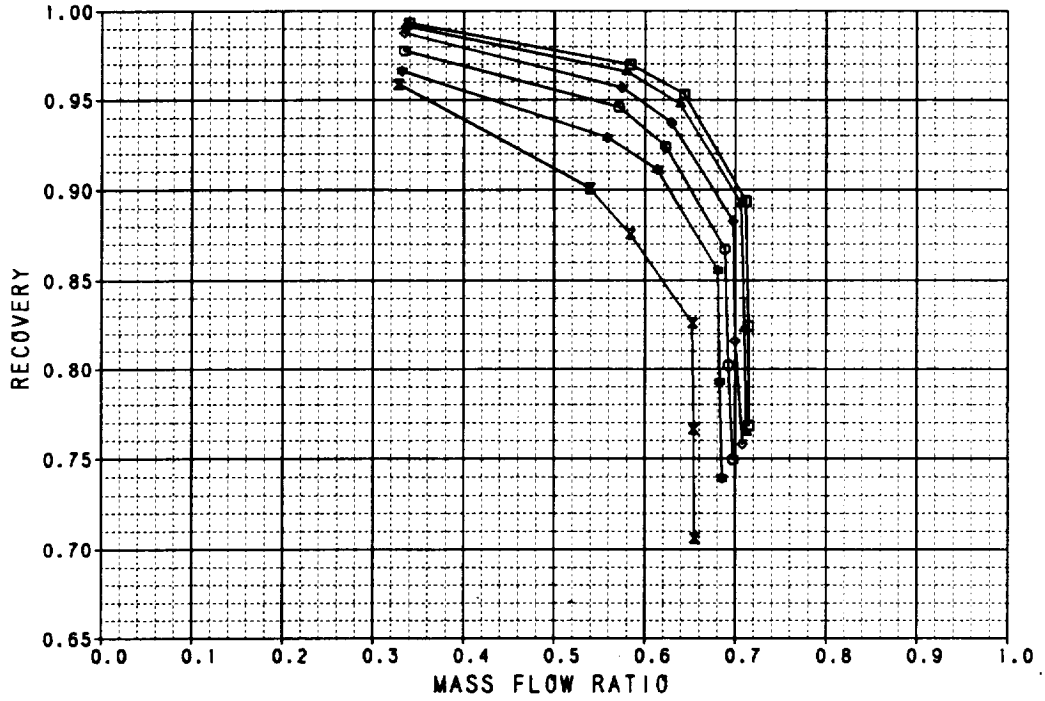

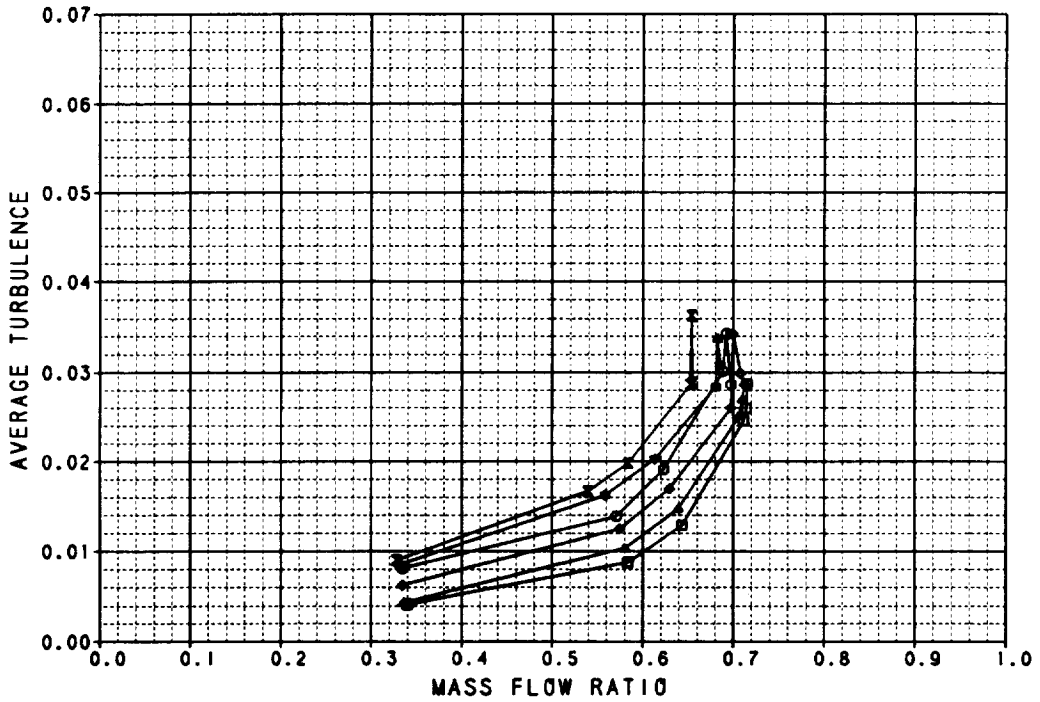

Figure B-10. Performance Data
Axisymmetric Inlet With 40° Cowl Lip
$M_0 = 0.9$

SYM	TEST	RUN	RMACH	RALPHA	RBETA	CONFIG	DESCRIPTION
□	41	64	1.2093	-0.0863	0.0882	4.0000	AXI INLET WITH 40 DEG DROOP LIP
△	41	65	1.2098	9.9775	0.0937	4.0000	AXI INLET WITH 40 DEG DROOP LIP
◇	41	66	1.2103	20.089	0.0648	4.0000	AXI INLET WITH 40 DEG DROOP LIP
○	41	67	1.2090	25.144	0.0820	4.0000	AXI INLET WITH 40 DEG DROOP LIP

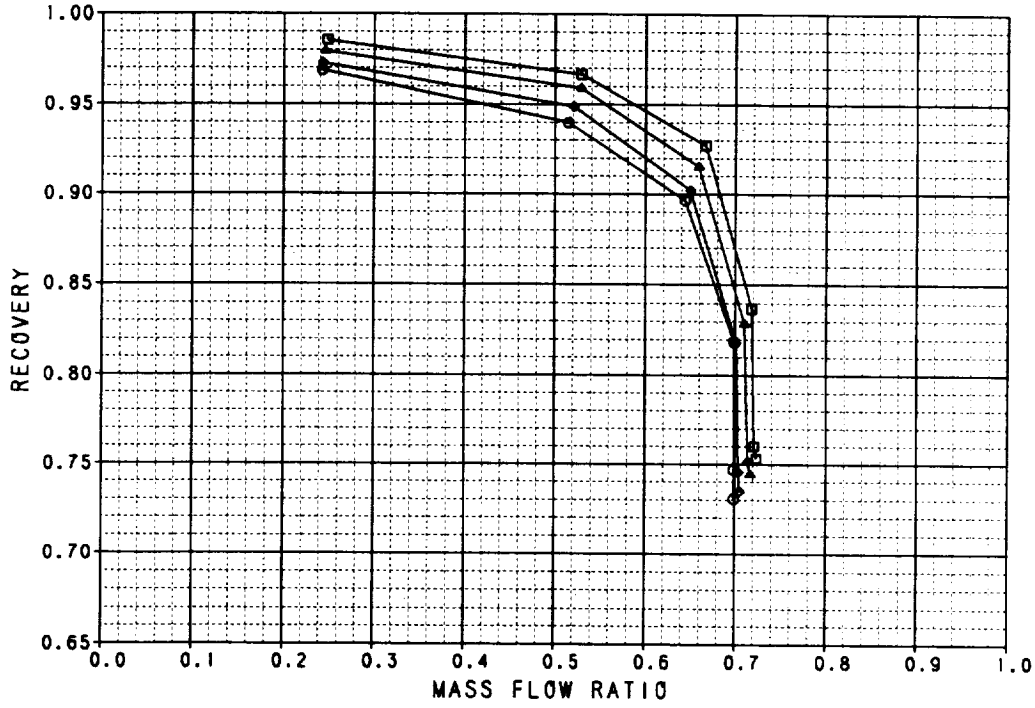

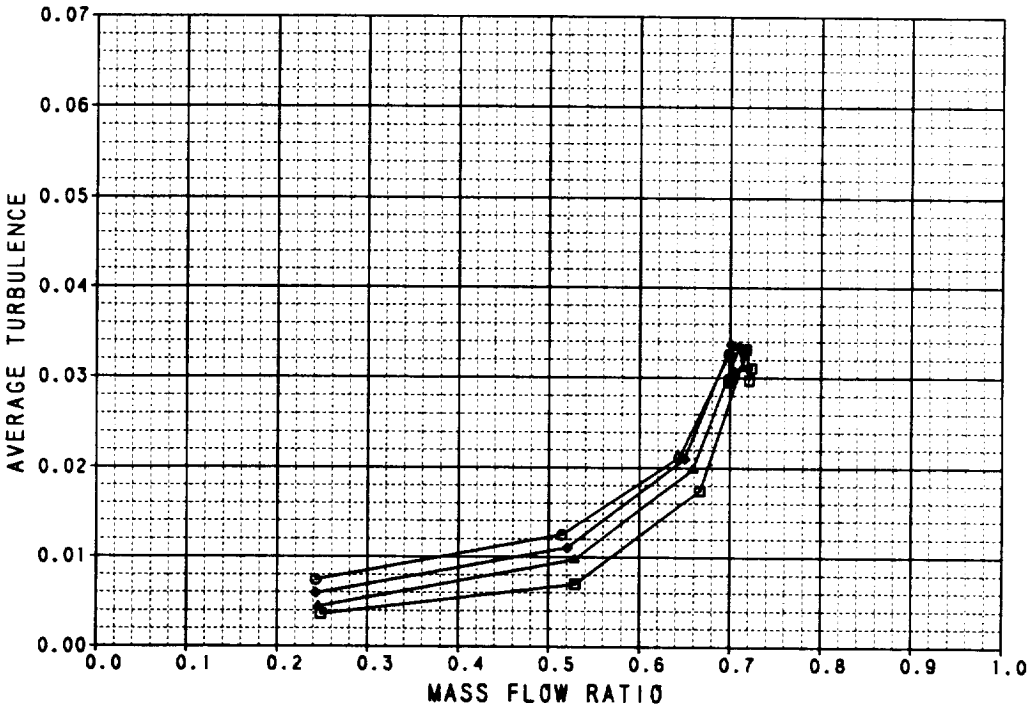

Figure B-11. Performance Data
Axisymmetric Inlet With 40° Cowl Lip
$M_0 = 1.2$

SYM	TEST	RUN	RMACH	RALPHA	RBETA	CONFIG	DESCRIPTION
□	41	73	1.4037	-0.1097	0.0972	4.0000	AXI INLET WITH 40 DEG DROOP LIP
▲	41	74	1.4006	4.8592	0.1005	4.0000	AXI INLET WITH 40 DEG DROOP LIP
◆	41	75	1.3998	9.7588	0.1055	4.0000	AXI INLET WITH 40 DEG DROOP LIP
⊙	41	76	1.3998	15.118	0.0897	4.0000	AXI INLET WITH 40 DEG DROOP LIP
●	41	77	1.3971	20.115	0.0987	4.0000	AXI INLET WITH 40 DEG DROOP LIP

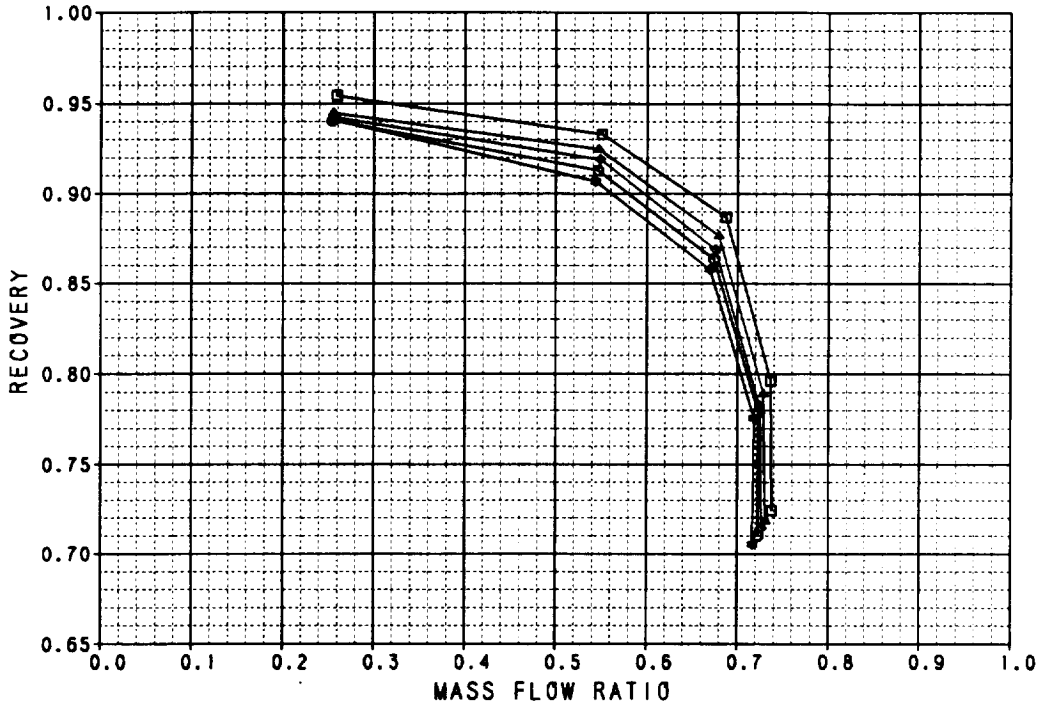

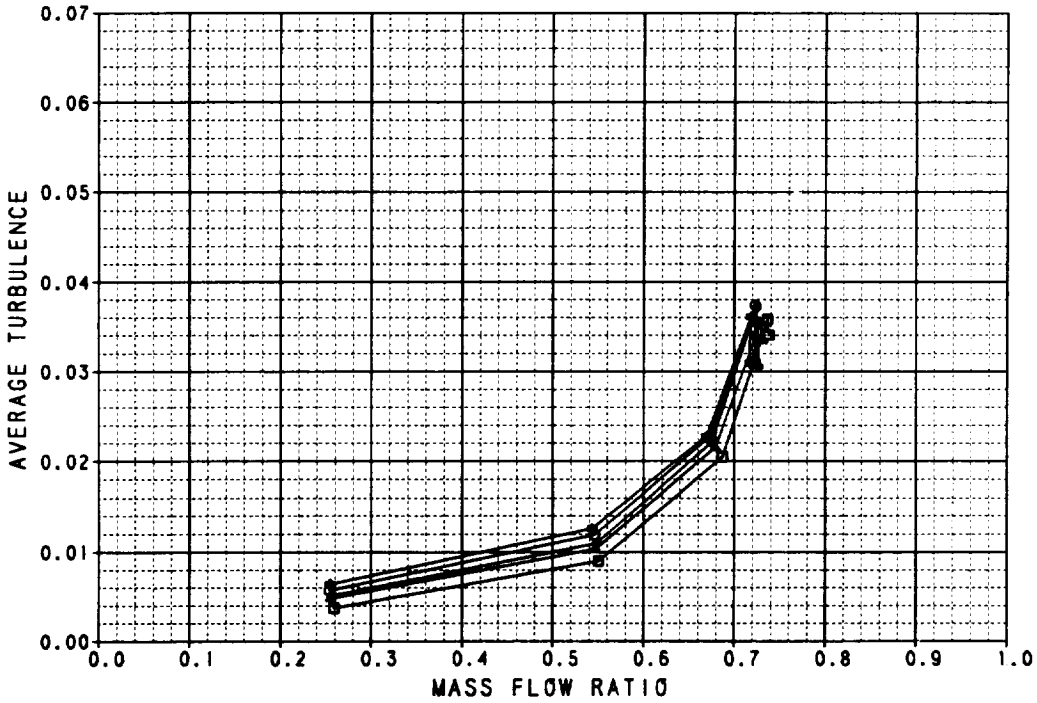

Figure B-12. Performance Data
Axisymmetric Inlet With 40° Cowl Lip
$M_0 = 1.4$

SYM	TEST	RUN	RMACH	RALPHA	RBETA	CONFIG	DESCRIPTION
□	41	19	0.6046	-0.1038	0.0884	1.0000	AXI INLET WITH RETRACTED SIDEPLATES
▲	41	20	0.6051	19.910	0.0936	1.0000	AXI INLET WITH RETRACTED SIDEPLATES
◆	41	21	0.6063	38.604	0.0903	1.0000	AXI INLET WITH RETRACTED SIDEPLATES

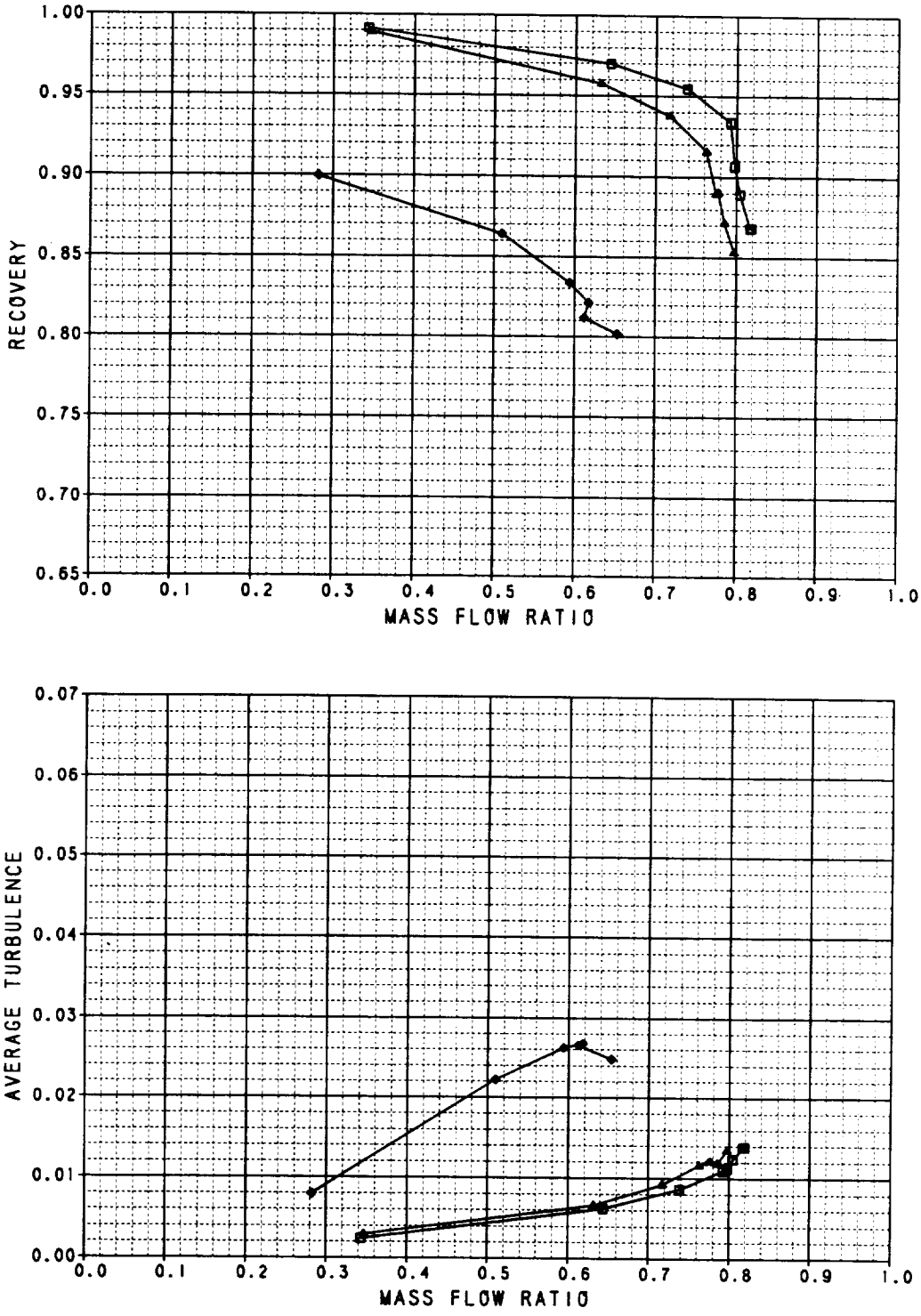

Figure B-13. Performance Data
Axisymmetric Inlet With Retracted Sideplates
$M_0 = 0.6$

SYM	TEST	RUN	RMACH	RALPHA	RBETA	CONFIG	DESCRIPTION
▫	41	22	0.8962	-0.1187	0.0712	1.0000	AXI INLET WITH RETRACTED SIDEPLATES
▲	41	25	0.9026	19.858	0.0583	1.0000	AXI INLET WITH RETRACTED SIDEPLATES
◆	41	28	0.9041	39.864	0.0788	1.0000	AXI INLET WITH RETRACTED SIDEPLATES

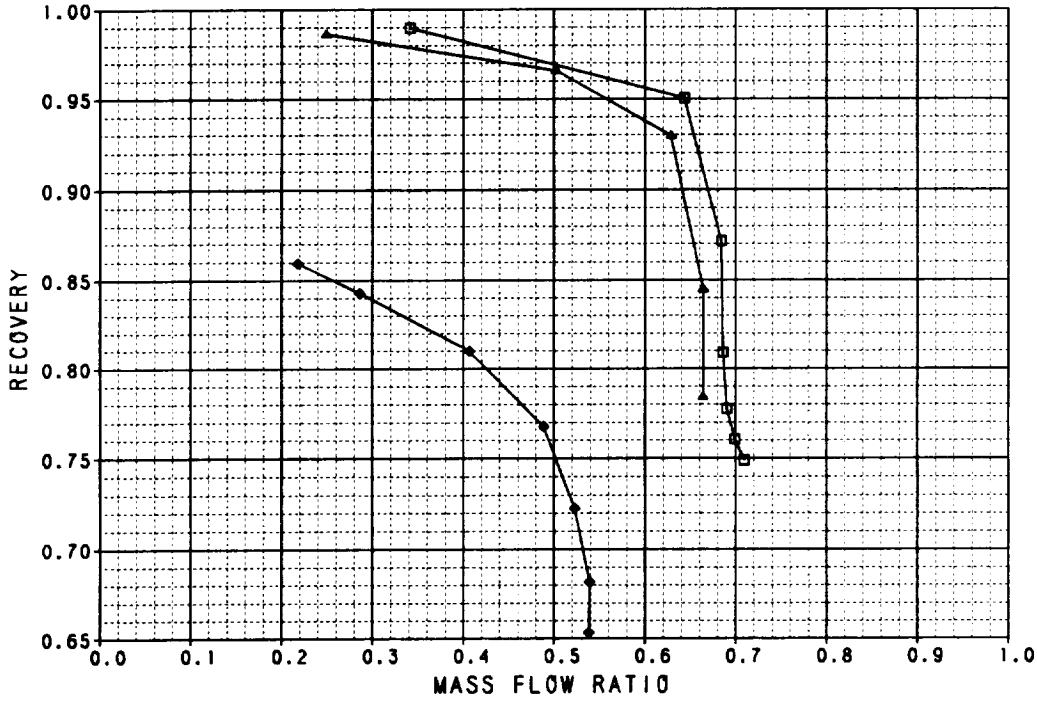

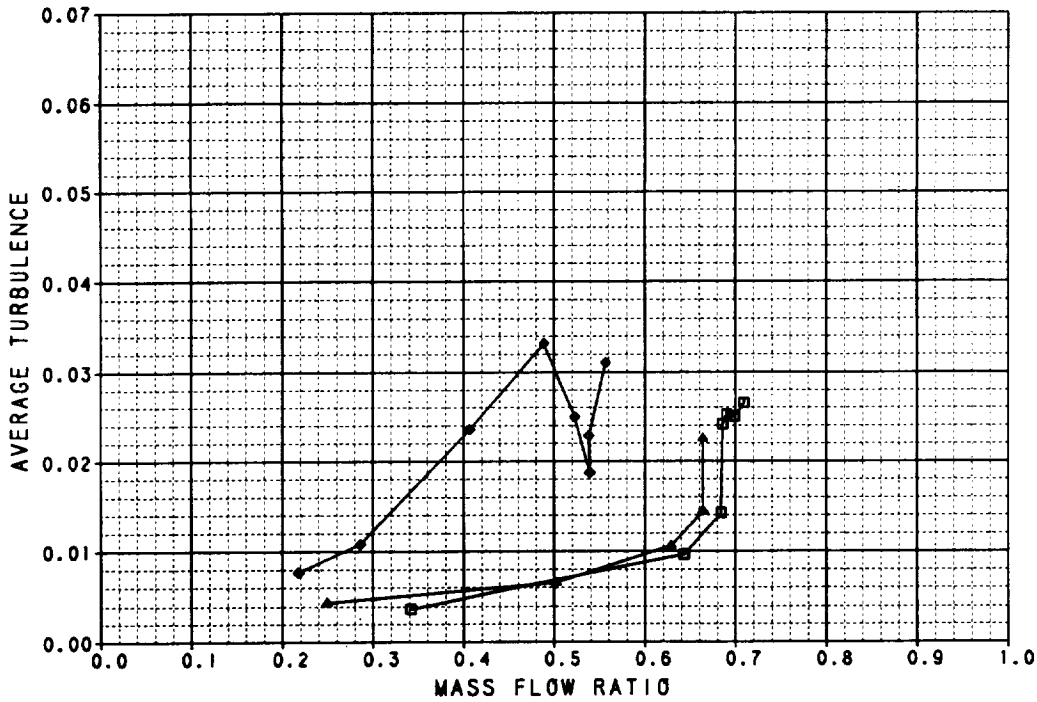

Figure B-14. Performance Data
Axisymmetric Inlet With Retracted Sideplates
$M_0 = 0.9$

SYM	TEST	RUN	RMACH	RALPHA	RBETA	CONFIG	DESCRIPTION
□	41	83	1.4038	-0.1848	0.0881	1.0000	AXI INLET WITH RETRACTED SIDEPLATES
▲	41	84	1.4012	5.0148	0.0815	1.0000	AXI INLET WITH RETRACTED SIDEPLATES
◆	41	85	1.4019	10.151	0.0724	1.0000	AXI INLET WITH RETRACTED SIDEPLATES
⊙	41	86	1.3941	15.060	0.0627	1.0000	AXI INLET WITH RETRACTED SIDEPLATES
*	41	87	1.3908	19.985	0.0496	1.0000	AXI INLET WITH RETRACTED SIDEPLATES

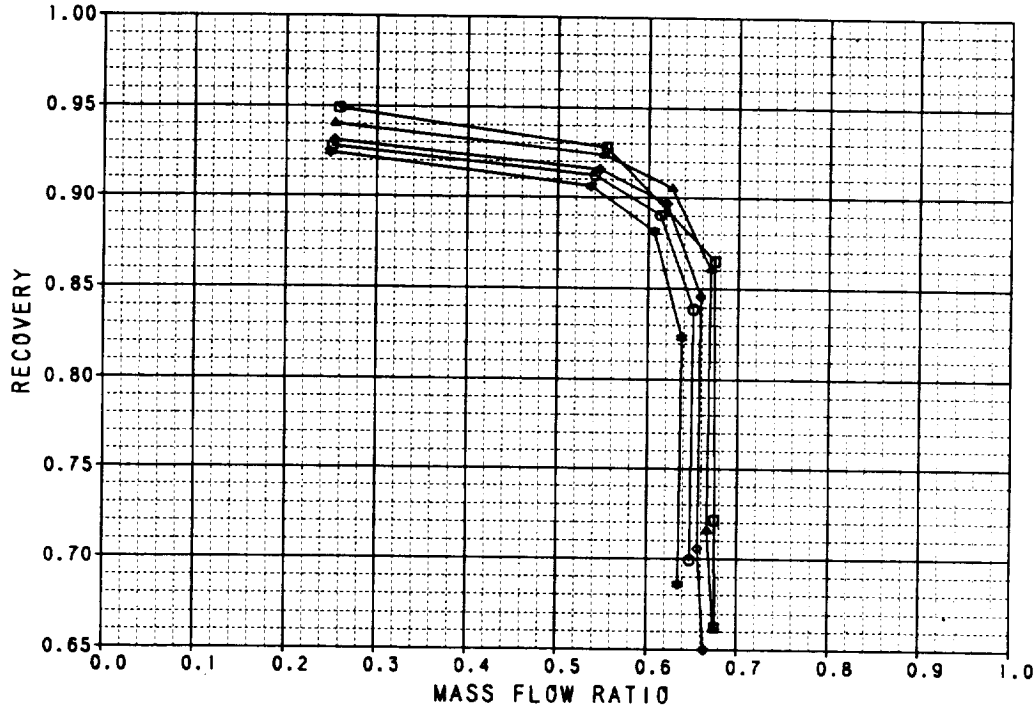

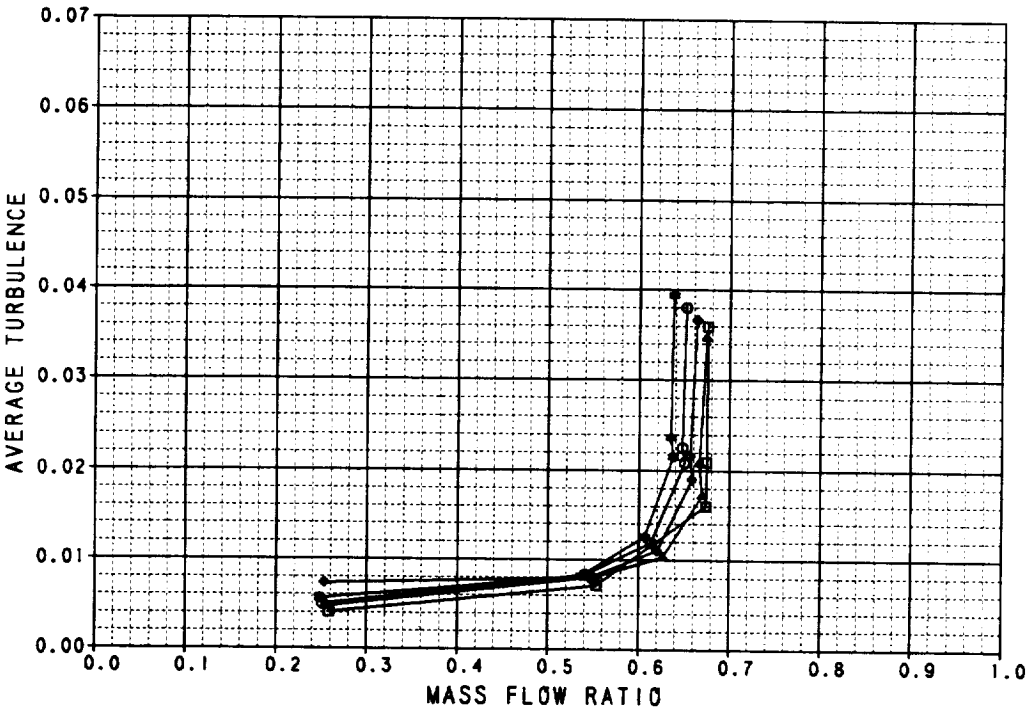

Figure B-15. Performance Data
Axisymmetric Inlet With Retracted Sideplates
$M_0 = 1.4$

SYM	TEST	RUN	RMACH	RALPHA	RBETA	CONFIG	DESCRIPTION
□	41	121	0.6026	-0.1312	0.0675	6.0000	AXI INLET,LOWER AUX INLETS OPEN 100%
▲	41	122	0.6048	10.022	0.0758	6.0000	AXI INLET,LOWER AUX INLETS OPEN 100%
◆	41	123	0.6050	20.162	0.0751	6.0000	AXI INLET,LOWER AUX INLETS OPEN 100%
⊙	41	124	0.6065	30.184	0.0765	6.0000	AXI INLET,LOWER AUX INLETS OPEN 100%
✱	41	125	0.6088	39.967	0.0648	6.0000	AXI INLET,LOWER AUX INLETS OPEN 100%

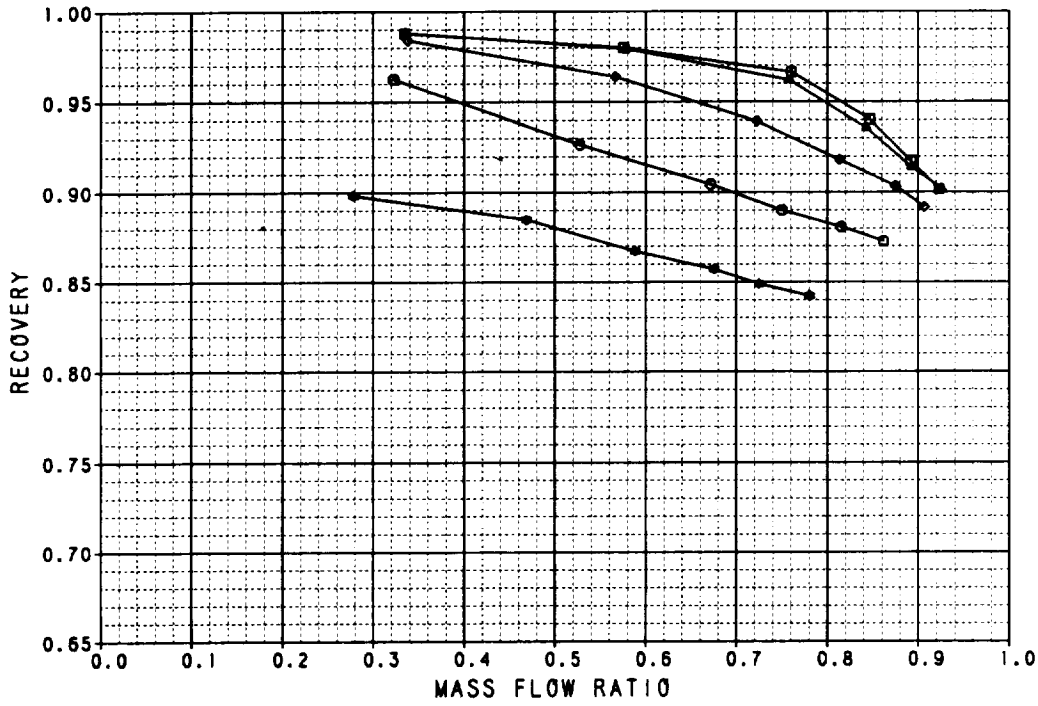

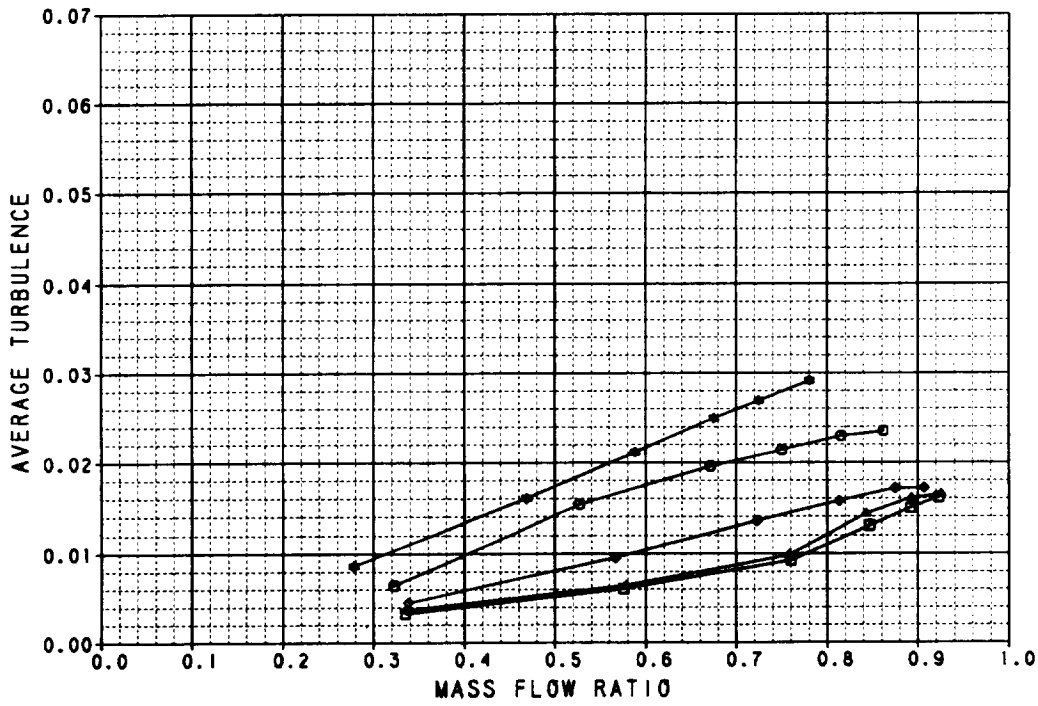

Figure B-16. Performance Data
Axisymmetric Inlet Lower Auxiliary Inlets Open 100%
$M_0 = 0.6$

SYM	TEST	RUN	RMACH	RALPHA	RBETA	CONFIG	DESCRIPTION
□	41	103	1.4026	-0.3182	0.0489	6.0000	AXI INLET,LOWER AUX INLETS OPEN 100%
▲	41	104	1.4028	5.0209	0.0351	6.0000	AXI INLET,LOWER AUX INLETS OPEN 100%
◆	41	105	1.4025	10.018	0.0310	6.0000	AXI INLET,LOWER AUX INLETS OPEN 100%
⊙	41	106	1.4020	14.975	0.0524	6.0000	AXI INLET,LOWER AUX INLETS OPEN 100%
✱	41	107	1.3981	20.247	0.0375	6.0000	AXI INLET,LOWER AUX INLETS OPEN 100%

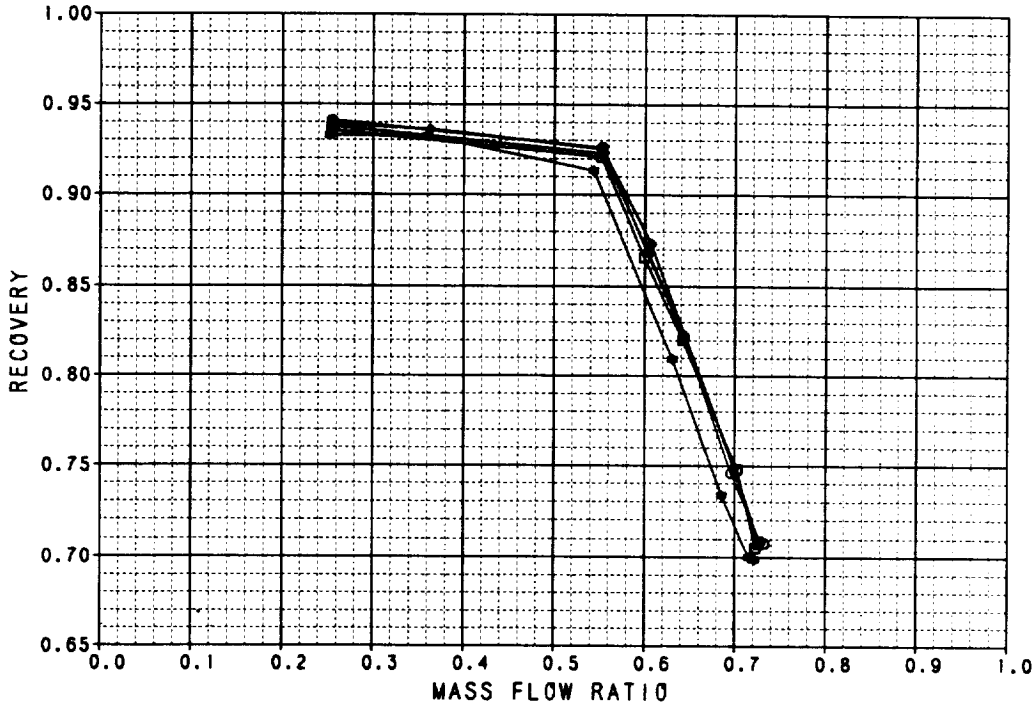

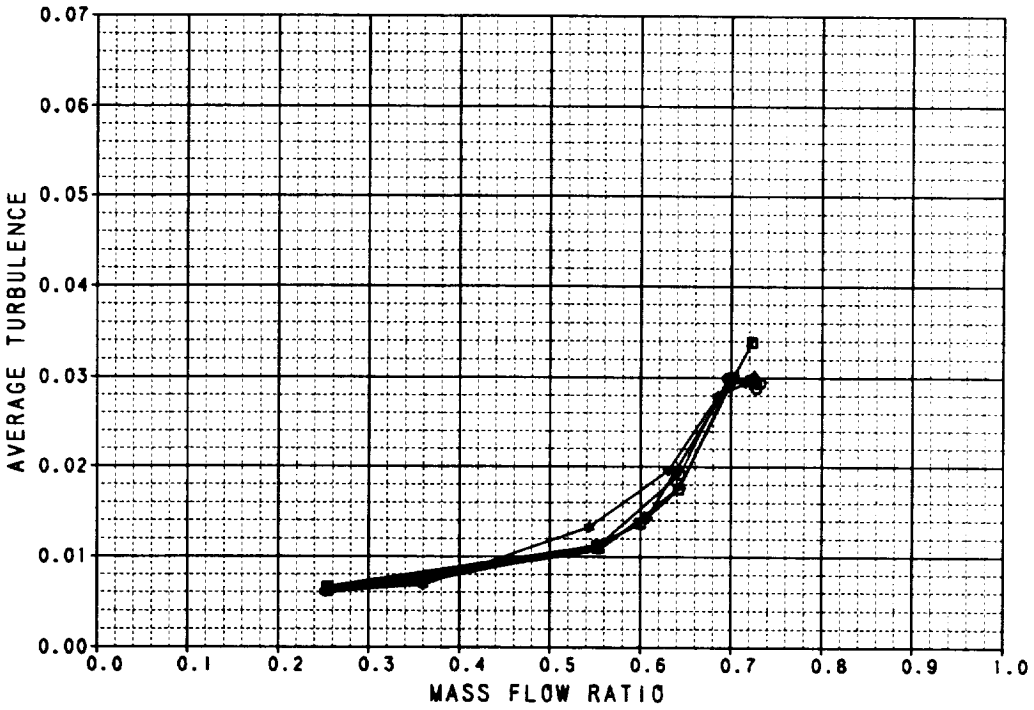

Figure B-17. Performance Data
Axisymmetric Inlet Lower Auxiliary Inlets Open 100%
$M_0 = 0.9$

SYM	TEST	RUN	RMACH	RALPHA	RBETA	CONFIG	DESCRIPTION
□	41	112	0.8974	-0.1779	0.0220	6.0000	AXI INLET,LOWER AUX INLETS OPEN 100%
▲	41	115	0.9008	9.9632	0.0856	6.0000	AXI INLET,LOWER AUX INLETS OPEN 100%
◆	41	116	0.8993	20.130	0.0620	6.0000	AXI INLET,LOWER AUX INLETS OPEN 100%
⊙	41	119	0.9006	30.090	0.0856	6.0000	AXI INLET,LOWER AUX INLETS OPEN 100%
✱	41	120	0.8978	39.978	0.0896	6.0000	AXI INLET,LOWER AUX INLETS OPEN 100%

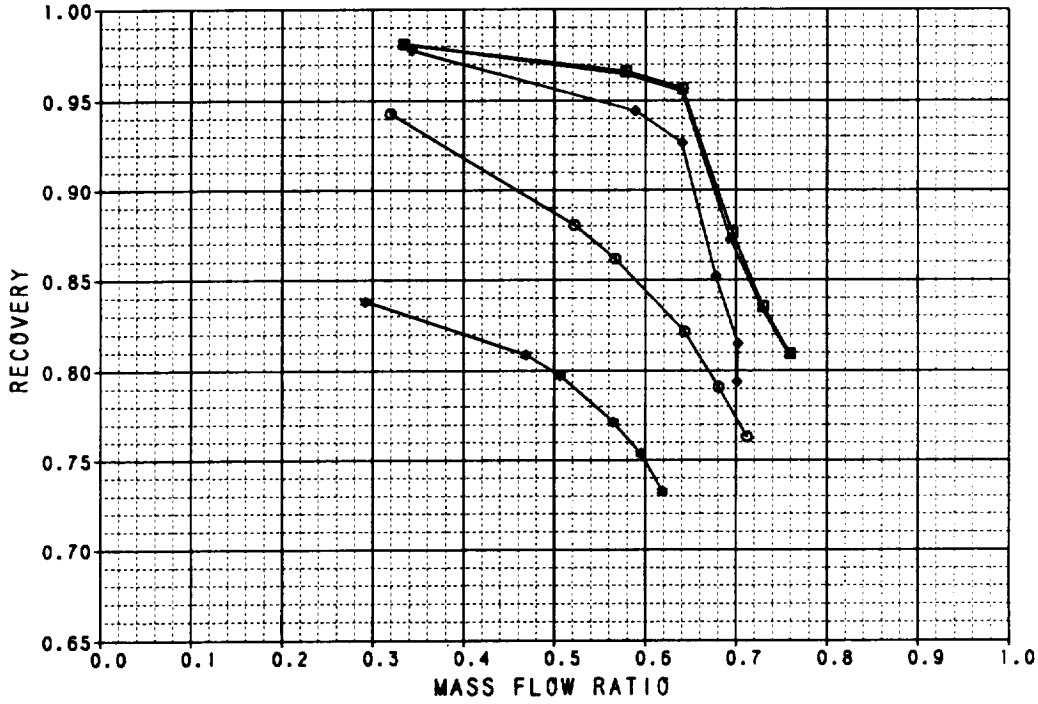

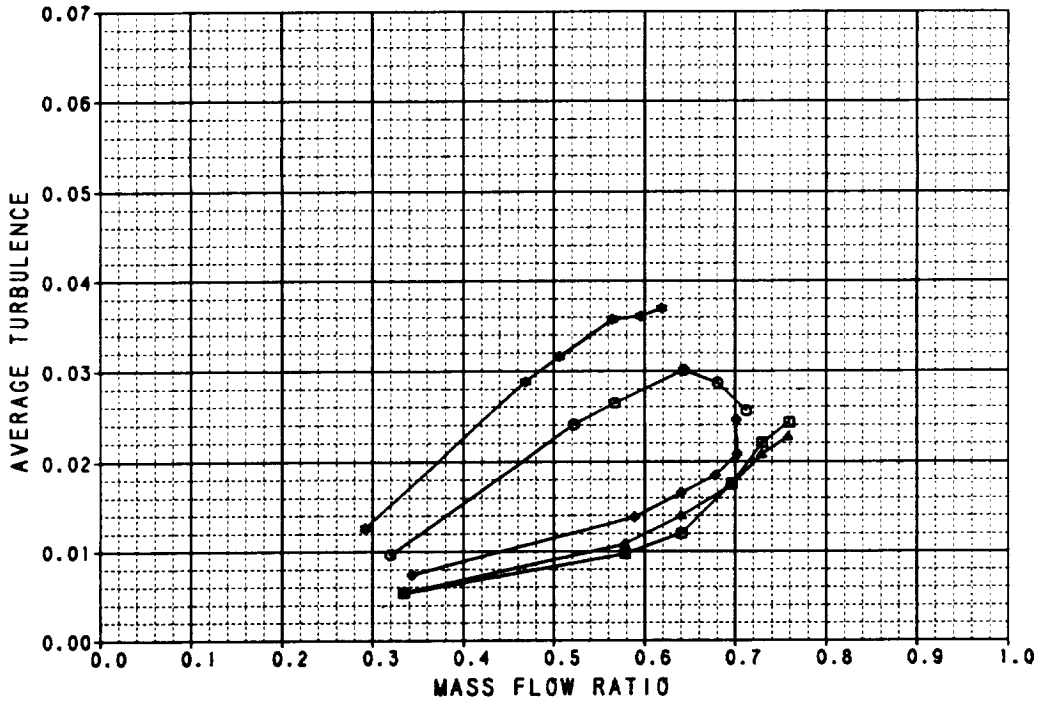

Figure B-18. Performance Data
Axisymmetric Inlet Lower Auxiliary Inlets Open 100%
$M_0 = 1.2$

SYM	TEST	RUN	RMACH	RALPHA	RBETA	CONFIG	DESCRIPTION
□	41	108	1.2035	-0.2179	0.0185	6.0000	AXI INLET,LOWER AUX INLETS OPEN 100Z
▲	41	109	1.2046	9.9938	.00342	6.0000	AXI INLET,LOWER AUX INLETS OPEN 100Z
◆	41	110	1.2033	20.049	.00618	6.0000	AXI INLET,LOWER AUX INLETS OPEN 100Z
⊙	41	111	1.2035	25.417	0.0288	6.0000	AXI INLET,LOWER AUX INLETS OPEN 100Z

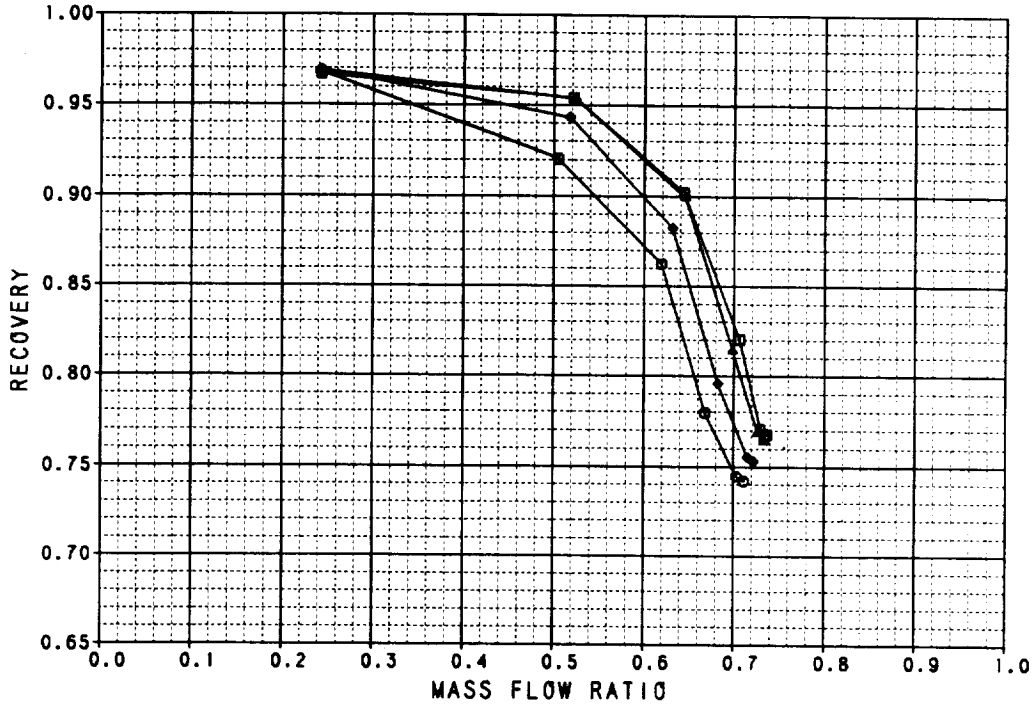

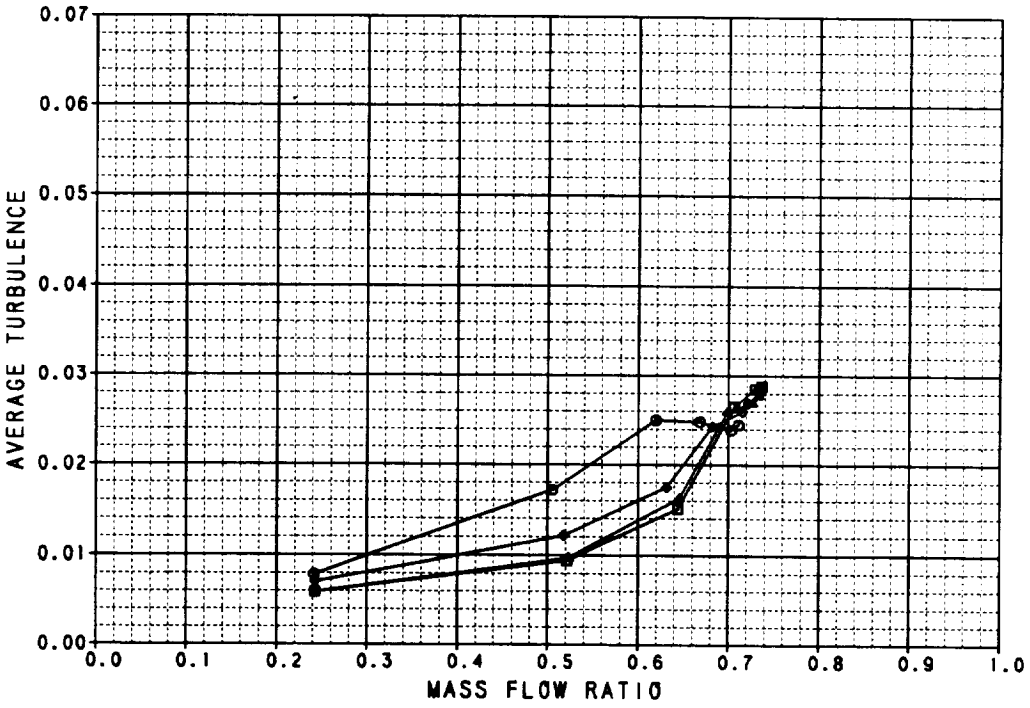

Figure B-19. Performance Data
Axisymmetric Inlet Lower Auxiliary Inlets Open 100%
$M_0 = 1.4$

SYM	TEST	RUN	RMACH	RALPHA	RBETA	CONFIG	DESCRIPTION
□	41	88	0.6061	0.0482	0.0668	7.0000	AXI INLET,LOWER AUX INLETS OPEN 50%
▲	41	89	0.6062	20.104	0.0524	7.0000	AXI INLET,LOWER AUX INLETS OPEN 50%
◆	41	90	0.6066	40.075	0.0599	7.0000	AXI INLET,LOWER AUX INLETS OPEN 50%

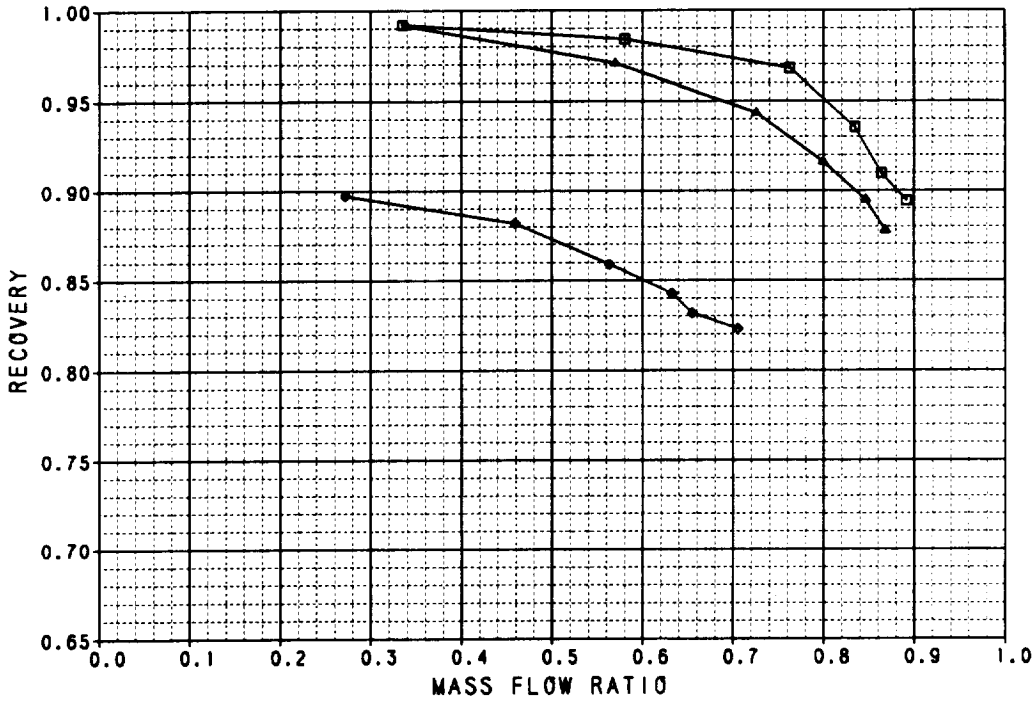

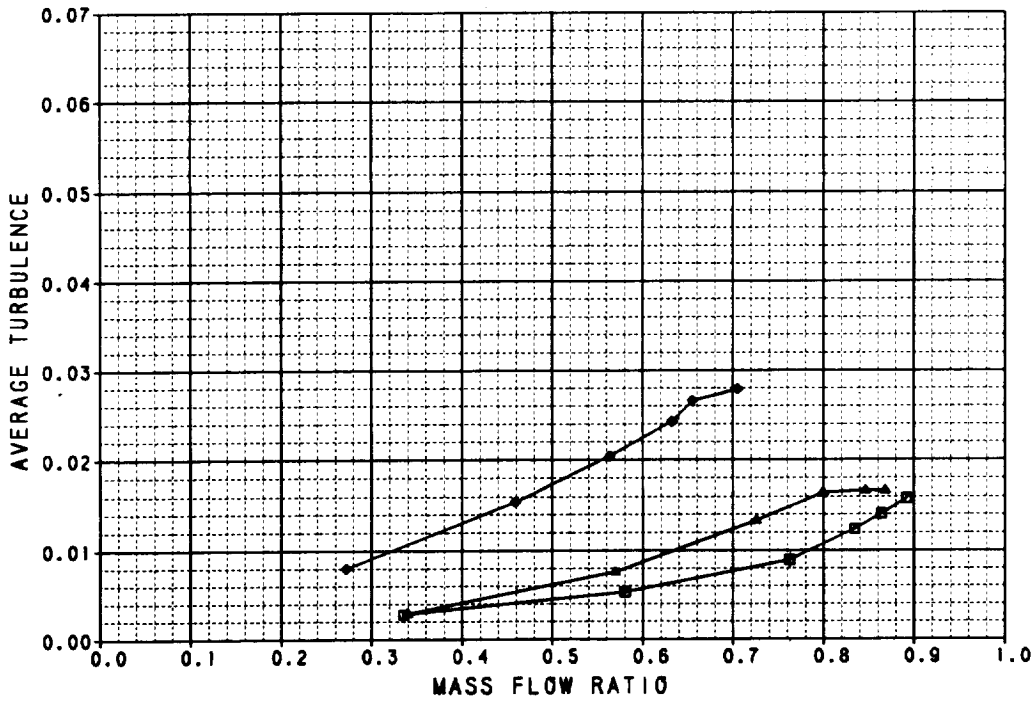

Figure B-20. Performance Data
Axisymmetric Inlet Lower Auxiliary Inlets Open 50%
$M_0 = 0.6$

SYM	TEST	RUN	RMACH	RALPHA	RBETA	CONFIG	DESCRIPTION
□	41	91	0.9032	-0.0707	0.0586	7.0000	AXI INLET,LOWER AUX INLETS OPEN 50%
▲	41	94	0.8990	20.062	0.0551	7.0000	AXI INLET,LOWER AUX INLETS OPEN 50%
◆	41	97	0.9026	40.166	0.0854	7.0000	AXI INLET,LOWER AUX INLETS OPEN 50%

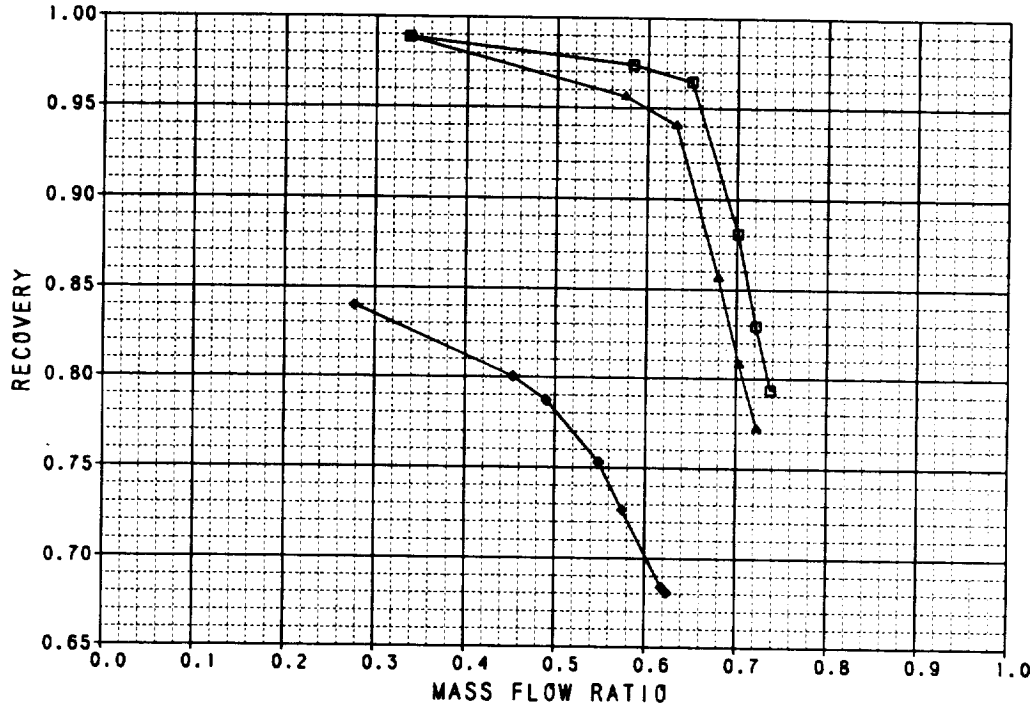

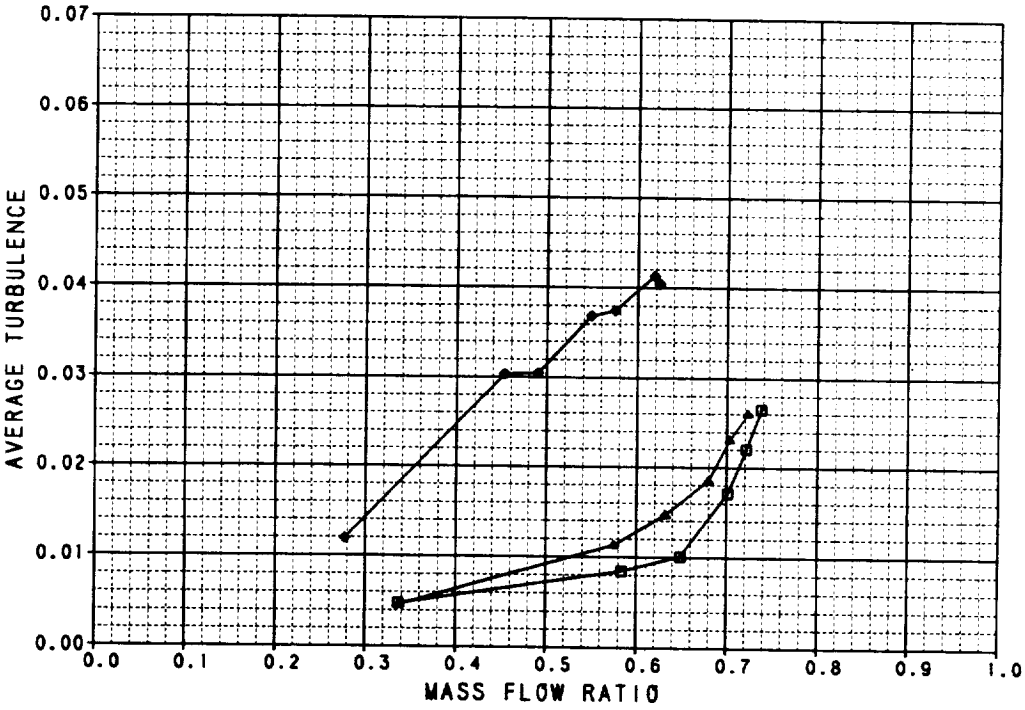

Figure B-21. Performance Data
Axisymmetric Inlet Lower Auxiliary Inlets Open 50%
$M_0 = 0.9$

SYM	TEST	RUN	RMACH	RALPHA	RBETA	CONFIG	DESCRIPTION
□	41	187	0.6011	-0.1315	-.00800	8.0000	AXI INLET,UPPER AND LOWER AUX INLETS OPEN 50Z
▲	41	188	0.6041	20.089	-0.0157	8.0000	AXI INLET,UPPER AND LOWER AUX INLETS OPEN 50Z
◆	41	189	0.6057	39.950	-0.0541	8.0000	AXI INLET,UPPER AND LOWER AUX INLETS OPEN 50Z

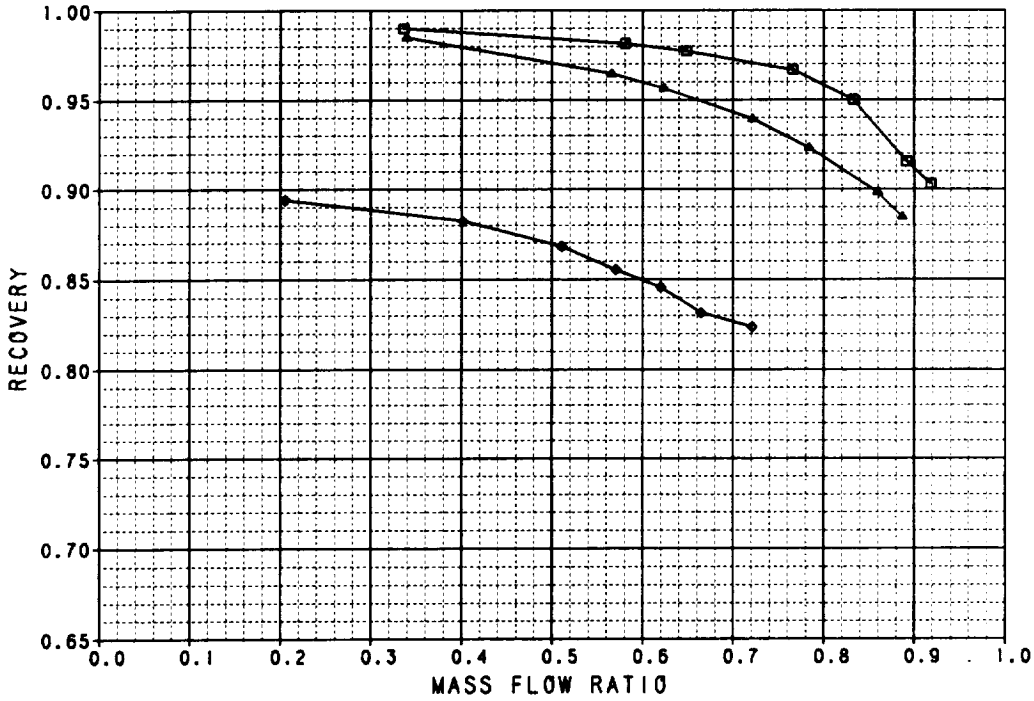

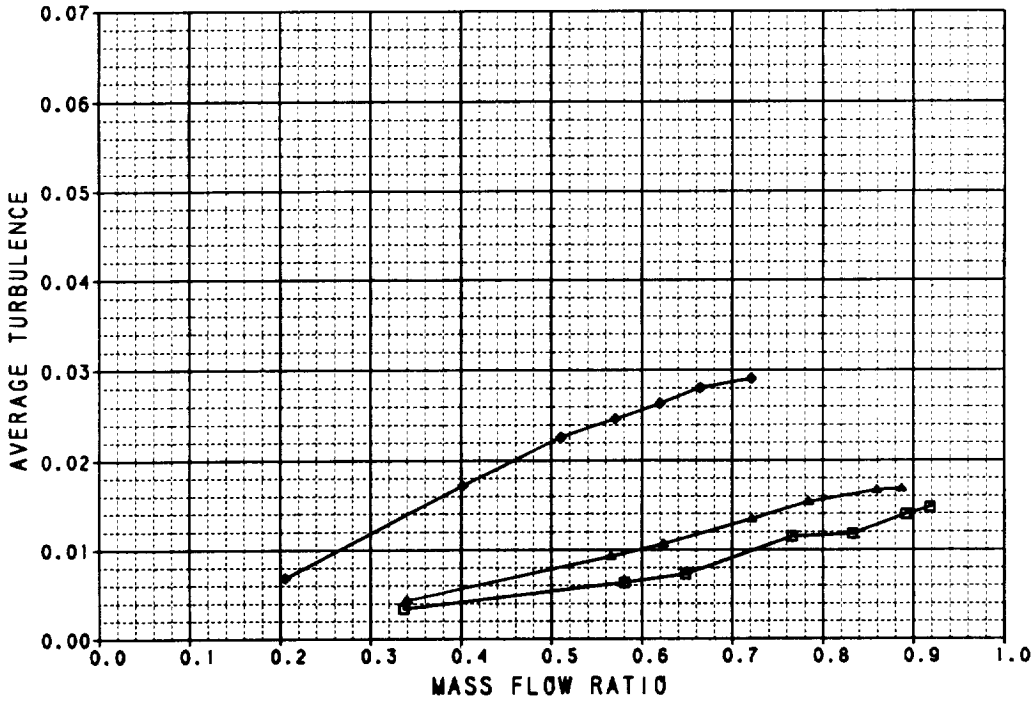

Figure B-22. Performance Data

Axisymmetric Inlet Upper and Lower Auxiliary Inlets Open 50%

$M_0 = 0.6$

SYM	TEST	RUN	RMACH	RALPHA	RBETA	CONFIG	DESCRIPTION
□	41	190	0.8989	-0.1147	-0.0189	8.0000	AXI INLET,UPPER AND LOWER AUX INLETS OPEN 50%
▲	41	193	0.9042	20.088	0.0310	8.0000	AXI INLET,UPPER AND LOWER AUX INLETS OPEN 50%
◆	41	196	0.9007	40.074	0.0180	8.0000	AXI INLET,UPPER AND LOWER AUX INLETS OPEN 50%

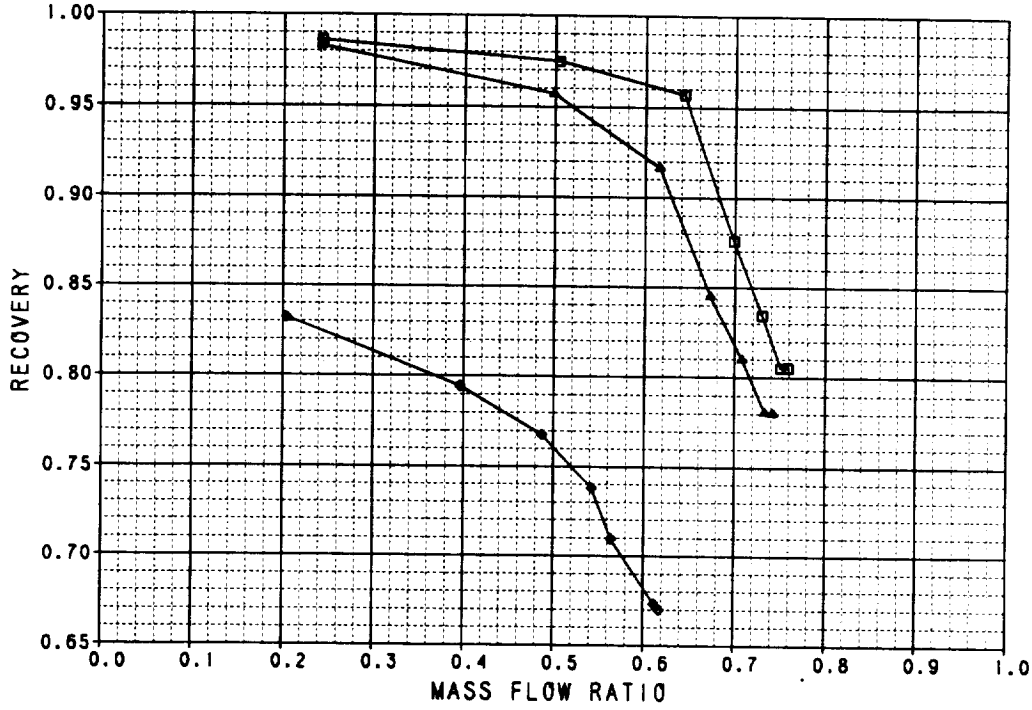

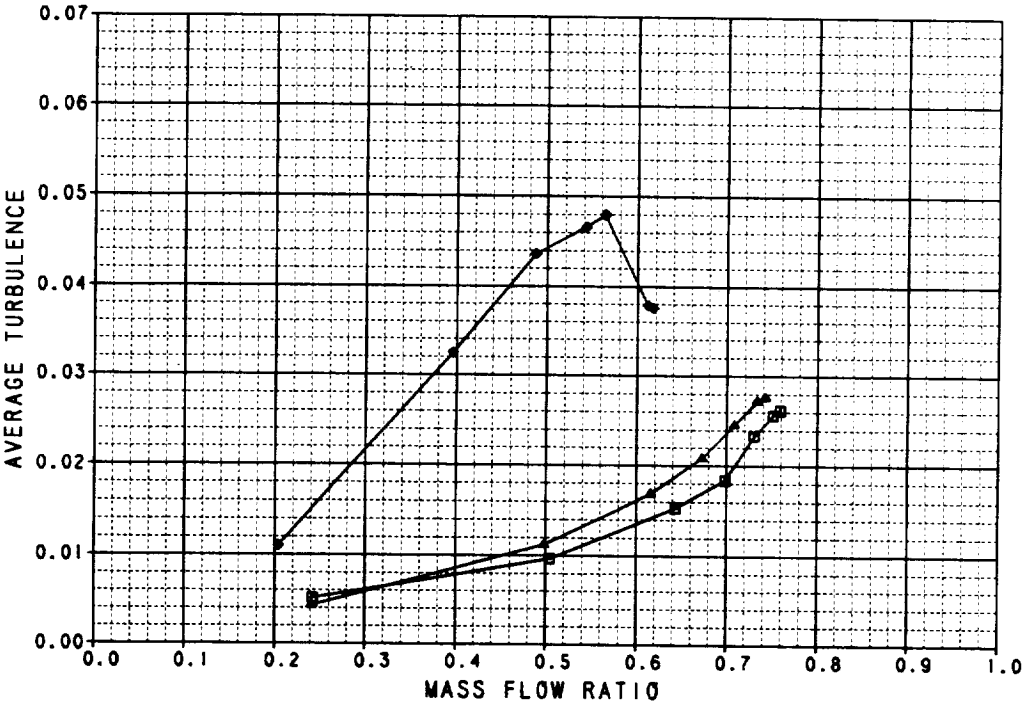

Figure B-23. Performance Data
Axisymmetric Inlet Upper and Lower Auxiliary Inlets Open 50%
$M_0 = 0.9$

SYM	TEST	RUN	RMACH	RALPHA	RBETA	CONFIG	DESCRIPTION
□	41	159	0.6058	0.0443	0.0138	9.0000	AXI INLET,UPPER AND LOWER AUX INLETS OPEN 100%
▲	41	160	0.6052	9.9716	0.0103	9.0000	AXI INLET,UPPER AND LOWER AUX INLETS OPEN 100%
◆	41	161	0.6048	20.074	0.0188	9.0000	AXI INLET,UPPER AND LOWER AUX INLETS OPEN 100%
○	41	162	0.6066	30.157	0.0180	9.0000	AXI INLET,UPPER AND LOWER AUX INLETS OPEN 100%
●	41	163	0.6050	39.910	0.0108	9.0000	AXI INLET,UPPER AND LOWER AUX INLETS OPEN 100%

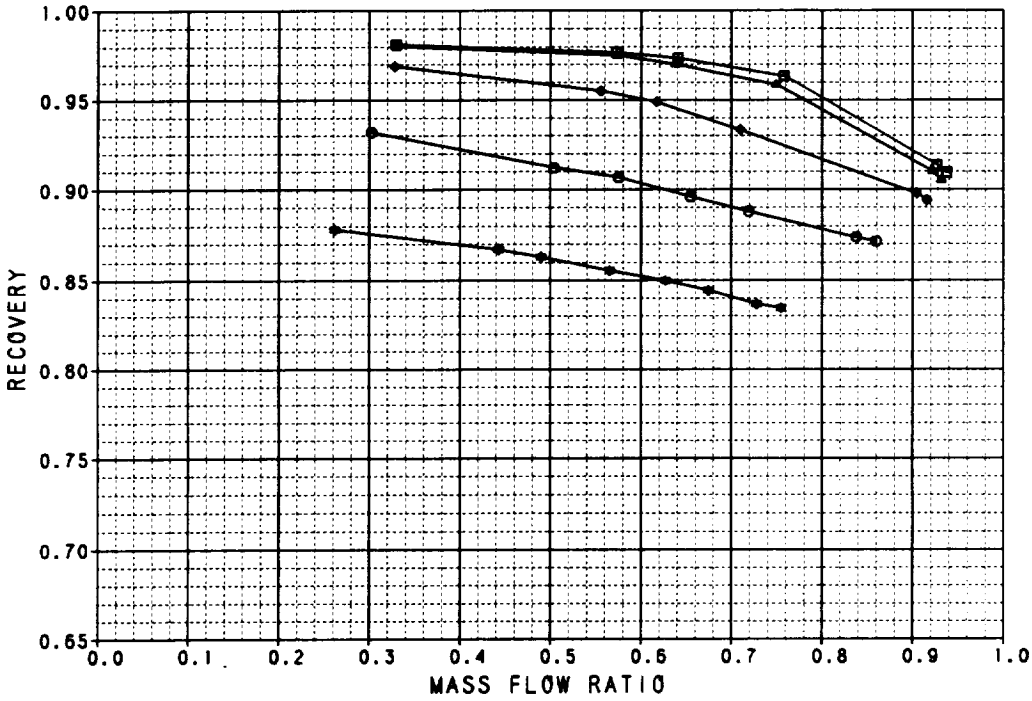

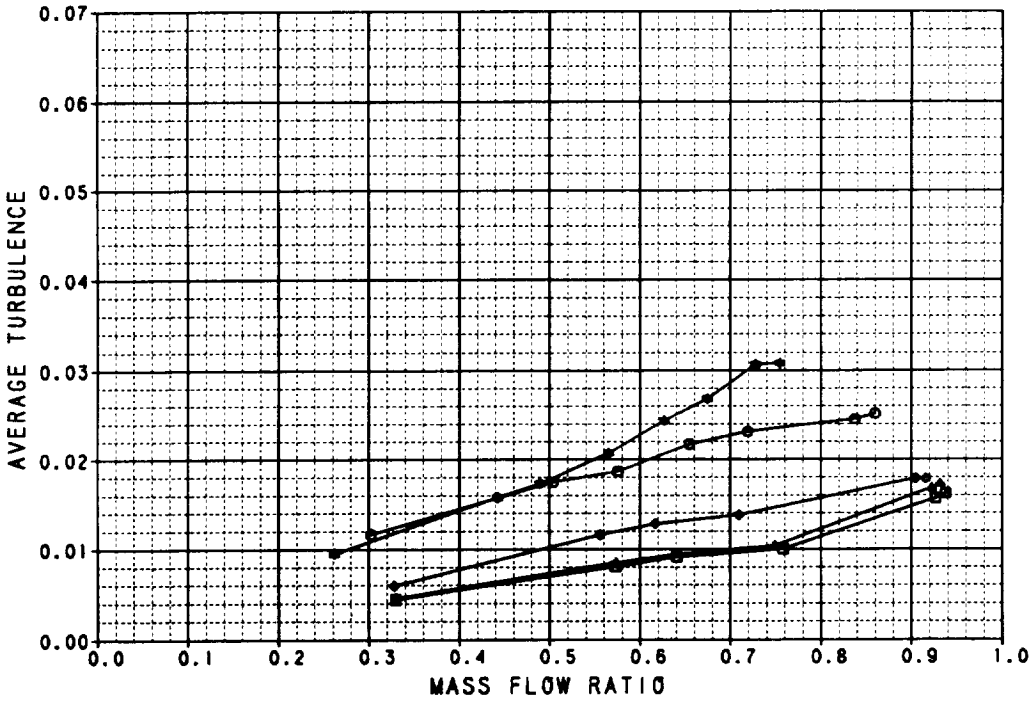

Figure B-24. Performance Data
Axisymmetric Inlet Upper and Lower Auxiliary Inlets Open 100%
$M_0 = 0.6$

SYM	TEST	RUN	RMACH	RALPHA	RBETA	CONFIG	DESCRIPTION
□	41	150	0.9010	-0.0980	0.0737	9.0000	AXI INLET,UPPER AND LOWER AUX INLETS OPEN 100%
▲	41	153	0.8997	9.9898	0.0110	9.0000	AXI INLET,UPPER AND LOWER AUX INLETS OPEN 100%
◆	41	154	0.9005	20.217	-.00822	9.0000	AXI INLET,UPPER AND LOWER AUX INLETS OPEN 100%
○	41	157	0.9026	30.149	0.0144	9.0000	AXI INLET,UPPER AND LOWER AUX INLETS OPEN 100%
✱	41	158	0.9029	40.085	0.0103	9.0000	AXI INLET,UPPER AND LOWER AUX INLETS OPEN 100%

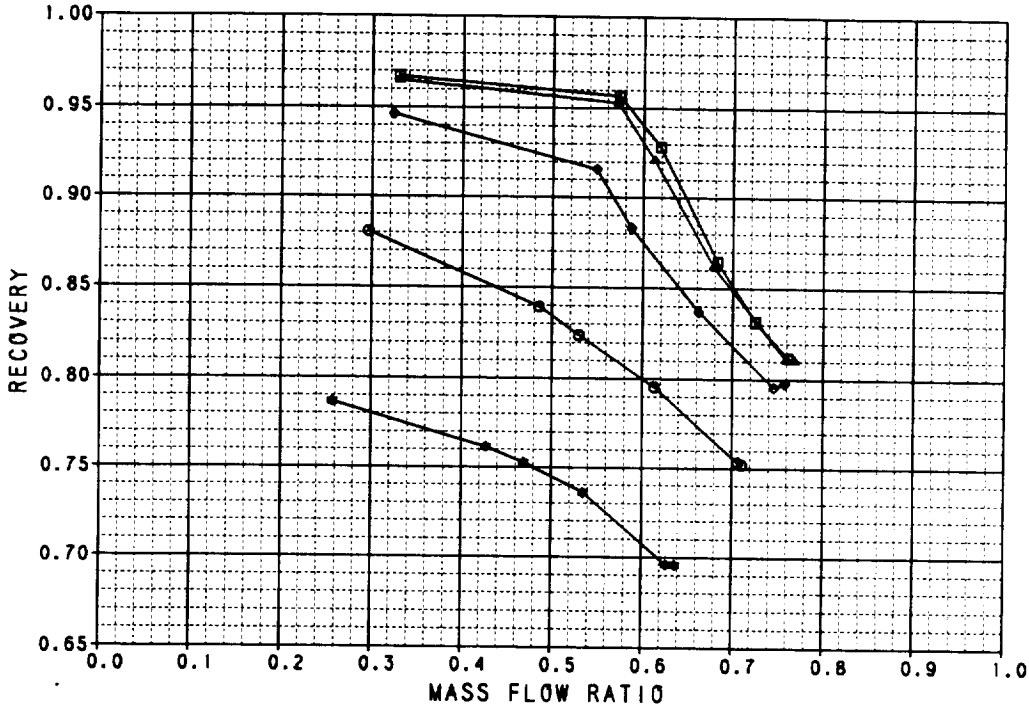

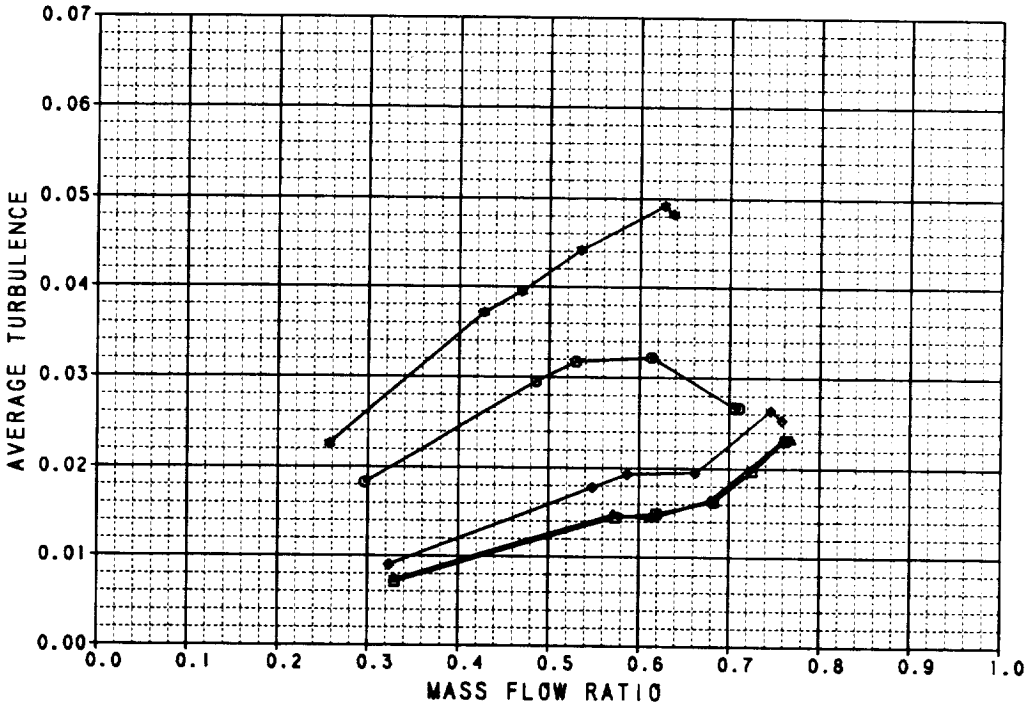

Figure B-25. Performance Data

Axisymmetric Inlet Upper and Lower Auxiliary Inlets Open 100%

$M_0 = 0.9$

SYM	TEST	RUN	RMACH	RALPHA	RBETA	CONFIG	DESCRIPTION
□	41	147	1.2058	-0.1156	0.0841	9.0000	AXI INLET,UPPER AND LOWER AUX INLETS OPEN 100%
▲	41	148	1.1992	9.9185	0.0837	9.0000	AXI INLET,UPPER AND LOWER AUX INLETS OPEN 100%
◆	41	148	1.2002	20.225	0.0469	9.0000	AXI INLET,UPPER AND LOWER AUX INLETS OPEN 100%

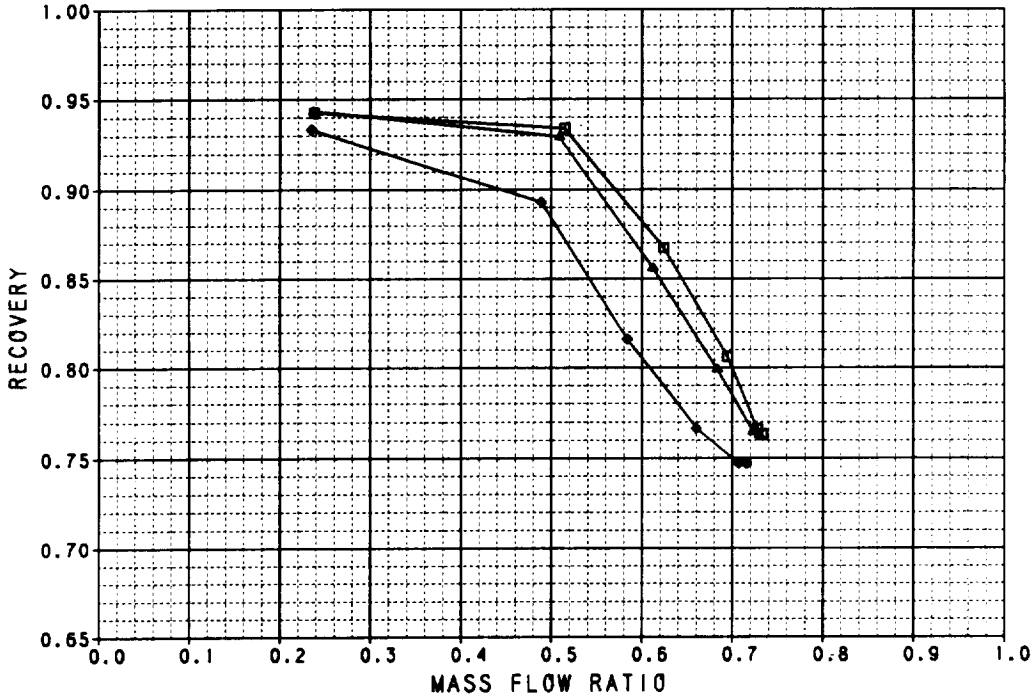

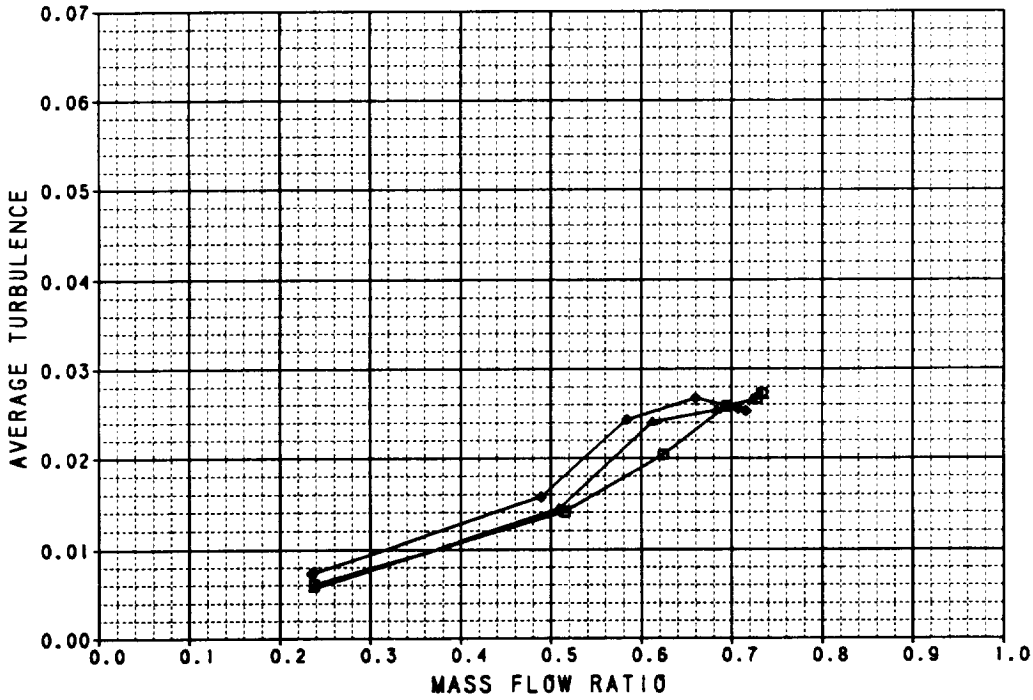

Figure B-26. Performance Data
Axisymmetric Inlet Upper and Lower Auxiliary Inlets Open 100%
$M_0 = 1.2$

SYM	TEST	RUN	RMACH	RALPHA	RBETA	CONFIG	DESCRIPTION
□	41	142	1.4053	-0.1721	0.0799	9.0000	AXI INLET, UPPER AND LOWER AUX INLETS OPEN 100%
▲	41	143	1.4028	4.8315	0.0648	9.0000	AXI INLET, UPPER AND LOWER AUX INLETS OPEN 100%
◆	41	144	1.3985	9.9775	0.0779	9.0000	AXI INLET, UPPER AND LOWER AUX INLETS OPEN 100%
○	41	145	1.3987	14.918	0.0634	9.0000	AXI INLET, UPPER AND LOWER AUX INLETS OPEN 100%
✱	41	146	1.3992	20.108	0.0751	9.0000	AXI INLET, UPPER AND LOWER AUX INLETS OPEN 100%

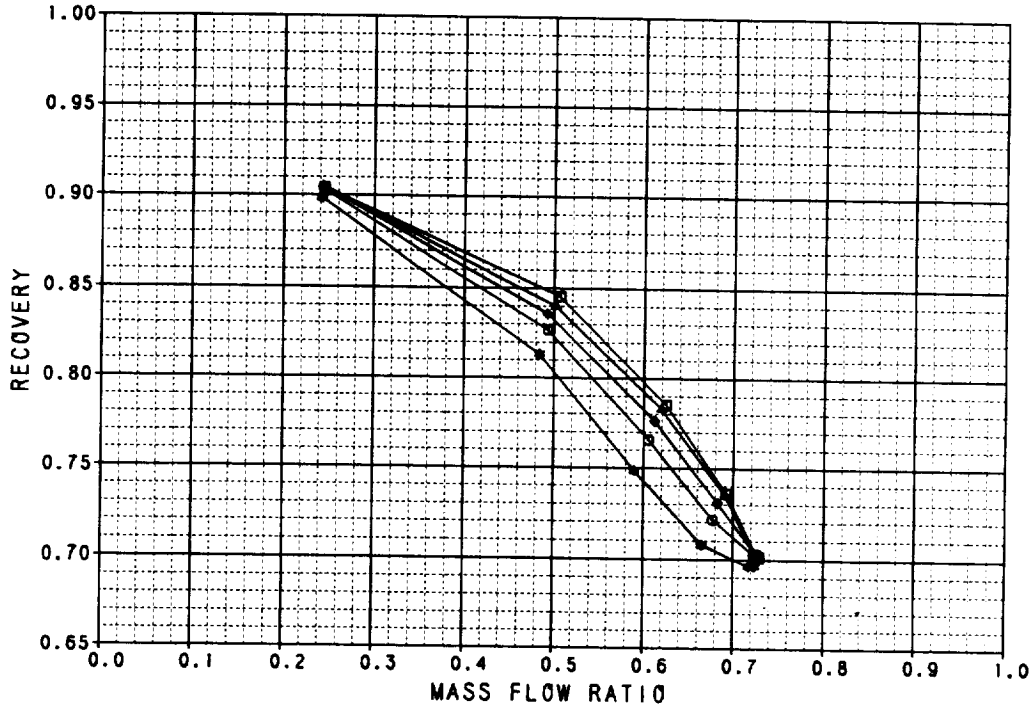

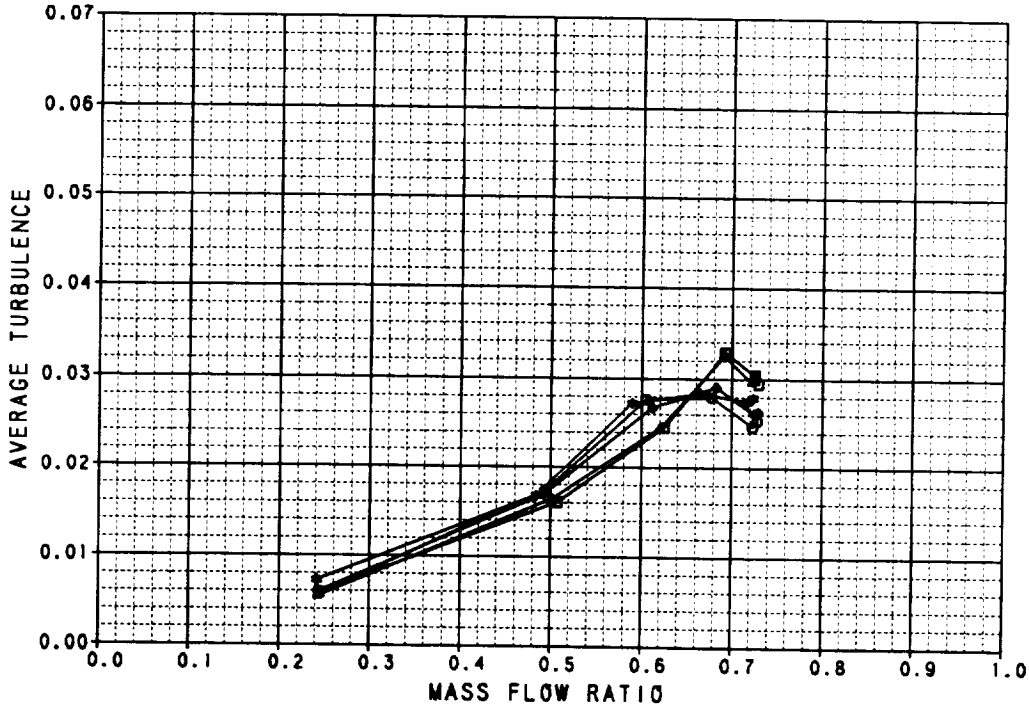

Figure B-27. Performance Data

Axisymmetric Inlet Upper and Lower Auxiliary Inlets Open 100%

$M_0 = 1.4$

SYM	TEST	RUN	RMACH	RALPHA	RBETA	CONFIG	DESCRIPTION
□	41	164	0.6039	-0.1832	0.0174	10.000	AXI INLET,UPPER AUX INLETS OPEN 100%
▲	41	165	0.6045	10.051	0.0156	10.000	AXI INLET,UPPER AUX INLETS OPEN 100%
◆	41	166	0.6054	20.147	0.0150	10.000	AXI INLET,UPPER AUX INLETS OPEN 100%
⊙	41	167	0.6059	30.172	0.0127	10.000	AXI INLET,UPPER AUX INLETS OPEN 100%
●	41	168	0.6063	39.986	.00854	10.000	AXI INLET,UPPER AUX INLETS OPEN 100%

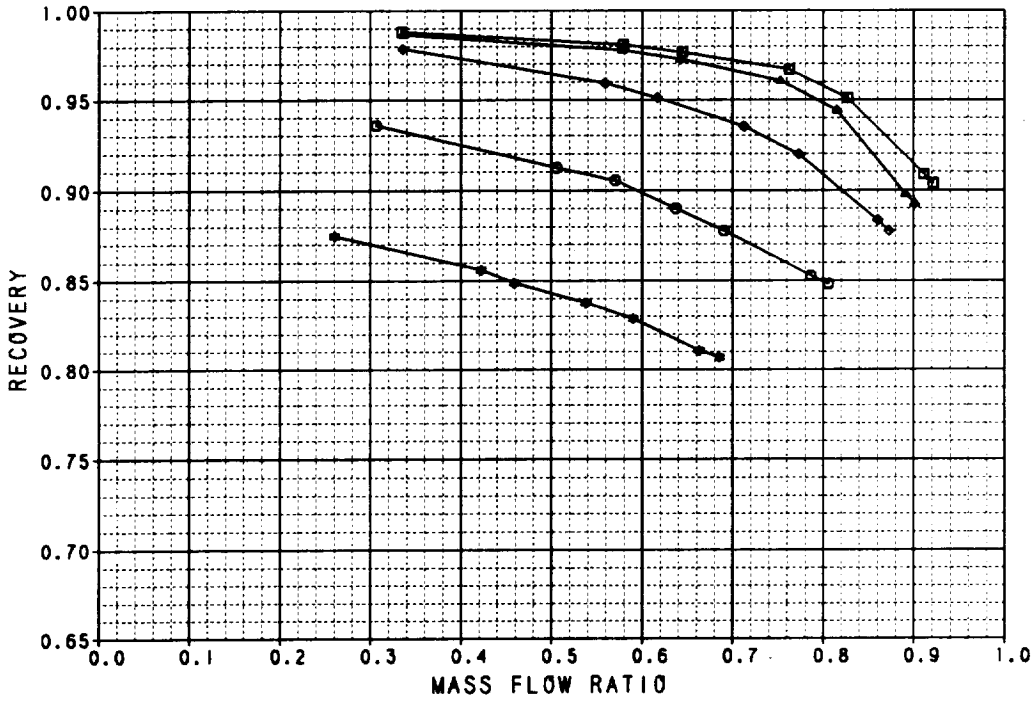

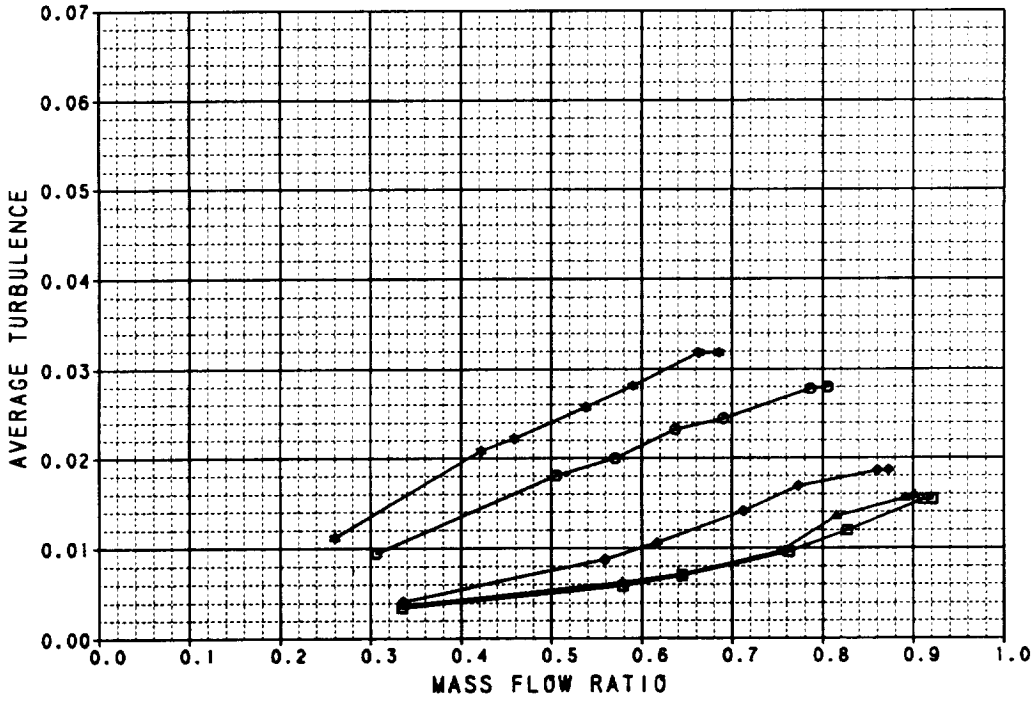

Figure B-28. Performance Data
Axisymmetric Inlet Upper Auxiliary Inlets Open 100%
$M_0 = 0.6$

SYM	TEST	RUN	RMACH	RALPHA	RBETA	CONFIG	DESCRIPTION
□	41	174	0.9002	-0.0579	0.0274	10.000	AXI INLET, UPPER AUX INLETS OPEN 100%
▲	41	177	0.9005	9.9408	0.0930	10.000	AXI INLET, UPPER AUX INLETS OPEN 100%
◆	41	178	0.9029	19.866	0.0882	10.000	AXI INLET, UPPER AUX INLETS OPEN 100%
⊙	41	181	0.9000	30.120	0.0117	10.000	AXI INLET, UPPER AUX INLETS OPEN 100%
●	41	182	0.8983	39.855	.00342	10.000	AXI INLET, UPPER AUX INLETS OPEN 100%

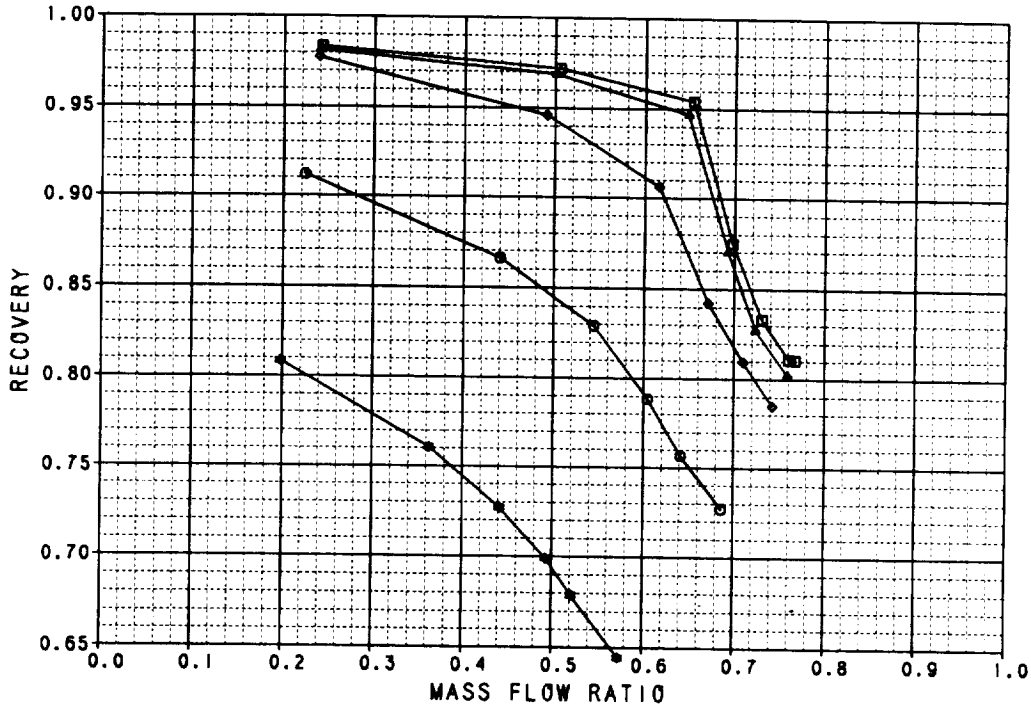

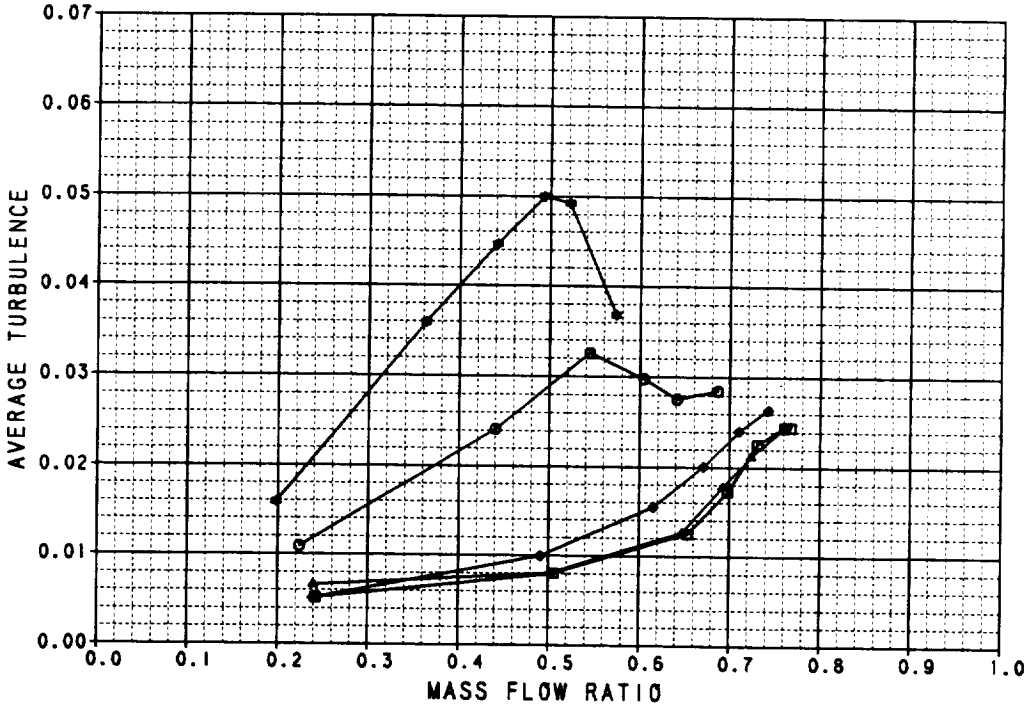

Figure B-29. Performance Data
Axisymmetric Inlet Upper Auxiliary Inlets Open 100%
$M_0 = 0.9$

SYM	TEST	RUN	RMACH	RALPHA	RBETA	CONFIG	DESCRIPTION
□	41	183	1.2102	-0.0278	.00136	10.000	AXI INLET,UPPER AUX INLETS OPEN 100%
▲	41	184	1.2101	9.9776	0.0131	10.000	AXI INLET,UPPER AUX INLETS OPEN 100%
◆	41	185	1.2113	20.045	-0.0234	10.000	AXI INLET,UPPER AUX INLETS OPEN 100%
○	41	186	1.2067	25.372	-0.0221	10.000	AXI INLET,UPPER AUX INLETS OPEN 100%

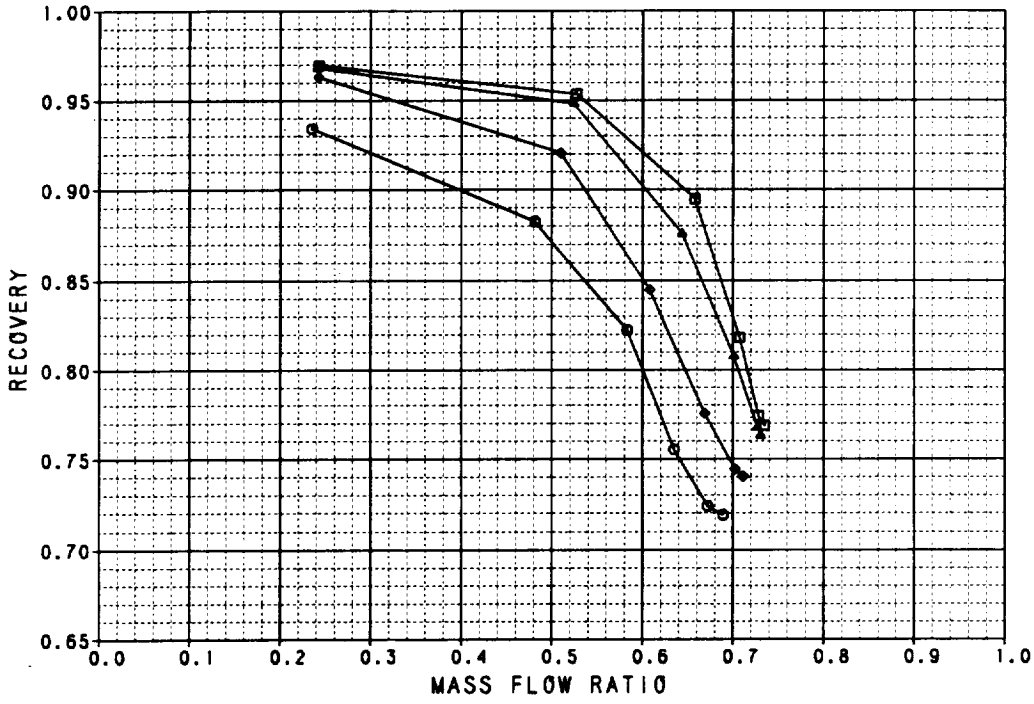

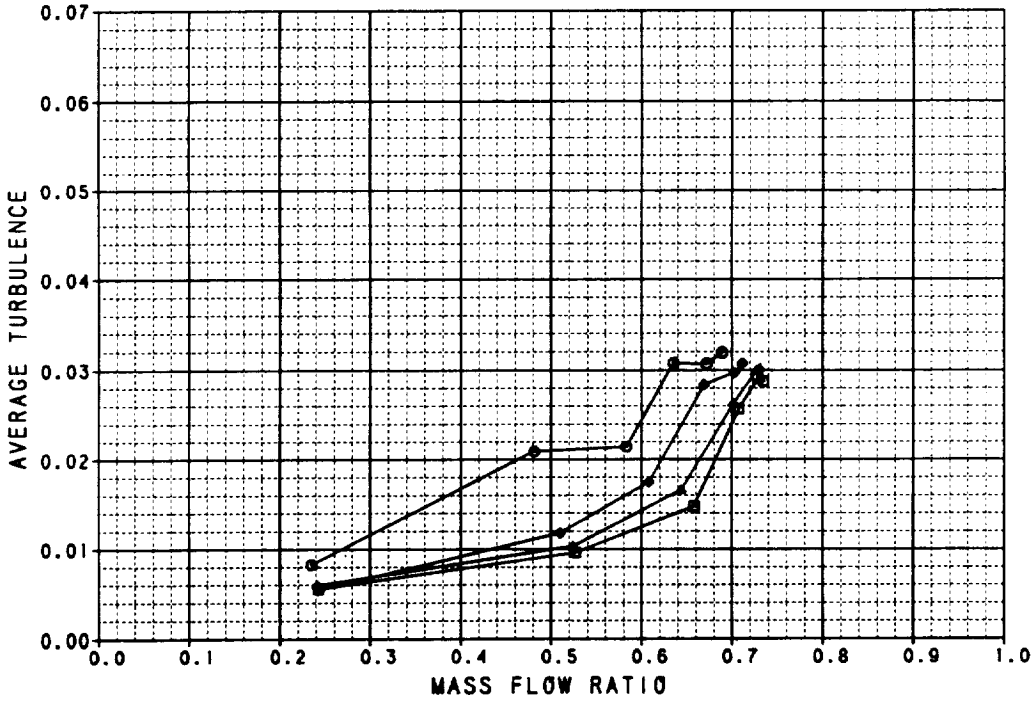

Figure B-30. Performance Data
Axisymmetric Inlet Upper Auxiliary Inlets Open 100%
$M_0 = 1.2$

SYM	TEST	RUN	RMACH	RALPHA	RBETA	CONFIG	DESCRIPTION
□	41	137	1.3959	-0.2168	0.0944	10.000	AXI INLET,UPPER AUX INLETS OPEN 100%
△	41	138	1.3987	4.8831	0.1046	10.000	AXI INLET,UPPER AUX INLETS OPEN 100%
◇	41	139	1.4101	10.000	0.0993	10.000	AXI INLET,UPPER AUX INLETS OPEN 100%
○	41	140	1.4094	15.139	0.0785	10.000	AXI INLET,UPPER AUX INLETS OPEN 100%
●	41	141	1.4073	20.538	0.0765	10.000	AXI INLET,UPPER AUX INLETS OPEN 100%

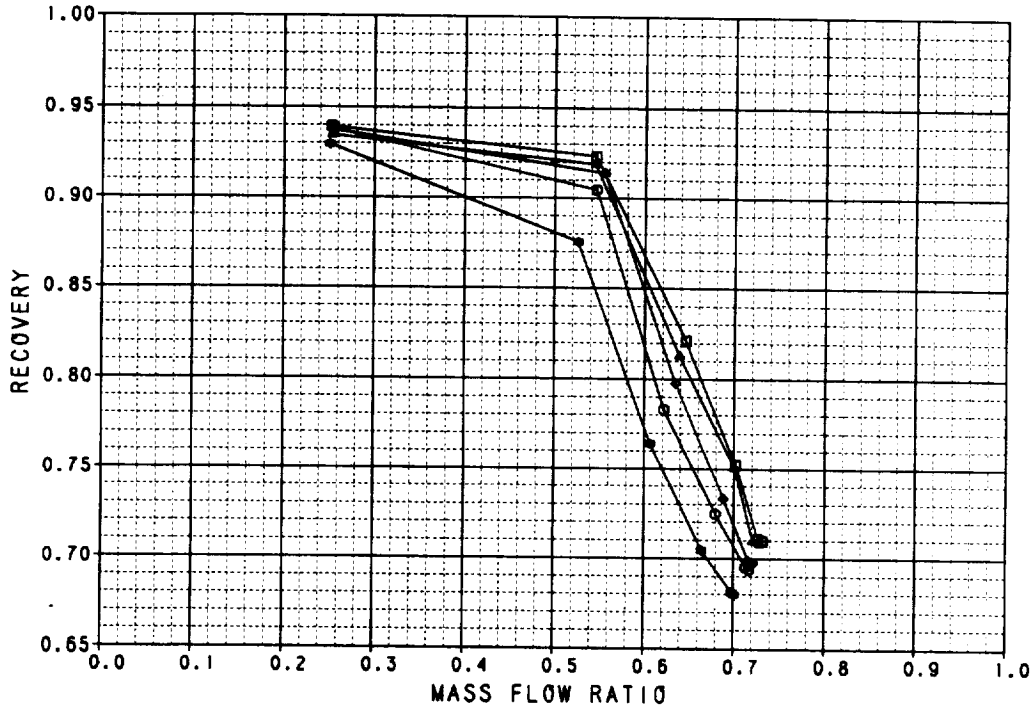

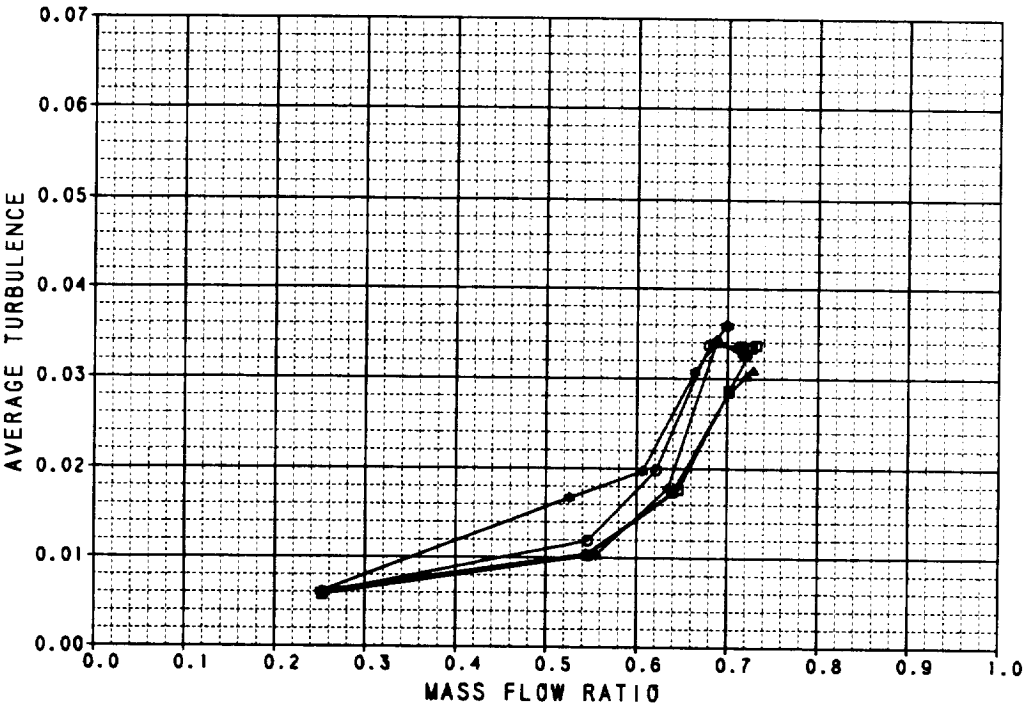

Figure B-31. Performance Data
Axisymmetric Inlet Upper Auxiliary Inlets Open 100%
$M_0 = 1.4$

SYM	TEST	RUN	RMACH	RALPHA	RBETA	CONFIG	DESCRIPTION
□	41	197	0.6029	-0.1078	0.0696	11.000	AXI INLET,UPPER AUX INLETS OPEN 50%
▲	41	198	0.6038	17.292	0.0540	11.000	AXI INLET,UPPER AUX INLETS OPEN 50%
◆	41	199	0.6061	37.135	-8.1E-4	11.000	AXI INLET,UPPER AUX INLETS OPEN 50%

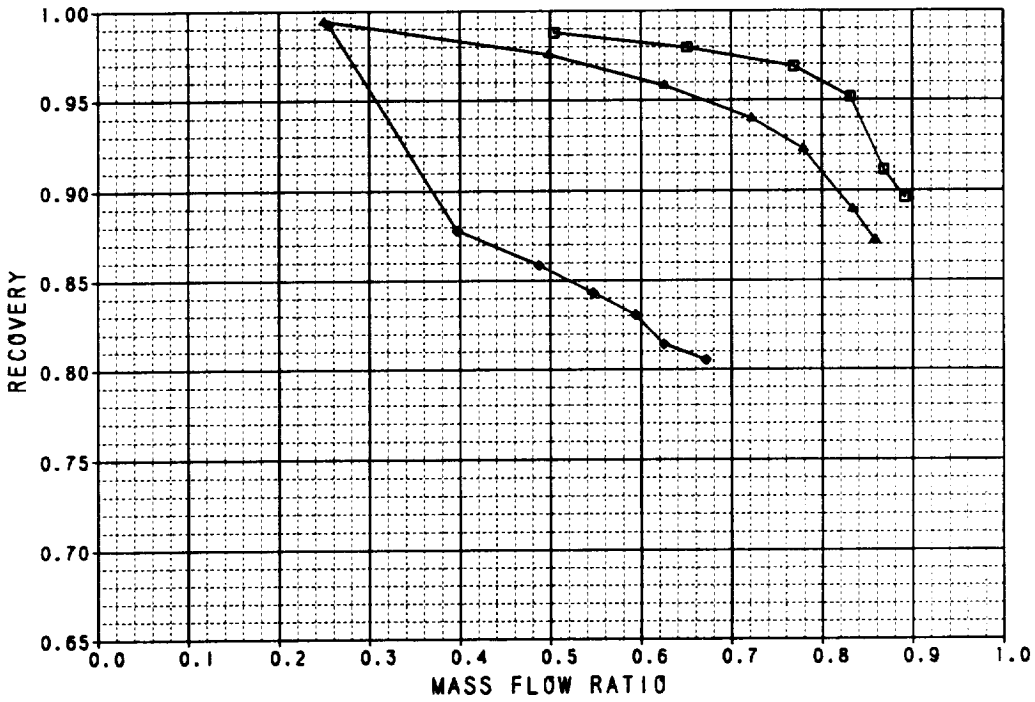

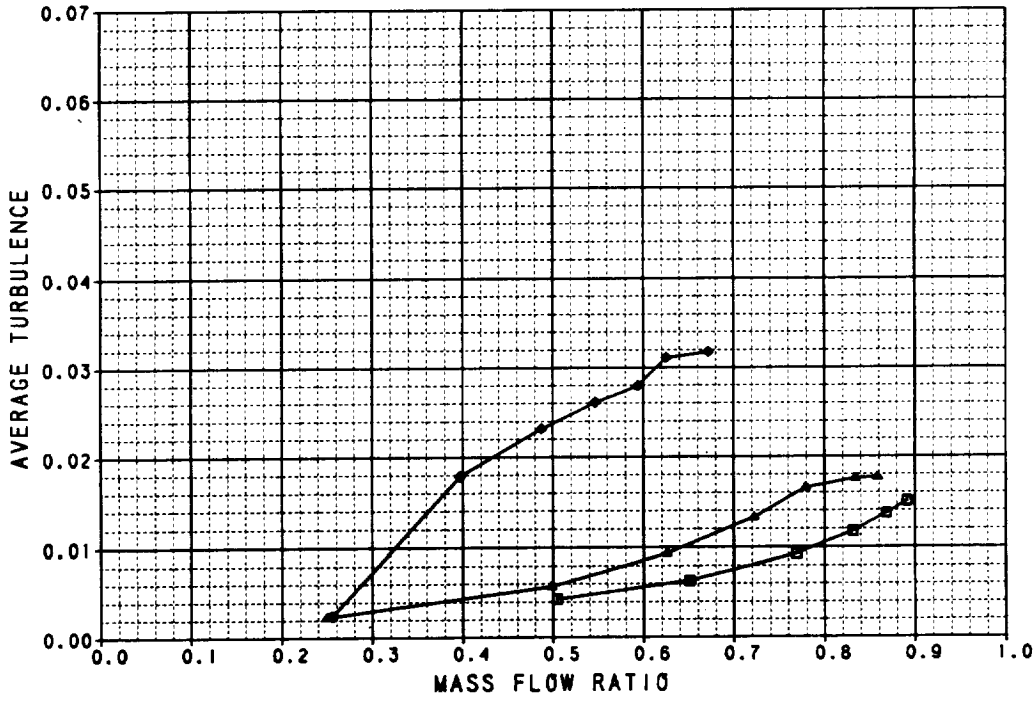

Figure B-32. Performance Data
Axisymmetric Inlet Upper Auxiliary Inlets Open 50%
$M_0 = 0.6$

SYM	TEST	RUN	RMACH	RALPHA	RBETA	CONFIG	DESCRIPTION
□	41	200	0.8598	5.8258	0.0304	11.000	AXI INLET,UPPER AUX INLETS OPEN 50%
▲	41	201	0.9012	17.325	-0.0198	11.000	AXI INLET,UPPER AUX INLETS OPEN 50%
◆	41	202	0.9000	37.614	-0.0140	11.000	AXI INLET,UPPER AUX INLETS OPEN 50%

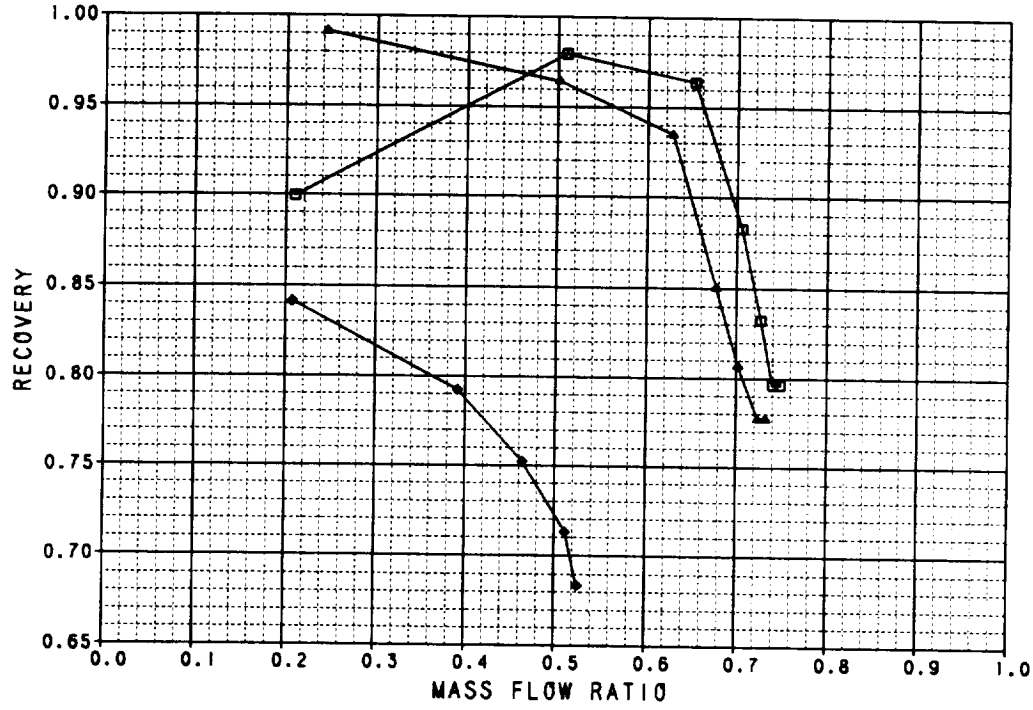

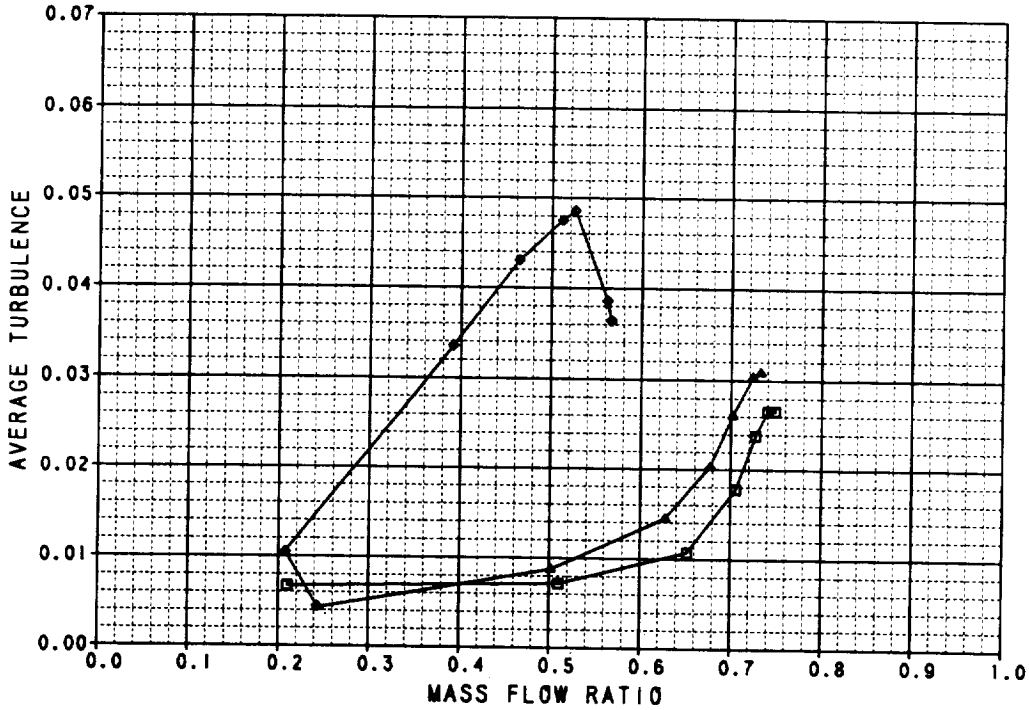

Figure B-33. Performance Data
Axisymmetric Inlet Upper Auxiliary Inlets Open 50%
$M_0 = 0.9$

SYM	TEST	RUN	RMACH	RALPHA	RBETA	CONFIG	DESCRIPTION
□	41	126	0.6015	-0.2035	0.0793	12.000	AXI INLET WITH RETRACTED C.B.
▲	41	127	0.6028	10.985	0.0834	12.000	AXI INLET WITH RETRACTED C.B.
◆	41	128	0.6057	30.344	0.0724	12.000	AXI INLET WITH RETRACTED C.B.

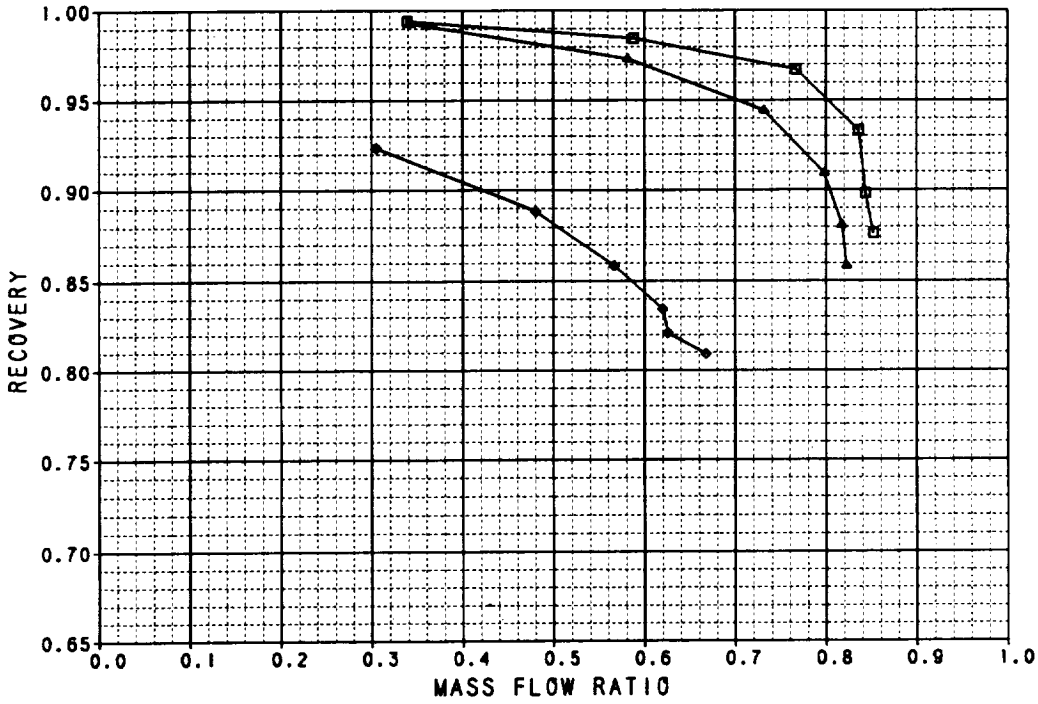

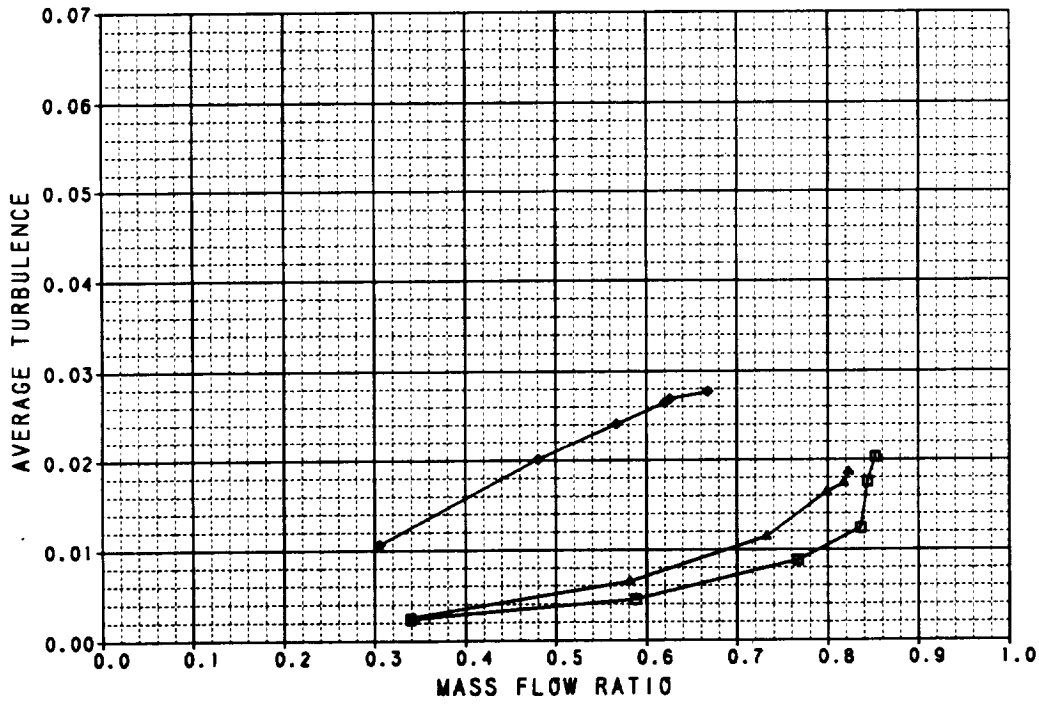

Figure B-34. Performance Data
Axisymmetric Inlet With Retracted Centerbody
$M_0 = 0.6$

SYM	TEST	RUN	RMACH	RALPHA	RBETA	CONFIG	DESCRIPTION
□	41	129	0.9003	-0.2558	0.0579	12.000	AXI INLET WITH RETRACTED C.B.
△	41	132	0.9005	20.166	0.0972	12.000	AXI INLET WITH RETRACTED C.B.
◇	41	135	0.9027	30.158	0.0820	12.000	AXI INLET WITH RETRACTED C.B.
○	41	136	0.8985	39.766	0.0986	12.000	AXI INLET WITH RETRACTED C.B.

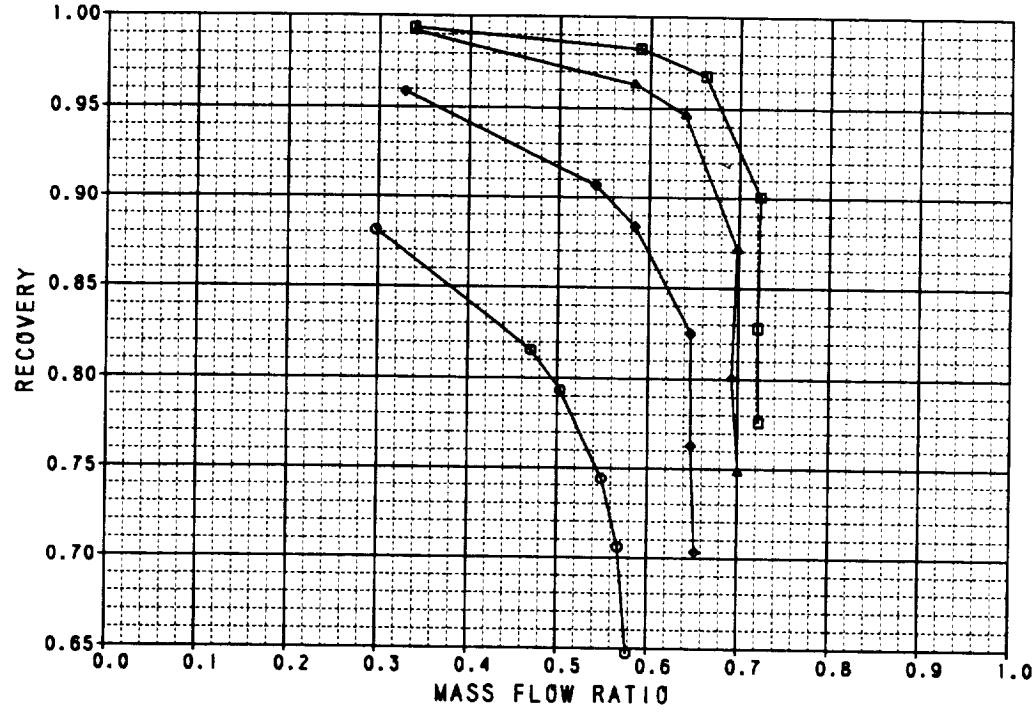

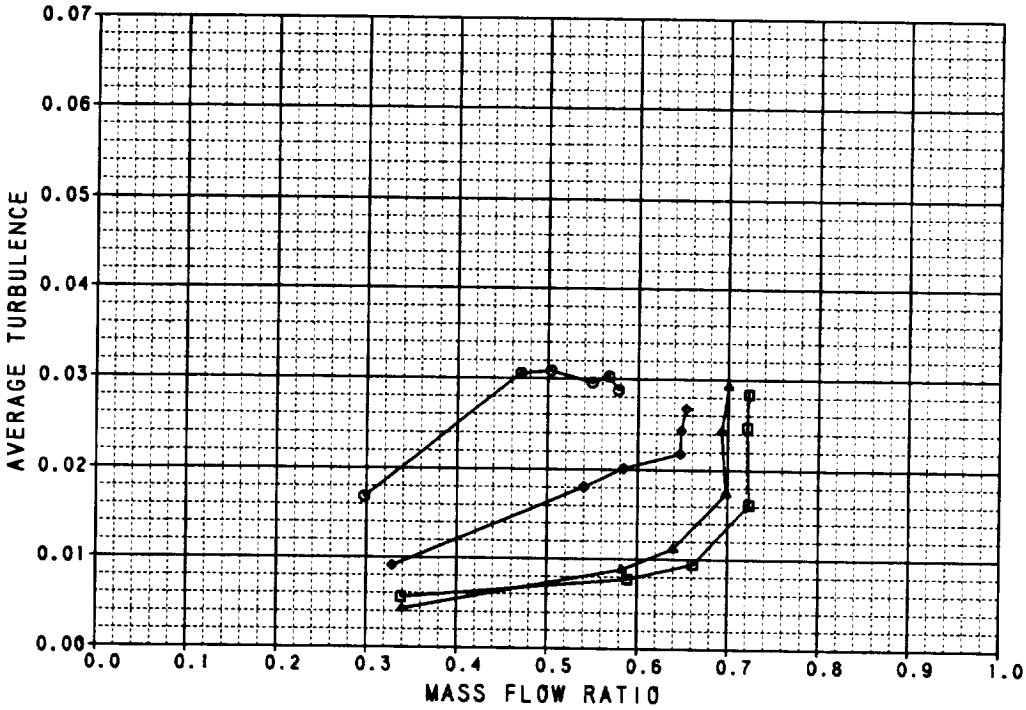

Figure B-35. Performance Data
Axisymmetric Inlet With Retracted Centerbody
$M_0 = 0.9$

SYM	TEST	RUN	RMACH	RALPHA	RBETA	CONFIG	DESCRIPTION
□	41	226	0.6083	-.00442	0.0174	15.000	AXI INLET,20 DEG DROOP LIP AND LOWER AUX INLETS OPEN 100%
▲	41	227	0.6093	9.8867	0.0204	15.000	AXI INLET,20 DEG DROOP LIP AND LOWER AUX INLETS OPEN 100%
◆	41	228	0.6066	20.147	0.0221	15.000	AXI INLET,20 DEG DROOP LIP AND LOWER AUX INLETS OPEN 100%
○	41	229	0.6093	29.977	0.0328	15.000	AXI INLET,20 DEG DROOP LIP AND LOWER AUX INLETS OPEN 100%
●	41	230	0.6089	40.090	-3.2E-4	15.000	AXI INLET,20 DEG DROOP LIP AND LOWER AUX INLETS OPEN 100%

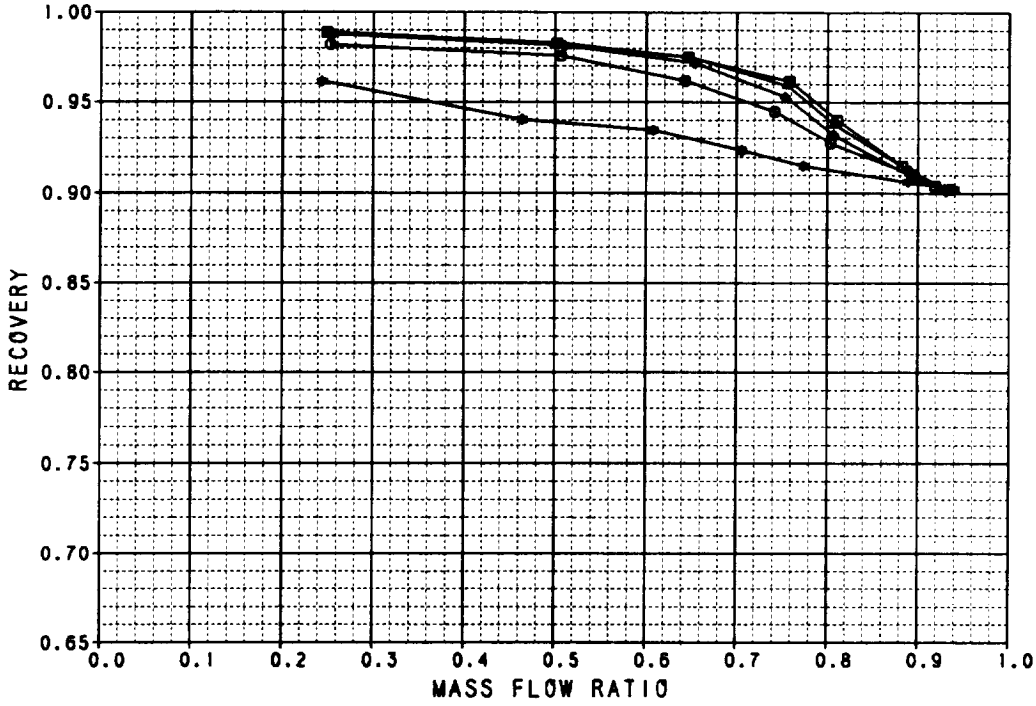

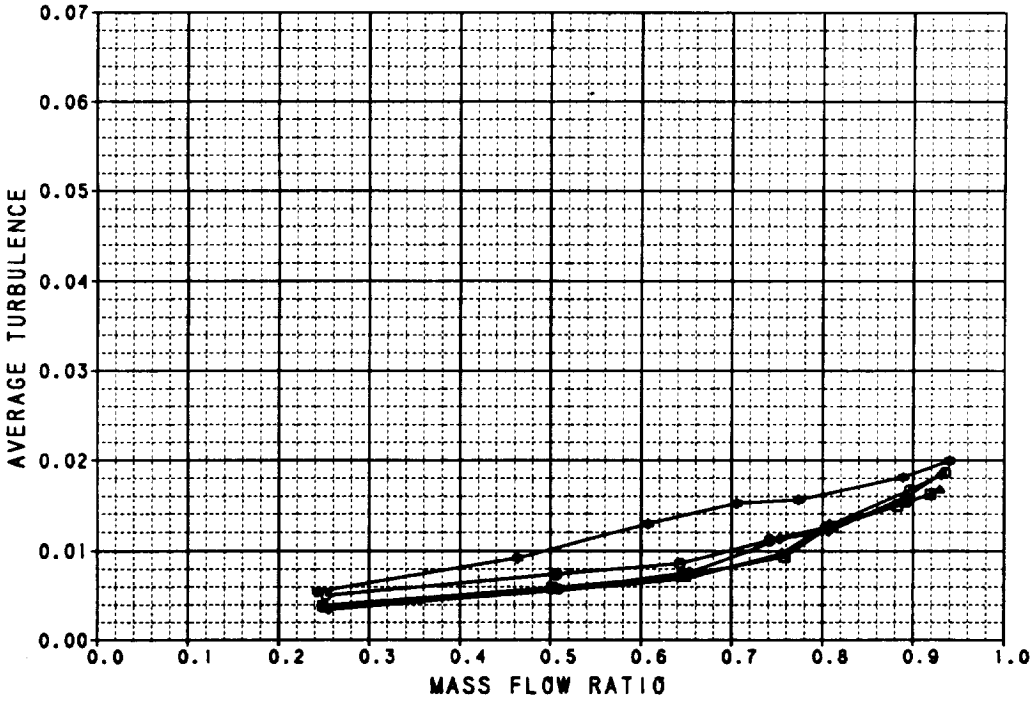

Figure B-36. Performance Data

Axisymmetric Inlet 20° Cowl Lip Lower Auxiliary Inlets Open 100%

$M_0 = 0.6$

SYM	TEST	RUN	RMACH	RALPHA	RBETA	CONFIG	DESCRIPTION
□	41	216	0.8995	-5.1225	-0.0387	13.000	AXI INLET,20 DEG DROOP LIP AND LOWER AUX INLETS OPEN 100%
▲	41	217	0.8960	-0.0796	-0.0434	13.000	AXI INLET,20 DEG DROOP LIP AND LOWER AUX INLETS OPEN 100%
◆	41	219	0.9035	10.098	0.0317	13.000	AXI INLET,20 DEG DROOP LIP AND LOWER AUX INLETS OPEN 100%
⊙	41	220	0.9048	20.081	-7.1E-4	13.000	AXI INLET,20 DEG DROOP LIP AND LOWER AUX INLETS OPEN 100%
✱	41	221	0.9010	30.162	-.00416	13.000	AXI INLET,20 DEG DROOP LIP AND LOWER AUX INLETS OPEN 100%
⊠	41	222	0.8996	40.253	-0.0287	13.000	AXI INLET,20 DEG DROOP LIP AND LOWER AUX INLETS OPEN 100%

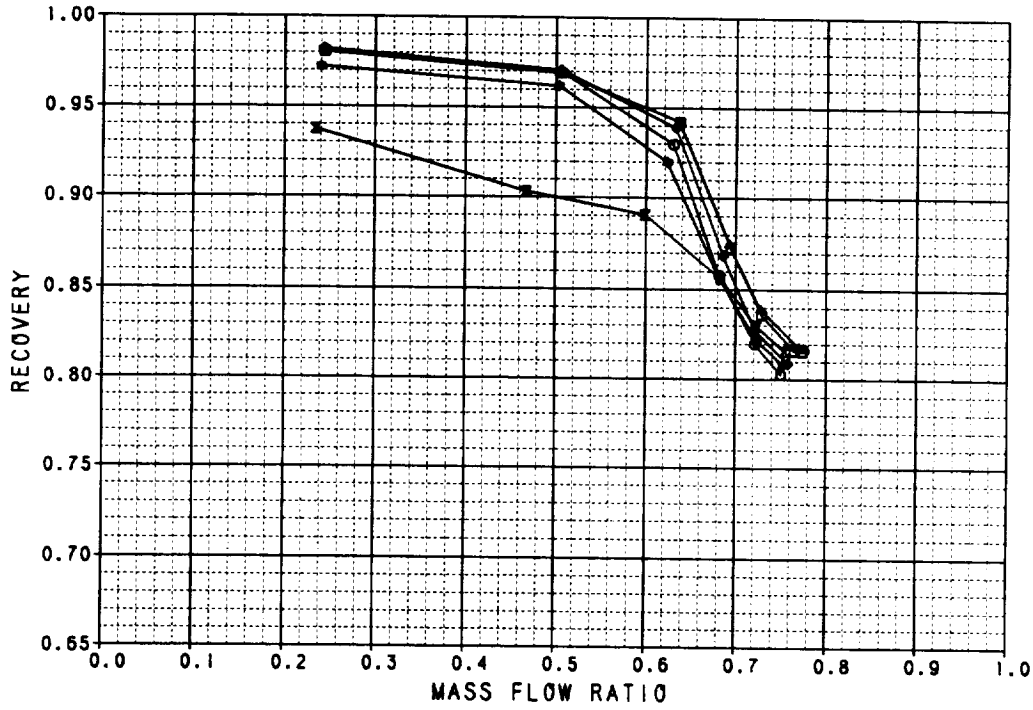

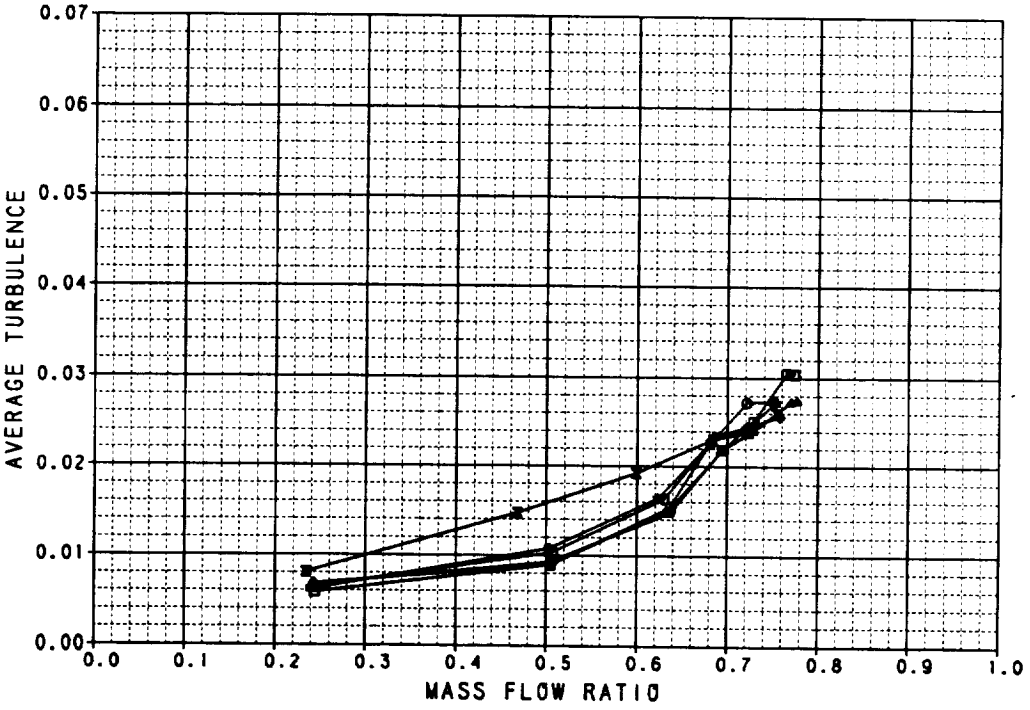

Figure B-37. Performance Data

Axisymmetric Inlet 20° Cowl Lip Lower Auxiliary Inlets Open 100%

$M_0 = 0.9$

SYM	TEST	RUN	RMACH	RALPHA	RBETA	CONFIG	DESCRIPTION
□	41	251	1.2057	0.1614	-.00347	13.000	AXI INLET,20 DEG DROOP LIP AND LOWER AUX INLETS OPEN 100%
▲	41	254	1.2027	9.9082	-0.0117	13.000	AXI INLET,20 DEG DROOP LIP AND LOWER AUX INLETS OPEN 100%
◆	41	252	1.2031	20.119	-0.0178	13.000	AXI INLET,20 DEG DROOP LIP AND LOWER AUX INLETS OPEN 100%
○	41	253	1.2012	25.155	-0.0235	13.000	AXI INLET,20 DEG DROOP LIP AND LOWER AUX INLETS OPEN 100%

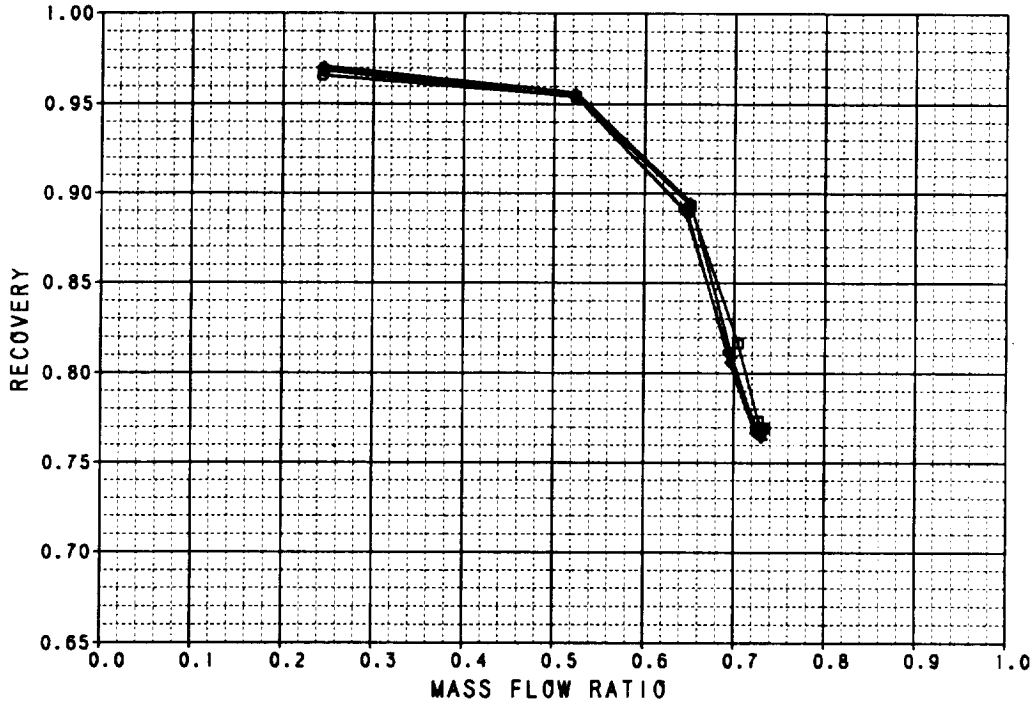

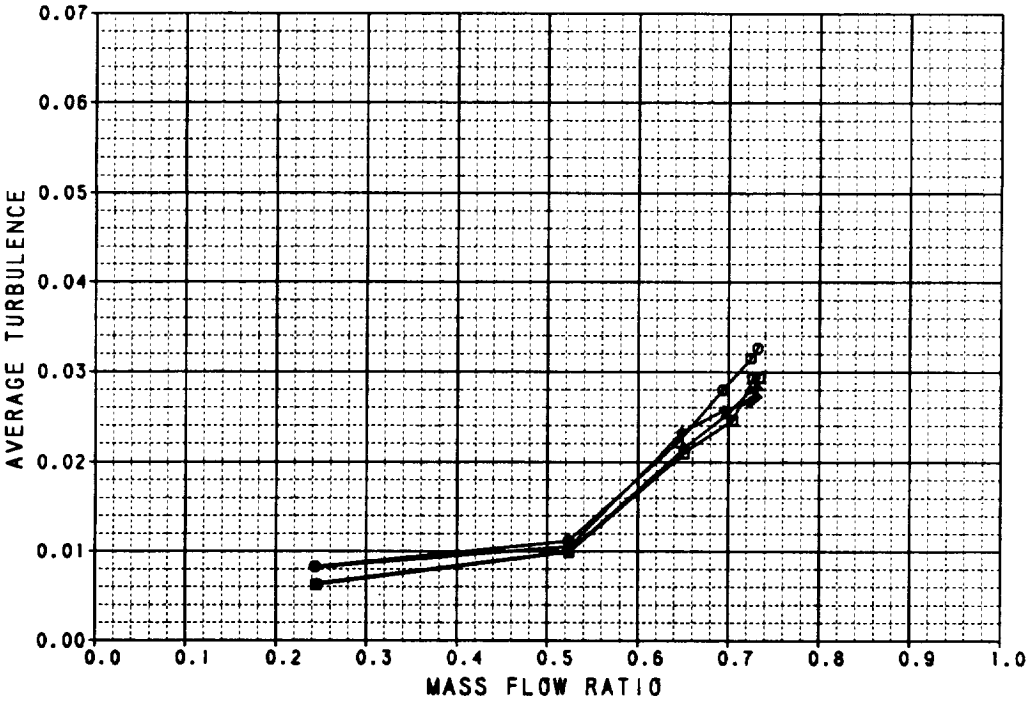

Figure B-38. Performance Data

Axisymmetric Inlet 20° Cowl Lip Lower Auxiliary Inlets Open 100%

$M_0 = 1.2$

SYM	TEST	RUN	RMACH	RALPHA	RBETA	CONFIG	DESCRIPTION
□	41	205	0.5999	-0.2317	-0.0289	14.000	AXI INLET,20 DEG DROOP LIP,L AUX INLETS OPEN 100%,RETD C.B.
△	41	206	0.6003	10.091	-0.0198	14.000	AXI INLET,20 DEG DROOP LIP,L AUX INLETS OPEN 100%,RETD C.B.
◇	41	207	0.6038	20.142	-0.0245	14.000	AXI INLET,20 DEG DROOP LIP,L AUX INLETS OPEN 100%,RETD C.B.
○	41	208	0.6068	30.005	-0.0422	14.000	AXI INLET,20 DEG DROOP LIP,L AUX INLETS OPEN 100%,RETD C.B.
⋆	41	209	0.6064	39.972	-0.0569	14.000	AXI INLET,20 DEG DROOP LIP,L AUX INLETS OPEN 100%,RETD C.B.

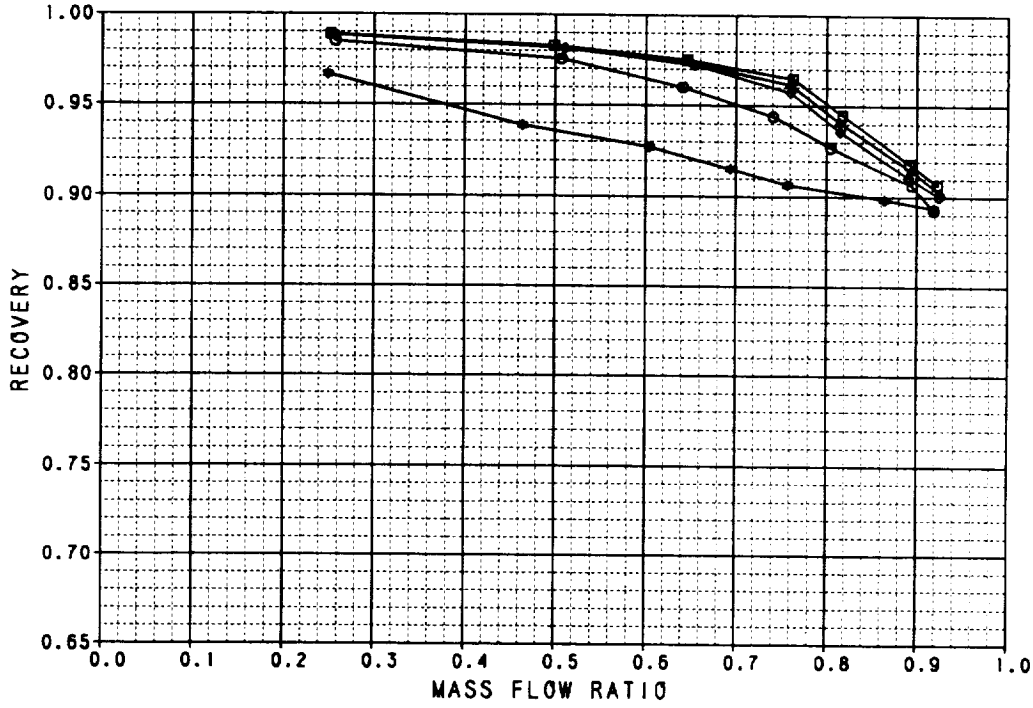

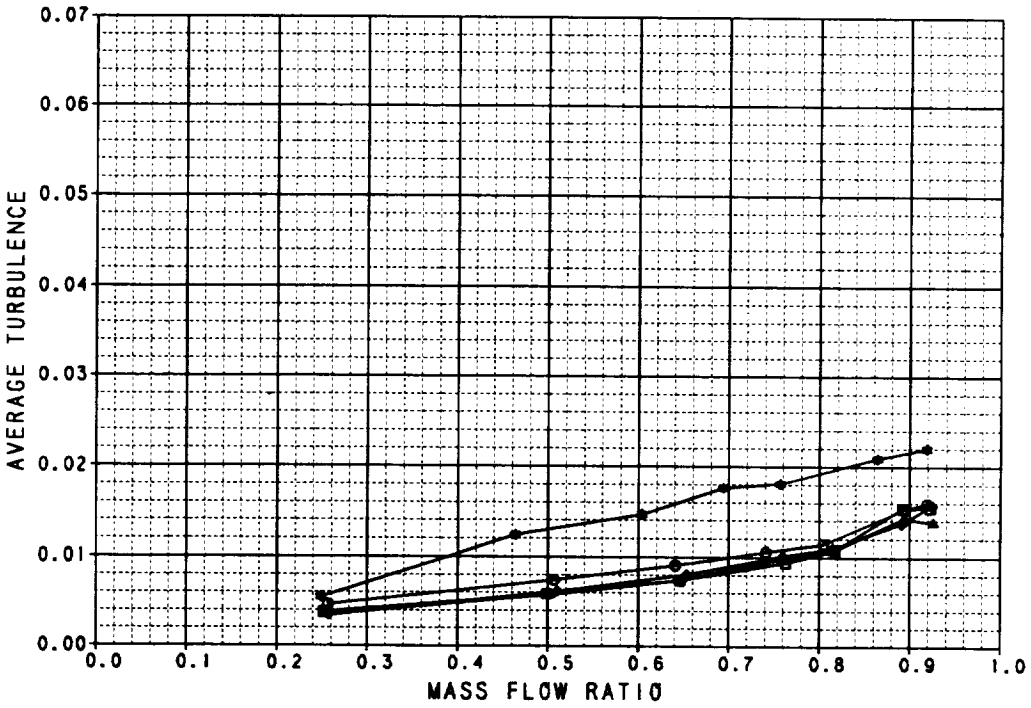

Figure B-39. Performance Data
Axisymmetric Inlet 20° Cowl Lip
Lower Auxiliary Inlets Open 100% Retracted Centerbody
$M_0 = 0.6$

SYM	TEST	RUN	RMACH	RALPHA	RBETA	CONFIG	DESCRIPTION
□	41	210	0.9021	-4.9479	-0.0287	14.000	AXI INLET,20 DEG DROOP LIP,L AUX INLETS OPEN 100%,RETD C.B.
▲	41	211	0.9019	-0.1498	-0.0375	14.000	AXI INLET,20 DEG DROOP LIP,L AUX INLETS OPEN 100%,RETD C.B.
◆	41	212	0.9015	9.8709	-0.0304	14.000	AXI INLET,20 DEG DROOP LIP,L AUX INLETS OPEN 100%,RETD C.B.
○	41	213	0.9019	19.978	-0.0348	14.000	AXI INLET,20 DEG DROOP LIP,L AUX INLETS OPEN 100%,RETD C.B.
●	41	214	0.9012	30.088	-0.0340	14.000	AXI INLET,20 DEG DROOP LIP,L AUX INLETS OPEN 100%,RETD C.B.
⧗	41	215	0.9017	40.285	-0.0487	14.000	AXI INLET,20 DEG DROOP LIP,L AUX INLETS OPEN 100%,RETD C.B.

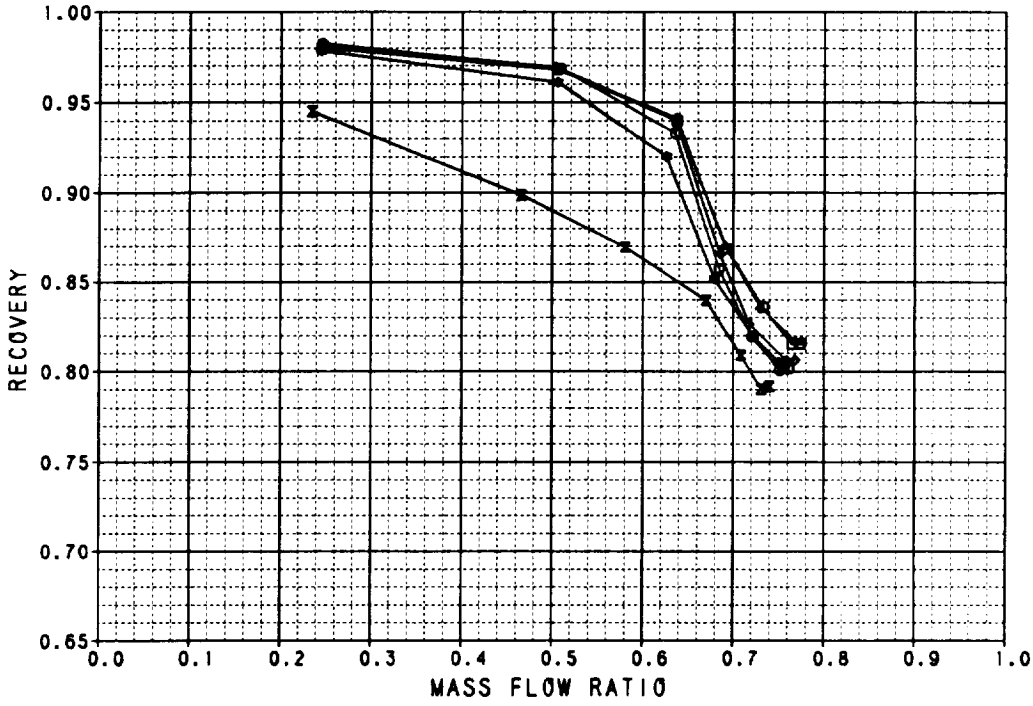

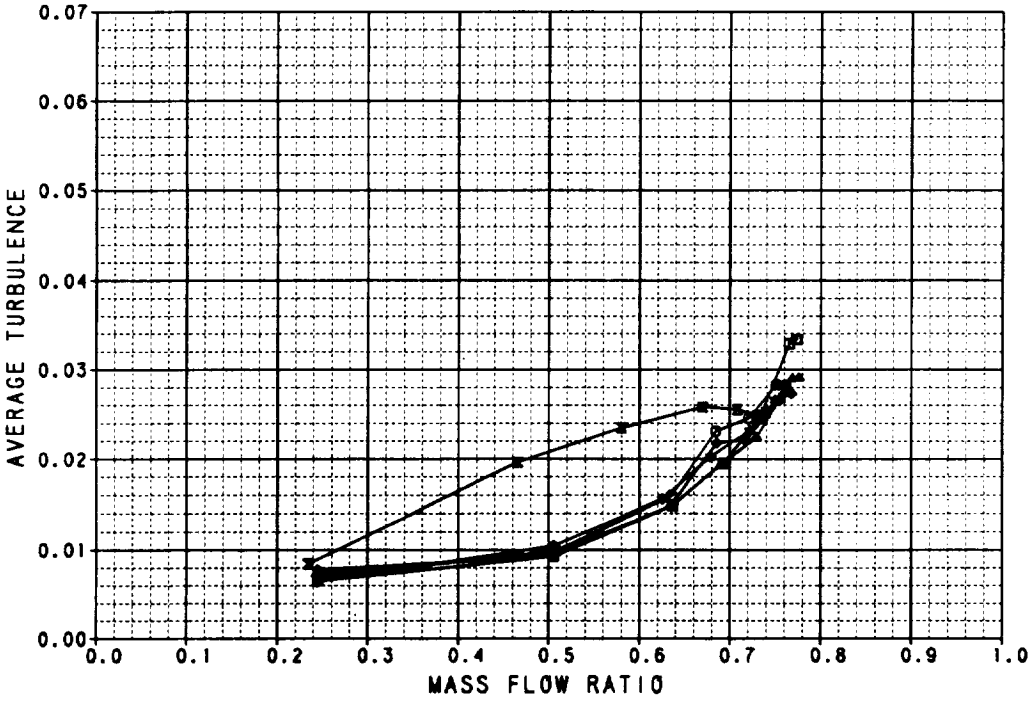

Figure B-40. Performance Data
Axisymmetric Inlet 20° Cowl Lip
Lower Auxiliary Inlets Open 100% Retracted Centerbody
$M_0 = 0.9$

SYM	TEST	RUN	RMACH	RALPHA	RBETA	CONFIG	DESCRIPTION
□	41	249	0.6053	-0.1281	0.0280	15.000	2-D INLET WITH SHORT DIFFUSER
▲	41	250	0.6035	10.011	0.0331	15.000	2-D INLET WITH SHORT DIFFUSER
◆	41	251	0.6062	20.027	0.0233	15.000	2-D INLET WITH SHORT DIFFUSER
○	41	252	0.6076	30.155	0.0182	15.000	2-D INLET WITH SHORT DIFFUSER
●	41	253	0.6087	39.970	.00877	15.000	2-D INLET WITH SHORT DIFFUSER

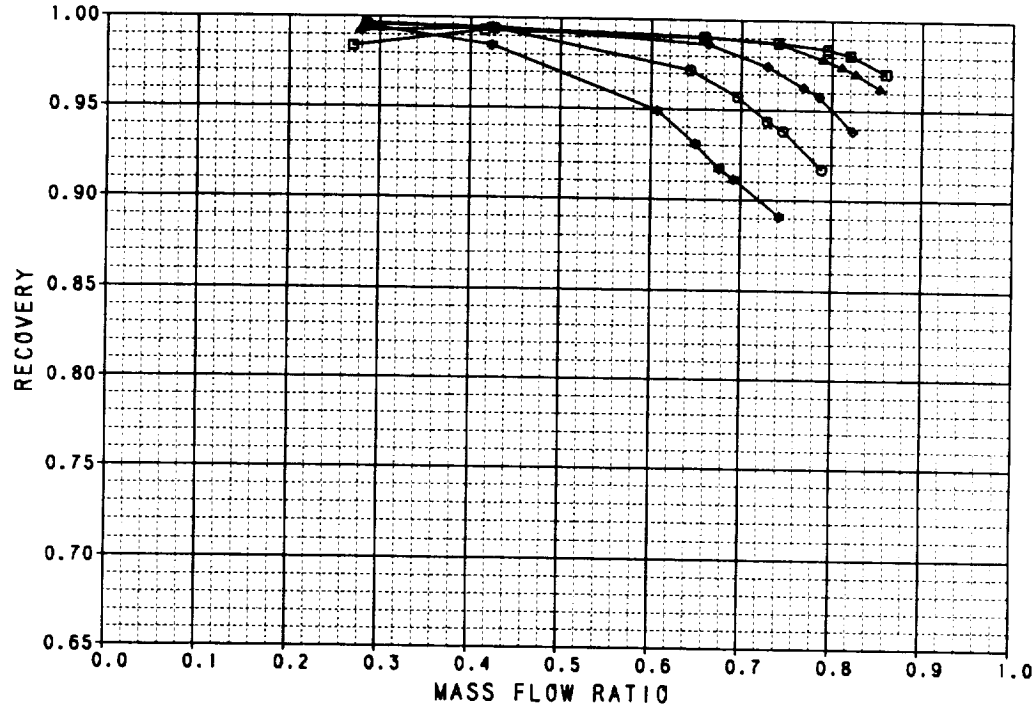

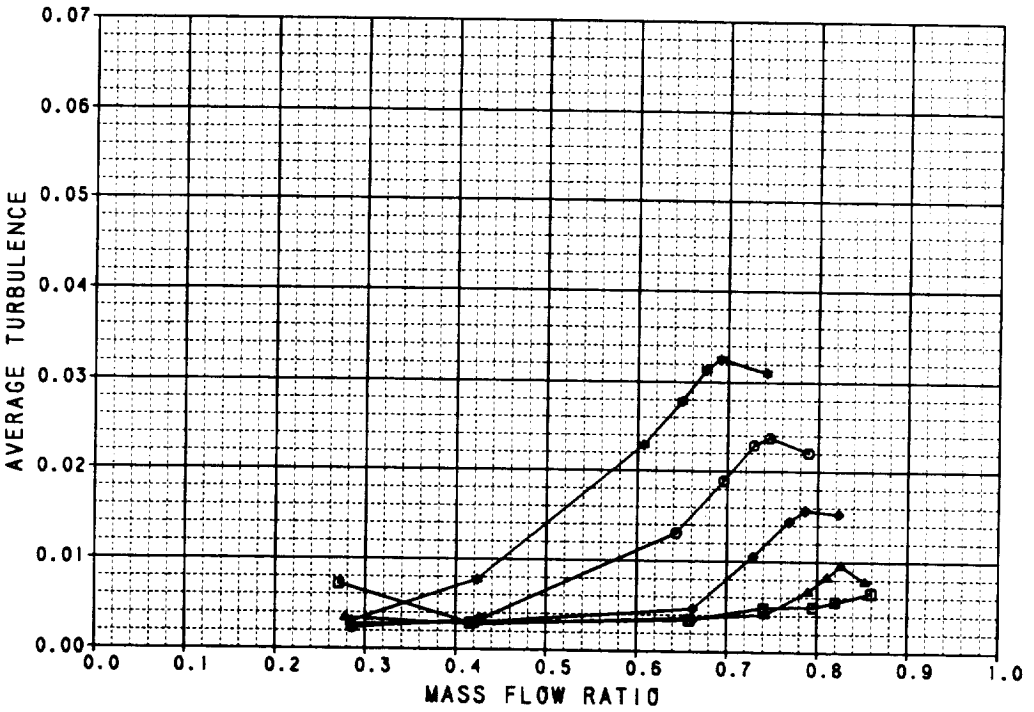

Figure B-41. Performance Data
2-D Inlet With Short Diffuser
$M_0 = 0.6$

SYM	TEST	RUN	RMACH	RALPHA	RBETA	CONFIG	DESCRIPTION
□	41	243	0.9044	-4.8891	-.00583	15.000	2-D INLET WITH SHORT DIFFUSER
▲	41	239	0.9031	-0.0454	-0.0522	15.000	2-D INLET WITH SHORT DIFFUSER
◆	41	242	0.9000	10.087	0.0156	15.000	2-D INLET WITH SHORT DIFFUSER
⊙	41	244	0.8985	20.068	-0.0202	15.000	2-D INLET WITH SHORT DIFFUSER
⬟	41	247	0.9006	30.075	-.00681	15.000	2-D INLET WITH SHORT DIFFUSER
⧗	41	248	0.8989	39.856	-0.0334	15.000	2-D INLET WITH SHORT DIFFUSER

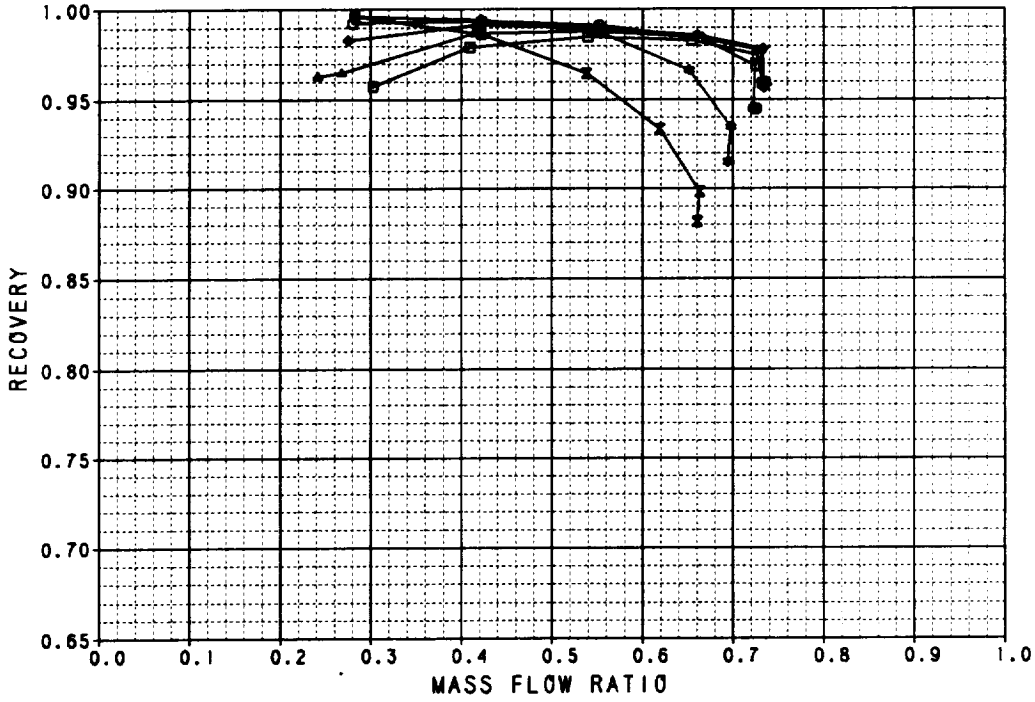

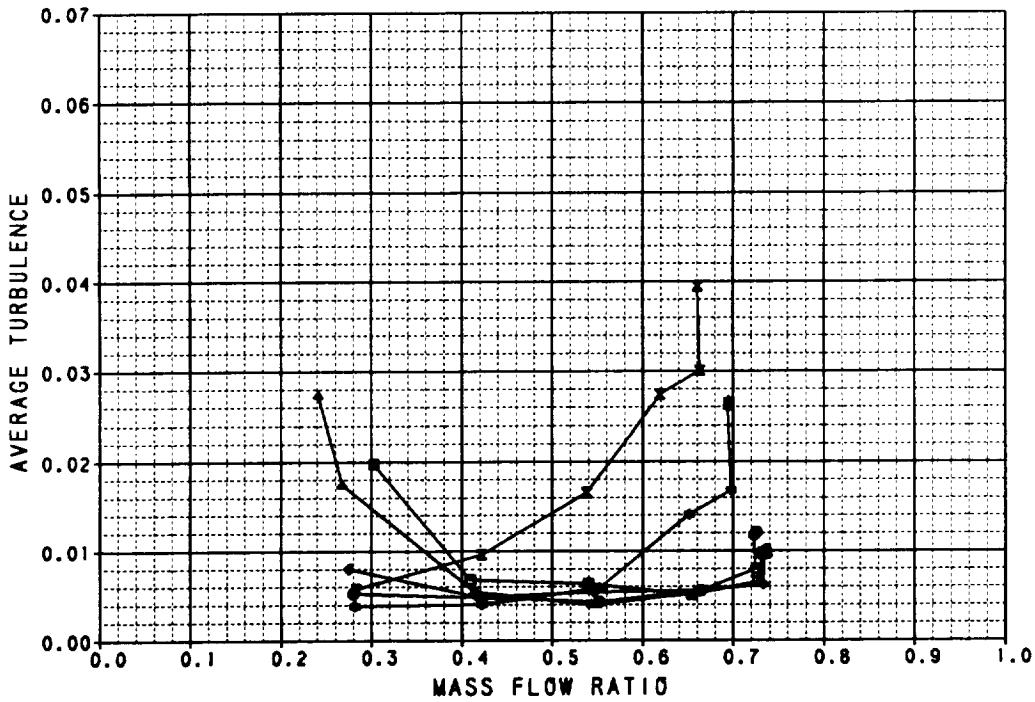

Figure B-42. Performance Data
2-D Inlet With Short Diffuser
$M_0 = 0.9$

SYM	TEST	RUN	RMACH	RALPHA	RBETA	CONFIG	DESCRIPTION
□	41	235	1.2119	-0.2370	-0.0393	15.000	2-D INLET WITH SHORT DIFFUSER
▲	41	236	1.2122	10.028	-.00726	15.000	2-D INLET WITH SHORT DIFFUSER
◆	41	237	1.2105	20.010	-0.0342	15.000	2-D INLET WITH SHORT DIFFUSER
○	41	238	1.2094	24.585	-0.0295	15.000	2-D INLET WITH SHORT DIFFUSER

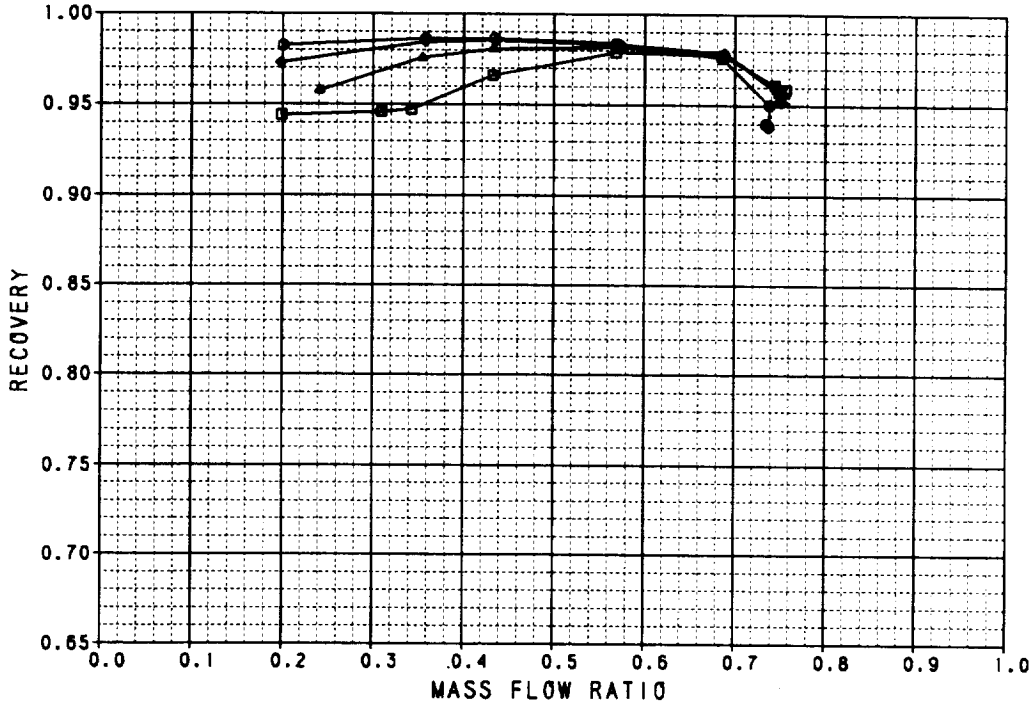

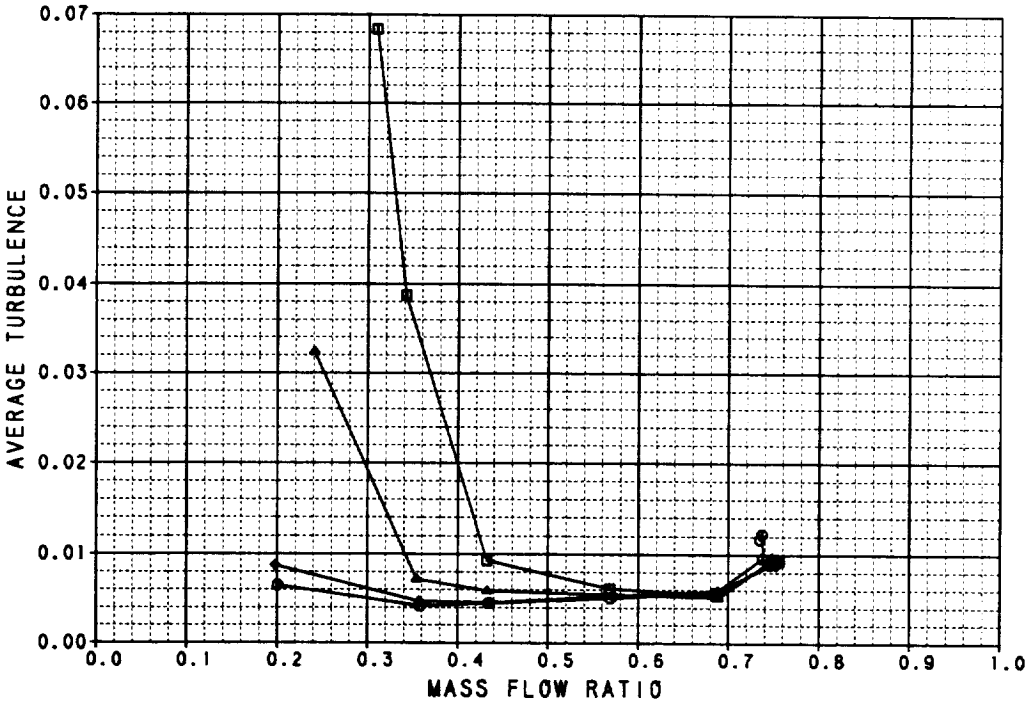

Figure B-43. Performance Data
2-D Inlet With Short Diffuser
$M_0 = 1.2$

SYM	TEST	RUN	RMACH	RALPHA	RBETA	CONFIG	DESCRIPTION
□	41	258	0.6070	-.00611	.00736	16.000	2-D INLET WITH SHORT DIFFUSER,20 DEG DROOP LIP
▲	41	259	0.6051	10.123	0.0160	16.000	2-D INLET WITH SHORT DIFFUSER,20 DEG DROOP LIP
◆	41	260	0.6062	20.081	.00441	16.000	2-D INLET WITH SHORT DIFFUSER,20 DEG DROOP LIP
⊙	41	261	0.6086	30.067	0.0162	16.000	2-D INLET WITH SHORT DIFFUSER,20 DEG DROOP LIP
●	41	262	0.6075	40.186	0.0192	16.000	2-D INLET WITH SHORT DIFFUSER,20 DEG DROOP LIP

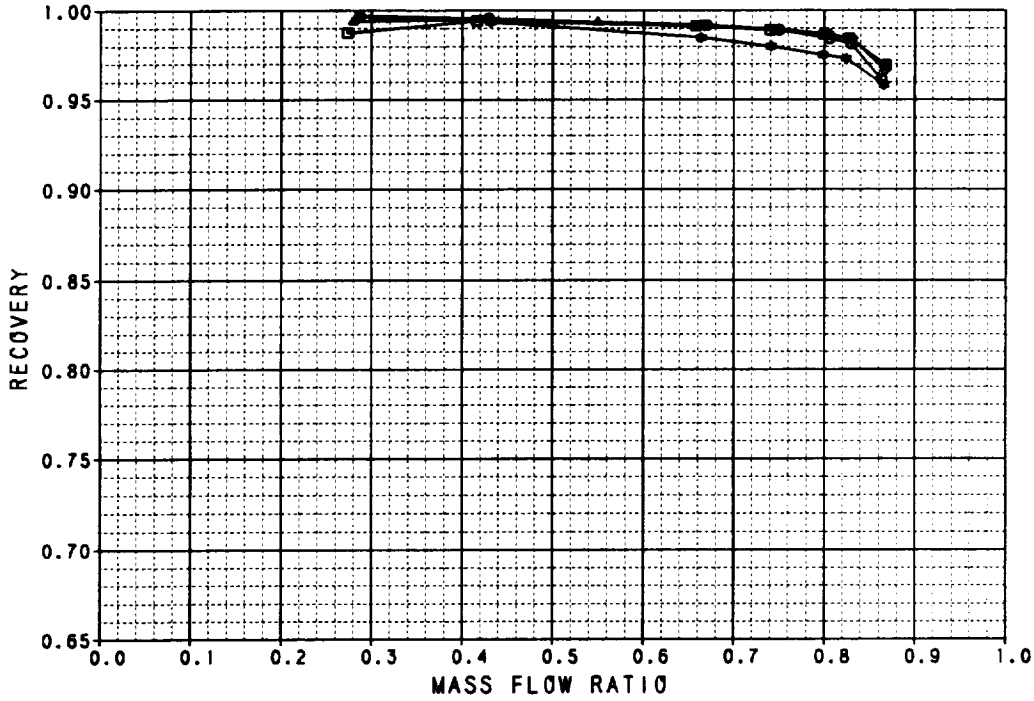

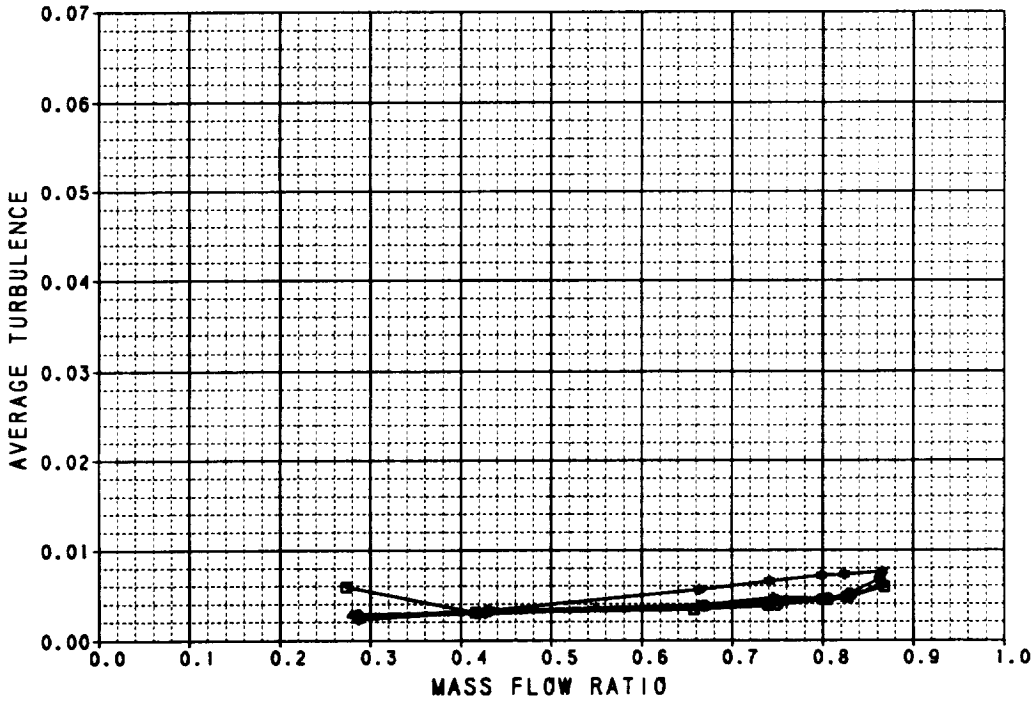

Figure B-44. Performance Data
2-D Inlet 20° Cowl Lip
$M_0 = 0.6$

SYM	TEST	RUN	RMACH	RALPHA	RBETA	CONFIG	DESCRIPTION
□	41	266	0.8998	-4.9244	0.0775	16.000	2-D INLET WITH SHORT DIFFUSER,20 DEG DROOP LIP
△	41	263	0.8980	-0.1253	0.0112	16.000	2-D INLET WITH SHORT DIFFUSER,20 DEG DROOP LIP
◇	41	267	0.8978	10.066	0.0796	16.000	2-D INLET WITH SHORT DIFFUSER,20 DEG DROOP LIP
○	41	268	0.8977	20.205	0.0527	16.000	2-D INLET WITH SHORT DIFFUSER,20 DEG DROOP LIP
◆	41	271	0.9005	30.009	.00913	16.000	2-D INLET WITH SHORT DIFFUSER,20 DEG DROOP LIP
⊠	41	272	0.8972	39.845	.00795	16.000	2-D INLET WITH SHORT DIFFUSER,20 DEG DROOP LIP

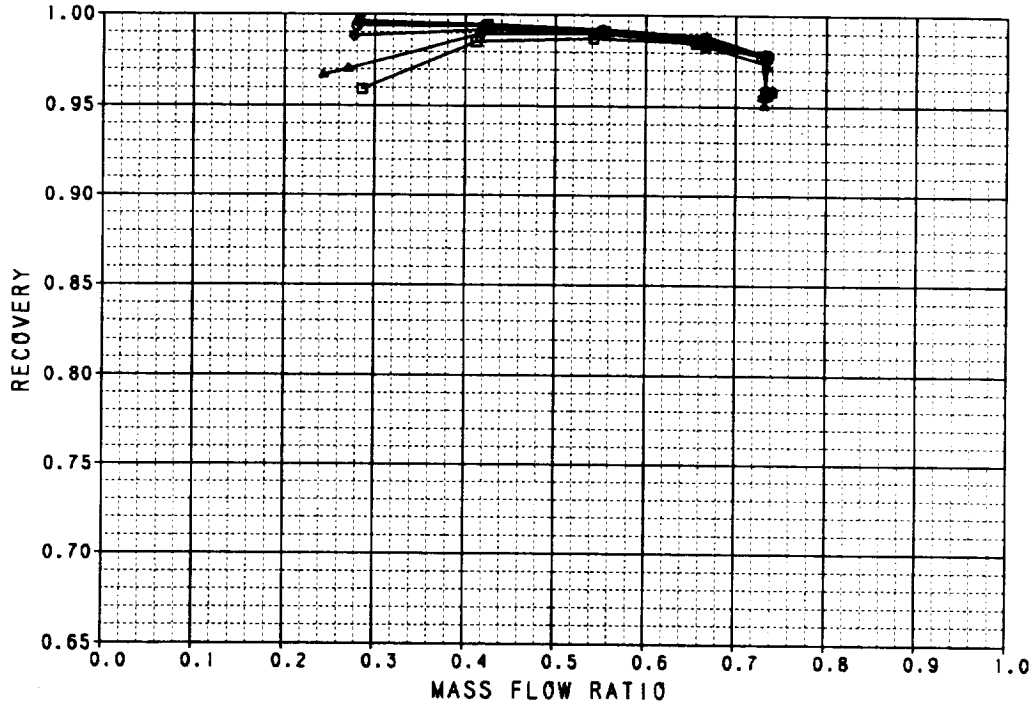

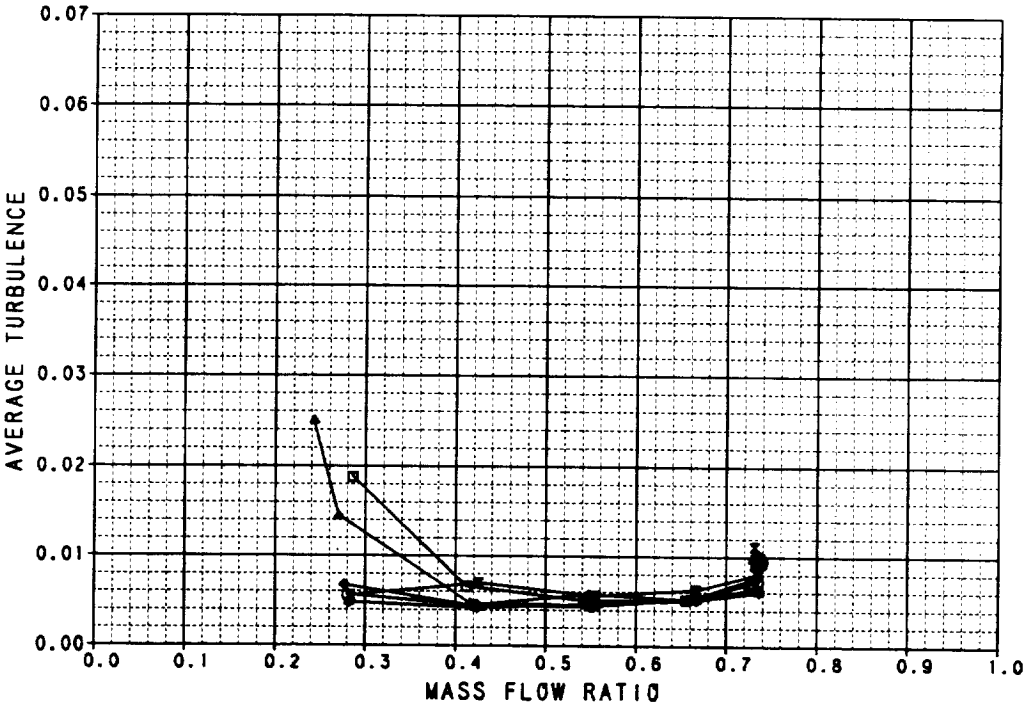

Figure B-45. Performance Data
2-D Inlet 20° Cowl Lip
$M_0 = 0.9$

SYM	TEST	RUN	RMACH	RALPHA	RBETA	CONFIG	DESCRIPTION
□	41	254	1.2109	-0.0834	-0.0259	16.000	2-D INLET WITH SHORT DIFFUSER,20 DEG DROOP LIP
▲	41	255	1.2092	10.020	.00308	16.000	2-D INLET WITH SHORT DIFFUSER,20 DEG DROOP LIP
◆	41	256	1.2050	20.034	-0.0228	16.000	2-D INLET WITH SHORT DIFFUSER,20 DEG DROOP LIP
○	41	257	1.2051	25.073	-0.0300	16.000	2-D INLET WITH SHORT DIFFUSER,20 DEG DROOP LIP

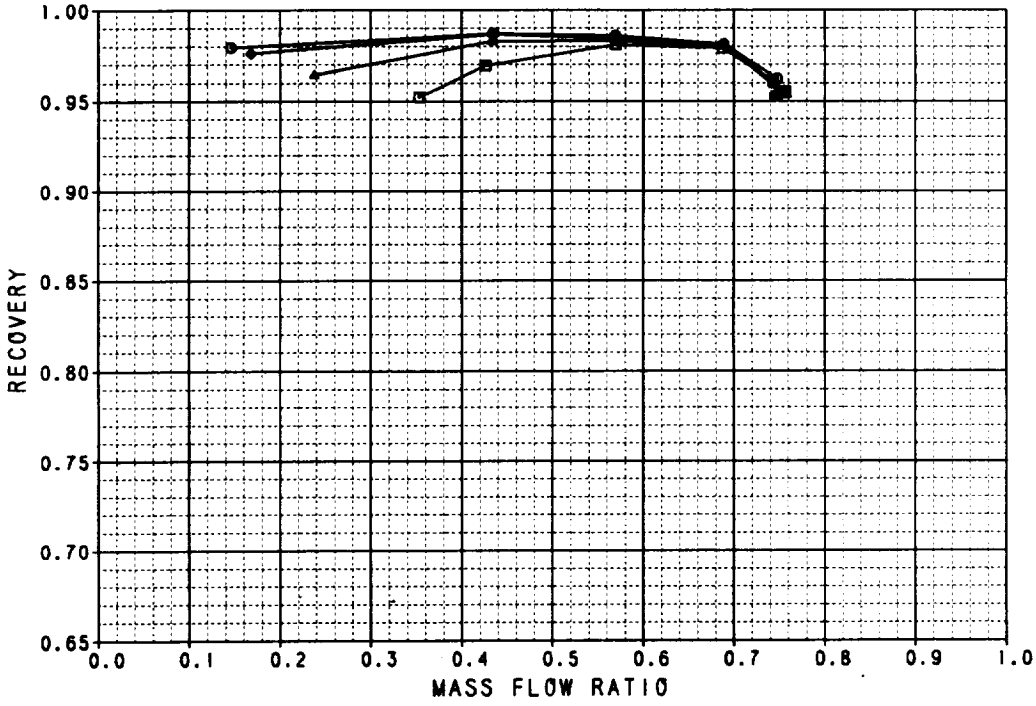

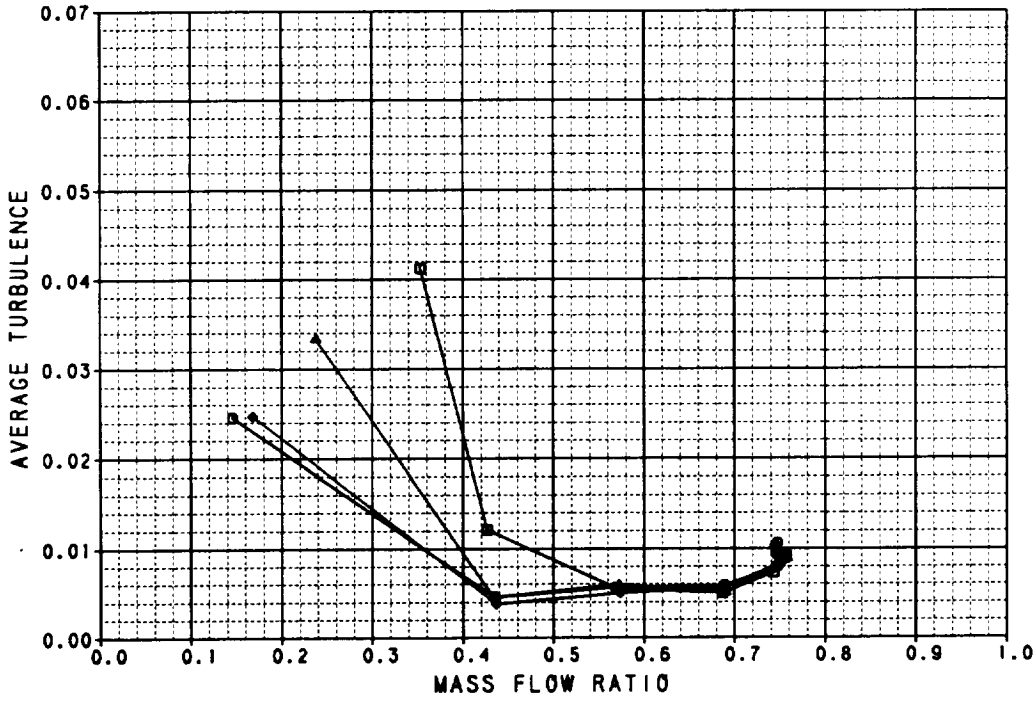

Figure B-46. Performance Data
2-D Inlet 20° Cowl Lip
$M_0 = 1.2$

SYM	TEST	RUN	RMACH	RALPHA	RBETA	CONFIG	DESCRIPTION
□	41	287	0.6059	-.00611	0.0289	17.000	2-D INLET WITH SHORT DIFFUSER,40 DEG DROOP LIP
△	41	288	0.6057	9.9617	0.0286	17.000	2-D INLET WITH SHORT DIFFUSER,40 DEG DROOP LIP
◇	41	289	0.6069	20.062	0.0204	17.000	2-D INLET WITH SHORT DIFFUSER,40 DEG DROOP LIP
○	41	290	0.6071	30.026	.00913	17.000	2-D INLET WITH SHORT DIFFUSER,40 DEG DROOP LIP
⬟	41	291	0.6063	40.056	-.00859	17.000	2-D INLET WITH SHORT DIFFUSER,40 DEG DROOP LIP

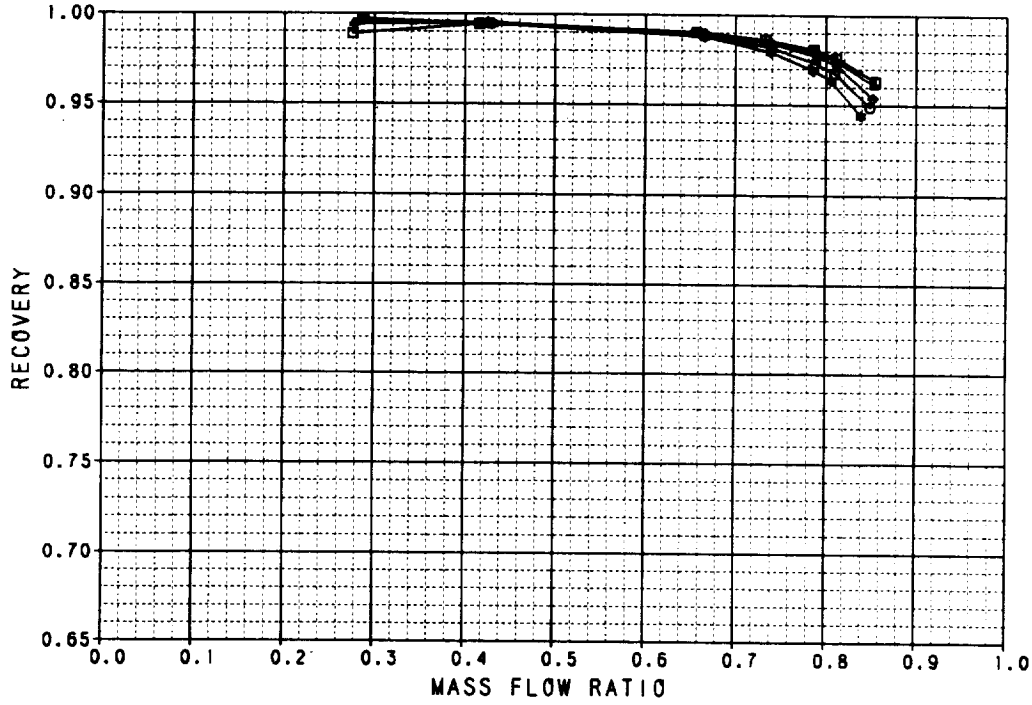

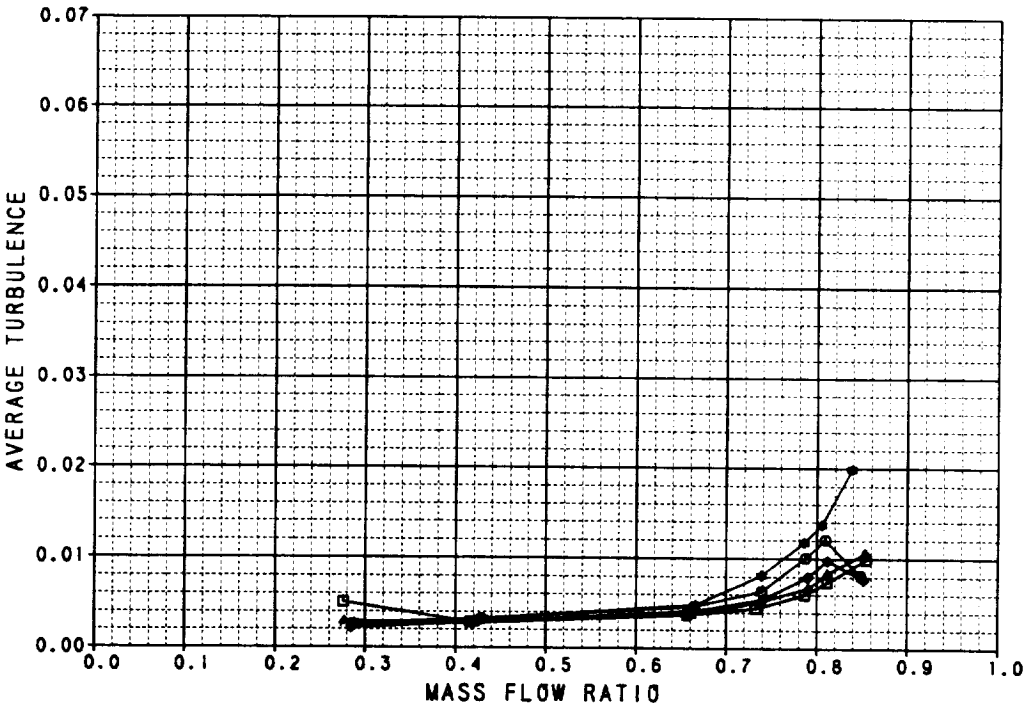

Figure B-47. Performance Data
2-D Inlet 40° Cowl Lip
$M_0 = 0.6$

SYM	TEST	RUN	RMACH	RALPHA	RBETA	CONFIG	DESCRIPTION
□	41	280	0.9002	-5.1584	-.00504	17.000	2-D INLET WITH SHORT DIFFUSER,40 DEG DROOP LIP
▲	41	277	0.9006	-0.1477	-0.0166	17.000	2-D INLET WITH SHORT DIFFUSER,40 DEG DROOP LIP
◆	41	281	0.8995	10.026	-.00741	17.000	2-D INLET WITH SHORT DIFFUSER,40 DEG DROOP LIP
⊙	41	282	0.9016	20.058	-0.0287	17.000	2-D INLET WITH SHORT DIFFUSER,40 DEG DROOP LIP
●	41	285	0.9018	30.293	-0.0192	17.000	2-D INLET WITH SHORT DIFFUSER,40 DEG DROOP LIP
⧗	41	286	0.9022	38.941	-0.0239	17.000	2-D INLET WITH SHORT DIFFUSER,40 DEG DROOP LIP

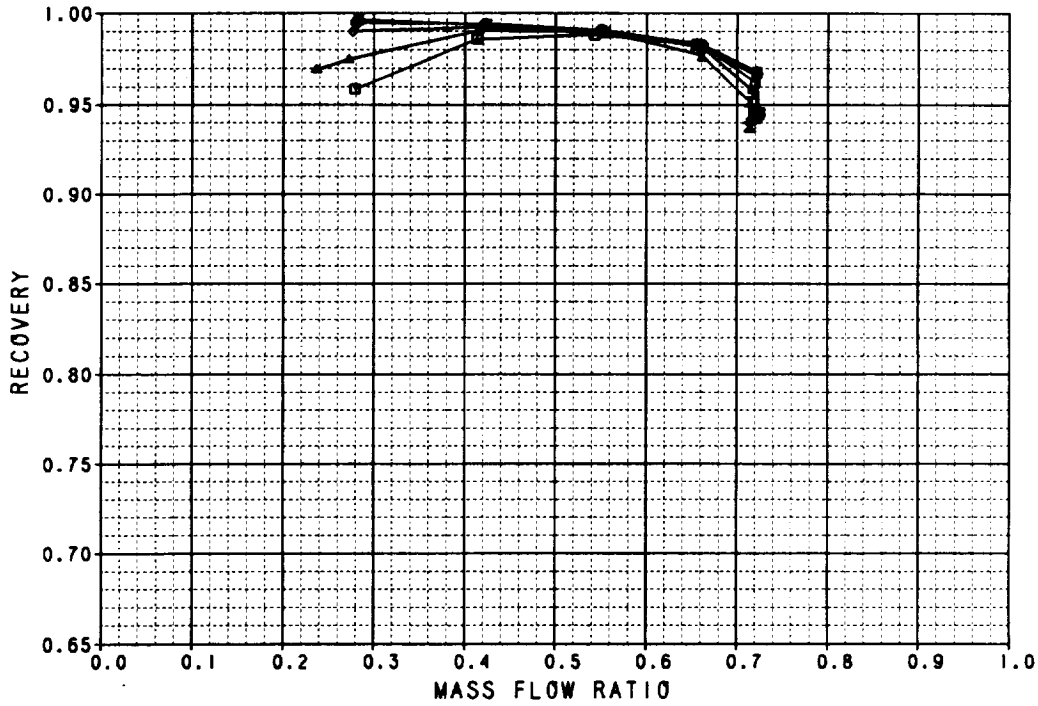

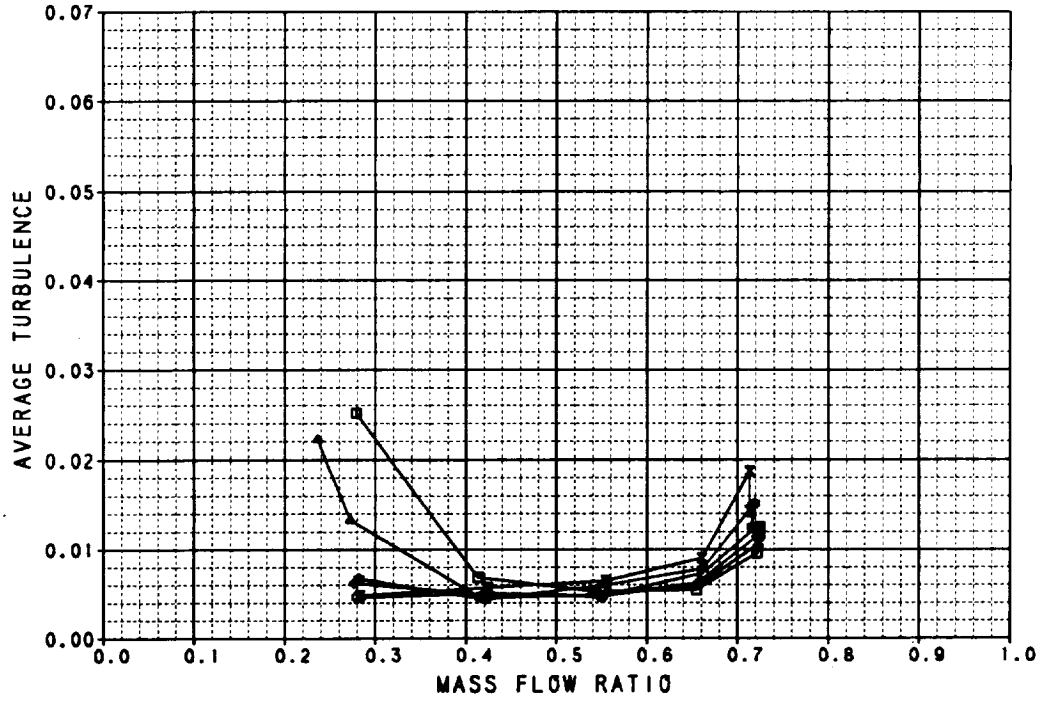

Figure B-48. Performance Data
2-D Inlet 40° Cowl Lip
$M_0 = 0.9$

SYM	TEST	RUN	RMACH	RALPHA	RBETA	CONFIG	DESCRIPTION
□	41	273	1.2139	-0.1314	.00736	17.000	2-D INLET WITH SHORT DIFFUSER,40 DEG DROOP LIP
▲	41	274	1.2123	10.030	.00677	17.000	2-D INLET WITH SHORT DIFFUSER,40 DEG DROOP LIP
◆	41	275	1.2101	20.089	-0.0328	17.000	2-D INLET WITH SHORT DIFFUSER,40 DEG DROOP LIP
⊙	41	276	1.2075	24.851	-0.0393	17.000	2-D INLET WITH SHORT DIFFUSER,40 DEG DROOP LIP

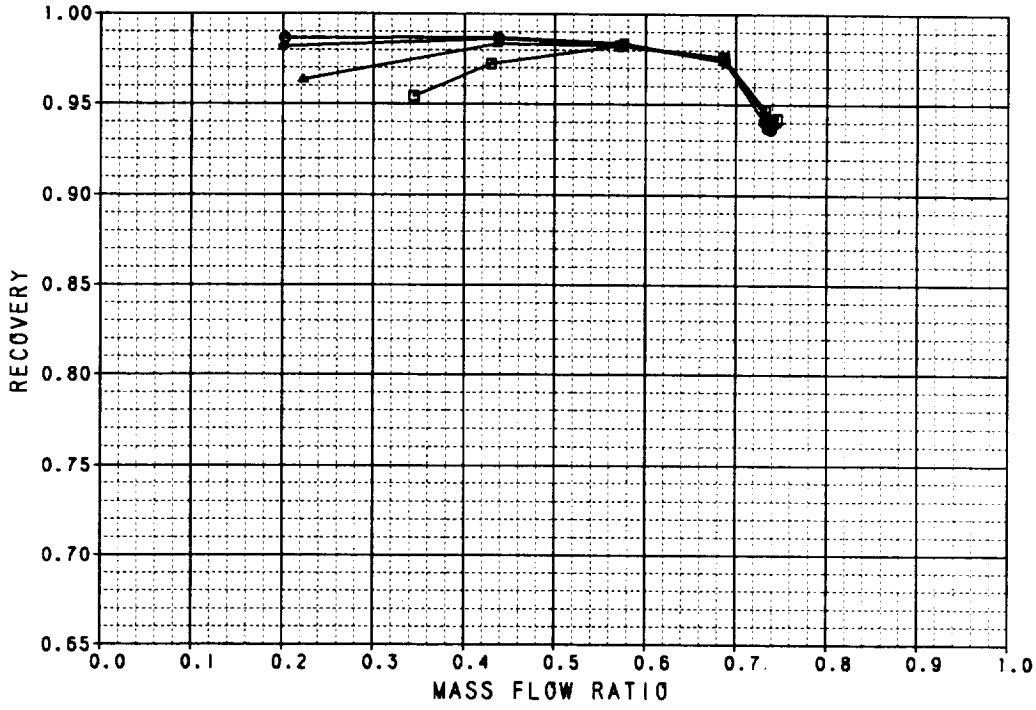

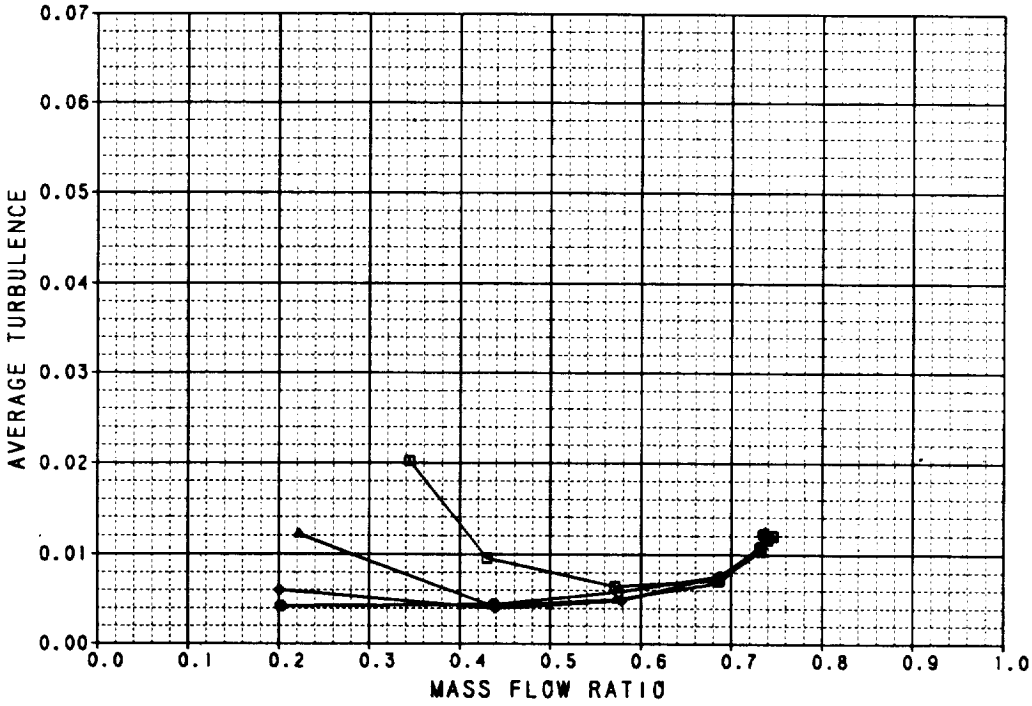

Figure B-49. Performance Data
2-D Inlet 40° Cowl Lip
$M_0 = 1.2$

SYM	TEST	RUN	RMACH	RALPHA	RBETA	CONFIG	DESCRIPTION
□	41	308	0.6063	-0.1715	0.0215	18.000	BASELINE 2-D INLET,NO BLEED
▲	41	309	0.6043	9.9375	0.0221	18.000	BASELINE 2-D INLET,NO BLEED
◆	41	310	0.6064	20.145	2.7E-4	18.000	BASELINE 2-D INLET,NO BLEED
○	41	311	0.6075	30.058	-0.0269	18.000	BASELINE 2-D INLET,NO BLEED
●	41	312	0.6081	39.857	-0.0233	18.000	BASELINE 2-D INLET,NO BLEED

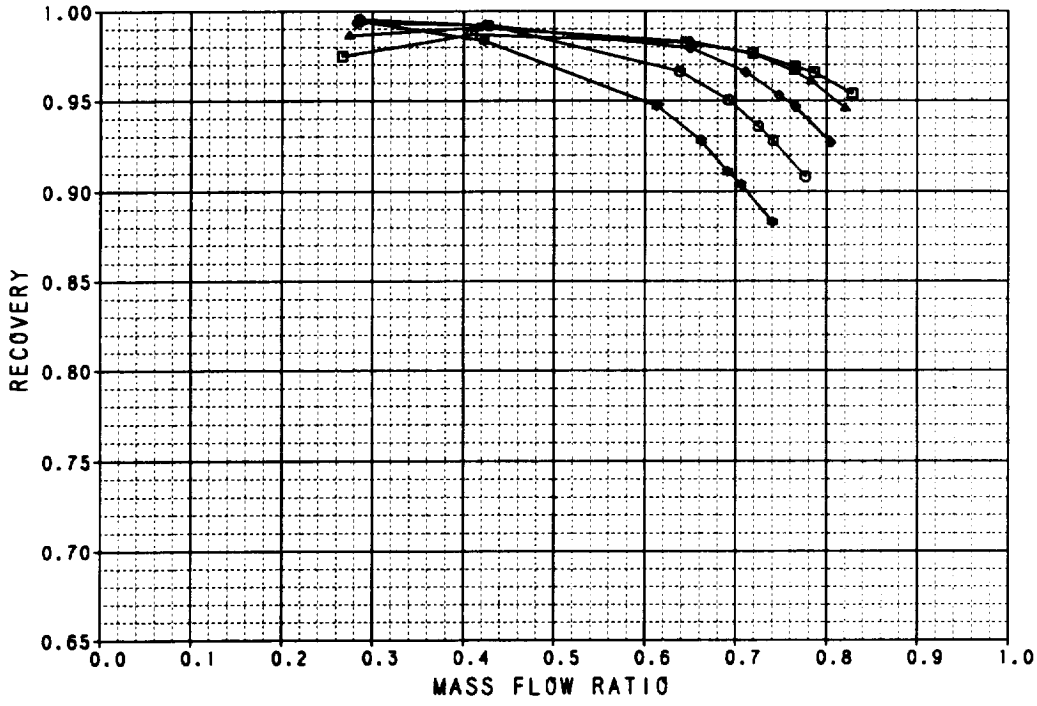

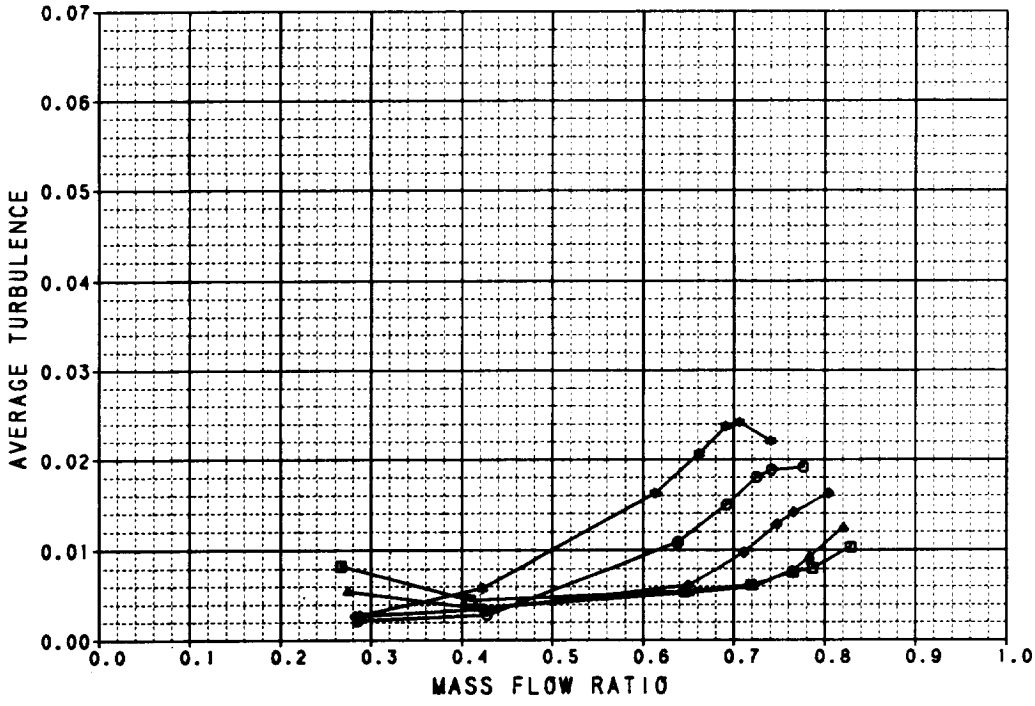

Figure B-50. Performance Data
2-D Inlet With Long Diffuser
$M_0 = 0.6$

SYM	TEST	RUN	RMACH	RALPHA	RBETA	CONFIG	DESCRIPTION
□	41	302	0.9019	-5.0572	0.0279	18.000	BASELINE 2-D INLET, NO BLEED
△	41	303	0.9013	-0.1711	0.0180	18.000	BASELINE 2-D INLET, NO BLEED
◇	41	304	0.8948	9.8828	-.00157	18.000	BASELINE 2-D INLET, NO BLEED
○	41	305	0.9031	20.144	-5.4E-4	18.000	BASELINE 2-D INLET, NO BLEED
⬟	41	306	0.9001	30.132	.00870	18.000	BASELINE 2-D INLET, NO BLEED
⧗	41	307	0.9013	38.887	-0.0279	18.000	BASELINE 2-D INLET, NO BLEED

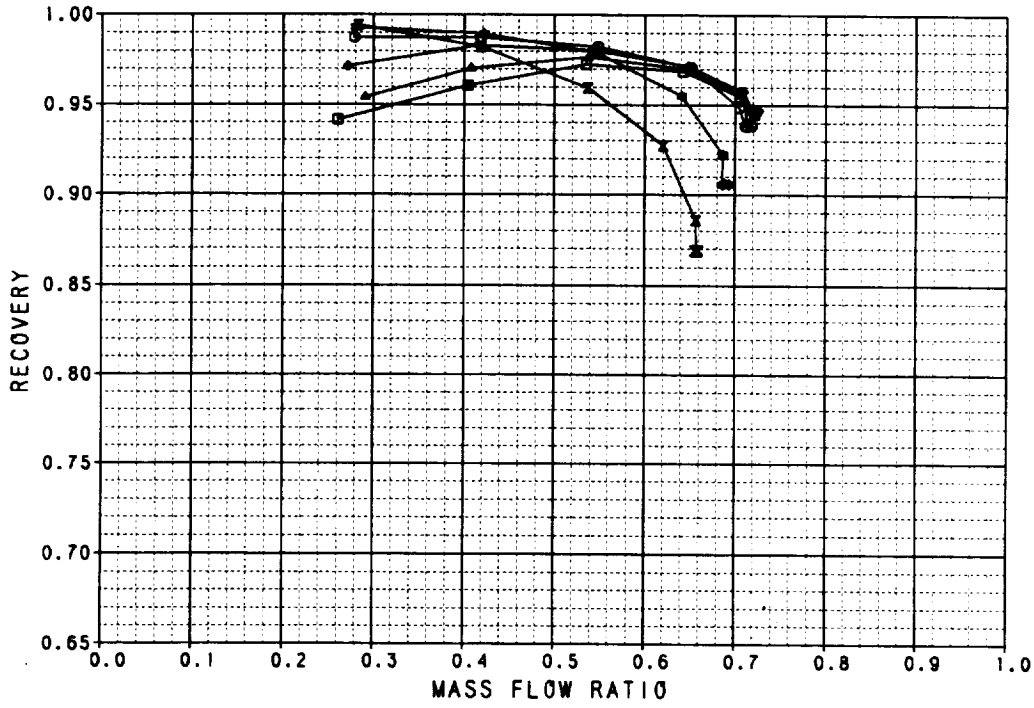

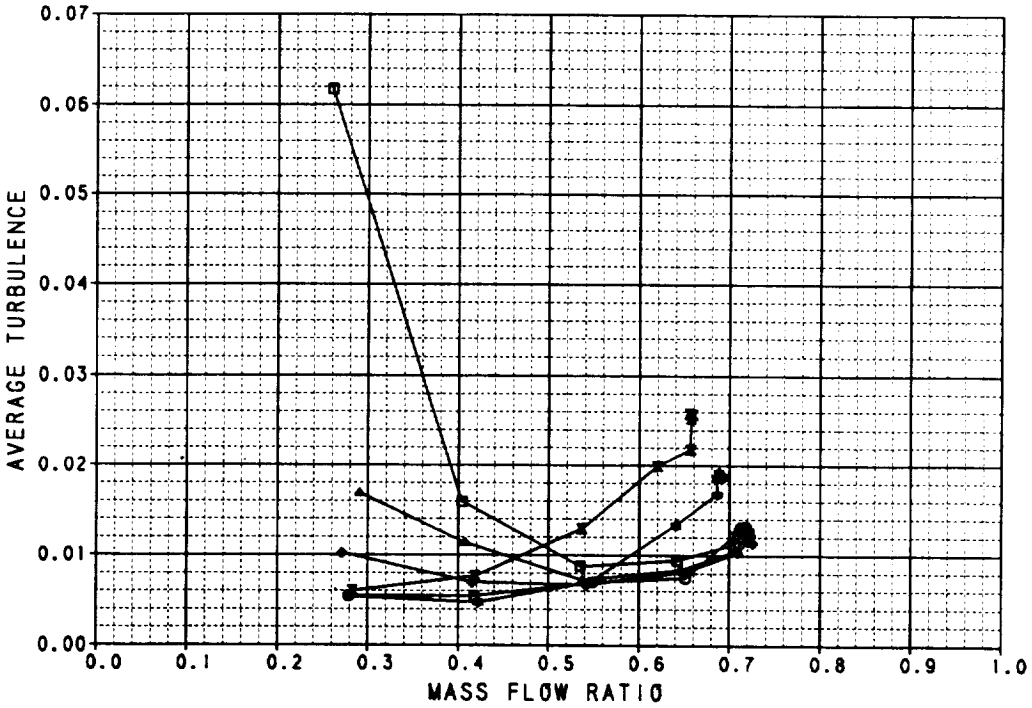

Figure B-51. Performance Data
2-D Inlet With Long Diffuser
$M_0 = 0.9$

SYM	TEST	RUN	RMACH	RALPHA	RBETA	CONFIG	DESCRIPTION
⊡	41	298	1.2133	0.0758	-0.0281	18.000	BASELINE 2-D INLET,NO BLEED
▲	41	299	1.2104	10.035	-0.0304	18.000	BASELINE 2-D INLET,NO BLEED
◆	41	300	1.2084	20.310	-0.0289	18.000	BASELINE 2-D INLET,NO BLEED
⊙	41	301	1.2107	25.288	-0.0239	18.000	BASELINE 2-D INLET,NO BLEED

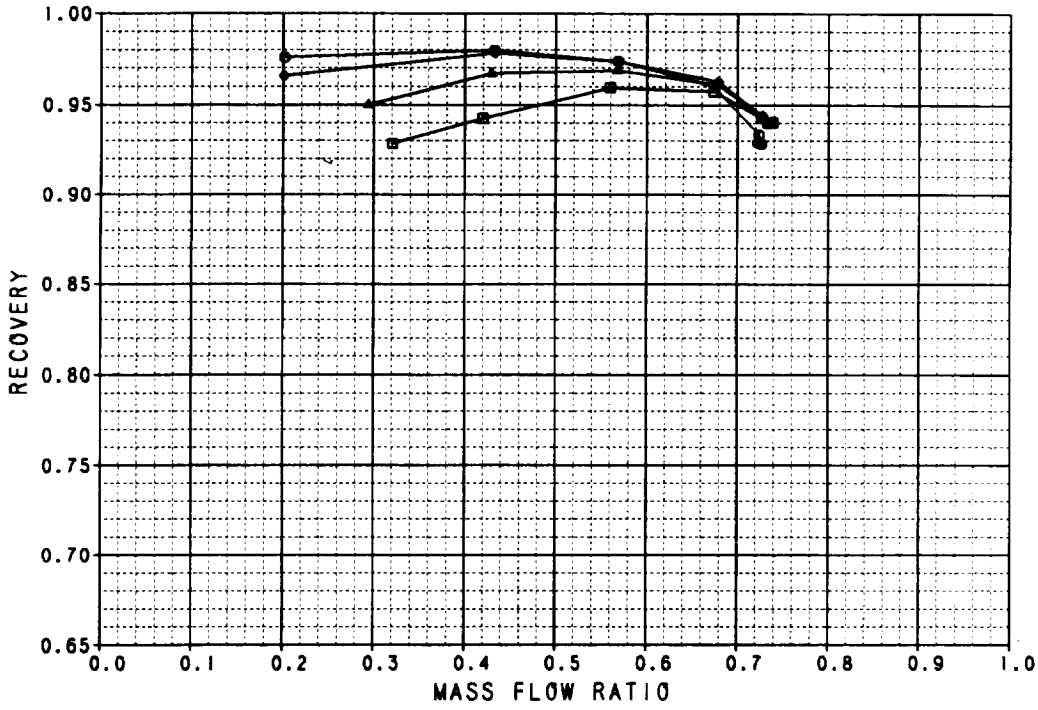

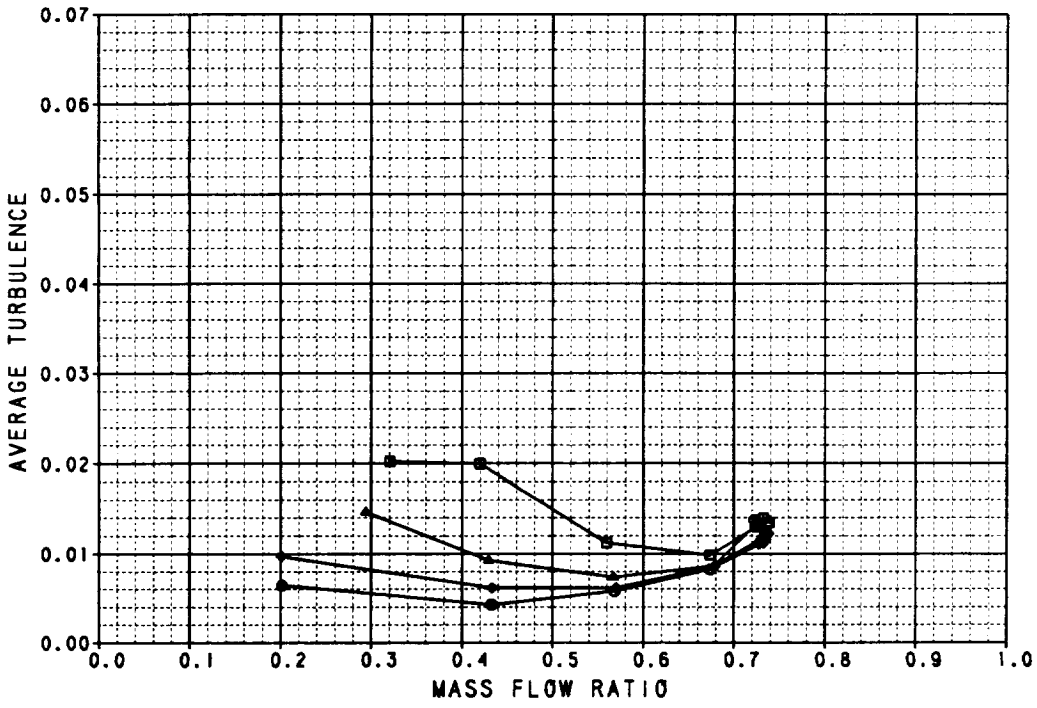

Figure B-52. Performance Data
2-D Inlet With Long Diffuser
$M_0 = 1.2$

SYM	TEST	RUN	RMACH	RALPHA	RBETA	CONFIG	DESCRIPTION
□	41	292	1.4040	-5.0419	-.00898	18.000	BASELINE 2-D INLET,NO BLEED
△	41	293	1.4033	0.0205	-.00778	18.000	BASELINE 2-D INLET,NO BLEED
◇	41	294	1.4026	4.7158	-0.0114	18.000	BASELINE 2-D INLET,NO BLEED
○	41	295	1.4090	9.8400	-0.0207	18.000	BASELINE 2-D INLET,NO BLEED
✱	41	296	1.4046	15.040	-0.0331	18.000	BASELINE 2-D INLET,NO BLEED
⧗	41	297	1.4032	20.192	-0.0259	18.000	BASELINE 2-D INLET,NO BLEED

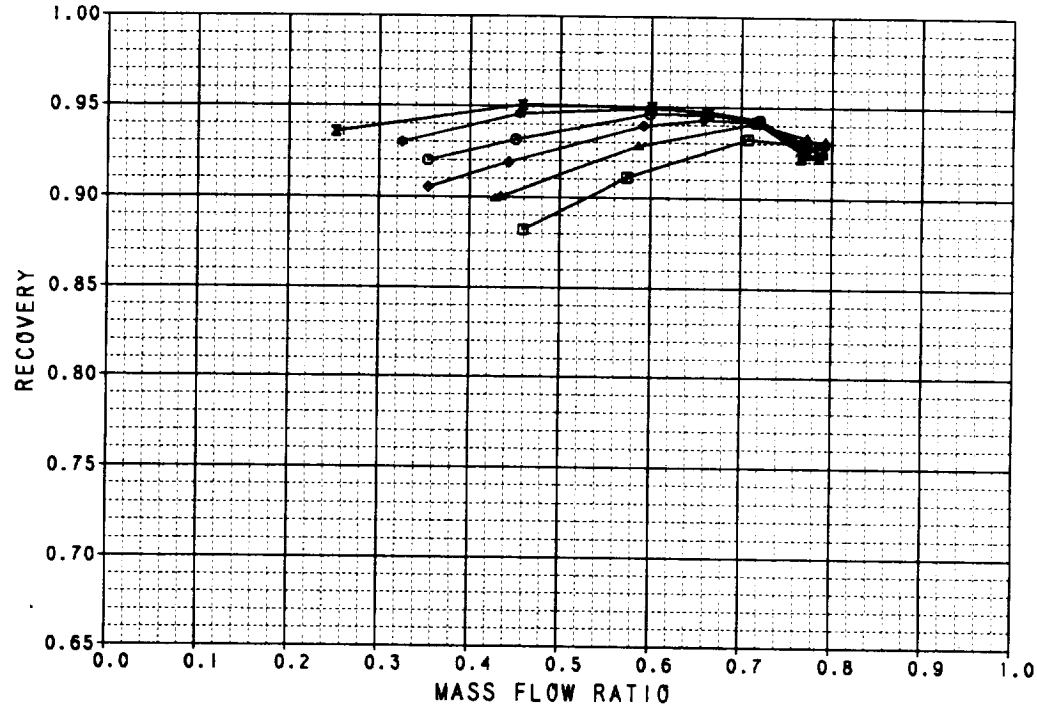

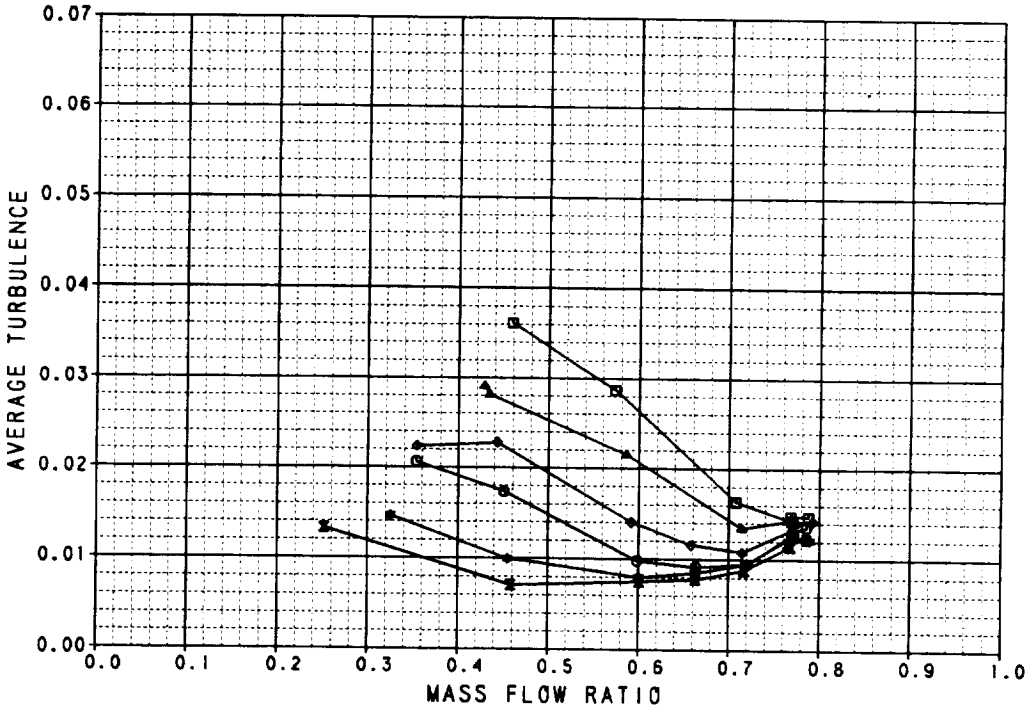

Figure B-53. Performance Data
2-D Inlet With Long Diffuser
$M_0 = 1.4$

1. Report No.	2. Government Accession No.	3. Recipient's Catalog No.
NASA CR-179544		

4. Title and Subtitle	5. Report Date
ISOLATED TESTING OF HIGHLY MANEUVERABLE INLET CONCEPTS	December 1986
	6. Performing Organization Code

7. Author(s)	8. Performing Organization Report No.
W. P. Norby and B. A. Haeffele, McDonnell Aircraft Company and R. R. Burley, NASA Lewis Research Center	10. Work Unit No.

9. Performing Organization Name and Address	11. Contract or Grant No.
McDonnell Aircraft Company P.O. Box 516 St. Louis, MI 63166	See Supplementary Notes
	13. Type of Report and Period Covered
	Contractor Report
12. Sponsoring Agency Name and Address NASA Lewis Research Center 21000 Brookpark Road Cleveland, Ohio 44135	14. Sponsoring Agency Code

15. Supplementary Notes

PROJECT MANAGER: Richard R. Burley, NASA Lewis Research Center, 21000 Brookpark Road, Cleveland, Ohio 44135

(This report was not a result of a contract or grant. The report was written per an informal agreement with the contractor.)

16. Abstract

Ten percent scale models of a Mach 2.2 two-dimensional inlet and a Mach 2.0 axisymmetric inlet were tested in the NASA Lewis Research Center 8'x6' Supersonic Wind Tunnel as part of a cooperative effort with the McDonnell Aircraft Company. The objective of this effort was to test methods designed to increase the maneuvering performance of fighter aircraft inlets. Maneuvering improvement concepts were tested up to 40° angle-of-attack for Mach numbers of 0.6 and 0.9, and up to 25° for Mach numbers 1.2 and 1.4.

Maneuvering improvement concepts included a rotating cowl lip, auxiliary inlets aft of the inlet throat, and a retracting centerbody for the axisymmetric inlet. Test results show that the rotating cowl design was effective in improving subsonic maneuvering performance for both inlets. Auxiliary inlets did not produce significant performance increases for either model. The retracted centerbody resulted in some performance benefits at high angles-of-attack. None of the maneuvering improvement concepts were effective at Mach 1.2 and 1.4.

17. Key Words (Suggested by Author(s))	18. Distribution Statement
Auxiliary inlets, droop lips, highly maneuverable inlet design, subsonic and transonic inlet performance	UNCLASSIFIED [redacted] UNTIL DECEMBER 1988 STAR CATEGORY 7

19. Security Classif. (of this report)	20. Security Classif. (of this page)	21. No. of pages	22. Price*
UNCLASSIFIED	UNCLASSIFIED	166	

[redacted]